THE ELECTROKINTIC (EK) EFFECT AS THE BASIS FOR A NON-INVASIVE GROUND INVESTIGATION TOOL

May 2004

Kenneth Alwyn O'Hara-Dhand

A thesis submitted in fulfilment of the requirements of
The Nottingham Trent University
for the degree of Doctor of Philosophy

This thesis is dedicated to the
memory of my late mother and father
Ethel Maud and Daniel Patrick O'Hara

Also to my mother and late father in law
Kundan Lal and Raj Ranee Dhand

Venerable mother!

All else who live and suffer take from thee

Some comfort; flowers, and fruits, and happy sounds,

And love, though fleeting; these may not be mine.

But mine own words, I pray, deny me not.

PROMETHEUS UNBOUND
A lyrical drama in four acts Act 1 190
Percy Byshee Shelley 1792 - 1822

And in appreciation of my four children
Jason, Rachael, Suneela and Sameer

Certificate of Originality

This is to certify that I am responsible for the work submitted in this thesis, that the content is my own except where specified in the acknowledgements and that neither the thesis nor the original work contained therein has been submitted to this or any other institution for a higher degree

Signature.....

Kenneth Alwyn O'Hara-Dhand

Abstract

This thesis presents research relating to the detection of acoustically generated electromagnetic (EM) waves by a novel dipole aerial system in two differing geological environments. Both field and laboratory studies were conducted that concentrated on the electromagnetic response due to a compressional wave crossing a seismically contrasting boundary. The field investigation results revealed clear electromagnetic responses from a depth down to 30 metres and an indication of responses from the water table and fracture zones. Correlation of the EM responses was demonstrated by comparison to other geotechnical measurements. A method has been devised to detect the water table using the variation in the measured amplitude of the dipole distribution of the electric field away from the shot point, eliminating the need for extensive seismic refraction surveying. Laboratory studies on a consolidated sandstone sample, representative of the geology of one of the field locations, demonstrated clear electromagnetic responses from a water saturated bedding plane flaw. Readings were also taken with the sample reversed with a clear correlation of the EK responses in both cases. The laboratory results were comparable to those obtained for the field investigations. The encouraging results of the laboratory investigations have pointed the way forward for further research, such as similar carefully controlled laboratory experiments with other geological samples such as clay and consolidated limestone. The results demonstrate that the Electrokinetic technique will provide another useful technique to existing geophysical methods such as seismic refraction, electromagnetics, resistivity, GPR, etc for shallow ground investigation.

Keywords: Acoustic waves, compressional wave, seismic refraction, dipole aerial, Electrokinetic, electromagnetic waves, acoustic source.

ACKNOWLEDGEMENTS

Professor Michael Rosenbaum, my initial principle supervisor, whom I have known for the last 30 years, for his enthusiastic support and advice on the geological and other many aspects of the research.

Dr. Ian Jefferson. My present principle supervisor, for his ever enthusiastic support and patience.

Dr. Peter Thomas, my second supervisor, Head of the Machine Control Group within the Department of Computing, for many useful discussions and advice on the software , the overall system and layout of the thesis.

Dr. Roger Hill, my third supervisor, Reader in physics in the Department of physics and chemistry, for his help and advice in the more mathematical and physical aspects of this thesis.

Dr. David Beamish of the British Geological Survey (BGS) at Keyworth for the loan of a 'Terraloc' seismic recorder with vertical and horizontal geophones for the month of July 2001.

Dr. Nigel Cassidy, for his help and advice in the final stages of this thesis.

Professor Ian Smalley for his enthusiasm and many helpful discussions.

Mr Robert Evans for his assistance in some of the field work

Mrs Judith Prest, soils laboratory technician, for her enthusiastic help in the laboratory tests and EK experiments.

Mr. Lawrence Dickenson, surveying stores technician, for his willing help in the supply of field equipment.

Mr Steve Goodman, Mr Alan Freeby, Mr Colin Chambers and Mark Flanagan, workshop technicians, for their help in the mechanical construction of the preamplifier unit and other experimental items.

The technicians in the Electrical Engineering Department for their help in the loan of equipment in order to carry out the laboratory EK experiments and in particular Mr. Jeffrey Baines his help in the supply of components and the loan of various measuring instruments.

Toray Textiles for making their site avail for a number of the EK investigations and in particular Mr Mark Fisher, works manager, from whom permission was obtained on a number of occasions

Mr Brian Parks, Works manager, Cremer Whiting & Co. For making the site at Ospringe in Kent available for a number of geophysical investigations.

Mr John Dean of 'Worlds Farm', Costock, for permission to use his field for the EK investigations.

Mr. Paul Bagley. A colleague who was working on a PhD at Keele University for use of equipment used to conduct the field work at the Mansfield site on the 6th February 2000

The Ordinance Survey for use of their free map service.

Finally and not least to my dear wife for her patience and understanding during the three and a half years (part time) I have spent in doing this research.

TABLE OF CONTENTS

Appendices

List of tables

List of figures

LIST OF PLATES

NOTATION

Please note that where appropriate all units are quoted in the SI system of units unless otherwise specified.

BGS	British Geological Survey
C	Capacitance in Farads
C	Current source density
D	Electric flux density
DCP	Dynamic Cone penetrometer
DPA	Dipole aerial
E	Electric field strength. volt per metre (V/m)
EDL	Electric Double Layer
EK	Electrokinectic
E	Electric field strength
EM	Electromagnetic
W	Energy (Watts)
ε_0	Permittivity of free space = $8.85.10^{-12}$ farad per metre $\left(\frac{F}{m}\right)$
ε_r	Relative permittivity of free space
f	f_f fluid force
G	Electrical conductance siemans (S)
H	Magnetic field strength Amperes per metre (A/m)
Hz	Frequency in cycles per second
I	Electric current Steady or rms value Amperes (A)
I	Identity tensor
J	Current density amperes per square metre (A/m^2)
K_G	Gassmann's bulk modulus
$L(\omega)$	Electrokinetic coupling tensor
f_0	Resonant frequency Hz
IHP	Inner Helmholtz Plane
l	Inductance in Henry's (H)
λ	Wavelength of an acoustic or electromagnetic wave
$\lambda\!\!\!^{-}$	Radian wavelength $\lambda/2\pi$
mah	milli-ampere hour i.e. amperes x 10^{-3} per hour
ms	Milliseconds i.e. seconds x 10^{-3}.

η	fluid shear viscosity
OHP	Outer Helmholtz Plane
ω	Radian measure of frequency = $2\pi f$ (Hz)
Ψ	Electric flux
P	Pore-fluid pressure
p	fluid pressure
Q	Electrical charge, Coulombs (C)
R	Resistance ohms
SPT	Standard Penetrometer Test
τ	bulk stress tensor
μ	1×10^{-6}
μ_e	Effective permeability of ferrite rod
μ_0	Permeability of free space = $4\pi x10^{-7}$
UHMW	Ultra High Molecular Weight
USR	Ultrasonic receiver
UST	Ultrasonic transmitter
V	Potential difference volt
v	Velocity m/s

With them the seed of Wisdom did I sow
And with mine own hand wrought to make it grow
And this was all the Harvest that I reap'd
I came like Water, and like Wind I go.

Rubaiyat of Omar Khayyam
Verse 28
Translation by Edward FitzGerald

Introduction

On Physical Lines of Force:-

We can scarcely avoid the inference that light consists in the traverse undulations of the same medium which is the cause of electric and magnetic phenomena.

James Clarke Maxwell 1862 upon the realisation that Electromagnetic phenomena are related to light when he discovered that they travelled at the same speed.

The research described in this thesis is concerned with the Electro-Kinetic (EK) effect and its application as a shallow ground investigation tool in the built environment. This thesis describes the application of a novel dipole aerial for the detection of the electro-kinetically induced electromagnetic radiation and outlines development of an EK spectrometer for the recording and collection of data during shallow ground investigations. Software has been written to analyse these data on a desktop personal computer. Specific applications relate to and include the assessment of the location the water table. EK investigations have been conducted at two sites with different geological profiles.

The EK technique developed in this thesis will not only stand alone in its application but will also be a useful addition to existing geophysical techniques.

The seismoelectric effect has four known components, namely:

(1) The change in ground electrical resistance, in which currents flow upon passage of a seismic wave, as reported by Thompson (1936).

(2) Seismically induced EK effects or streaming potentials (Ivanov, 1939, 1940; Thompson and Gist, 1993).

(3) The piezoelectric effect as first described by (Pierre and Jacques Curie, (1880) and subsequently in a geological context by Volarovich *et al.*, (1959; Volarovich *et al.* (1962) and Russell *et al.* (1992).

(4) Seismically induced EK responses of the second kind. Pride, (1994). In addition Non-linear processes that generate radio frequency impulsive (EK)

responses resulting in the generation of electromagnetic (EM) waves in sulphide rich rocks. Kepic *et al.* (1995).

This thesis will concentrate on the fourth component.

For the majority of the geophysical investigations described in this thesis, the recommendations as laid down in the two publications, namely the Construction Industry Research and Information Association (CIRIA) report (C562), and "Geophysics Engineering Investigations" (McDowell *et al.*, 2000) have been observed.

In most geological profiles electromagnetic waves travel considerably faster than the seismic waves. As a result a delay occurs between the shot instant and the reception of an EK response. This equates to the time for the seismic wave to travel from the shot point to the first fluid filled contrasting layer. However, there may be a number of varying seismic velocity profiles above the contrasting layer due to the stratigraphy of the ground. These velocities have been calculated for correlation with the EK data.

These seismically induced electro-kinetic responses are the result of a coupling between fluid and electric current flow. They arise because of the electric double layer, which exists on the surface of the soil grains. The existence of an electric double layer in a clay was first suggested by Reuss (1808). A model to describe this layer was first described by Helmholtz (1879) and subsequently developed by Gouy (1910) and Chapman (1913).

The double layer exists at a solid–liquid interface and consists of a layer of ions absorbed on the matrix of the solid or soil particle. In addition, a parallel diffuse layer of counter ions exist within the pore fluid with part of the diffuse layer being free to move with this fluid. Thus, the flow of fluid relative to the solid surface allows the possibility of charge separation and the development of an electric field. Biot's equation's for elastic wave propagation (Biot, 1956) were extended by Neeve and Yeates, (1989), to calculate the electro-kinetic effects accompanying seismic compressional waves in the quasi-static case. Subsequently, Haarstsen and Pride, (1994) developed a method for solving the general time-varying problem, in which Maxwell's electromagnetic and Biot's mechanical wave equations are linked through electro-kinetic coupling. Haarstsen and Pride, (1994) also predicted that seismic body waves in layered media

produce two types of seismoelectric effects:

(1) Non-radiating fields that accompany the body waves in layered media. These are only observed when the waves pass by an EM detector and receiving apparatus.

(2) EM fields that are generated by seismic waves traversing a contrasting boundary, where there is a change in the elastic or electrical properties, e.g. fluid chemistry and ground permeability.

Ivanov (Ivanov 1939, 1940) reported seismoelectric effects in sedimentary media. He proposed an electro-kinetic mechanism for these electroseismic effects. He observed two effects. The first he called seismic effects of the first kind namely, the modulation of earth electrical resistivity by seismic pressure. The second effect Ivanov called "seismoelectric effect of the second kind". This is the EK effect as examined in this thesis. These results were followed by further reports of EK phenomena, (Frenkle, 1944 and Martner and Sparks, 1959). Further papers, mainly of a theoretical nature, appeared later, e.g. Biot 1956, 1957 and 1962.

With advances in electronic technology and signal processing techniques over the last fifteen years, interest in EK has been rekindled; Butler *et al.* (1996) investigated the EK effect, detecting EK responses emanating from a shallow boundary approximately 3.0 m. Further work includes investigations by Dietrich *et al.* (1996) and Haarstsen and Pride, (1997).

Most of the recent field data so far reported have been collected from depths of less than 10 m. Additional data has been collected under laboratory conditions where a method for measuring the electro-kinetic coefficients of porous media for a number of geological series, such as limestone and sandstone (Ishido, 1981). He used an electrochemical cell. Jiang *et al.* (1998) later used a different experimental arrangement, which comprised a cell to measure electro-kinetic coefficients in the range 20 to 100 Hz. EK experiments using ultrasonic waves of frequency 100 kHz were conducted by Haartsen *et al.* (1995), using a specially prepared sandstone model. In addition crosshole seismoelectric measurement in borehole models were conducted to detect fractures, (Zhena and Toksöz, 2001).

It has been theoretically shown that when an elastic wave transverses a fluid saturated porous seismically contrasting layer, a charge disturbance or imbalance occurs, which generates a small but measurable electromagnetic response (Pride, 1996). This process is shown in diagrammatically in figures 1.1, 1.2 and 1.3.

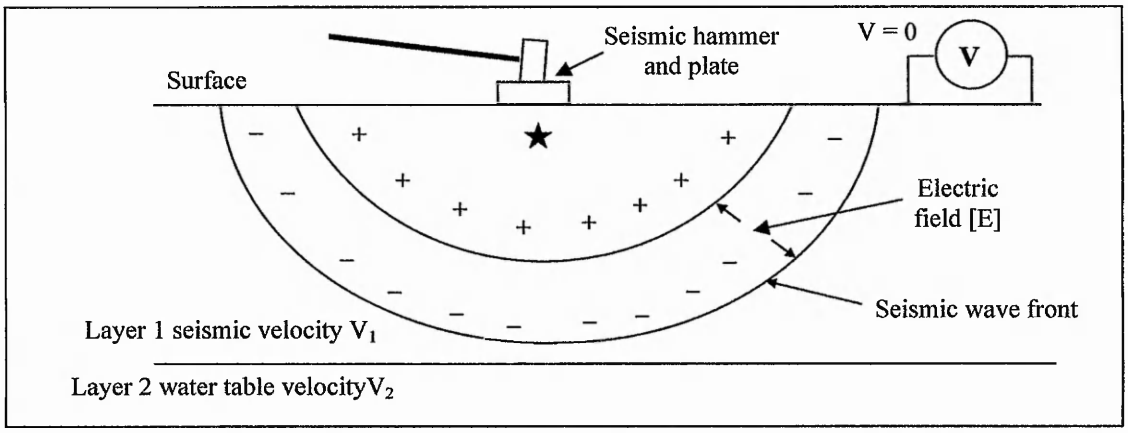

Figure 1 Stage 1: Depicts the seismic wave propagating out from the shot point with electrical charges distributed on the leading edge of the wave, i.e. a travelling electric field with no external extent.

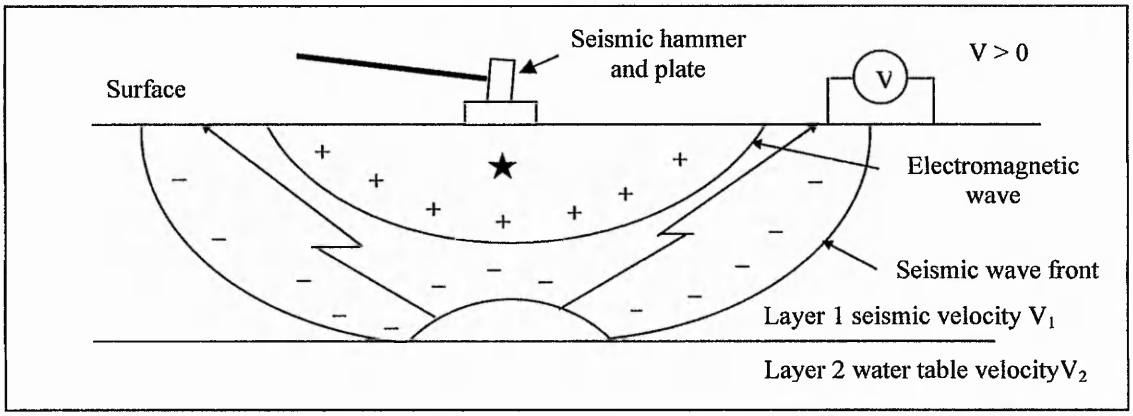

Figure 2 Stage 2: The seismic wave encounters a contrasting interface. The start of the electrical charge displacement takes place giving rise to an electromagnetic wave varying with the frequency of the seismic wave.

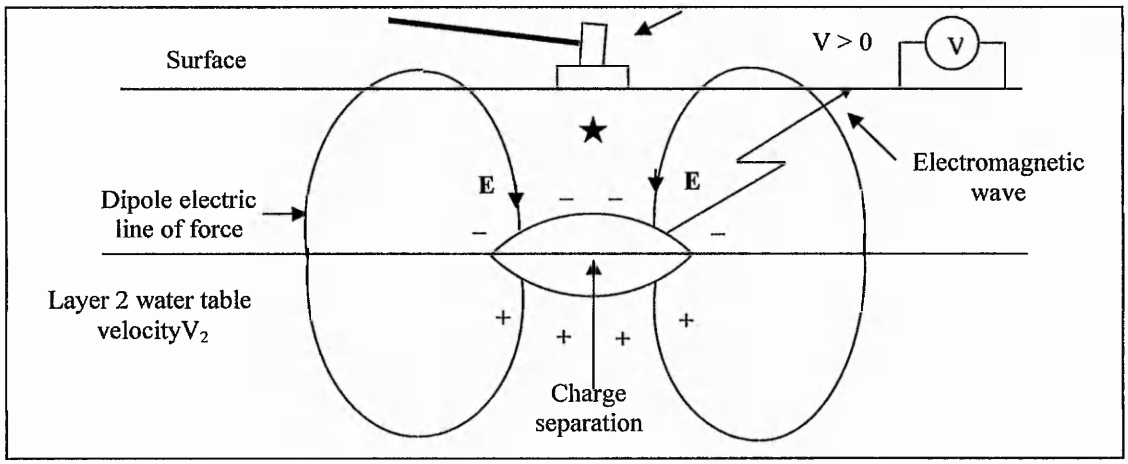

Figure 3 Stage 3: The seismic wave front has now traversed the interface resulting in charge separation giving rise to a transitory flow of electric current resulting in the generation of an EM wave.

The literature review (Chapter 1) highlights key areas requiring further work in particular the detection of EK phenomena in different geological profiles. This review showed that the theoretical nature as of the EK generation process is reasonably well understood. However, little research has been conducted to relate the theory described so far, to field behaviour. Specifically measurements made in the field can be used to define various geological profiles.

Very little practical development has taken place due in part to the lack of portable robust apparatus of sufficient sensitivity to detect the low-level signals encountered. These are typically in the low millivolt to microvolt range. In addition other more established geophysical techniques have dominated most geophysical investigations. Other researchers have tended to investigate electro-kinetic effects down boreholes, targeted specifically at petroleum or hydro geological studies e.g. (Miller and Clark, 1995) and (Hunt and Worthington, 2000).

Research aim. *To establish the extent to which the EK effect can be reliably detected at shallow subsurface of less than 50 metres.*

The research has the following objectives:

1. To develop a non-destructive ground investigation tool based on EK using a novel electric dipole aerial detection system, thereby overcoming most of the difficulties experienced with other detection methods.

2. To establish the range of the EK response in at least two contrasting geological profiles. These will be used to test the assertion made by Pride (1996).

3. To evaluate the usefulness of EK in detecting the start of the fully water saturated zone and further establish the maximum useful depth over which EK signals can be reliably detected.

4. Investigate the dependence of the wave shape of the received EK signal in relation to the capillary region above the fully water saturated zone.

5 To correlate the relationship of EK responses obtained in the field to theory as predicated by Pride (1996) and to laboratory EK investigations.

6 To conduct laboratory experiments with a simple two layer model in order to observe results in carefully controlled conditions.

The work outlined in this thesis makes an original contribution to knowledge in the following ways:

1 The use of the novel dipole aerial for detecting an EK signal that gives enhanced signal sensitivity.

2 The increased of sensitivity of detection allows a more reliable correlation between theoretical models and field data.

3 The study of EK wave shape change makes it feasible to determine porosity *in situ*.

4 The location of the depth to the fully water saturated ground can be reliably detected using the EK technique.

Chapter 1 Review of the Electrokinetic Effect

In a memoir presented to the academy in 1784,
I determined by experiment the laws of force of
torsion of a metallic wire……
I submit today to the Academy an electric balance
constructed on the same principle; it measures very
exactly the state and the electric force of a body
however slightly it is charged ……
…. we go on to give the method which we have used
to determine the fundamental law according to
which the electrical bodies repel each other.

Charles Augustin de Coulomb, Mémoires sur et le magnétisme,
Mem. Acad.Roy. Sc., pp 569 ff (1788)

1.1 General overview of the Electrokinetic Effect

The Electrokinetic (EK) seismic effect, relates the displacement of electrical charge due to an elastic wave causing their physical movement. This has been known for some considerable time. Early references include Reuss (1808), Helmholtz (1879). Later Gouy (1910) and Chapman (1913) who proposed that the electro-kinetic phenomena are due to the existence of a double layer, consisting one layer of ions and another layer of counter ions, which form at the solid-liquid interface of a particulate medium. However, the Gouy–Chapman theory can predict impossibly large ion concentrations next to the surface, because the theory assumes ions are point charges. The Gouy-Chapman theory has subsequently been modified to take into account finite ion size e.g. (Stern, 1924 and Carnie, 1984).

Smoluchowski (1914) was the first to derive an equation to correctly calculate the zeta (ζ) potential. Zeta potential is the electric potential at the shear or slipping plane of a double layer resulting from electro-kinetic mobility. This shear plane is an imaginary surface separating the thin layer of liquid bound to a solid surface showing elastic behaviour, from the rest of liquid showing normal viscous characteristics. Although,

still popular, Smoluchowski assumed the electrostatic force is opposed by the frictional force that occurs at the slippage plane with all other effects ignored.

At present there is a considerable amount of research into the exact nature of the double layer in relation to colloids (McBride and Baveye, 2002). However, very little research has been undertaken with regard to how the double layer forms in various geological media such as sandstone, limestone or clay. Laboratory investigations were conducted by (Jiang *et al.*, 1998) to determine the electro-kinetic coupling coefficients of porous media.

Debye, (1934) described the electro-kinetic effect in colloidal solutions and suggested its potential as an analytical tool. The application of ultrasonic waves to a colloidal or an emulsion generates an electrical response. This technique now known as 'electro-acoustical' method, and is applied in the determination of the electro-kinetic potential at ultrasound frequencies. This has become a traditional tool for the industry/laboratory characterization of colloids and emulsions (Dukhin and Goetz, 2001).

Early research of seismoelectric phenomena in the geological environment observed two electrical effects. Stathem and Blau (1935) in an internal memo of the Humble Oil Company first suggested variation of the earth resistivity with elastic deformation, such as caused by a seismic wave. Thompson (1936) conducted an experiment in which he passed a current into the ground using a storage battery and a pair of metal electrodes. The primary of a transformer was connected in series with one terminal of the storage battery and one of the current electrodes. A variation in the current due the passage of a seismic wave was observed on the secondary of the transformer, where it was passed to an amplifier and recording apparatus. Essentially he described a $\Delta[R]$ change of ground resistance, producing a voltage $\Delta[v] = [R]\times[i]$, where $[R] = R_0 + \Delta r(t)$ with R_0 being the resistance observed with no passing seismic wave and $\Delta r(t)$ being the time varying change in resistance due to the passage of the seismic wave. Thompson called this the seismic electric effect. However, it was only one of the two seismic electric effects as described by Ivanov (1939) who referred to electro-seismic effects of the 'first' and 'second' kind. The seismoelectric effect of the first kind was similar to that described by Thompson. The seismoelectric effect of the second kind or 'E-effect' was reported by Ivanov. He observed an electric response across grounded electrodes corresponding to the passage of a seismic wave front. He did not link these responses to a subsurface

interface. Ivanov (1940) described further work relating to his 1939 paper. However, Martner and Sparks (1959) documented clear seismoelectric responses from the base of a weathered layer. The seismoelectric effect of the second kind resulted from a travelling electric field carried along in a seismic head wave with no external extent and that this was readily detectable using grounded metallic electrodes. This is shown in figure 1.1 a and b:

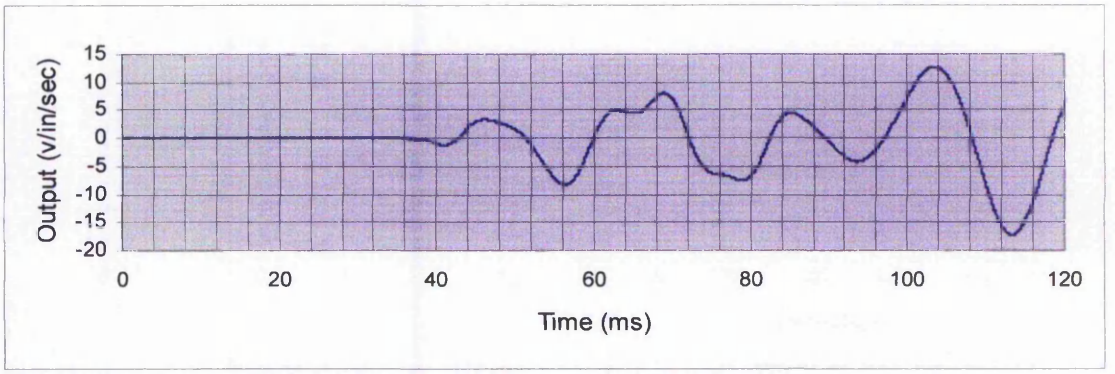

Figure 1.1, (a) Geophone response placed at the mid point of the electrodes.

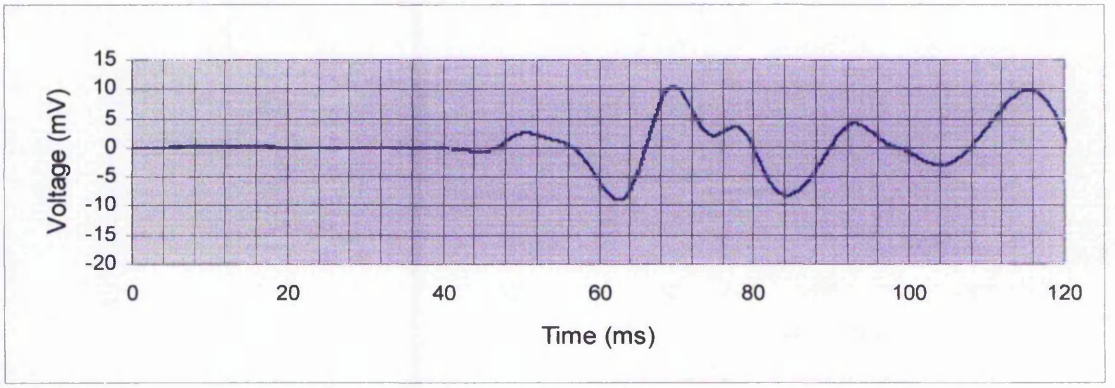

Figure 1.1, (b). Electrode response. Observation will note minor differences in wave shape. The electrode spacing was 1 metre with the geophone at their midpoint.

The papers by Ivanov (1939, 1940) were the first to propose a theory of seismoelectric phenomena and importantly reported field measurements to verify the theory, a not inconsiderable feat for the time. However, important papers followed Biot (1955, 1956, 1957 and 1962) although not proposing EK they laid the down the foundation and basic principles relating to the propagation of elastic waves through porous media. They were to prove important in the further development of EK theory providing a means to which Maxwell's equations could be coupled, so correctly describing the EK effect Pride (1994).

1.2 EK phenomena

All of the work described so far refers to seismoelectric effects of the first and second kind. However, the author feels this does not define a true EK response. *A true EK response I will define as electromagnetic radiation originating from electrical charge displacement due to the passage of a seismic wave through a particle water boundary.* This will be demonstrated through the work presented in this thesis.

The foundation of principles leading to an understanding of the EK effect began with a paper by Frenkel (1944) who related the seismoelectric effect of the second kind, due to a seismic disturbance of the double layer that existed at the soil water boundary. The presence of such layers helped to explain the connection between the flow of water in capillary spaces of the soil and the transfer of electrical charges, which gave rise to the electric field. According to the theory of Helmholtz and Smoluchowski the difference between hydrostatic pressure, Δp, between two points of the soil must be connected with a difference of electrical potential, ΔV.

$$\Delta V = \frac{\varepsilon \zeta \Delta p}{4\pi\mu\sigma} \qquad (1.1)$$

Where ζ is the zeta potential.

μ the viscosity of the water.

σ the electrical conductivity of the water.

ε The electrical permittivity of the water.

One of the more significant papers was by Pride (1994), which gave a very thorough and comprehensive physical and mathematical analysis of the seismo-electric and EK effects. Noubrecht (1995) expanded this work further in his thesis. This was followed by another important paper by Haartsen and Toköz (1996) which dealt with among other issues, the factors affecting ground permeability, such as the electrical conductivity which decreases with increasing ground permeability. Further papers by Hartzen and Pride (1997) and a number of other papers describing field studies of the EK effect; these include Long and rivers (1975), Murty, (1985), Butler and Russell (1993) and Beamish and Peart (1997). All these papers describe the use of grounded electrode dipole pairs as a means of EK detection. As a point of interest borehole

measurements by Parkhomenko and Gaskarov (1971) reported seismoelectric responses in limestone were consistently stronger than those observed in clay.

Currently, EK responses have been recorded using metal dipole pairs with a variety of dipole spacing. The EK response is mainly dependent on the charge separation in the double layer and the energy in the seismic 'P' wave. For example the separation of the electrostatic charges in a double layer for clay where water distributed evenly on the surface, would be in the order of 17–100 Å. This depends on the molar concentration and the grain size, which for clay is typically < 0.002mm. Furthermore, the total charge calculated over a $1m^2$ surface of clay is 0.1 C, very large indeed (Mitchell, 1993). However, the typical grain size for fine sand is in the range 0.06 – 0.20 mm. The water grain interface is thus considerably different from that of clay, even after taking into account the chemical nature of the difference. The effects of cementation between grains would also have to be taken account of where clay could be involved. The differences between the main clay groups and the nature of the grain boundary at the interface are also important. These issues are discussed more fully later in the thesis.

The generation of EK responses should not be confused with piezoelectric phenomena. These are not involved in the generation of EK described in this thesis. The electric field generated is due to a completely different mechanism. Normally the signals generated are much smaller than the corresponding EK responses (Pride 1994).

Piezoelectric phenomena describe the mechanism whereby when mechanical strain is applied to minerals such as quartz (S_iO_2) or to a number of man-made materials such as barium titanate ($BaTiO_3$) it is converted to electrical energy. In this latter material the piezoelectric effect results from mechanical movement caused by application of a voltage. The piezoelectric effect was discovered by Pierre Curie and his brother in the early 1880's.

However, it is possible piezoelectric phenomena may play a part in electromagnetic emissions observed in volcanic disturbances and earthquakes. As a point of interest EK phenomena have been reported to have occurred prior to a volcanic eruption (Adler *et al.*, 1999, Zlotnicki and Morgan, 1990). The signals detected were found to be in the low frequency region, (7-15 Hz) and were of electromagnetic origin. However, the nature of the mechanism generating such signals is not yet fully understood.

Over the course of the EK investigations contained in this thesis it has become clear that although the double layer model has served as the basis for all geophysical aspects of EK investigations, there are a number of questions still unanswered such as the nature of the double layer in different geological profiles and the dependency of the EK response on this.

1.3 Generation of an EK response.

When a seismic 'P' wave propagates through the ground a relative fluid-solid motion is induced that transports the counter ions relative to the fixed charge thus inducing an electrical 'streaming current'. This streaming current is the source for electromagnetic coupling. For compressional waves in a homogenous porous medium, the streaming current leads to a build up of counter charge in the rarefactions (also called dilations of the wave) and depletion in the compressions as shown in figure 1.2. The effect is similar to that of a shunting train when the carriages are seen to bunch and pull apart along its length. In essence a compressional wave can be seen to travel along the carriages.

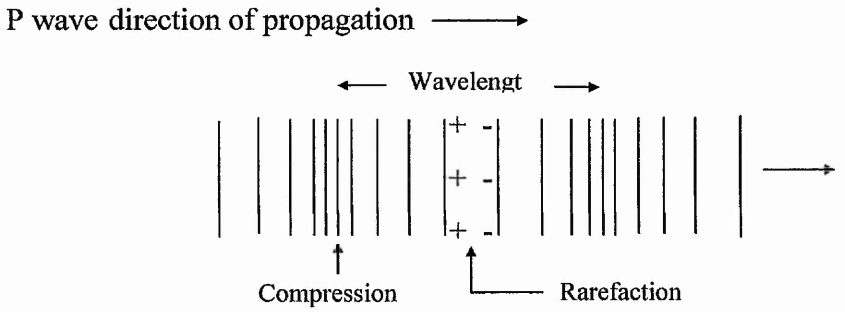

Figure 1.2 Illustration of a compressional wave showing the compressions and rarefactions that occur. A typical hammer plate strike has a dominant frequency of a 100 Hz. For ground with a seismic 'P' wave velocity of 800 m/s the wavelength will be 8 m.

The resultant electric field drives a conduction current that exactly balances the streaming current thereby fixing the amplitude of the charge separation within the wave. This travelling electric field is what gives rise to the response seen in figure 1.1. As there is no net flow of current within the wave, no electromagnetic field is generated.

As a compressional wave propagates through the ground, there is a constant electric field, which is fixed within the seismic head wave. There is no action, i.e., no electromagnetic waves are generated. However, when the compressional wave is

incident at a seismically contrasting boundary, there is a variation in the streaming current charge distribution while the wave is traversing the interface. This leads to a charge separation that varies with the shape of the wave. This time varying charge separation causes a small but detectable current and generates an electromagnetic signal that can be recorded with suitable detectors, such as the new dipole aerial detector see (Chapter 2). The frequency of the electromagnetic wave (EM) wave follows that of the seismic wave, typically 100 Hz.

In recent theoretical and experimental studies into electro-kinetic conversation at seismic frequencies (Pride, 1994) proposed that diffuse slow waves predicted in Biot's (low frequency) theory (Biot, 1956) and acoustic 'P' wave propagation in saturated porous rocks radiated electromagnetic (EM) energy, is generated when the seismic energy crosses a contrasting boundary. The EM generation is due to the large decoupling of the fluid-rock grain electric double layer creating a transitory change in charge distribution, thus giving rise to a current flow in porous and permeable strata, as described by Debye (1933), and Bockris and Reddy (1970). The model for the electric double layer is shown in figure 1.3,

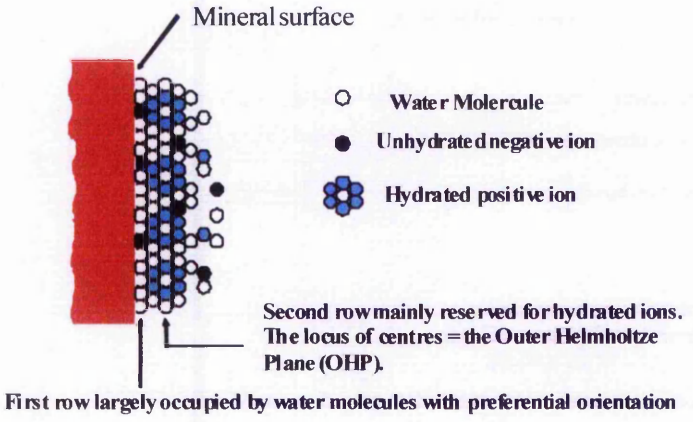

Fig. 1.3. Schematic representation of the electric double layer at a pore wall, (Bockris and Reddy 1970)

The partially fixed part of the electric double layer (EDL) is called the Stern layer and is, in general divided into two layers; one the inner Helmholtz plane (IHP) and the other the Outer Helmholtz plane (OHP). The IHP is populated by partially desolvated ions stuck to a bare solid with specific absorption forces. The OHP is populated by hydrated

ions, which touch a hydrated solid rather than stick to it. The variation in zeta potential, (ζ_P), is shown in figures 1.4 for the negative case and 1.5 the positive case as a function of distance from the solid surface, normally in the order of angstrom units.

$\xi_p < 0$

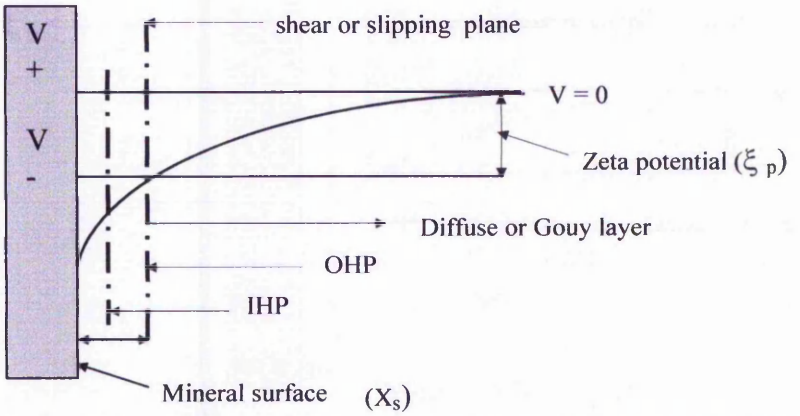

Fig.1.4 Diagrammatic view of the variation in ionic potential as a function of distance from the mineral surface: negative case.

Under certain conditions the Stern layer may contain more counter charge than is required to balance V, so that the diffuse Gouy layer is charged to the same sign as V +, the potential variation is therefore as shown in figure 1.5

$\xi_p > 0$

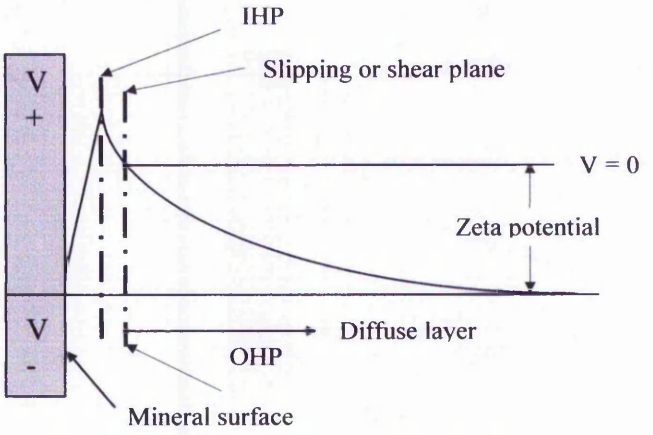

Fig. 1.5 Diagrammatic view of the variation in ionic potential as a function of distance from the mineral surface: positive case.

The relationship between the differential pressure (∇P) and resulting electro-kinetic voltage (∇V) is given by the Helmholtz-Schmouchowski equation (Overbeek, 1952, and Mizutani, 1981).

$$\nabla V = C \cdot \nabla P \qquad (1.2)$$

where C is the streaming potential coefficient.

The Helmholtz-Schmouchowski theory is mainly a large pore theory because it assumes a negative extension of the counter ion layers into the pores. It also fails to account for an excess of ions over those needed to balance the surface charge.

1.4 Detection of an EK response

To date most of the EK fieldwork conducted, as described by Butler *et al.* (1994) and Beamish and Peart (1997) employed various types of grounded electrodes. Also in these studies geophones were placed at the mid point of the dipole pairs giving rise to the possibility of electromagnetic pick up from the small but measurable EM field that is generated when they are excited. In some cases porous pots and lead electrodes have been used, the lead electrodes being used mainly in borehole investigations. This is described in more detail in Chapter 2, together with the effects of seismic attenuation in various geological profiles and the associated attenuation of the electromagnetic wave.

So far little practical development has taken place for specifically detecting and recording the EK effect. There is no robust and reliable equipment available and so investigations continue to be restricted to the use of more established (and better understood) geophysical techniques. The key to the research reported herein is the development of a novel dipole aerial which is insulated and adjustable length for the detection of EK signals. This facilitated identifying the limits of detection of the EK signal in two geological environments, namely sandstone and loess.

A number of points have to be considered when conducting EK investigations. These are listed below, sections 1.4.1 - 1.4.3:

1.4.1 *Effect of the seismic or acoustic wave on the generation of an EK response.*

The largest EK response is observed when the first Fresnel zone of the acoustical or seismic wave intercepts the boundary layer. This is coved in more detail in Chapter 2.

A frequency and range dependent area of a reflector from, which most of the energy of a reflection is returned, and arrival times differ by less than half a period from the first break. These were first named by French physicist Augustin-Jean Fresnel (1788 to 1827). Waves with such arrival times will interfere constructively and so be detected as a single arrival. Subsurface features smaller than the Fresnel zone usually cannot be detected using seismic waves. Figure 1.6 shows the lateral resolution of the Fresnel Zone.

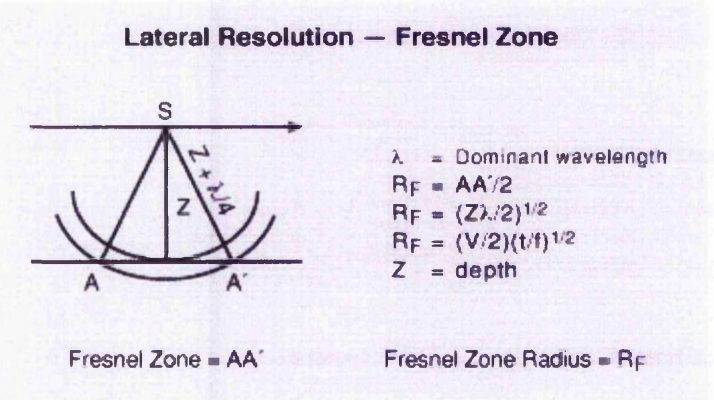

Figure 1.6 Diagram of Fresnel zone resolution

1.4.2 *Seismic wave attenuation*

This is discussed in greater detail in Chapter 2. However, the depths from which EK signal were obtained, i.e. ~ 15 metres or less the seismic wave attenuation was not a problem.

To date little or no work has been done to investigate the amplitude of the EK response of various geological profiles and also relate the wave shape to the nature of the underlying strata. The field and laboratory results gained have been very carefully analysed to determine such relationships. The results of these investigations are discussed in greater detail in Chapter 9, and details of fieldwork data are given in Appendices A, B and H.

1.4.3 *Noise.*

A common source of noise occurs from power lines, which in the UK and most of Europe is of a frequency of 50Hz. Software has been written to remove any 50Hz component and its higher harmonics. Another type of noise is seismic which can be

wind generated or vibrations from nearby plant. Truly random noise can be reduced by a process of stacking which enhances the signal and reduces random noise. This is normally decided when setting up in the field prior to conducting any investigations.

1.5 Justification of research aims and objectives.

The aim was to establish the extent to which the EK responses can be reliably detected at shallow subsurface of less than 50 metres depth.

At the in Mansfield site most of the investigations were carried out close to a specific borehole, which had a depth of 82 metres and a full geological log. The depth of the water table was carefully measured prior to starting any investigations. Fracture zones above and below the water table were clearly evident on the geological log. By noting were EK responses occurred on the seismic recording these could be correlated with depth. More importantly it was expected to have a large EK response at the interface with the water thus aiding the interpretation of other EK responses with features on the geological log. All of the results were obtained using a composite plate and 4.5 kg seismic hammer. Most of the EK results were obtained using an early two metre dipole aerial. However, some results were recorded for the new improved dipole aerial for comparison.

1.5.1 *Objectives.*

1) The field EK experiments were conducted using a purpose designed EK spectrometer, based on a ruggedised laptop computer. This is described in more detail in Chapter 6. The system can also be used to gather conventional seismic data using geophones. A fieldwork operating manual and methodology has also been prepared on the use of the field EK spectrometer (Appendix T). For some of the EK experiments a Geometrics 2400 24 channel seismic recorder was used.

2) Further field experiments were conducted with a loop aerial and dipole aerial to investigate if an EK response could be related to the shear wave. This effect is not predicted for a completely homogeneous media by the currently accepted theory as set down by Pride (1994). However, Garamboise and Dietrich (2001) describe EK responses for traverse *SH*- and *SV*- waves. These results have been compared to conventional geophone responses and the use of metal stake dipole pairs.

3) At present a seismic survey is conducted in addition the dipole aerial investigations. From the results of the seismic survey velocities in the geological layers can be determined. Using theses velocities and the time of arrival of the EK response the depth to the fully water saturated zone can be determined. However, during the course of the EK investigations another method of determining the depth of the fully saturated zone has been suggested which eliminates the need for the seismic survey. This is described in more detail in Chapter 2.

4) Careful analysis of the received EK signal will be undertaken to relate the ratio amplitude of the capillary zone EK response to that of the response at the fully water saturated zone. A Fourier Transform and power spectrum analysis will be applied to both EK responses to analyse their frequency components.

5) Two geological profiles are to be investigated, Sherwood Triassic sandstone and Pleistocene loess. A criteria based on these two studies will be established carefully noting all prevailing conditions.

6) The practical limitations of the dipole aerial will be determined using a composite hammer plate and 4.5 Kg seismic hammer.

1.6. Laboratory studies

Laboratory studies of the EK effect in rock-water systems to determine the electro-kinetic coefficients of porous media have been conducted by Ishido *et al.* (1981). These were based on measurements of the zeta and streaming potentials using an electrochemical cell. A laboratory method of was described by Jiang *et al.* (1998) using a 10mm diameter cylindrical cell which contained a sample. Pressure was applied to one end of the sample via a rod attached to a loudspeaker cone. The frequency of the load speaker was variable over the range 20 to 1000 Hz producing a pressure change ΔP in the order of 1 Pa. The potential was measured via electrodes attached to either end of the sample.

Laboratory experiments were then conducted order to gain a better insight of the exact nature of the generated EK signal when crossing a well-defined contrasting boundary (see Chapter 5). A simple two layer model was used to represent the Sherwood Sandstone Formation. The energy source for each experiment employed a 50 and 150 kHz ultrasonic transducer. An identical transducer and receiver were used to verify the passage of the ultrasonic pulse through the test medium. This also enabled the velocity of the ultrasonic pulse to be calculated. The results are described and discussed in more detail Chapter 5.

1.7 Data analysis.

A number of signal processing techniques have been developed and applied to the EK measurements, details in Chapter 8. These include fast Fourier transforms, digital filtering and a least squares mains noise removal technique as described by Butler and Russell (1993).

Chapter

2

EK DETECTION METHODS

The most beautiful thing we can experience is the mysterious. It is the source of all true art and science

What I Believe. Albert Einstein 1879 - 1955

2.1 Introduction

The description provided in this chapter will mainly relate to surface EK detection methods, although modifications of some of the detection systems described below have been used in borehole EK investigations, see (Hunt and Worthington, 2000). To date all of the reported fieldwork relating to the detection of EK responses has utilised grounded electrode dipole pair metal stake systems (Butler *et al.* 1996).

One of the main problems encountered to date in the detection of EK signals with metal stake dipole pairs, has been their very low amplitude, typically in the order of a few tens of micro-volts. This is barely above the noise level of the received signal and more often or not below it. With most modern seismographs signal stacking can enhance the received signal above normal background noise. However, it does not significantly enhance the signal above mains borne noise. A mains, 50 or 60 Hz, noise reduction technique was described by Butler and Russell (1993). A version of this technique has been employed during the research described in this thesis to reduce mains borne noise down to a very low level. The programme is described in more detail in Chapter 8.

2.2 Existing methods of EK signal detection

It is important to note that with grounded electrodes and other existing methods, the amplitude of the EK signals is in the order of a few tens of micro-volts and this could be after a number of stacks: a process which enhances the signal above the background noise. However, in some cases additional noise removal techniques are required to recover the EK signal as described by Butler and Russell (1993). It is also dependent on the electrode spacing as described by Long and Rivers (1975), who obtained a peak amplitude of 75μV for a 4.5 metre electrode spacing and a response of 160μV at an electrode spacing of 9 metres. For a spacing of 1metre the response would be in the

order of 16μV. Long and Rivers, also reported noise problems. Murty (1985) conducted field experiments reporting EK responses. However, these results were unclear with no supporting evidence.

The more common electrode is a type 316 stainless steel rod typically 12 – 15 mm in diameter and 500 mm in length. It is thought these were used as they are commonly employed in resistivity investigations and are easily available. This type of electrode has a considerable number of disadvantages. These include the effectiveness of their electrical contact with the ground under differing conditions of moisture content, consistency of the depth to which they are inserted in the ground and that they are normally connected to the recording device via flying leads to a conventional geophone take off cable. An additional problem is that movement due to the passing seismic wave would induce a voltage associated with the earth's magnetic field. However, calculations of the possible amplitude of this effect, confirmed it would be in of the order of pico-volts and so was discounted.

All of these possible sources of error give rise to problems with poor contact with the ground, poor contact with the flying leads and cross talk between the twisted pairs within the geophone cable. Other types of electrodes have been used such as lead, these are mainly used in borehole studies and magneto-telluric surveys (Simpson *et al.* 1994) and copper sulphate porous pots (Pattalla, 1997).

Again these detection methods are not without their own problems including electrical, contact noise together with low sensitivity and difficulties in repeating results. The electrode systems described in the above paragraph will in principle detect true EK signals but are not suitable due to their low sensitivity, problems with reproducibility of results and contact noise.

2.3 New and original EK detection system.

A completely new approach has been developed in which a fully insulated adjustable length dipole aerial has been used as the EK detection device. The main advantage of this means of detection is that it has no physical contact with the ground, thus eliminating ground contact problems and can easily be adjusted to increase its length and hence the sensitivity of the dipole. The EK signal detected by the dipole aerial is fed

into a low noise single twisted pair microphone cable with an outer screen thus eliminating the possibility of cross talk. It is particularly important to note that if a signal is detected it must therefore be EK and electromagnetic in origin as there is no physical contact with the ground whatsoever. In the original EK experiments a sponge rubber mat was laid under the dipole aerial to absorb any ground vibrations. However, it was found to be unnecessary as any induced voltage would be in the order of pico-volts.

The other three important criteria for the detection of EK signals are:

(1) There must be no increase in the time of the first arrival of the EK response with the move out associated with that of the seismic signal.

(2) There must be a 180° phase shift of EK responses taken in diametrically opposite lines about the shot plate. However, it is sensitive to the orientation of the EM field, which is normally a vertical dipole; therefore when starting out on an EK investigation tests must be made to confirm the precise orientation of the electric dipole field. This is achieved at the start of a survey by taking EK readings with the dipole aerial at a right angle to the hammer plate then rotating it through steps of 90° and finally with the aerial held vertical noting at each position the peak amplitude of the EK response.

(3) There must be a fall off in EK peak amplitude response with distance.

2.3.4 *Design and constructional details of the electric dipole aerial*

The theory relating to the detection characteristics of an electric dipole aerial is given in section 2.5.1. Originally a fully insulated two-metre dipole aerial was constructed to detect the electric component of the EM field. It was constructed using a two metre 12 mm diameter plastic tube, for support and rigidity, with two one metre lengths of 16/0.2 mm poly vinyl chloride (PVC) covered wire threaded through the middle, brought out at the centre, connected permanently to a screened two way microphone cable and sealed with a silicon rubber compound. The wire was secured at each end of the plastic tube and sealed with silicon rubber compound, see plate 2.1.

The original aerial was still used in some EK surveys for comparison purposes, as although the signal strength was low, it had a better resolution of the detail of the EK

when compared to the new adjustable length dipole aerial. The results obtained at the Mansfield site used both the original 2 metre dipole aerial and the new improved adjustable length dipole aerial. The response of the new aerial was two orders of magnitude larger when compared to the original one.

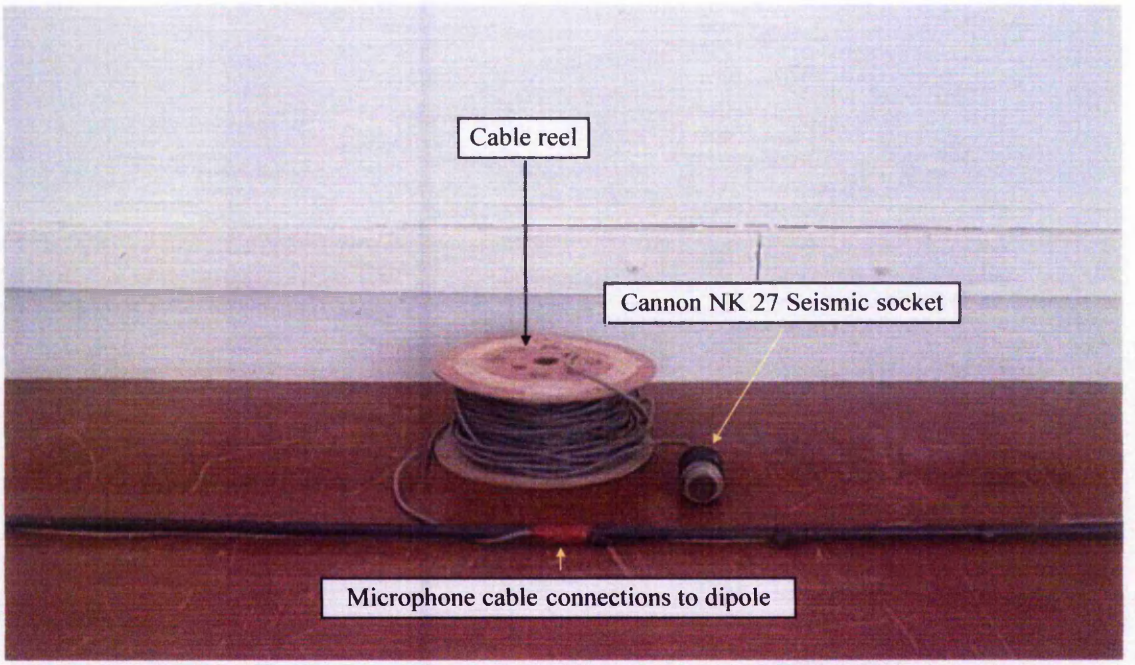

Plate 2.1 Original dipole aerial which was used to obtain most of the Mansfield EK readings. However, the new dipole aerial was used to gather results at the end of the Mansfield EK survey for comparison purposes. (For details see section 2.3.2)

2.3.4.1 *Design of improved dipole aerial system.*

Following fieldwork (see Chapter 4, section 4.5.4) it was decided to design a new EK aerial. This used standard 15 mm, 22 mm, 28 mm and 42 mm diameter copper plumbing pipe. This was to enable experiments to be carried out to determine the effects of the different diameters on the characteristics of the received EK signal.

The dipole aerial sections have all been made in precise one-metre lengths with a brass insert at each end to enable them to be screwed together using stainless steel studding to make any multiple of 1 metre length. These one-metre lengths are joined at the centre with a specially designed adapter to which the signal cable can be plugged into, (see plate.2.2). This has the advantage that the new dipole aerial is easily transportable and can rapidly be assembled in the field.

The one-metre lengths of copper pipe have been covered with yellow heat shrink

sleeving in order to provide electrical insulation from the ground. Therefore it would be proved beyond any doubt that if a signal were received with this device it would be due to the true EK response and not the electro-seismic response where an electric field is propagated within the seismic head wave. The latter is detected with grounded electrodes.

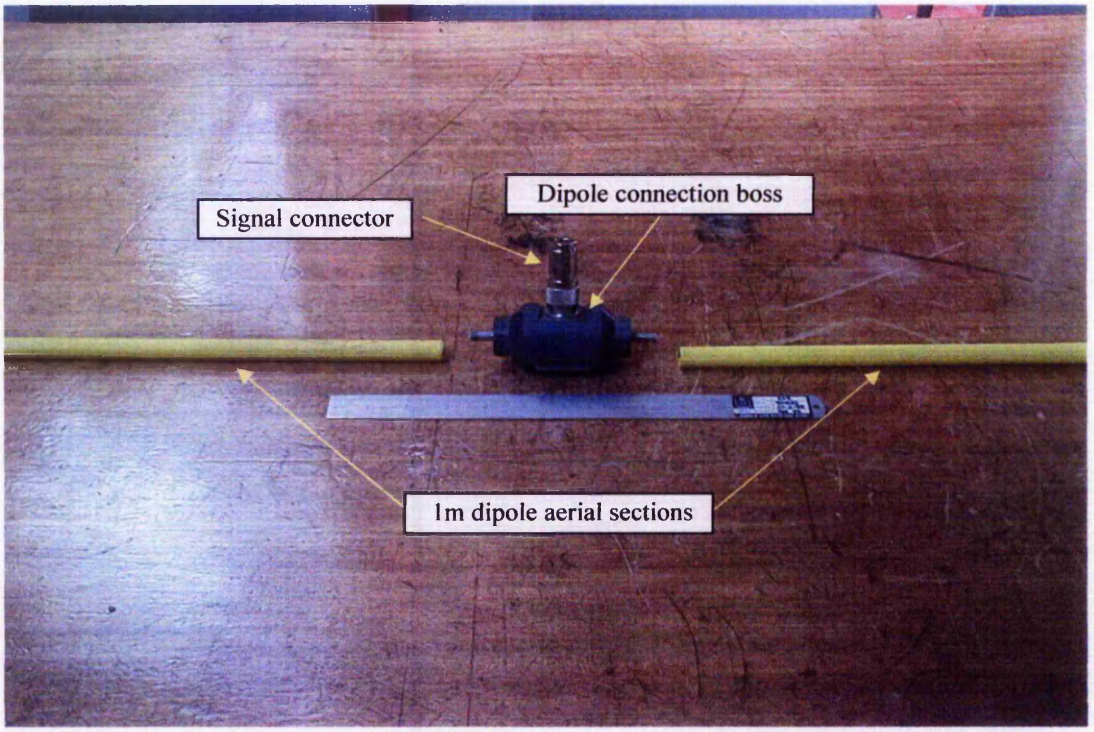

Plate 2.2 New dipole aerial. Note the two dipole aerial sections are shown unscrewed from the central connecting boss, the signal connecter is projecting up from the centre of the boss. A 300 mm steel rule is shown for scale purposes.

2.3.4.2 *Magnetic dipole aerial construction*

The aerial to detect the magnetic component of the EM field was constructed using 7/0.2 mm PVC covered wire. For economy and ease of use the diameter of the coil was set at 2 metres. This gave a total of 80 turns from a 500 metre reel. The loop aerial was constructed by simply winding up the number of turns and then holding the turns together with PVC insulating tape. A demountable wooden frame was designed in order to facilitate the mounting of the aerial and its orientation. This enabled it to be easily stowed for transport and to be quickly laid out in the field. It need not be a perfect circle when laid out, as what is important is the inner area it covers and the magnetic flux passing through it. This is seen by reference to the equations contained in the theory relating to the detection of the magnetic component of an EM wave using a coil aerial, (section 2.5.2)

2.3.4.3 *Seismic source*

The seismic source used for all of the experiments reported in this thesis was a high impact Ultra High Molecular Weight (UHMW) polyethylene plate and seismic hammer. A sledgehammer of weight 4.5 kg normal fitted with an impact sensor for triggering a seismic recorder. It has been shown by Keiswetter *et.al.* (1995), that most of the seismic energy generated by this arrangement is concentrated around 100Hz. This has been verified from a power spectrum analysis performed on the data the details of which are given in Chapter 8.

2.4 Static and time variant electromagnetic fields

To understand the shape of the electric and magnetic dipole fields an analysis of the dipole field distributions for the static and dynamic or varying fields has been undertaken, as there are some important differences between the two. This relates to the field case, i.e. where the point from the dipole is very much greater than the distance separating the dipoles. The point in question is the difference in the relationship of the far field distance $\frac{1}{r^n}$ for the static and time variant dipole field distributions, where n is 2 in the static case and the dynamic case. The main point in the analysis of the dynamic case is the relationship between the near and far dipole fields in relation to the length of the dipole. The analysis for the magnetic dipole is not presented as the main topic of this thesis relates to the electric dipole field. However, the analytical approach is very similar, (see Lorrain and Corson (1970)) for further details.

2.4.1 *Static case: Electric and potential field distribution of a classical electric dipole*

The theory developed in this section and section (2.4.2) is more fully described in (Lorrain and Corson 1970). The electric dipole shown in Figure 2.1 is one type of charge distribution that is frequently encountered. The electric dipole consists of two charges of equal magnitude, one positive and the other negative. They are separated by a distance S, which is small compared to the distance r to the point P at which the electric potential 'V' and electric field intensity 'E' are to be determined

$$\text{At 'P'} \qquad V = \frac{QS}{4\pi\varepsilon_0}\left\{\frac{1}{r_b} - \frac{1}{r_a}\right\} \qquad (2.1)$$

Where ε_0 is the permittivity of free space = $8.85.10^{-12}$ F/m

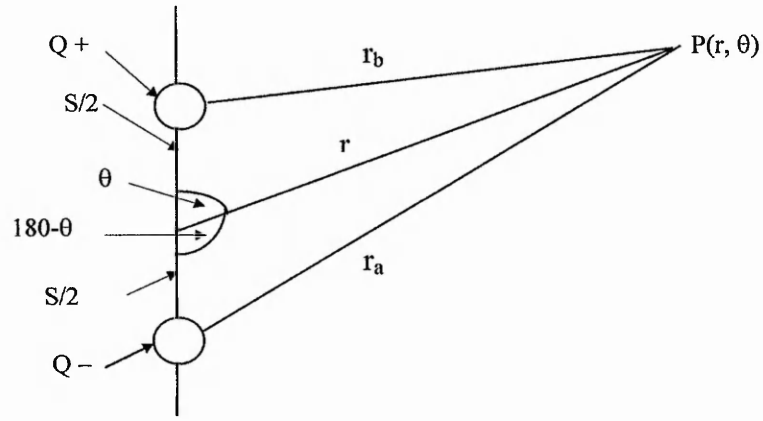

Figure 2.1 The two charges + Q and – Q form a dipole. The electric potential at P is the sum of the potentials due to the individual charges.

By the cosine rule $r_a^2 = (S/2)^2 + r^2 + 2r(S/2)\text{Cos}(180-\theta)$.....(2.2)

Note $\text{Cos}(180-\theta) = -\text{Cos}(\theta)$

Therefore $r_a^2 = (S/2)^2 + r^2 - 2r(S/2)\text{Cos}(\theta)$.....(2.3)

Rearranging $r_a^2 = r^2\{(S/2r)^2 + 1 - (S/r)\text{Cos}(\theta)\}$.....(2.4)

$\therefore$ $r/r_a = \{1 + [(S/2r)^2 - (S/r)\text{Cos}(\theta)]\}^{-0.5}$.....(2.5)

To simplify the following expansion of the term $\{1 - [(S/2r)^2 - (S/r)\text{Cos}(\theta)]\}^{-0..5}$, in

(2.5), the binomial expansion $(1 + a)^n$ will be used where $a = [(S/2r)^2 - (S/2)\text{Cos}(\theta)]$

Note the binomial expansion of $(1 + a)^n$ the following conditions hold.

(i) For n positive and $a > 1$ the binomial expansion is

$$\frac{1^n a^0}{0!} + \frac{n(1^{n(n-1)})a^1}{1!} + (n(n-1)(\frac{1^{n(n-1)(n-2)}a^2}{2!}) + \cdots (n(n-1)(n-2)\cdots\frac{(n-r+1)1^{n-r}a^r}{r!})...(2.6)$$

This is a finite binomial series

(ii) For n negative and or < 1 then a must be < 1 as the binomial series has no limit and is therefore infinite.

For the expansion to follow it must be proved that condition 2 is met.

The term $\{(S/2r)^2 - (S/2r)\text{Cos}(\theta)\}$ must be < unity.

S is the dipole separation and is typically in the order of $50\text{x}10^{-9}$ m, (see Chapter 1 page 2), in the condition being considered r >> S, thus the term S/2r is << 1 and n is also negative i.e. -0.5.

As cos(θ) has maximum values of ± 1 then the term $\{(S/2r)^2 - (S/2r)\text{Cos}(\theta)\}$ is << 1

Expanding the binomial expression for $(1\text{-}0.5)^1$:

$$1 - \frac{0.5.a^1}{1!} - \frac{0.5(-0.5\text{-}1)a^2}{2!} - \frac{0.5(-0.5\text{-}1)(-0.5\text{ -}2).\,a^3}{3!} + \cdots\frac{(n\text{-}r+1)1n\text{-}ra^r}{r!} \quad \text{.....(2.7)}$$

Taking terms up to a^2 as $a^3 \sim 0$, $(1+a)^{-0.5} = 1 - (1/2)a + (3/8)a^2$ .....(2.8)

Substituting in $(1+a)^{-0.5}$ for 'a' we have $a = \{1 + [(S/2r)^2 - (S/r)\text{Cos}(\theta)]\}^{-0.5}$ .....(2.9)

Expanding 5 using the binomial theorem:

$$1 - \frac{1}{2}\left[\left(\frac{S}{2r}\right)^2 - \frac{S\text{Cos}(\theta)}{r}\right] + \frac{3}{8}\left[\left(\frac{S}{2r}\right)^2 - \frac{S\text{Cos}(\theta)}{r}\right]^2 \quad \text{.....} \quad (2.10)$$

Expanding the last term

$$\frac{r}{r_a} = \{1 - \left(\frac{1}{2}\right)\left(\frac{S}{2r}\right)^2 + \left(\frac{S\text{Cos}(\theta)}{2r}\right) + \frac{3}{8}\left[\left(\frac{S}{2r}\right)^4 - 2\left(\frac{S}{r}\right)^2\left(\frac{S\text{Cos}(\theta)}{r}\right) + \left(\frac{S}{r}\right)^2 \text{Cos}^2(\theta)\right]\} \quad 2.11$$

Neglecting powers higher than $(S/2r)^2$

$$\frac{r}{r_a} = \{1 - \left(\frac{1}{2}\right)\left(\frac{S}{2r}\right)^2 + \left(\frac{S\text{Cos}(\theta)}{2r}\right) + \frac{3}{8}\left[\left(\frac{S}{r}\right)^2 \text{Cos}^2(\theta)\right] \quad \text{.....(2.12)}$$

Similarly $$\frac{r}{r_b} = \{1 - \left(\frac{1}{2}\right)\left(\frac{S}{2r}\right)^2 - \left(\frac{S\text{Cos}(\theta)}{2r}\right) + \frac{3}{8}\left[\left(\frac{S}{r}\right)^2 \text{Cos}^2(\theta)\right]\} \quad \text{.....(2.13)}$$

Note $$\{\frac{r}{r_b} - \frac{r}{r_a}\} = \frac{1}{r} \times \frac{S\,\text{Cos}(\theta)}{r} = -(S/r^2)\text{Cos}(\theta) \quad \text{..... (2.14)}$$

Substituting in (1) for $1/r_b - 1/r_a$ we have $V = QS\text{Cos}(\theta)/4\pi\varepsilon_0 r^2$ .....(2.15)

Note the potential falls off as $1/r^2$.

QS is defined as the dipole moment, symbol p. This is actually a vector $\mathbf{p} = Q\mathbf{S}$ where **S** is defined as pointing from – Q to + Q.

Equation (15) can be written as $V = p\text{Cos}(\theta)/4\pi\varepsilon_0 r^2$

or as $p \bullet \check{\mathbf{r}} = p\cos(\theta)$ where $\check{\mathbf{r}}$ is the unit vector along r.

$\therefore V = p \bullet \check{\mathbf{r}}/4\pi\varepsilon_0 r^2$ ..... .(2.16)

To find **E,** use $\mathbf{E} = -\nabla V$. However, for convenience the cylindrical form of ∇ is used.

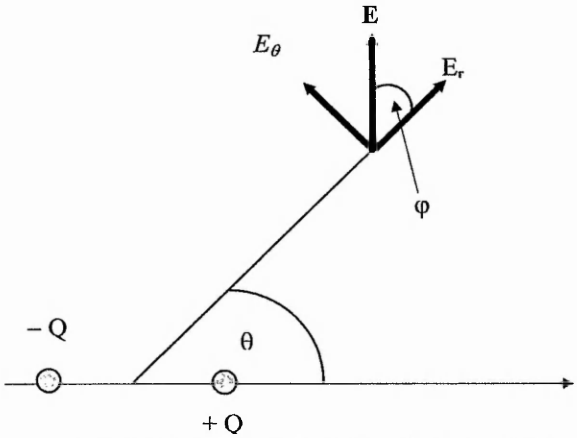

Figure 2.2 Model for the electric field at a distance r >> S

With reference to figure 2.2 the following equations are deduced:

$$E_r = \partial V/\partial r = \frac{2p\cos(\theta)}{4\pi\varepsilon_0 r^3} \quad \text{.....} \quad (2.17)$$

$$E_\theta = 1/r.\partial V/\partial\theta = \frac{p\sin(\theta)}{4\pi\varepsilon_0 r^3} \quad \text{.....(2.18)}$$

The total E-field has magnitude given by

$$E = (E_r^2 + E_\theta^2)^{0.5} = \frac{p(4\cos^2\theta + \sin^2\theta)^{0..5}}{4\pi\varepsilon_0 r^3} = \frac{p(1 + 3\cos^2\theta)^{0..5}}{4\pi\varepsilon_0 r^3} \quad \text{..... (2.19)}$$

The angle φ with respect to r is given by $\tan(\varphi) = E_\theta/E_r = 0.5\tan\theta$ ..... (2.20)

Figure 2.3 shows the electric field lines emanating from the positive charge Q + to the negative charge Q -. Equipotential lines are shown surrounding each charge. Note figure 2.3 represents what is defined as the near field diagram. Also there is inserted a hypothetical surface representing the ground. It is easy to see how the equipotential lines and electric field lines vary on the surface away from immediately above the two charges.

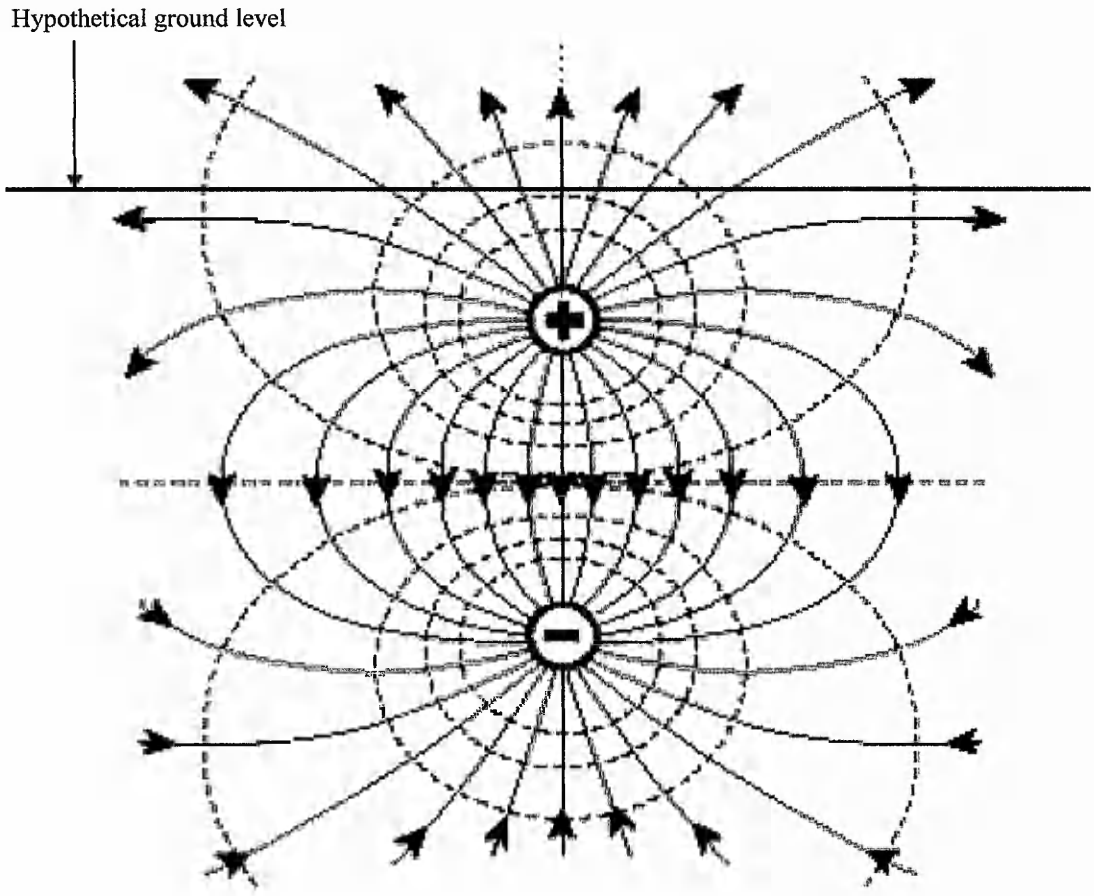

Figure 2.3 Electric field distribution with equipotential lines shown. The separation two charges are shown much larger than they would be in practice for the sake of clarity.

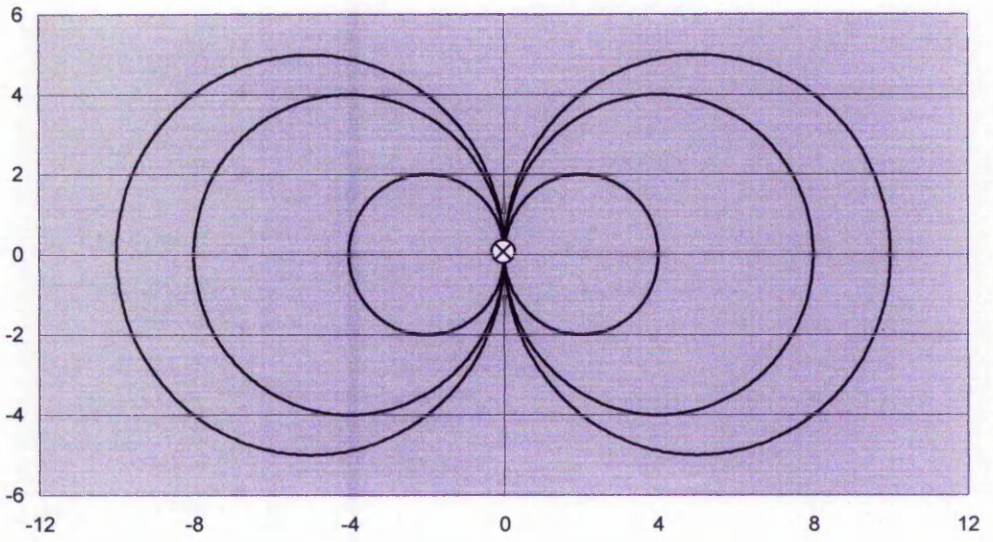

Figure 2.4. Plan view of figure 2.3 showing the dipole electric field distribution.

(2.4.2) Dynamic case: *Electric and potential field distribution of a classical electric dipole*

Consider the electric dipole given in figure 2.5

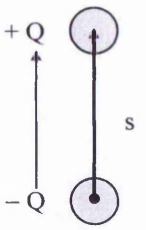

Figure 2.5. An electric dipole. The total charge is zero and the vector s is directed from – Q to + Q

In the oscillating electric dipole

$$Q = Q_0 e^{j\omega t} \quad \text{.....(2.21)}$$

$$\mathbf{p} = Q_S = Q_0 s e j^{\omega t} = \mathbf{p}_0 e^{j\omega t} \quad \text{.....(2.22)}$$

$$p_0 = Q_{0s} \quad \text{.....(2.23)}$$

Where 'Q' is the time varying charge and '**p**' the time varying dipole moment.

If say a current flows in a thin wire connecting the two charges and an alternating current

As $\frac{dQ}{dt} = I = j\omega t\, Q_0 e^{j\omega t}$ .....(2.24)

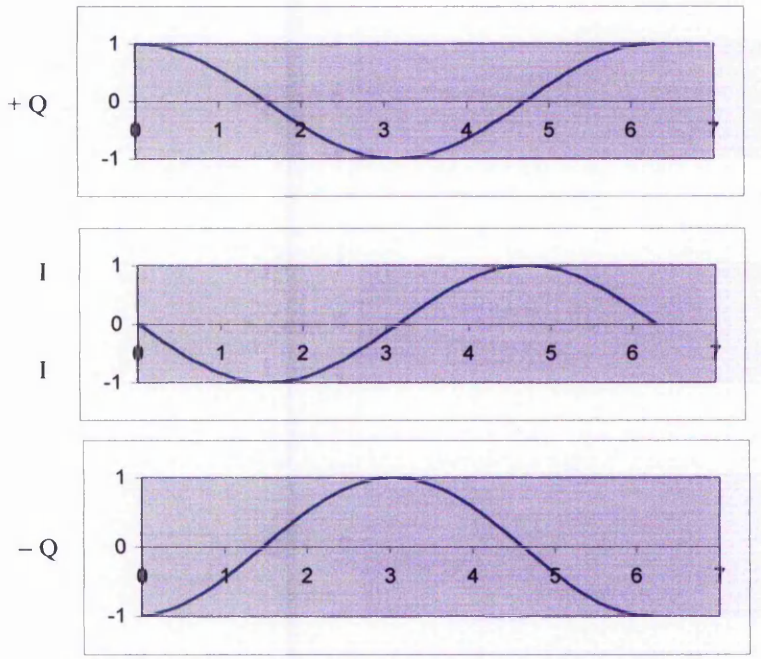

Figure 2.6 The charge + Q, the current I and the charge + Q are functions of time of the oscillating dipole

It will be shown that the scalar potential **V** can be expressed as

$$\mathbf{V} = \{p_0 / 4\pi\, \varepsilon_0\, r\, \hat{\lambda}\}\, \exp(j\omega[t - r/c]\left(\frac{\hat{\lambda}}{r} + j\right)\mathrm{Cos}\,(\theta) \quad \text{.....(2.25)}$$

Where r and θ are as in figure 2.7

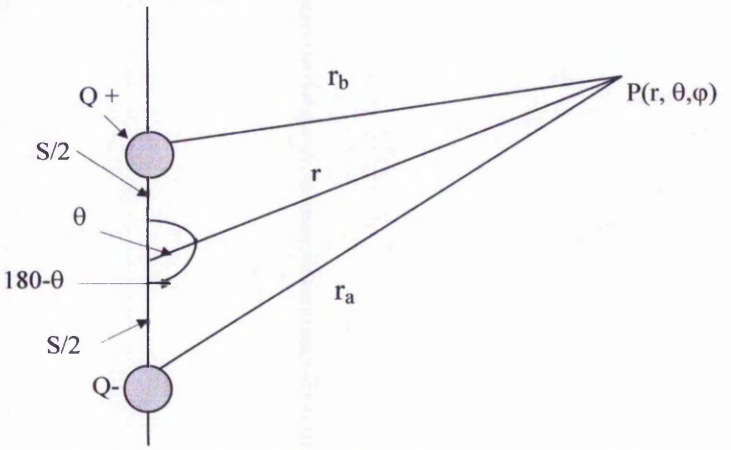

Fig. 2.7 Oscillating electric dipole and point P where the scalar potential is V.

$$V = \frac{Q_0 \exp j\omega(t - r_b/c)}{4\pi\varepsilon_0 r_b} - \frac{Q_0 \exp j\omega(t - r_a/c)}{4\pi\varepsilon_0 r_a} \quad \text{.....(2.26)}$$

Where the numerators are charges, as they appear at the point P(r, θ,φ) of figure 2.7 at time t.

Note the charges –Q and + Q give scalar potentials which differ not only in amplitude but also in phase. The amplitudes differ because of the terms r_a and r_b in the denominators, and the phases differ because of the $\frac{r_a}{c}$ and $\frac{r_b}{c}$ terms in the exponentials.

A more convenient expression can be derived for equation (26)

$$r_a \sim r + [s/2]\,\mathrm{Cos}(\theta) \quad \text{.....(2.27)}$$

$$r_b \sim r - [s/2]\,\mathrm{Cos}(\theta) \quad \text{.....(2.28)}$$

then $$\omega(t - r_b/c) \sim \omega(t - r/c + \{s\,\mathrm{Cos}(\theta)\}/2c) \quad \text{.....(2.29)}$$

$$\omega(t - r/c) \sim \omega(t - r/c) + \{s/2\lambda\!\!\!^{-}\}\mathrm{Cos}(\theta)\} \quad \text{.....(2.30)}$$

NB. In eq'n (29) the term $\{\omega s\,\mathrm{Cos}(\theta)\}/2c = \{S\,\mathrm{Cos}(\theta)\}/2\lambda\!\!\!^{-}$ as $\omega / c = 1/\lambda\!\!\!^{-}$

Where $\lambda\!\!\!^{-} = \frac{\lambda}{2\pi}$ is the radian wave length.

Now $$V \sim \frac{Q_0 \exp j\omega (t - r_b/c)}{(4\pi\varepsilon_0 r)} \{\exp(j\,[S/2\lambda\!\!\!^{-}]\mathrm{Cos}(\theta)) - \exp(-j\,[S/2\lambda\!\!\!^{-}]\mathrm{Cos}(\theta))\} \quad \text{.....(2.31)}$$
$$\{1 - [S/2r]\,\mathrm{Cos}(\theta) \qquad 1 + [S/2r]\,\mathrm{Cos}(\theta)\}$$

Expanding the two exponential function within the braces as a power series neglecting terms of third order or higher.

Noting that $$e^x = \frac{x^0}{0!} + \frac{x^1}{1!} + \frac{x^2}{2!} + \ldots\ldots\ldots + \frac{x^n}{n!} \quad \text{.....(2.32)}$$

$$\exp(j\,[s/2\lambda]\mathrm{Cos}(\theta)) = 1 + \frac{js\mathrm{Cos}(\theta)}{2\lambda} + \frac{(js\mathrm{Cos}(\theta))^2}{2 \times 4x\,\lambda^2} + \text{--} + \frac{(js\mathrm{Cos}(\theta))^n}{n!\lambda^n} \quad \text{.....(2.33)}$$

$$\exp(-j\,[s/2\lambda]\mathrm{Cos}(\theta)) = 1 - \frac{js\mathrm{Cos}(\theta)}{2\lambda} + \frac{(js\mathrm{Cos}(\theta))^2}{2 \times 4x\,\lambda^2} + (-1)^n\frac{(jscos(\theta))^n}{n!\lambda^n} \quad \text{.....(2.34)}$$

$\therefore$ $$\frac{\{\exp(j\,[s/2\lambda\mathrm{Cos}(\theta)) - \exp(-j\,[s/2\lambda]\mathrm{Cos}(\theta))\}}{\{1 - [s/2r]\,\mathrm{Cos}(\theta) \qquad 1 + [s/2r]\,\mathrm{Cos}(\theta)\}} \quad \text{.....(2.35)}$$

Taking the term in braces and replacing the exponential terms by the two powers series we have for equation 35 the expression below (36):

$$\frac{\left[1+\left(\frac{j\cos(\theta)}{2\lambda}\right)+\left(\frac{j\cos(\theta)^2}{8\lambda^2}\right)\right]\left[1+\left(\frac{s}{2r}\right)\cos(\theta)\right]-\left[1-\frac{j\cos(\theta)}{2\lambda}+\left(\frac{j\cos(\theta)^2}{8\lambda^2}\right)\right]\left[1-\left(\frac{s}{2r}\right)\cos(\theta)\right]}{1^2+\left[\frac{s\cos(\theta)}{2r}\right]} \quad \text{.....(2.36)}$$

Multiplying out and rationalising terms:

$$\left(\frac{js\cos(\theta)}{\lambda}\right)+\left(\frac{s\cos(\theta)}{r}\right) = s\cos(\theta)\left[\frac{j}{\lambda}+\frac{1}{r}\right] = \lambda\, s\cos(\theta)\left[j+\frac{1}{r\lambda}\right] \quad \text{.....(2.37)}$$

Substituting this expression back in to (31) we have:

$$V \sim \frac{Q_0 \exp j\omega\left(t-\frac{r}{c}\right)}{4\pi\varepsilon_0 r}\{\underline{s\cos(\theta)}\left[j+\frac{1}{r\lambda}\right] \quad \text{.....(2.38)}$$

as $p_0 = Q_0 s$ from eq'n (23)

$$V = \_p_0 \frac{Q_0 \exp j\omega\left(t-\frac{r}{c}\right)}{4\pi\varepsilon_0 r\lambda}\cos(\theta)\left[j\lambda+\frac{1}{r}\right] \quad \text{.....(2.39)}$$

It has been assumed that the length of the dipole s to be very much smaller than r and λ
$\therefore$ $s << r$ and $s << \lambda$ and where r and θ are as in figure 2.8

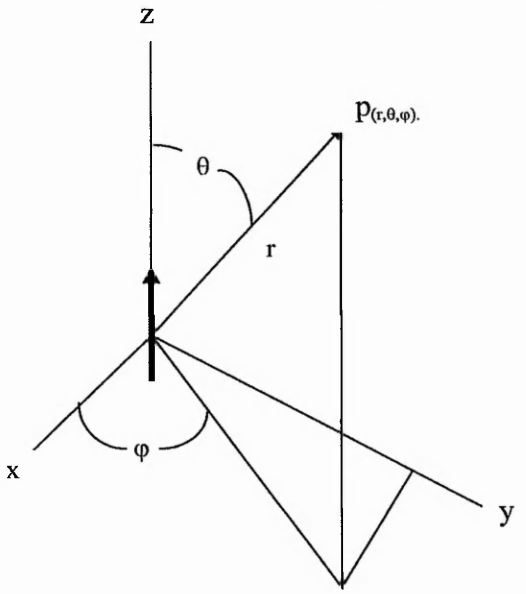

Figure 2.8 An oscillating electric dipole situated at the origin gives rise to a scalar potential V at the point P(r,θ,φ).

For a non zero frequency, the exponential term appears to show that 'V' propagates as a wave at phase velocity 'c'. This however, is not quiet correct, because of the complex factor ($\lambda\!\!\!^{-}$ /r + j). Rewriting the complex factor in exponential form,

$$V = [p_0/4\pi\varepsilon_0 r\,\lambda\!\!\!^{-}\,](\lambda\!\!\!^{-}\,^2/r^2 + 1)^{0.5} \exp\{j\omega(t - r/c - [1/\omega] \arctan(r/\lambda\!\!\!^{-}\,)\}\mathrm{Cos}\,(\theta) \quad \ldots\ldots (2.40)$$

For $r >> \lambda\!\!\!^{-}$, arctan $(r/\lambda\!\!\!^{-}) \sim \pi/2$ and is almost independent of r. The phase velocity is then c. However, close to the dipole, where r is not much larger than $\lambda\!\!\!^{-}$, arctan $(r/\lambda\!\!\!^{-})$ is not constant. The effect of this term is to give a phase velocity larger than c.

The scalar potential V varies as Cos (θ) and is zero in the equatorial plane, see figure 2.8, where the fields of the two charges cancel exactly, just as in the static case. The scalar potential varies as $1/r^2$ as in the electrostatic case, but only as 1/r when $r >> \lambda\!\!\!^{-}$ in the electrodynamic case. However, when $V >> r$ it varies as $1/r^2$.

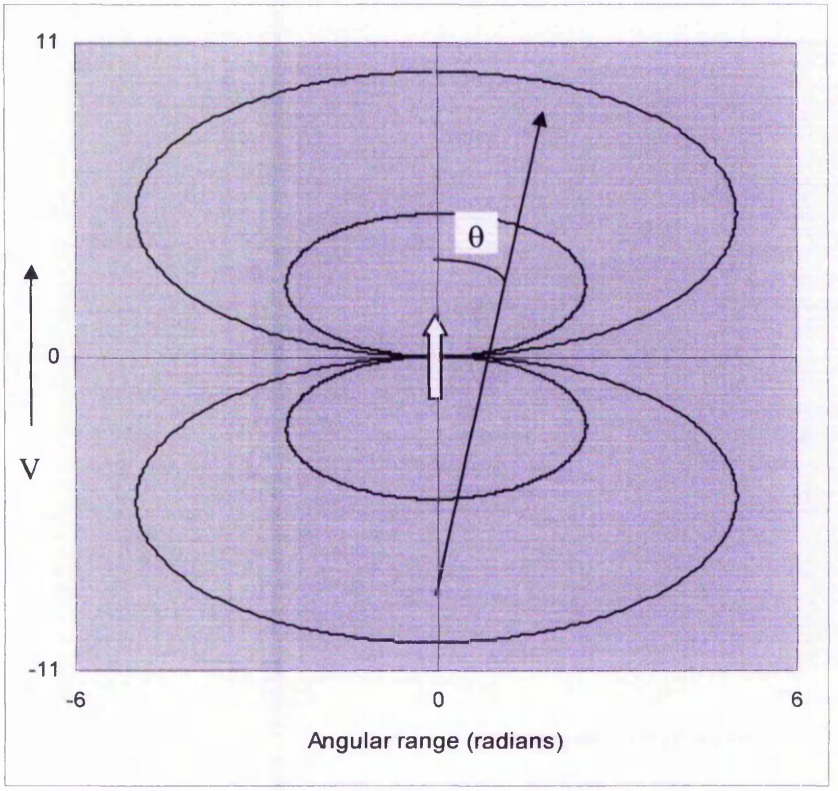

Figure 2.9 Vertical dipole field distribution for equation (38). The dipole is shown by the block arrow

In figure 2.9 two contour lines are shown for the scalar potential 'V', the outer contour being the maximum value of 'V'.

The contour lines will vary in proportion to the exp(jωt) term from zero to a maximum according to the frequency, f.

Lastly as an example, for this section a value for the scalar potential 'V' will be calculated using equation (39). First assume the value of 0.1 coulomb/m^2 as given on page 2 of Chapter 1 for the soil-water interface. Now consider the term $p_0 /4\pi\varepsilon_0 r \lambda$, the radian wavelength λ is given by c/2πf, where f = 100 Hz, and in this case is equal to $4.78x10^5$ m, also assume Cos(φ) = 1.The area of the wave front crossing the water table is found by considering figure 2.10 which assumes a 40 degree cone of spherical radiation.

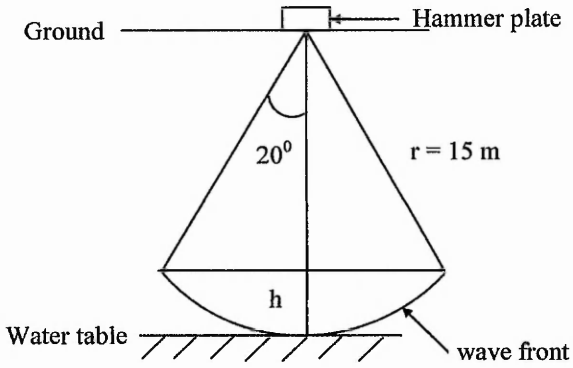

Figure 2.10 Diagram of seismic wave front propagation.

$15Cos(20^0) = 14.10$ m, $h = 15 - 15Cos(20^0) = 15 - 14.10 = 0.90$ m

Area of conical surface = $2\pi rh = 2\pi x15x.0.9 = 84.8\ m^2$

$$\therefore \quad v = \frac{p_0}{4\pi\varepsilon_0 r\lambda} = \frac{p_0 \times 1.88\times 10^5}{r} \qquad \text{.....(2.41)}$$

Now consider the term $\sqrt{\frac{\lambda^2}{r^2}+1}$ and assuming a value of 1 metre for r

$$\sqrt{\frac{\lambda^2}{r^2}+1} \approx 4.78x10^5 \qquad \text{.....(2.42)}$$

$$\therefore \quad \frac{p_0}{4\pi\varepsilon_0 r\lambda\!\!\!^{-}} \cdot \sqrt{\frac{\lambda\!\!\!^{-2}}{r^2}+1} = p_0 \times 9.1\times10^{9} \quad \text{..... (2.43)}$$

$p_0 = Q_0 S$ where for example $Q_0 = 0.1$ Cm^2 and $S = 50\times10^{-9}$ m

$$\therefore \quad \frac{p_0}{4\pi\varepsilon_0 r\lambda\!\!\!^{-}} \sqrt{\frac{\lambda\!\!\!^{-2}}{r^2}+1} = 0.1\times 84.8 \times 50 \times10^{-9} \times 9.1 \times 10^{9} = 3858 \text{ volts} \quad \text{..... (2.44)}$$

for r = 10 m the value for V now becomes 38.58 V ..... (2.45)

for r = 15 m the value for V now becomes 17.14 V..... (2.46)

The calculations for the dipole scalar voltage 'V' have not taken into account the term $\exp\{j\omega\,(t - \frac{r}{c} - [\frac{1}{\omega}]\arctan(\frac{r}{\lambda\!\!\!^{-}})\}$, which only affects the frequency variation of the exciting source.

At a 100 Hz the wavelength of the EM wave is 3×10^6 m. The ratio of the two metre dipole aerial to 3×10^6 m is 1.5×10^6:1. Therefore the voltage found in equation (2.46) can be scaled down to give $\frac{17.14}{1.5\times10^6} = 11.43\times10^{-6}$ volts. The value of the voltage calculated for the 15 m depth is reasonably close to the peak value of 13.0μv obtained for the Mansfield site investigations for the 2 metre dipole aerial after correcting for the dipole aerial length in relation to the wavelength of the EM radiation.

These theoretical results clearly show the means by which data can be gleaned from the EK response and can be used to estimate the charge held on a double layer.

2.5 Detection of the electric field and magnetic field components of a time variant electromagnetic wave.

Two means of detecting the two components of an EM wave are described in sections 2.5.1 and 2.5.2. First, the case of a simple dipole aerial as a means of detecting the electric field component of a radiating electromagnetic wave, will be examined.

2.5.1 *Detection of the electric field component of an EM wave*

The induced voltage 'v' on a dipole aerial is given by

$$v = El \text{ Volts} \quad \ldots\ldots (2.47)$$

where E is the electric field and '*l*' the dipole length as shown in figure 2.11:

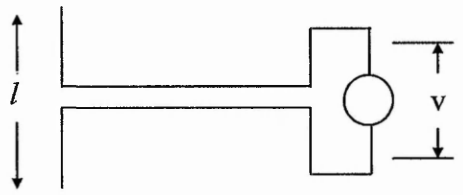

Figure 2.11 Schematic view of a simple dipole aerial of length 'l'. The circle represents a load across which appears a voltage as a result of the induced signal in the dipole aerial of length *'l'*

From experiments conducted at Mansfield, it was estimated that the peak electric field strength was in the order of 6.5 μv/m. The peak voltage induced in a 2 metre copper dipole aerial at 1 metre from the seismic source was 13.0μv. This was based on a single stack response of the raw data. Only the first 30 milliseconds of data are shown as this represents the time window of interest. (See Figure 2.12).

It was discovered when using a 6-metre dipole comprising two 3 metre lengths of standard 15 mm copper pipe that a much enhanced response was obtained, (See Figure 2.13). It appears that due to the increased sensitivity the fine detail is lost. This is not altogether surprising as in spectroscopy it is well known that for an increase in resolution the amplitude of the observed data decreases and vice-versa.

Note the EK responses in figures 2.12 to 2.14 are raw data and no noise removal techniques or filtering have been applied with the aerial at right angles to the source. Using this new result the electric field was calculated to be 267μv/m, an increase of more than two orders of magnitude. It is also of interest to note in both the graphs, that the first arrival occurs at 19 milliseconds, taking into account the 10ms delay seen as the blank portion at the start of the record.

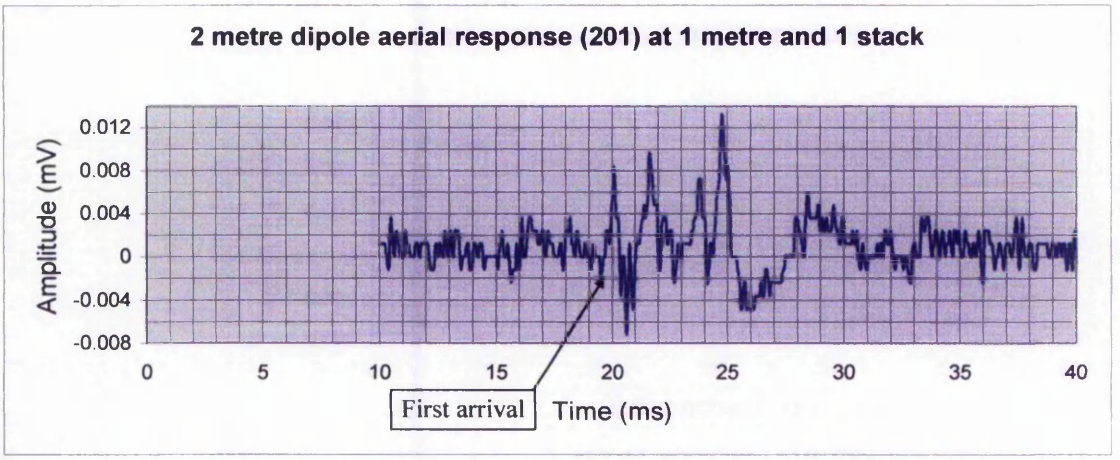

Figure 2.12. Recording of 2 metre dipole aerial response 1 metre from the shot point. Note the peak voltage at 25 ms has a maximum value of 12 μ-volt. The response at 18 ms was due to the measured water table at 15 metres depth. The blank part of the trace is due a 10ms delay set in the seismograph.

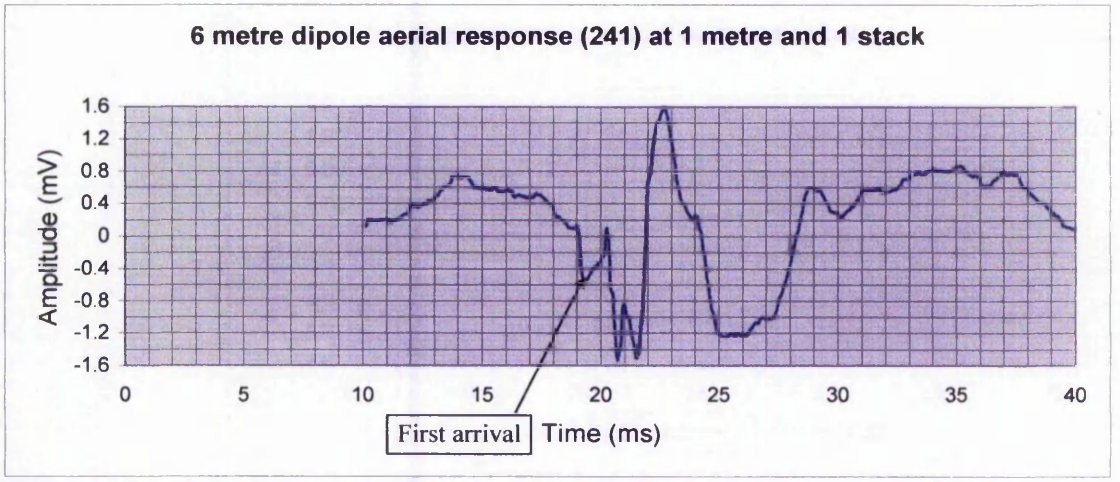

Figure 2.13 recording of 6 metre dipole aerial response 1 metres from the shot point. Note the increase in magnitude of the peak responses at 20 & 25 ms compared to figure 2.12.

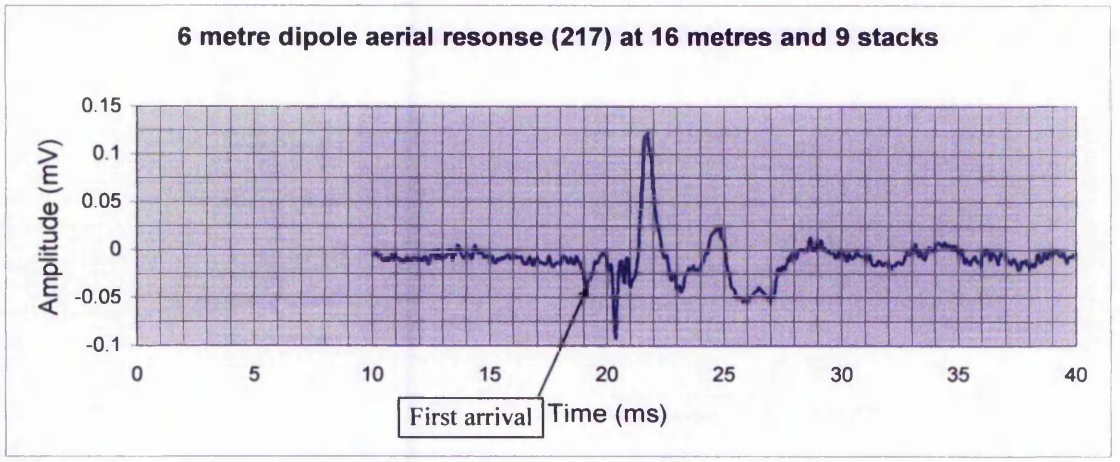

Figure 2.14 recording of 6 metre dipole aerial response 16 metres from the shot point. Note there is no move out of the EK response. Note also decrease in amplitude response compared to figure 2.14

2.5.2 *Magnetic dipole coil aerial*

For the magnetic dipole aerial, the induced electromotive force is

$$\int E \bullet .dl = -\int_c (\partial A/\partial t + \nabla v) \bullet dl = \int_s (\nabla \times \partial A/\partial t + \nabla \times \nabla v) \bullet da \quad \text{..... (2.48)}$$

where s is any surface bounded by the circuit. The second term on the right vanishes, since the gradient is identically equal to zero. Also, the order of the operations in the first term can be interchanged to give

$$\int E \bullet .dl = -\partial/\partial t \int_s \nabla \times A \bullet da = -\partial (\int_s B \bullet da)/\partial t \quad \text{..... (2.49)}$$

The induced electromotive force in the loop is therefore equal to the rate of change of the flux linking the loop. It is a maximum when the normal to the loop is parallel to the local field B.

A wound coil has also been constructed to complement the dipole aerial described above. This has been necessary in order to make simultaneous measurements of both the electric and magnetic components of the EK generated EM field. Pride (1996) stated that there is no magnetic component associated with the EK signal generated by a 'P' wave. However, it is essential to have a magnetic component detector in order to verify the correctness of the Pride assertion. Also quoted in the same paper was that no EK response was associated with the shear wave. Previous EK investigations conducted in 1997 and 1998 showed an electromagnetic response when using a coil of 500 turns of 28 standard wire gauge (swg) enamelled copper wire with a diameter of 0.5 metre, this was thought to be due to the shear wave or possibly a surface wave. Similar responses were obtained when a coil aerial designed for borehole studies was used for a selection of surface investigations. A schematic view of the magnetic field detection aerial is given in figure 2.15

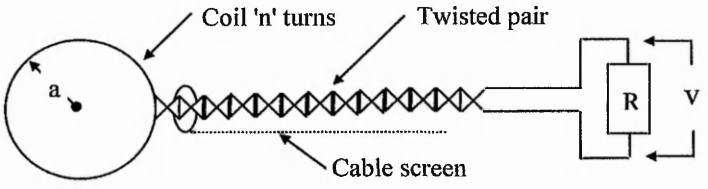

Figure. 2.15 Schematic view of the magnetic dipole aerial.

The design of the coil has taken into account that the main energy of the seismic hammer source has most of its energy centred around 100 Hz. In practice it would be a simple matter to tune the coil to a different frequency band if required by placing a capacitor of the appropriate value across the coil.

Another factor to be taken into account was the range of wavelengths most likely to be encountered. Taking the range of seismic velocities to be 300 to 6000 m/s the range of wavelengths would be 300/100 = λ =3 to 6000/100 = λ = 60 metres. The aerials used a $\frac{1}{4\lambda}$ design, i.e. 0.75 to 15m.

2.6 Electric dipole field distribution as a means of depth determination to the fully water saturated zone

The electric dipoles shown in Figures 2.5 and 2.10 are a type of charge distribution that is frequently encountered in the study of electrostatics and in this case in the EK investigations conducted at Mansfield and Ospringe. In particular the dipole electric field distribution due to a double layer.

However, figure 2.10 is of main interest as it represents the case for the time variant EM field. By measuring the reduction in amplitude of the EK response at measured points away from the point of impact to the point where the amplitude again increases it is possible to make an estimate of the depth at which the dipole is situated. Field experiments were undertaken to examine this. Therefore the need to carry out a seismic survey in order to determine the velocity depth profile is therefore eliminated.

2.7 Attenuation loss of a material.

An important factor to be taken into account in the detection of EK responses is the attenuation of both seismic and electromagnetic waves occur in traversing various geological media. A brief description of these is provided in sections 2.7.1 and 2.7.2

2.7.1 *Attenuation loss of an electromagnetic wave*

The attenuation loss is of considerable importance in the use of ground penetrating radar, which uses frequencies in the range 200 MHz to 2 GHz. Comparative

attenuations losses are shown in table 2.1. The important data for EK investigations are shown in column 2 of table2.1, i.e. loss at 100 Hz.

Table 2.1 Attenuation loss of various materials for different frequencies

Material	Loss at 100Hz	Loss at 100MHz	Loss at 1 GHz
	dB/m x 10^{-6}	dB/m	dB/m
Clay (moist)	5-300	5-300	50-3000
Loamy soil (moist)	1-60	1-60	10-600
Sand (dry)	0.01-2	0.01-2	0.1-20
Ice	0.1-5	0.1-5	1-50
Fresh water	0.1	0.1	1
Sea water	1000	1000	10,000
Concrete (dry)	.5-2.5	0.5-2.5	5-25
Brick	.3-2.0	0.3-2.0	3-20

The losses are quoted in db/m where db is defined as:

$$db = 20.\log\frac{V_1}{V_2} \qquad (2.50)$$

where V_1 and V_2 are the signal voltage before and after attenuation. For this expression to hold true the source and output impedances for V_1 and V_2 must be the same. For reference See table 2.2 shows gains in db in for a range of gains in standard format.

Table 2.2 List of gains for Vout/Vin in terms of dB

Gain Vout/Vin	Gain dB	Gain Vout/Vin	Gain dB
1	0	1,000	60
3.1623	10	3162.28	70
10	20	10,000	80
31.62	30	31622.8	90
100	40	100,000	100
316.22	50	316228	110

However, it is still important to know attenuation the loss at 100 Hz for various geological profiles. The extrapolated values for the attenuation loss at 100 Hz are shown in table 2.3. These are all seen be very close to zero for practical purposes.

However for the laboratory experiments where two ultrasonic transducers with resonant frequencies of 150 KHz and 50 KHz were used, the losses for some materials start to become noticeable, *e.g.* clay at 100KHz could be 0.1dB/m

2.7.2 *Attenuation and relative electrical permittivity*

The effects of both seismic attenuation and moisture content on the electrical relative permittivity for various soil and rock types need to be considered in order to determine their effect on the generation of an EK response. A selection of materials given in table 2.3, which compares their effect on the signal attenuation and relative electrical permittivity.

Table 2.3. Attenuation and relative permittivity of various materials measured at 100Hz. *(reported)*

Material	**Attenuation**	**Relative permittivity ε_r**	**Material**	**Attenuation**	**Relative permittivity ε_r**
	(db/m)	(F/m)		(db/m)	(F/m)
Air	0	1	Rock salt: dry	0.01 – 1	4 – 7
Ashhalt: dry	2 – 15	2-4	Sand: dry	0.01 – 1	4 – 6
Ashhalt: wet	2 – 20	6 –12	Sand: saturated	0.03 – 0.3	10 – 30
Clay	10 – 100	2 - 40	Sandstone: dry	2 – 10	2 – 3
Coal (UK): dry	1 – 10	3.5 - 9	Sandstone: wet	10 – 20	5 – 10
Coal (UK):	2 – 20	8.5 - 25	Seawater	1000	81
Concrete: dry	2 – 12	4 – 10	Seawater ice	10 – 30	4 – 8
Concrete: wet	10 – 25	10 - 20	Shale: saturated	10 - 100	6 – 9
Freshwater	0.1	80	Snow: firm	0.1 - 12	8 – 12
Freshwater ice	0.1 – 2	4	Soil: sandy dry	0.1 – 2	4 – 6
Granite: dry	0.5 – 3	5	Soil: sandy wet	1 - 5	15 –30
Granite: wet	2 – 5	7	Soil: loamy dry	0.5 – 3	4 –6
Limestone: dry	0.5 – 10	7	Soil: loamy wet	1 – 6	10 –20
Limestone: wet	2 – 5	8	Soil: clayey dry	0.3 – 3	4 – 6
Permafrost	0.1 – 5	4 – 8			

As electrical permittivity is a term contained in the equations for the theoretical derivation of how an EK response is generated, (Pride 1996), figure 2.16 is included to show how the relative permittivity is affected by moisture content in the ground.

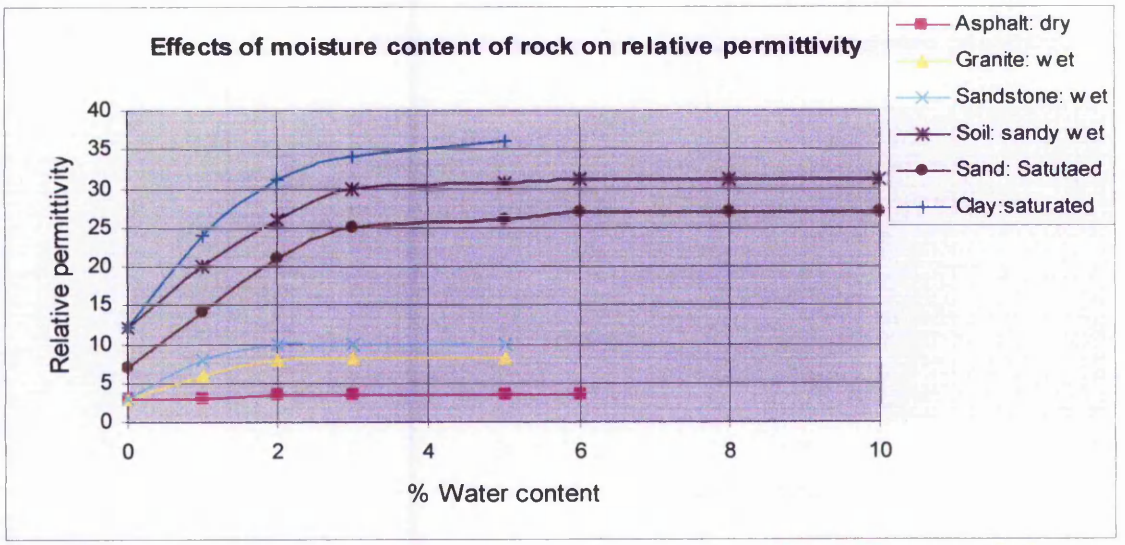

Figure 2.16 Effect of moisture content of rock on relative permittivity (after Hipp, 1974).

The attenuation loss (La) of a material is given by

$$La = 8.686 \times R \times 2 \times \pi \times f \times \sqrt{\frac{(\mu_0 \mu_r \varepsilon_0 \varepsilon_r)}{2}} \times \{\sqrt{(1+\tan^2\delta)} - 1\} dB \quad \text{..... (2.51)}$$

Where f = frequency, Hz

$\tan \delta$ = tangent loss of material

εr = relative permittivity of material

ε_0 = absolute permittivity of material

μ_r = relative magnetic susceptibility of material

μ_0 = absolute magnetic susceptibility of material

dB = gain in decibels = $20 \times \log \frac{(Vout)}{(Vin)}$.

For example, if the gain given by Vout/Vin is 10 then the gain in dB is 20xlog(10) = 20.

2.7.3 *Seismic attenuation.*

The seismic attenuation is normally expressed as a loss Q_s where

$$Q_s = \frac{1}{Attenuation} \qquad (2.52)$$

or

$$Q_s = \frac{4\pi W}{\Delta W} \qquad (2.53)$$

Where $4\pi W$ is the energy in the first cycle of the seismic wave and ΔW is the energy dissipated.

In practice, account must be taken of the ground stratigraphy, which may in certain cases complicate the determination of the overall attenuation (O'Hara-Dhand *et.al.*.1996). However, for the investigations conducted in this thesis this can be ignored. Figure 2.17 shows the attenuation over a range of frequencies.

At shallow depths down to 50 metres the spherical divergence is not too great and hence the seismic attenuation in later models of seismic recorders is compensated for by

automatic gain control, (AGC). In the case where the seismic wave gives rise to an EK response, the return loss of the seismic wave is not considered as:

(i) The loss of the seismic energy is small ~15% and is not involved in passage of the EK EM radiation from the interface to the surface.

(ii) Depth at which the EK response was generated was the main focus of the research reported in this thesis.

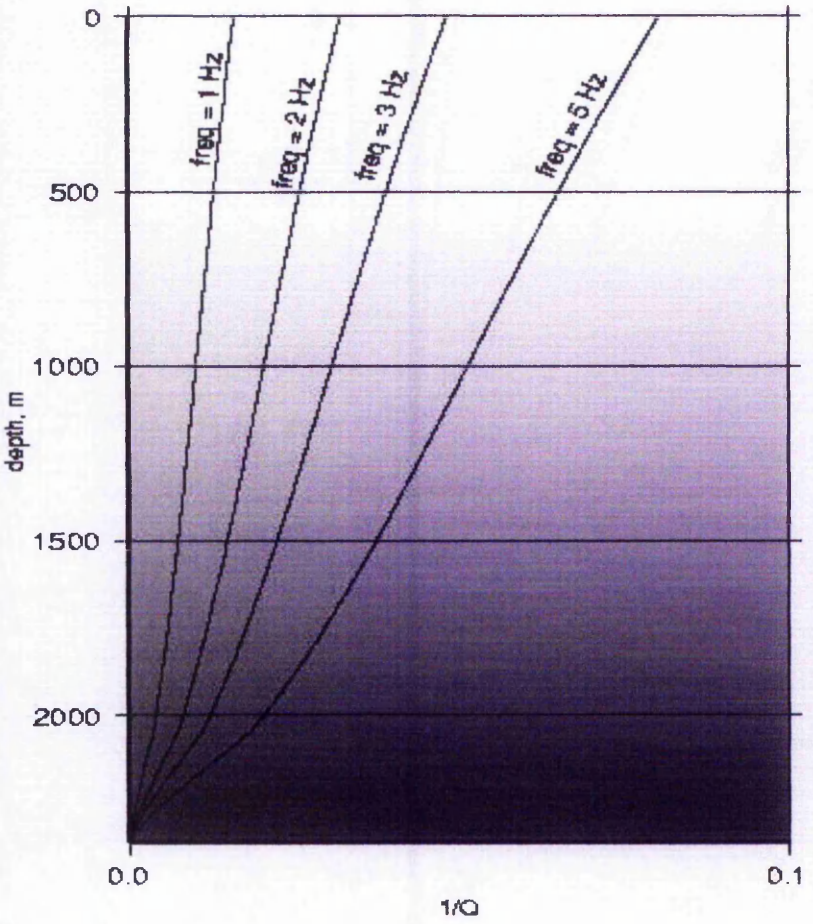

Figure 2.17 Attenuation losses per unit depth for a seismic wave. After Lensky *et.al*, 2000.

Note from table 2.3 where the attenuation at 100 Hz for dry sand is in the worst case i.e. $2x10^{-6}$ db/m, and an EK response generated at a depths 100 metre would be attenuated by $2x10^{-4}$ db/m, hardly significant. A useful paper used when considering the effects of seismic attenuation and dispersion is Wang *et al.*(2004).

2.8 Summary

The advantages of the new dipole aerial over these other electrode systems have been clearly demonstrated, e.g., no physical contact with the ground eliminating contact problems and improved EK signal sensitivity. Theoretical calculations of the magnitude of the EK response, assuming a spherical wave front, agree very closely to that measured,(See Chapter 4). Other problems associated with the detection of an EK response, such as the attenuation of an EM wave in various geological profiles, have been outlined. The important points to note are;

(i) Although the field EK results in section 2.4.2 agreed very well with the theoretical calculations further theoretical studies, both laboratory and field, have been undertaken to investigate the interaction of the seismic wave front with the soil water interface.

(ii) There is a small degree of attenuation for shallow depths, < 30m, in most geological profiles of the seismic attenuation, $\frac{1}{Q_s}$ is < 0.1db/m

(iii) Ground type and moisture content affect attenuation and the relative permittivity, ε_r. (This was not undertaken under taken because of time constraints).

Chapter 3

Field site descriptions and investigation methodology

My eyes, wide open,
had the run
Of some ten weeds to fix upon;
Among those few,
out of the sun,
The woodspurge flower'd,
three cups in one.

Dante Gabriel Rossetti (1828- 1882)

3.1 Introduction

In order to conduct the EK fieldwork a list of 61 potential sites with a varying range of geological profiles was drawn up, trying where possible to keep within the East Midlands catchment area. These were mainly sandstone, clay and silt. The main reasons for selecting these geological profiles were that previous EK investigations were conducted on road fill overlaying glacial till (Butler *et.al.* 1996) using metal dipole pairs. Beamish (1997) published results on EK studies conducted on the Sherwood sandstone aquifer among other sites. This offered the opportunity of comparing results with published work. A limestone site was also selected on which to carry out EK investigations, time allowing, as to the best of the authors knowledge there is no reported work of EK field investigations on a non fractured limestone dominated geological profile.

Most of the sites were visited in order to determine suitability for EK investigations and for those examined the following points were considered.

a) Ease of access.

b) If there were accessible boreholes. However, this was not always possible. Table 3.1, which originally contained details of 65 sites, provides an example of the spread sheet created to log details of all visits.

Table 3.1 Field sites investigated for potential EK experiments.

All of the sites below will be found by reference to Loughborough geological map, sheet 141 and the Geology of the Nottingham Area Map 1. (Boreholes and Trial Pits)								
Place name	Grid reference	BH.Ref.	Dia	Cased	WT	Owner	Access	Geology
Long Eaton	31.45 N, 49.40 E	NV	?	?	?	STW	Y	Alluvial Beds
Gotham	30.05 N, 51.75 E	"	"	"	"	"	Y	Red Marl with beds of Sandstone and bands of Gypsum
Barton Lodge	32.40 N, 53.10 E	"	"	"	"	"	Y	"
Gotham	32.65 N, 55.60 E	"	"	"	3m	KOHD	Y	"
Shepshed	21.40 N, 47.47 E	"	"	"	?	?	Y	Boulder Clay with under and overlaying Sand and
"	21.80 N, 47.40 E	"	"	"	"	"	?	Gravel
Hatheren	21.70 N, 50.75 E	"	"	"	"	"	"	Alluvium close to River Terraces (Gravel or clay) and
"	"	"	"	"	"	"	"	Red Marl with beds of Sandstone and bands of Gypsum
"	27.75 N, 40.90 E	"	"	"	"	"	"	River Terraces (Gravel or Clay)
Worthington	20.00 N, 41.85 E	"	"	"		"	"	Boulder Clay with under and overlaying Sand and Gravel
1.5 km south	28.45 N, 44.05 E	"	"	"	"	"	?	Alluvium
All of the sites below will be found by reference to Melton Mowbray geological map, sheet 142 and the Geology of the Nottingham Area Map 1. (Boreholes and Trial Pits)								
Place name	Grid reference	BH..Ref	Dia.	Cased	WT	Owner	Access	Geology
Ruddington and	34.30 N, 59.65 E	1	?	?	4.0 m	NCC	No	Housing development now covers a lot of the sites below
Surrounding area	33.62 N, 58.05 E	2	"	"	2.0 m	NCB	"	In most of the sites listed in 24 to 50 boreholes have either been
"	34.20 N, 59.45 E	3	"	"	2.0 m	NCB	"	covered over or filled in. See notes in appendix A
"	33.85 N, 59.17 E	12	7.125 m	Yes	1-2 m	"	"	"
Longer grange	31.50 N, 72.90 E							
Hose	29.05 N, 73.90 E							Mercia Mudstone overlaying sandy clays
All of the sites below will be found by reference to geological map sheet 113 Ollerton.								
Place name	Grid reference	BH.Ref	Dia.	Cased	WT	Owner	Access	Geology
Mansfield (Toray	36.17N, 45.57 E	32	76 mm	Part	16 m	Toray T	Y	Edge of Sherwood Triassic Sandstone
Factory site)	36.10N, 45.53 E	33	"	"		"	"	"
All of the sites below will be found by reference to geological map, sheet 273 (1953)								
Place name	Grid reference	BH.Ref	Dia.	Cased	WT	Owner	Access	Geology
Ospringe (Kent)	TQ 995611	19			12 m		Y	Loess (Brickearth)

Key: BH Borehole, WT Water Table, NCB, National Coal board, NLA No longer available, KOHD Ken O'Hara-Dhand, STW Seven Trent Water Toray T Toray Textiles, NV Not visible

c) If a borehole was still accessible, were the borehole log details available.

d) Locate owner of the site in order to gain permission to work.

Details for all field site visits and EK investigations were kept in a field notebook and then the relevant details transferred to an Excel spread sheet and in a word document. Details noted were site location, British National Grid Reference, brief geological profile, nearby power lines and any other relevant items. This information was transferred to an Excel spreadsheet, table 3.1 being a representative selection of sites visited showing the formatting of the spreadsheet. However, in a lot of cases where there were boreholes indicated on geological maps these were found to be either filled in or could not be located.

3.2 Field investigation methodology.

A geophysical site investigation methodology was adopted for all sites investigated in order to ensure uniformity in the measurement process between sites.

A thorough inspection of the geological maps of the area to be investigated was undertaken making notes of any special features observed. A site visit was undertaken prior to any measurements to ascertain the existence of boreholes, ease of access to the site and to locate the site owner in order to gain permission to work. Photographs were taken of the site.

Before starting any measurements a sketch and details of the field site were recorded in a field notebook, i.e. covering, weather conditions, date and time, magnetic orientation of the site, any nearby power lines or radio transmitters and position of the experiment. Power lines in the country environment are mainly of two types, one where there are pylons and the other overhead poles. The former is the national grid and are 400 to 132 kilo-volt and the latter local power lines at 11kV. In cases of heavy industrial users the overhead line can be 33kV. All can induce significant currents in the ground and in the case where metal stakes are used for EK investigations can completely swamp the EK signal.

Any boreholes on the site were located and dipped to determine the depth of the water

table and a sample of the water also taken for laboratory analysis to determine conductivity etc. A supply of preformatted $3\frac{1}{2}"$ floppy disks, at least two boxes of 10. At the time of writing this thesis memory pens have become available and providing there is a USB buss available on the seismic recorder. These are much more robust and can store 128 m-bytes or more of data, nearly 100 times more data than a floppy disc, certainly more than enough for at least five days records. They are not affected by magnetic fields and are powered from the USB port.

In all of the EK investigations described in this thesis a composite plate was used as the seismic source together with a 4.5kg sledge hammer to which an impact sensor was attached. This provided a trigger signal to the seismic recorder. The composite plate material consisted of a 30 mm thick, 300 mm diameter Ultra High Molecular Weight (UHMW) polyethylene disk. The UHMW plate is cost effective and overcomes the problems faced by using a metal plate which includes generation of electromagnetic (EM) signals. Metal plates are also prone to distortion and hammer impact damage.

All EK investigations were preceded by a conventional shallow seismic survey, using both vertical and horizontal geophones, over the area of interest to a depth of 40 -50 metres, a depth of approximately 20 metres below the water table. This was necessary in order to establish the ground stratigraphy and resulting seismic velocities. The geology was confirmed by reference to a geological map. If the borehole records were still available then these were obtained or inspected in order to gain knowledge of the down-hole geological profile. The British Geological survey (BGS) has a large number of borehole records for the East Midlands at their site in Keyworth.

It is necessary to take a noise reading at each survey line. These data were used to determine the mains bourne noise parameters used in the Butler and Russell least squares noise removal programme for 50Hz and its harmonics. This is very important in locations that have a high degree of mains bourn interference as it can completely obscure the EK signal. The noise recording is analysed by means of a fast Fourier transform (FFT) to determine both the presence of the mains frequency components and their relative amplitudes. The offending signals are selected from the FFT data and transformed back into the time domain using an inverse Fourier transform. They are then convolved with the EK recoding to subtract the selected noise components. Thus

with the offending noise removed the EK signal becomes clearer and more easy to identify.

When carrying out an EK survey careful note must be made to make sure there are no geophones left in the ground as these can generate a small but measurable magnetic field. Measurement of ground conductivity using either a "Megger" or ground resistivity meter such as the ABEM SAS 300 were made at a number of points along the survey line.

Where time allowed EK data were also gathered using stainless steel metal stakes, 15 mm diameter with a length of 500 mm, at a 1 metre spacing between electrodes and at a one metre spread. This was to correlate the EK data with the travelling electric field, i.e. Electroseismic (ES) wave. Also it was decided to use the same electrode layout to measure the ground electrical conductivity as these will not interfere with the dipole aerial. A noise reading was taken at each survey line. Trial runs were undertaken using 9 stacks, 16 stacks and 25 stacks. In certain cases a greater number of stacks were necessary to allow very small signals to be seen. Initial investigations confirmed that the signal level is enhanced over background noise, the amplitude of the signal increases in direct proportion to the number of hammer blows, while the random noise increases as $\frac{1}{\sqrt{n}}$, where n is the number of strikes. Therefore, with nine hammer strikes the signal is increased nine times and the random noise is reduced by 1/3 giving an overall improvement of signal to noise ratio of 30:1. The highest gain setting on the later range of 'Geometrics' seismic recorders is 120 db, a factor of 1,048,576 or a factor of $> 10^6$.

3.3 Details of field sites selected

The final sites selected reflected two main geological profiles in which the EK investigations would take place.

3.3.1 *Site 1. Lower Triassic Sherwood Sandstone Formation, Mansfield*

A site at Mansfield in Nottinghamshire adjacent to the Toray Textile Factory site was chosen as it had a large number of boreholes which were still accessible. The location is recorded by geological map 113 (Ollerton), (National Grid reference: SK572618 (457215 361880)). (See figure 3.1)

This site has been the source of intense geophysical investigations comprising EK down hole and surface surveys, seismic downhole and surface surveys and resistivity surveys.

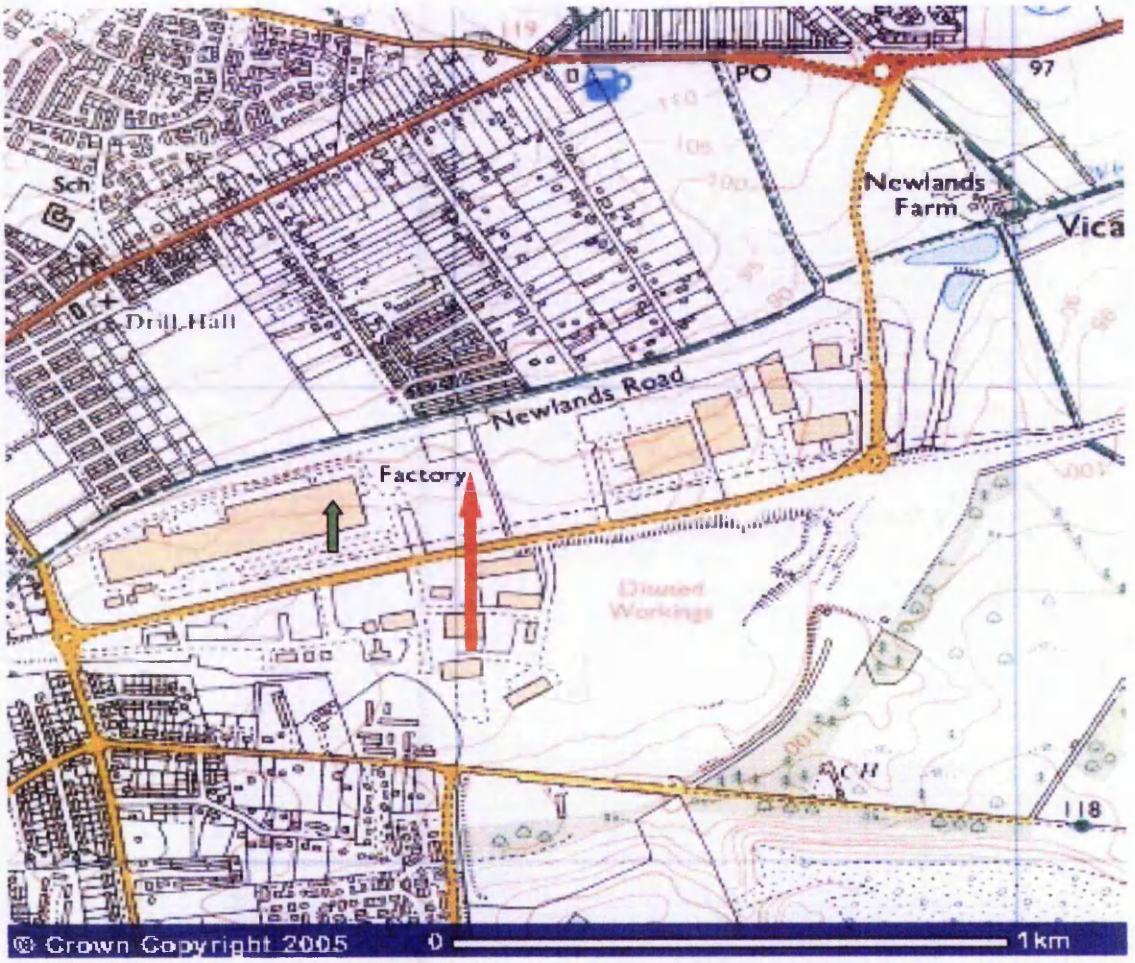

Figure 3.1 Location map for Ollerton, Mansfield Ospringe. The red arrow indicates the area of the geophysical and EK investigations. The green arrow is the Toray dye factory. *Image reproduced with kind permission of Ordnance Survey and Ordnance Survey of Northern Ireland.*

The Mansfield site, (see site map figure 3.1), consists an 80 m deep aquifer of Triassic Sherwood Sandstone overlying Permian Marls and lower Magnesia limestone. There were 34 boreholes mainly 76 mm diameter present on the site of various depths down to 80 metres, enabling the depth of the water table to be accurately determined. The results of measurements taken over a period of four years were used to determine the variation in depth of the water table (See table 3.2)

Table 3.2. Measured depths of the water table at borehole 32. Note that over a three year period the water table had risen by 2 metres.

Borehole	Date	Depth of water table (m)	Comments
32	17-01-1998	17.0 m	Seismic and EK investigations
32	6-02-2001	16.0 m	"
32	3-07-2001	15.0 m	"

Borehole logs and core samples were also available. The data for this site were obtained using a number of different seismic recorders. However, as the data were in SEGII format it was read into Excel and it was found there were no major difficulties. There have been a number of EK investigations carried out on this site dating back to 1998, however the main investigations fall into three sets. Those carried out prior to the year 2000, those carried out on the 6th February 2000 and those more recently in July 2001.

A site map is shown below in figure 3.2. It should be noted that the coking works were no longer in operation at the south west of the site and at the south east of the site there was a large spoil heap consisting mainly of building rubble overlain by approximately one metre of soil. This was noted as some of the results presented in Chapter 4 were obtained on this slope.

Most of the other EK investigations took place around borehole 32, shown by the block arrow on figure 3.2. Initially EK investigations were conducted at boreholes 10, 25 and 27. A number of the boreholes had piezometer instrumentation in place to monitor groundwater pressure. The rectangular area to the north of borehole 32 was a water overflow pit of approximately 12 metres in depth. The Toray factory is seen to the lower left of the map.

Overhead power lines ran along the north side of the road. It was noticed during the last visit to the site that there was a warehouse development taking place due east of the map. This is the area where borehole 10 is located (See figure 3.2).

Borehole 32 where most of the seismic and EK investigations were conducted is indicated by the block arrow, also boreholes 10 and 30 where some earlier investigations had taken place. The results of the earlier EK investigation are presented and discussed in Chapter 9. Since the last visit the site to the east where borehole 10 is located has had industrial units erected.

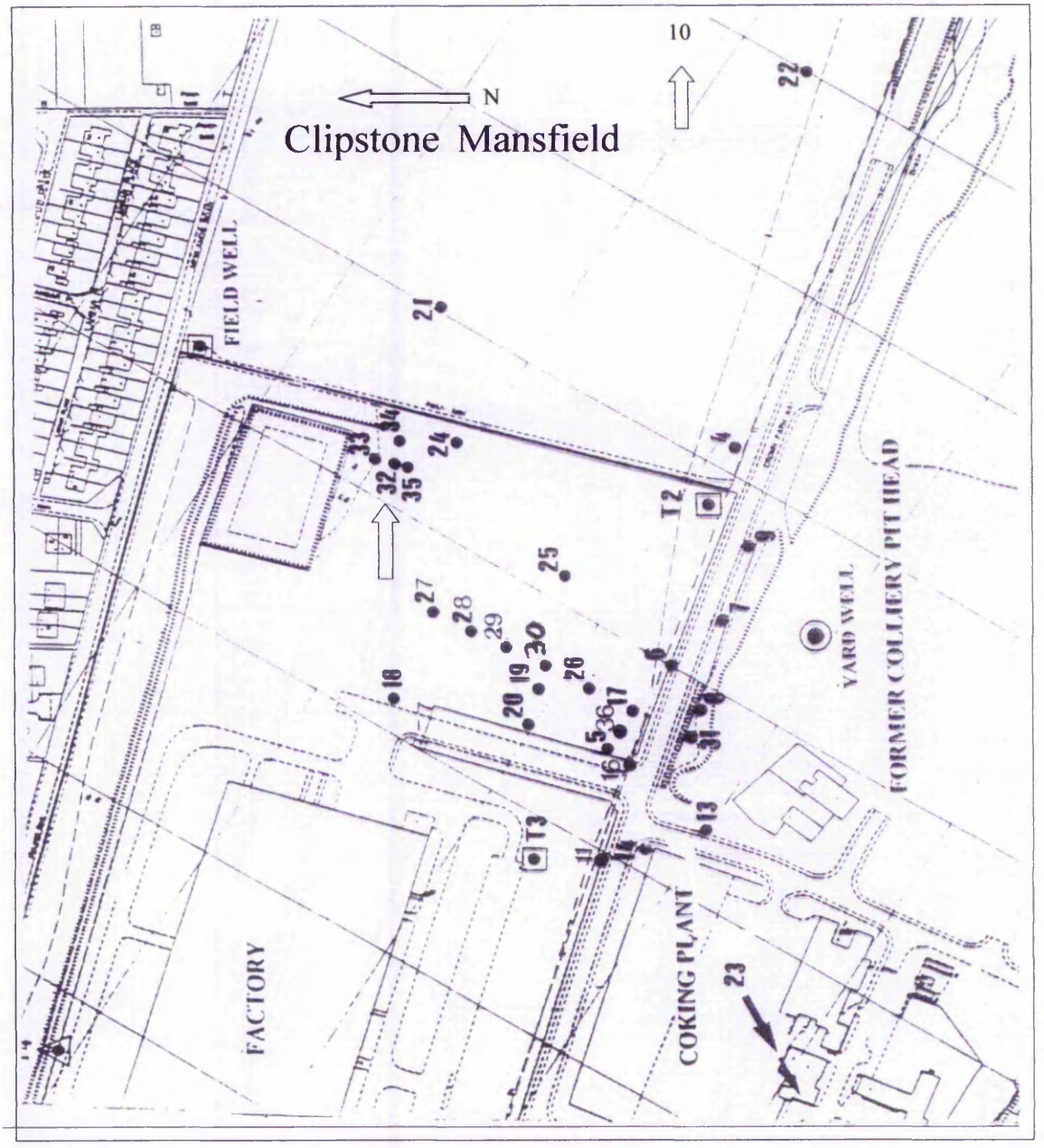

Figure 3.2 Site map of the Mansfield test area. Personal communication. The oblong structure to the north of borehole 32 is a water overflow lagoon approximately 12 metres deep. Courtesy Dr. C Hutton.

Plate 3.1 is a view of the investigation site near to borehole 32 looking from east to west. The Toray dye factory is in the distance. Borehole 32 is to the right of the author. The area around the vicinity of borehole 32 was flat. However, to the right the ground can be seen to slope upward.

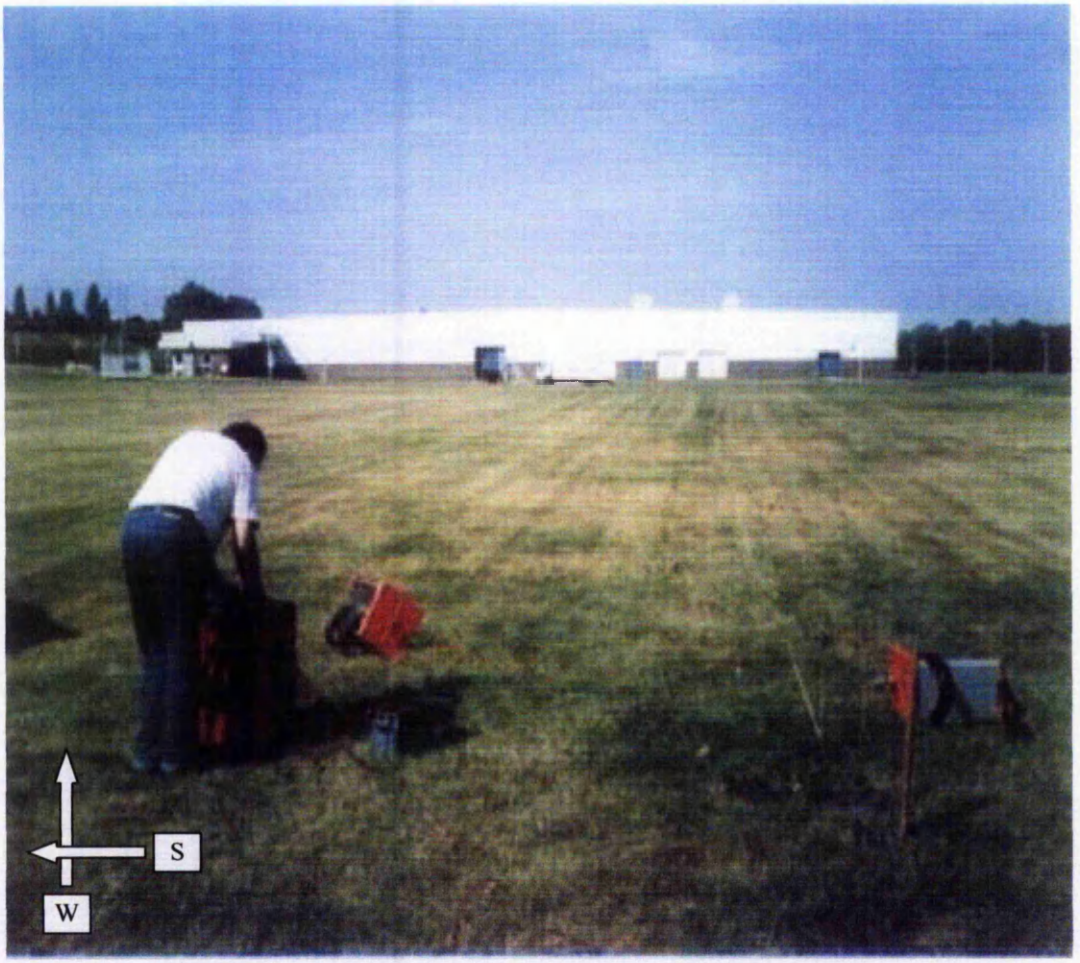

Plate 3.1 The seismic recorder near to borehole 32. The Toray Factory can be clearly seen in the background. To the left of the author was a slope leading up to the road where the power line were located. The entrance to the site is seen above middle left where a gatehouse can be observed.

From the geological log for borehole 32, table 3.3, it is seen that there are a considerable number of fracture zones starting at 13 metres continuing at various intervals down to 47 metres. Also noted was the compaction at 22 metres and cementation at 20 and 23 metres. Only the borehole log details down to 52 metres are shown as it was not expected to obtain EK responses below this level during these investigations. Unfortunately the section of the log from 9 to 13 metres was missing. However, the log will prove useful for any future work. The log for borehole 32 is given in Table 3.3

The subsurface geology of the local area, down to 468 metres is shown in figure 3.3. This will be referred to in Chapters 4 and 9. The data were taken form the geological section on the Ollerton map.

Table 3.3. Borehole log details for borehole 32. Details down to 82 metres. However, the information given here down to 52 metres is related to the depth at which EK responses can be reliably seen. Courtesy of Dr. Craig Hutton. Ex. Imperial college

Depth (m)	Geological description of core	EK resp.
0 - 9	Sand and some pebbles	Y
13 – 14.5	Coarse red Bunter sandstone with pebbles. Heterogeneous minerals. Lots of fractures due to bedding planes.	
14.5 - 16	Coarse red Bunter sandstone with pebbles. Heterogeneity in minerals. Lots of fractures due to bedding planes.	Y
16 - 17.5	Coarse red sandstone. Pebbles decrease. Bedding plane fractures	Y
17.5 – 19.0	Coarse red sandstone. Pebbles decrease. Rock unconsolidated. Bedding plane fractures	Y
19.0 – 20.5	Coarse red sandstone. Pebbles decrease. Rock unconsolidated. Bedding plane fractures. Cementation poor. Red Marl at 20.5 m.	Y
20.5 – 22.0	Coarse gravel red sandstone with small pebbles. Fairly well cemented. Small fractures every 5 –20 cm.	Y
22.0 – 23.5	Fairly compacted material but not well cemented.	Y
23.5 – 25.0	Fairly well cemented red sandstone with few pebbles. Material appears homogeneous. Horizontal fractures due to bedding planes.	Y
25.0 – 26.5	Change in composition. Two distinct rock types. Upper 10 cm very coarse yellow sandstone with lots of pebbles smaller than 0.5 cm. Colourful and heterogeneous minerals. Transition to compacted well cemented medium red sandstone. Appears heterogeneous. Horizontal spills at bedding planes. No significant fractures observed in both rock types	N
26.5 – 28.0	Red medium sandstone, compacted and well cemented but finer than the above. No observed fractures	Y
28.0 – 29.5	The first 15 cm consists of red medium sandstone compacted and well cemented with no significant fractures. Below this depth the material changes to coarse gravel yellow sandstone. The rock presents heterogeneity. No observed fractures.	Y
29.5 – 31.0	Coarse red sandstone, heterogeneous, compacted, well cemented with fractures on the bedding planes	Y
31.0 – 32.5	No recovery at this drilling stage.	Y
32.5 – 34.0	Cross bedding, heterogeneous, red and yellow sandstone with silty layers changing. Clays encountered. Fairly well sorted, compacted and cemented.	Y
34.0 – 35.5	The first 30 cm present a layer of coarse, yellow sandstone compacted and well cemented. The rest consists fine red sandstone, compacted and well cemented.	No EK signals observed
35.5 – 37.0	Medium, red sandstone, very broken.	this level
37.0 – 38.5	Red Mottled sandstone formation starting at a depth of approximately 37.5 m . Red sandstone is still predominant but with marls. The rock is very compacted. Grain compression seems visible but not very well cemented. A large vertical fracture is visible	"
38.5 – 40.0	Consistent Mottled sandstone. Laminations clearly visible. Lots of marl. Compact, coarse but not very strong. Breaks easily at the bedding plane boarders. One sub - vertical fracture at 39.0 m.	"
40.0 – 41.5	At 40.0 m medium red sandstone with less marl. At 40.9 m changes to very coarse sandstone. Heterogeneous with marl, grit and gravel. Grain size approximately 1 – 2mm.	"
41.5 – 43.2	Coarse red mottled sandstone. Some marls and grits are present approximately 1 mm. Sandstone is reddish with some yellow bands. Compacted and very well cemented. Some bedding plane fractures occur but les than above.	"
43.2 – 43.65	Pure marl, dark red – brown	"
43.65 – 47.3	Medium to fine sandstone less red than above, very compact, well cemented becoming slightly coarse and lighter towards the base. Less fractures and bedding planes than above.	"
47.3 – 49.0	Marl band and material broken. Weak and poorly cemented below 48m.	"
49.0 – 52.0	White, yellow, green red sandstone compacted and well cemented. Material is very heterogeneous and presents a few cracks. No marls are present. It is purely clean sandstone very heterogeneous and very fine.	"

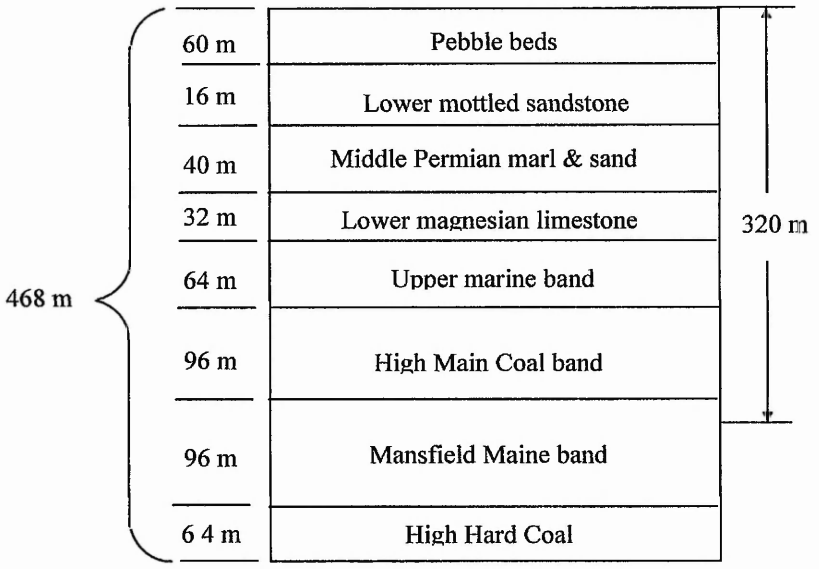

Figure 3.3.Subsurface geology near to the Mansfield site

3.3.2 *Second site: Representative of Pleistocene Loess Ospringe in Kent.*

3.3.2.1 Introduction to site details

This site is located on the western edge of the small town of Ospringe near Faversham in Kent, just north of the A2 and is recorded by Geological Sheet 273 (1953). The geology is Pleistocene Loess overlying lower Eocene sand with sandy clay seams, (National grid reference: TQ 995611 (599590 161190)).

The near surface consists of a drift deposit of Head Brickearth (loess) overlain by 0.40 m of topsoil. Below this is another layer of brickearth with a calcareous content, approximately 1.5 metres in depth. Nearby, there is evidence of white chalk outcrops with flints, and also outcrops of green-grey sand with shell beds and sandy clay (Thanet sand beds). All of this overlies the Upper Chalk of thickness 91 to 116 metres. An Ordinance Survey map of the site location is provided in figure 3.4.

A local brick works, Cremer Whiting & Co. Ltd, had excavated a shallow quarry approximately 1.5m deep, in order to use the brickearth soil in the brick manufacturing process. The excavation, and plant trafficking, has left a quarry floor with a disturbed surface, see plate 3.2.

This site presented a different geological profile to the other site described and offered a unique opportunity to compare EK surveys with a number of other geophysical investigations.

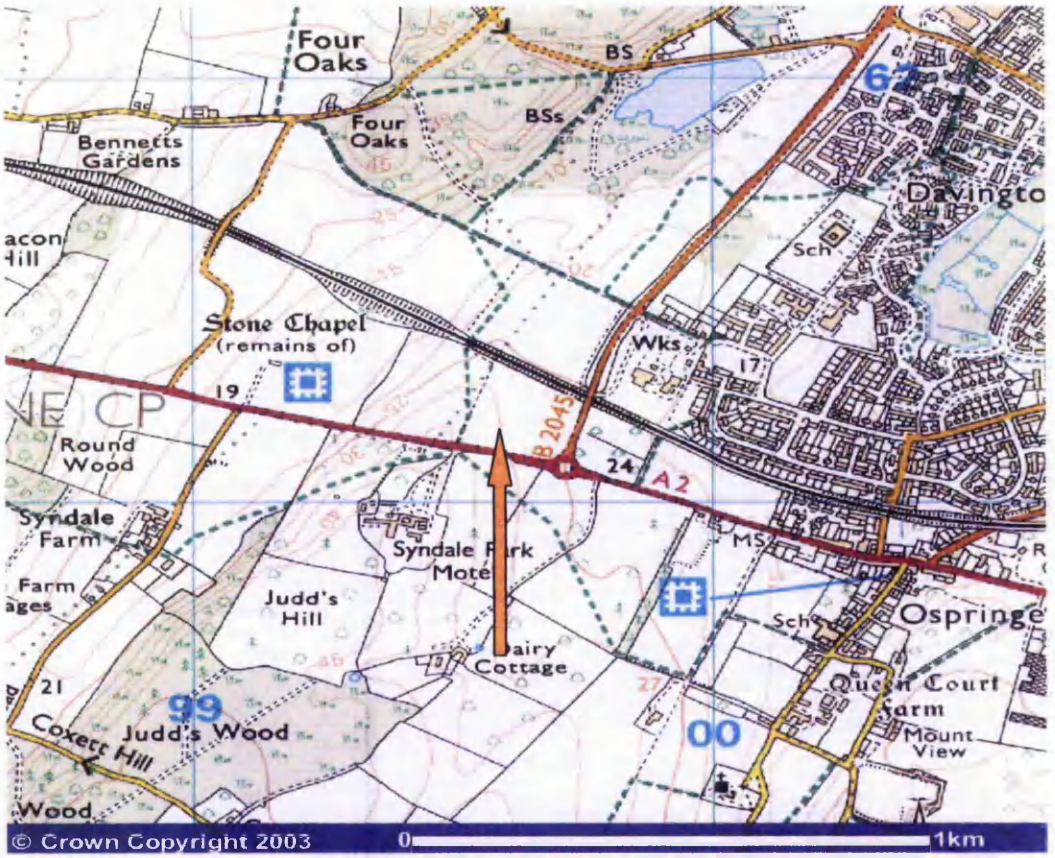

Figure 3.4 Location map for Ospringe. The orange arrow indicates the area of the geotechnical and EK investigations. *Image reproduced with kind permission of Ordnance Survey and Ordnance Survey of Northern Ireland.*

Plate 3.2. View of site, looking west, showing the disturbed condition of the ground. The east entrance to the quarry is seen on the slope to the bottom right of the plate.

Although boreholes were indicated on the original site map, none were traceable at the time of the investigation.

A Global Positing System (GPS) reading was taken on the position of the seismic hammer plate, near to borehole 10 on the site map. The GPS reading was TQ 99592, BRG 61192 with an altitude of 42 metres. The boreholes marked out on the site map were no longer visible on the site, see figure 3.5.

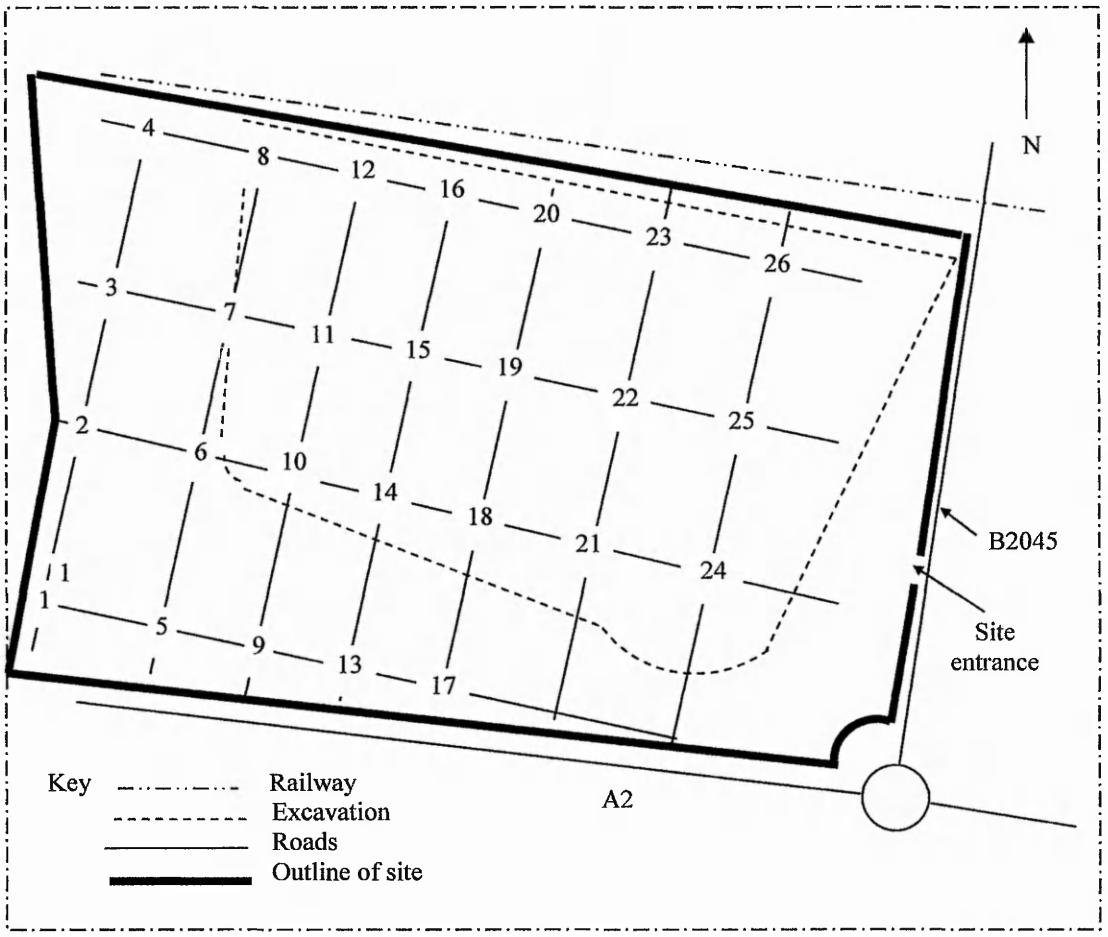

Figure 3.5 Sketch map of site showing location of bore holes

3.3.2.2 *Survey locations and additional details*

As indicated on the sketch map below of the site, figure 3.6, two main survey lines were used for all of the investigations in the quarry. The first ran west east at the southern end of the quarry. The second ran at approximately 45^0 to the first, in a south west to north east direction. Both lines used the shot point for the seismic surveys as a reference starting point.

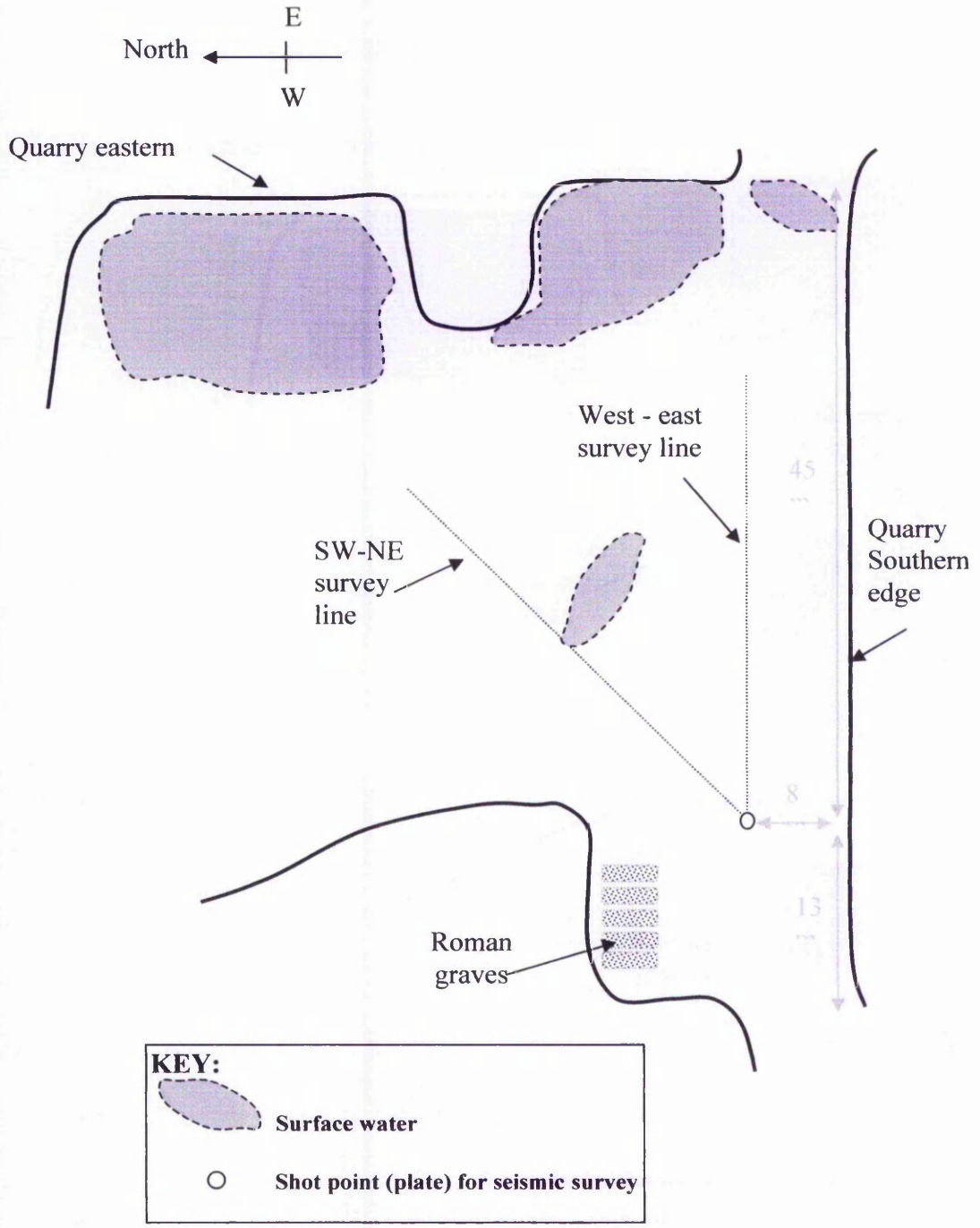

Figure 3.6 Sketch map of Ospringe brickearth site (not to scale)

The shallow quarry (approximately 1.5m maximum depth) was located in an open grass covered field and exposed brickearth (loess) deposits. When initially appraising the site, before commencing the geophysical and geotechnical testing, a 30 metre strip of loess at the southern end of the quarry was chosen as being most suitable for compaction. The west-east survey line, see figures 3.6, was selected for the main seismic survey, as this part of the quarry was most accessible and suitable for compaction. For comparison, a

seismic survey on the South West to North East line was also performed.

The seismic hammer plate (same point used for both surveys) was located at the western end of the line. Plate 3.3 shows the west - east seismic line looking east and plate 3.4 is the line looking west. This line was laid out with shot point near to the location of BH10 and the line passing near to BH's 14, 18 and 21. The log data for boreholes 10, 13, 14, 18, 19 and 21 are given in table 3.4.

Table 3.4. Data from boreholes (previously obtained at the Ospringe site). Drillers log. Only data near the survey area is included. Borehole results taken from Figure 3, in 'Bonding Mechanisms in Loess', NERC Project report, Documentation for the 6th meeting of the Steering Group. Northmore et.al. (2004)

BH	Topsoil	Sub-soil	Brickearth	Bottom	Other comments
1	230 mm	300 mm	Nil	3.05 m Flint and chalk	Driller's comments
5	230 mm	300 mm	Nil	2.44 m Flint and chalk	"
9	230 mm	300 mm	Nil	Clay & sand	"
10	230 mm	300 mm	Nil	Clay & sand	"
13	230 mm	230 mm	Nil	3.66 m Clay	"
14	230 mm	230 mm	Nil	3.66 m Clay and flint	"
18	230 mm	230 mm	Nil	3.66 m Flint and sand	"
19	230 mm	230 mm	3.05 m	Sand on bottom	"
21	230 mm	230 mm	3.66 m	Brickearth on bottom	"

From the above log there appears to be considerable variability in the under lying strata. This observation was confirmed when EM data of the site was made available from the BGS at Keyworth see (Chapter 9, figure 9.12).

Plates 3.3 and 3.4 are included to show:

1 The disturbed nature of the ground

2 The water still remaining on the site from the previous week's heavy rain.

3 The layout of the survey line

The samples taken for laboratory tests were taken from the pile of soil on site. Further soil samples were carefully dug out after the compaction and measurements were made. These were extracted halfway down the seismic line shown in plate 3.3

Plate 3.3 View of the west-east survey line, looking west. The author is shown setting up the seismic recorder.

Plate 3.4 View of site looking in an easterly direction. Note the heavily disturbed ground.

As a point of interest a typical loess structure is shown in plate 3.5. Note the columnar structure and dishing at the top of the plate, typical of loess. This photograph was taken near to the shot point.

As part of the EK and other geophysical investigations ground compaction was undertaken. This is described in Chapter 4.

Plate 3.5 Exposed brickearth on southern quarry wall, near to the author seen in figure 3.6.

3.3 Summary

A total of two sites with differing geological profiles were selected for the EK investigations. One further site representative of Ancaster Limestone was held in reserve permission to work the site, if needed, being granted from "Realstone" in Derbyshire. This was not undertaken due to time constraints

The site owned by Toray Textiles in Mansfield, representative of the Sherwood Triassic sandstone, was selected on the basis that earlier geophysical investigations that had been conducted in 1998. These consisted of EK measurements either side of borehole 25 using the original 2 metre dipole aerial in four different orientations at each offset from

the hammer plate. These results would assist in the analysis of the results obtained for this thesis, (See Chapter 9).

The second site was selected on the basis of its different geological profile, Loess. This site also offered the advantage of comparing EK results other geophysical data obtained by the British Geological Survey (BGS).

Chapter 4 EK Field investigation results

The poet in his lone yet genial hour
Gives to his eyes a magnifying power:
Or rather he emancipates his eyes
From the black shapeless accidents of size--
In unctuous cones of kindling coal,
Or smoke upwreathing from the pipe's trim bole,
His gifted ken can see
Phantoms of sublimity.

Samuel Taylor Coleridge
1772 -1834
Apologia pro Vita Sua
August 28, 1800, published 1822

4.1 Introduction.

In order to ensure the uniformity of all of the EK and geophysical measurements procedure a site investigation methodology as described in Chapter 3 was adhered to. This comprised a standard set of rules which were adopted for all sites investigated to ensure the uniformity of measurements between sites and enhance data interpretation.

4.2 EK Measurement details

Tests were conducted with the dipole aerial placed horizontally on the ground with the dipole facing north-south, east-west, south-north, west-east and finally with it raised 1 metre above the ground vertically and horizontally with respect to its centre. A demountable wooden test rig has been designed to accomplish this. It should be noted that wood will not affect the electromagnetic wave. As a precaution it was painted with yacht vanish to weather proof it.

An EK survey was taken either side of the seismic impact plate, taking care to note the orientation of the dipole aerial relative to the shot plate with red marker tape placed around one end of the dipole in order to identify the correct orientation. This was to

confirm the phase reversal between two diametrically opposing EK surveys. A demountable wooden rig was designed to allow the vertical dipole aerial to be rotated in set angular increments, in order to allow the angular responses to be observed. Care was taken to keep all measurement parameters constant, i.e. the same number of stacks and same dipole length, in order to make the estimation of the variation in EK response amplitude with distance more straightforward.

In order to correlate the EK field data, a measurement of the water table depth was performed for boreholes 32, 33 and 34. The results are shown in table 4.1.

Table 4.1 Details of water table depth and general conditions

Site details dry with a temperature at 08.00 hrs of 3°C			
Depth to water table (m) ± 2 mm		Distance between boreholes (m) ± 5 mm	
Borehole 32	15.12	BH32 – BH35	3.0
" 33	15.09	BH32 – BH33	9.9
" 34	15.00	BH32 – BH34	10.0

Finally, care was taken to make notes of all of the electrode, geophone and aerial positions and readings. Any unusual phenomena, no matter how trivial, were noted in order to attempt to correlate these with any other observations. Estimations of any errors, such as positioning of the dipole aerial and geophones that could affect the final results were noted.

4.2.1 *Effects of signal stacking*

Figures 4.1 and 4.2 show the effect of stacking the EK recordings. This process was also applied to the stacking of seismic recordings. The time axis has been expanded to show the effects of stacking on the noise amplitude, which is more easily observed after 35 ms on the recording. Figures 4.1 and 4.2 show an example of one stack versus 9 stacks clearly showing the improvement in signal to noise ratio. The amplitude of the peak occurring at 22 ms on figure 4.2 is seen to be 0.1 mV on figure 4.1 and 0.09 mV, an improvement by a factor of 9.

Providing there is an accurate trigger point relative to a seismic or EK response stacking can bring about an improvement of signal to noise ratio. In essence if the signal is coherent it will add with each stack and the noise, being random cancels out. This is sometimes referred to as coherent signal detection.

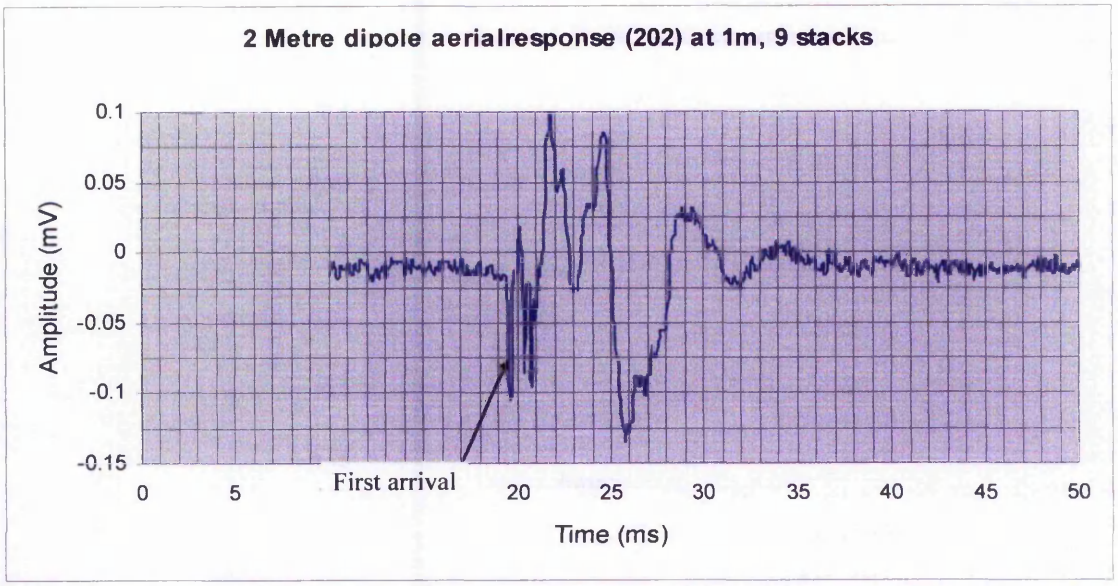

Figure 4.1 EK response using the original 2 meter dipole aerial at 1 metre and 9 stacks

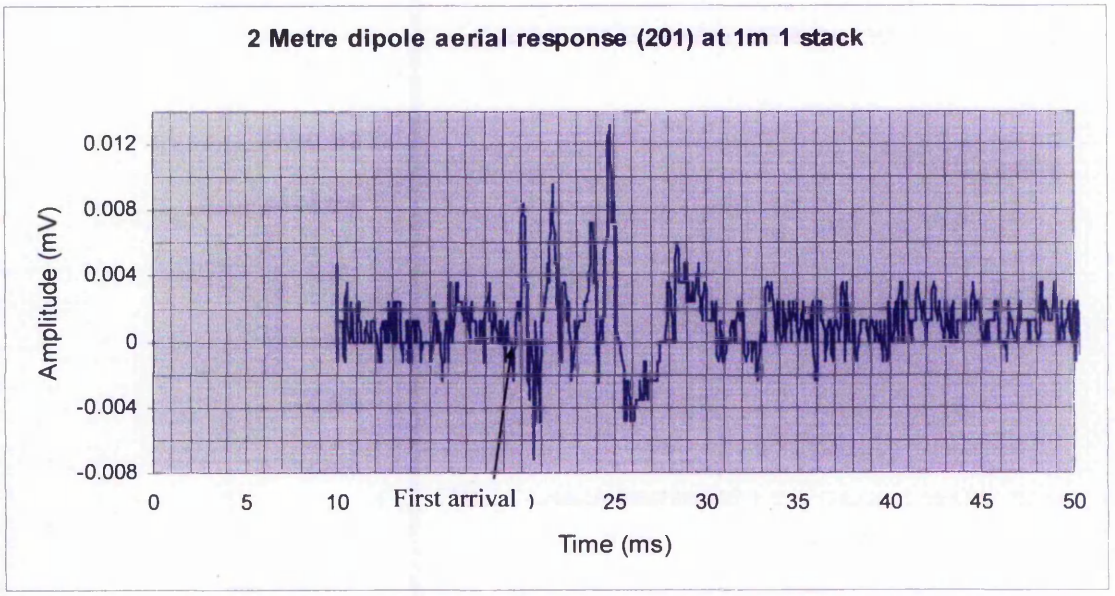

Figure 4.2 This is the EK response from the original 2 metre dipole aerial at 1 metre and one stack. Note the amplitude scale factor in relation to figure 4.1.

4.3 Society of Engineering Geologists (SEG) II Data format

For most of the EK investigations the SEGII data format was used for the recorded data. A sample of the data format for a Geometrics 'Smartseis' 24 channel seismic recorder is shown in Appendix B with the first few lines of the data. For more details on the SEGII format see Chapter 8.

4.4 Field work preparation

Prior to starting the fieldwork, tests were carried out to determine the response time of the impact sensor on the seismic hammer in order to determine the error in the trigger time of the seismic recorder. To obtain the recording a ultra high molecular weight (UHMW) polypropylene plate, placed on the floor of the laboratory, was struck with less force than would be applied in the field. A graph of the result of this test is shown in figure 4.3. The recording was obtained using a Tektronix TDS3032 digital phosphor oscilloscope. A 50% pre-trigger was set in order to record the event prior to the oscilloscope being triggered. The pre-trigger time of – 2ms is shown to the left of the '0' on the time axis.

The 'Geometrics' seismic recorder triggers on the positive edge of a pulse with an amplitude in the range of 0.2 to 5.0 volts. Thus from figure 4.3, 0.2 volts corresponds to a time of 0.9 ms. To this figure must be added an uncertainty of ± 0.8 ms. Thus the maximum error is 1.7 ms.

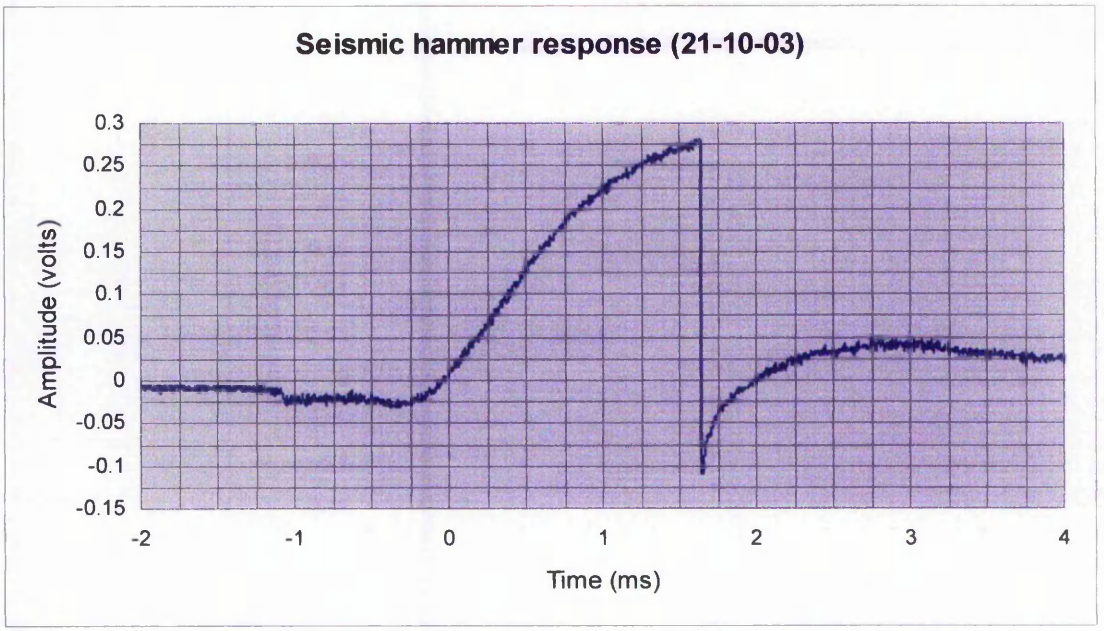

Figure 4.3 Response time of impact sensor attached to the seismic hammer used in the field tests.

4.5 Field results

The data gathered at the two sites are analysed below for each site. Only the salient features are presented in order to conserve space. However, all of the sources of data are contained in the appendices and are referred to where appropriate.

4.5.1 *Toray Factory Site Mansfield (Tuesday 6th February 2001).*

Previous visits to the site had taken place and initial EK experiments conducted using the original dipole aerial (Chapter 2, section 2.3.1). This visit offered the opportunity to test the improved version of the dipole aerial see (Chapter 2, section 2.3.2). However, to ensure compatibility the original 2 metre dipole aerial was used for most of the measurements and the new dipole aerial was used for the final ones.

Table 4.2 File references for main EK data. Note corrections for diagonal distance in table 4.3.

Centre of copper antenna	Dipole aerial in m from bh 32	Noise	1 shot	9 shot
20	1	130	131	133
"	"	134		
"	"	135		
"	"	136		
20	1	200	201	202
21	3	203	204	205
22	7	206	207	208
23	10	209	210	211
24	13	212	213	214
25	16	215	216	217
26	19	218	219	220
27	21	221	222	223
28	24	224	225	226
29	24 perpendicular	227	228	229
30	12 perpendicular	230	231	232
14	6 perpendicular	233	234,235	236
1	1m from bh 32 to bh 33	237	238	239
1	4m parallel to 2 metre aerial	240	241	242
1	2 m aerial 1 m high	243	244	255

4.5.2 *Results of EK investigations.*

The results of the EK survey are given in figures 4.5 to 4.17. These were all obtained with the old 2 metre dipole aerial. After the survey it was discovered that a 10 ms delay had been set in the seismic recorder Therefore this 10 ms has been added to the time axis on the graphs to aid interpretation, for all figures 4.5 to 4.17. The geometry of the survey is shown in figure 4.4. It was not possible to have the dipole aerial line from borehole 33 going east or west as other investigations were being conducted by another University along this line. Therefore the dipole aerial was positioned as shown in the sketch, figures 4.4. Table 4.3 is the data relating to the offset of the dipole aerial with regard to borehole 33.

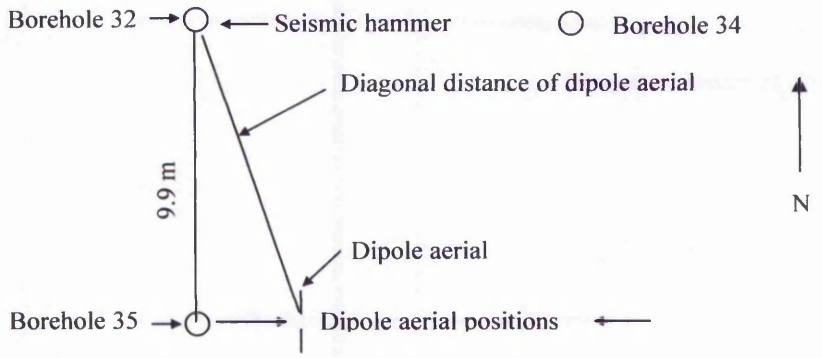

Figure 4.4 Sketch of borehole layout for EK investigations seismic hammer at BH 33. Distance from borehole 32 to 34 = 10.0m.

Table 4.3 Diagonal distances of dipole aerial at interval along the line bh32 going east

Dipole aerial distance from bh 32 to bh 34 due east of bh 32 (m)	Diagonal distance from bh 33 towards EK aerial position (m)
1.00	9.95
3.00	10.34
7.00	12.12
10.00	14.10
13.00	16.34
16.00	18.81
19.00	21.42
24.00	25.96

Figure 4.5 shows the noise recording taken at the 3 metre position from borehole 32 over the maximum recording time of 138 ms, with a sample interval of 62.5×10^{-6} second. This was to see if any responses over this period were present. The notch, high and low pass filters on the equipment were not selected. The noise recording was used in the noise removal process, (see Chapter 8). The amplitude scale was chosen to match that of the following EK responses for comparison purposes. It should be noted that the peak value of the noise is well below the 25μV per division.

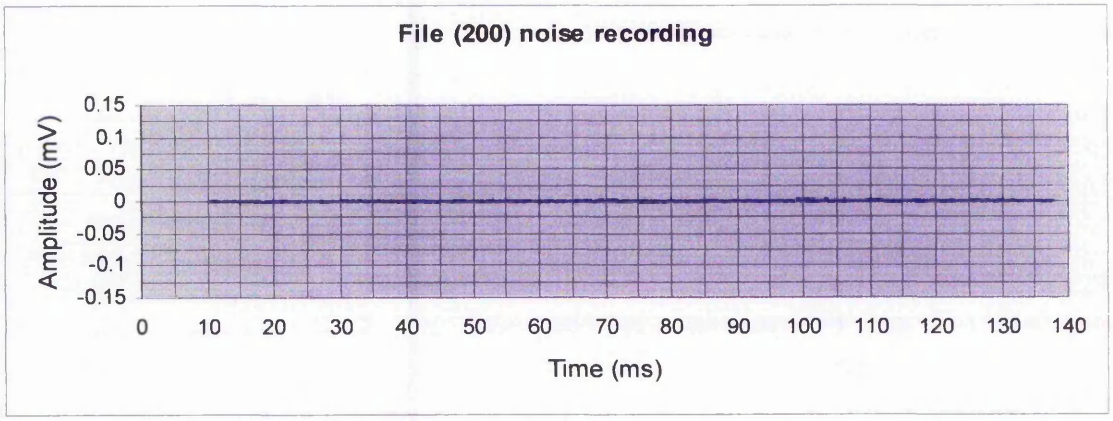

Figure 4.5 Noise recording shown on the same vertical scale as the figures below and for the complete recording cycle of 138 milliseconds.

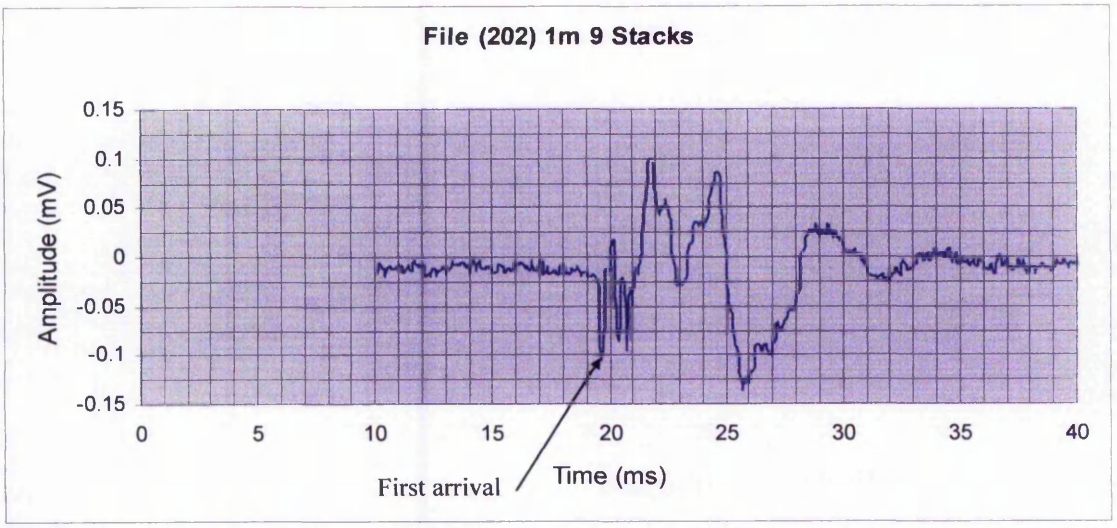

Figure 4.6 EK responses at 1m from the shot point. Note the first arrival at 19.25 ms and the EK responses following up to 35 ms.

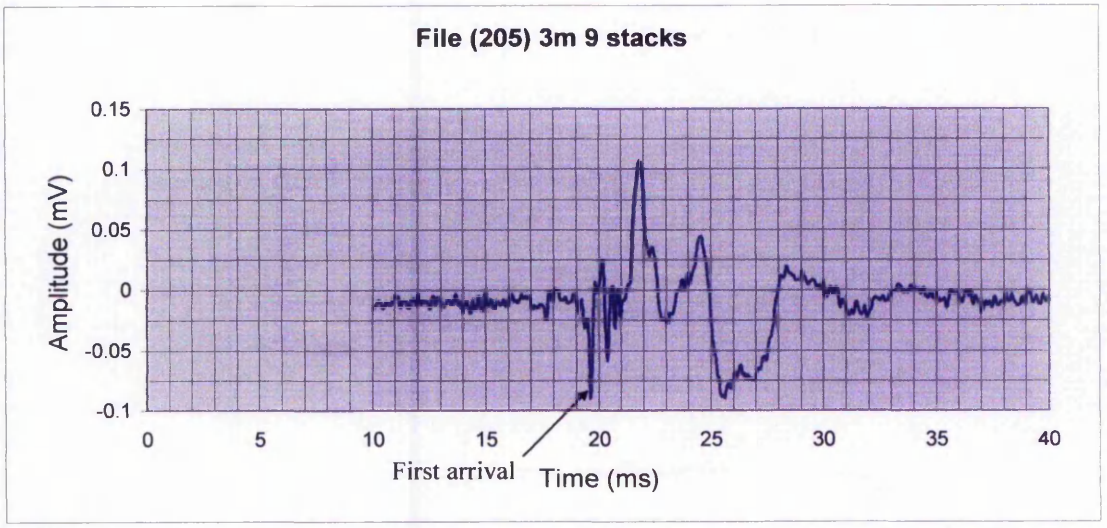

Figure 4.7 EK response at 3m from the shot point. Note the first arrival at 19.25 ms and the EK responses following up to 35 ms.

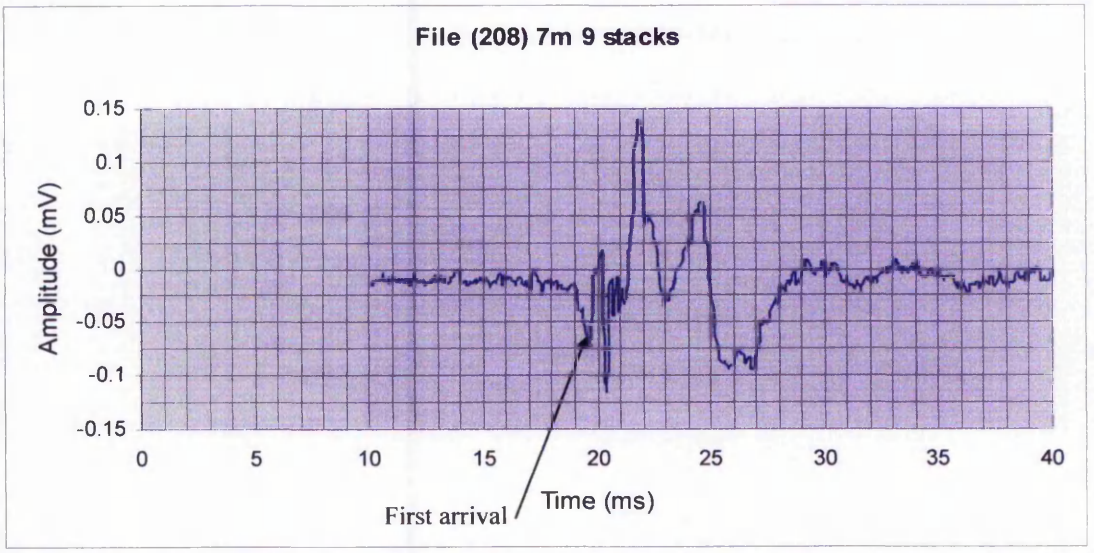

Figure 4.8 EK responses at 7m from the shot point. Note the first arrival at 19.25 ms and the EK responses following up to 35 ms.

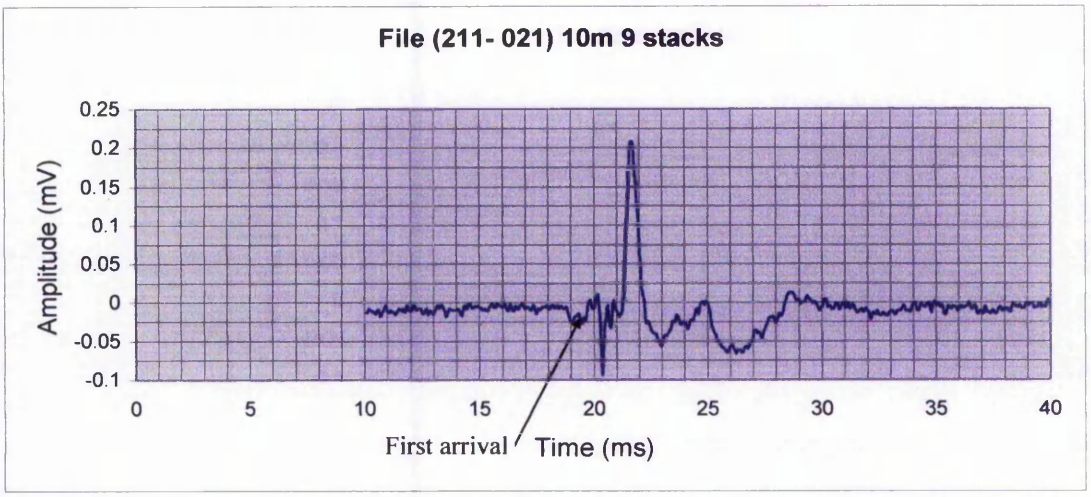

Figure 4.9 EK response at 9m from the shot point. Note the first arrival at 19.25 ms and the EK responses following up to 35 ms.

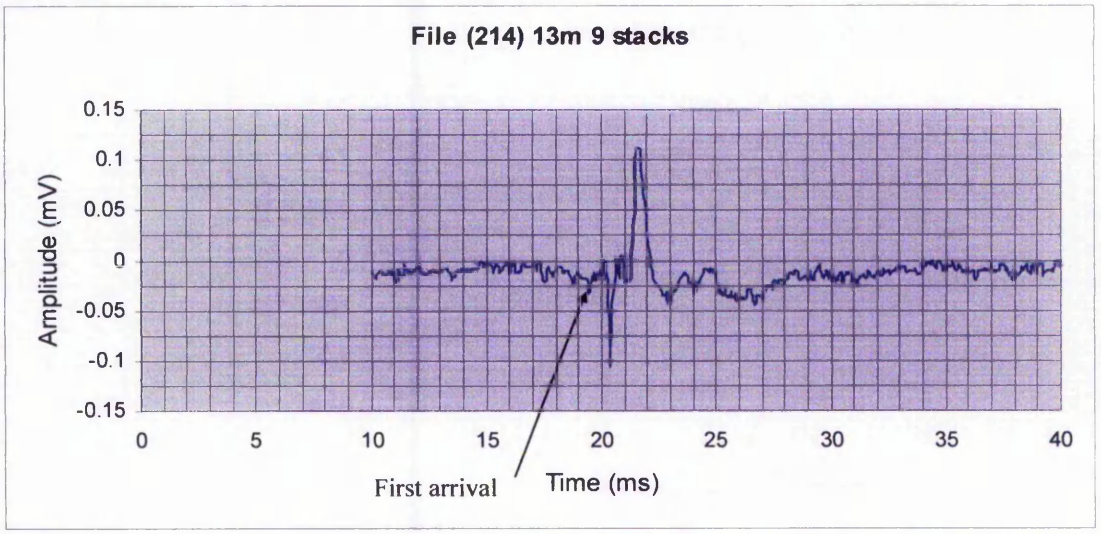

Figure 4.10 EK responses at 13m from the shot point. Note the virtual absence of a response at 19.25 ms.

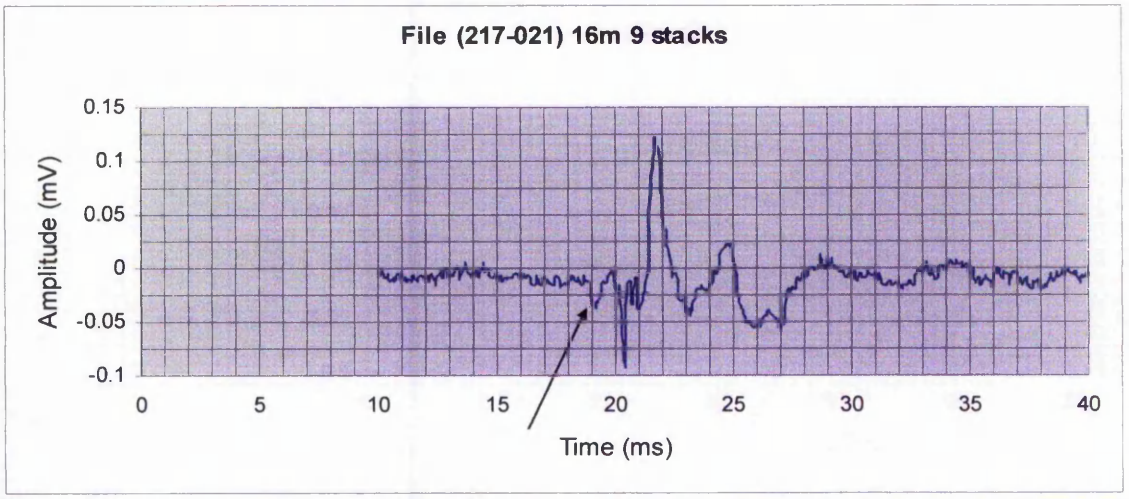

Figure 4.11 EK responses at 16m from the shot point. Note the reappearance of the first arrival at 19.0 ms and the EK responses following up to 35 ms.

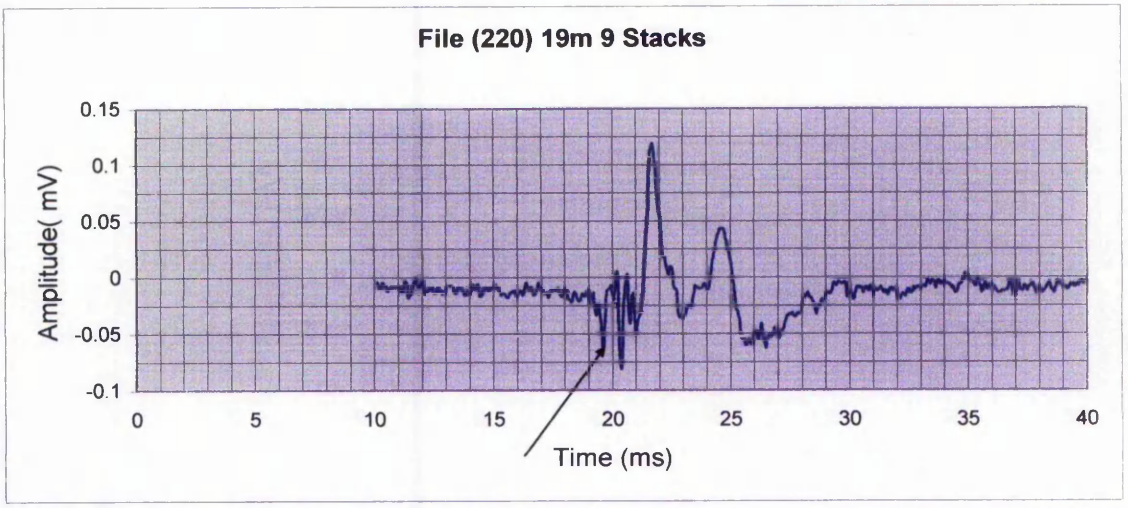

Figure 4.12 EK responses at 19m from the shot point. Note the first arrival at 19.25 ms and the EK responses following up to 35 ms.

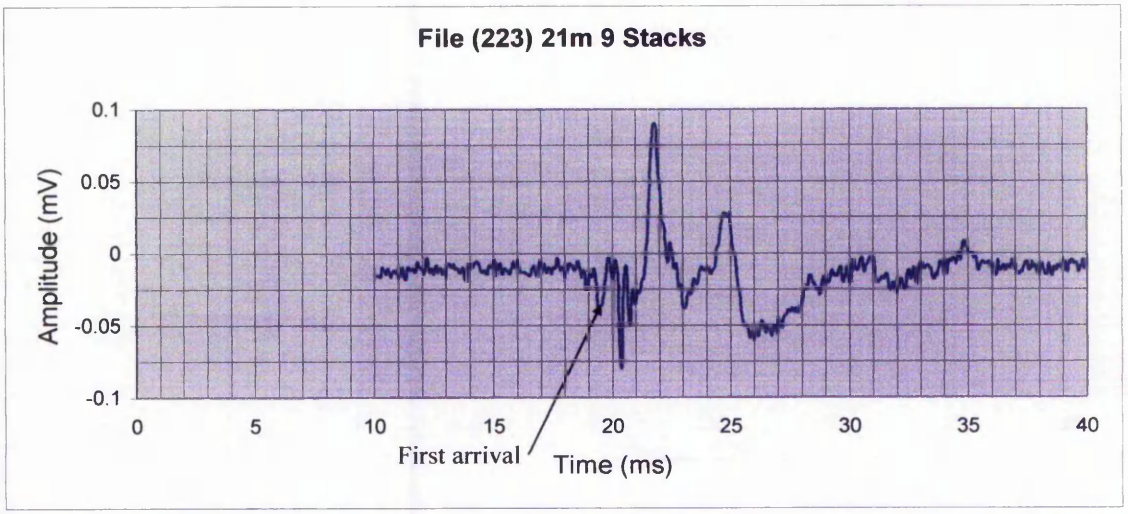

Figure 4.13 EK responses at 21m from the shot point. Note the first arrival at 19.25 ms and the EK responses following up to 35 ms.

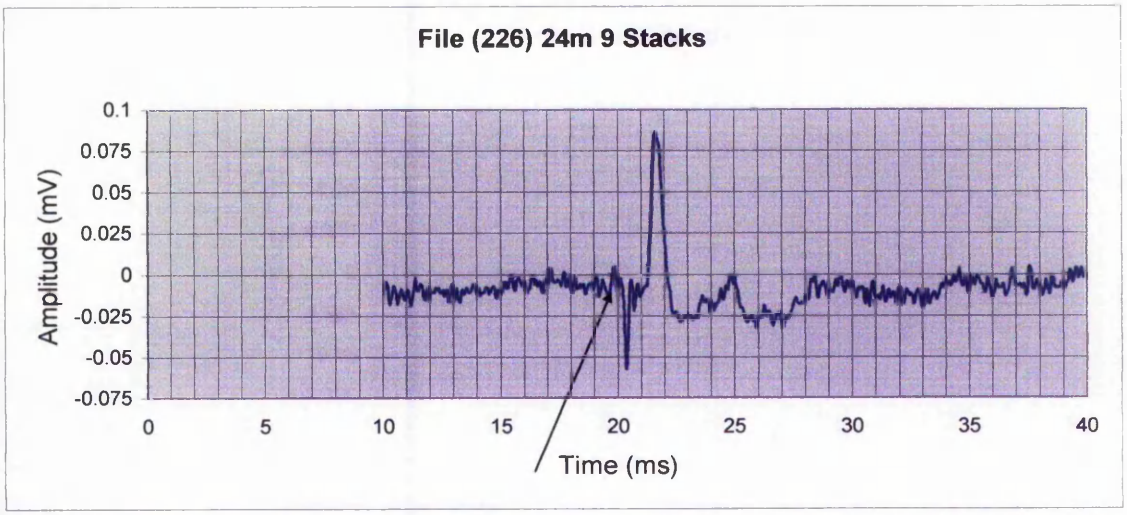

Figure 4.14 EK responses at 24m from the shot point. Note the virtual absence of first arrival at 19.25 ms and the EK responses following up to 35 ms.

Careful examination of all of the EK responses, figures 4.6 to 4.14, clearly show that there is no evidence of move out of the first arrival over a distance of the survey of 1 to 24 metres. There is some evidence of EK responses occurring earlier, as apparent at 10.5, 12.0 and 15 .0 ms on figure 4.13.

To gain a clearer understanding of the dipole field distribution it was decided to carry out a plot of the full off of EK amplitude response with distance away from the shot point. This was done to determine the nature of the amplitude of the EK response. Lorrain and Corson (1970) showed that for a radiating dipole the scalar potential varies as $\frac{1}{r}$ when $r >> \lambda$, where r is the radial distance from the point source and λ is the radian wavelength. For a static electric field the scalar potential varies as $\frac{1}{r^2}$ see (Chapter 2).

Table 4.4 shows the variation of the EK response amplitude with distance away from the shot point. Column 2 is the true distance that the dipole aerial was away from the shot point. The peak EK response was obtained from the first arrival at 19.25 ms.

Table 4.4 Variation of EK in amplitude response with diagonal distance from the shot point.

Dipole aerial distance (m) From bh 32 to 34	Diagonal distance (m) from bh 33 to EK aerial position	Tan(90-φ) Degrees	EK peak response (mv)
1	9.950377	84.33	- 0.10
3	10.34456	73.14	- 0.08
7	12.12477	54.74	- 0.053
10	14.0716	44.71	-0.020
13	16.34044	37.29	- 0.006
16	18.81515	31.75	-0.025
19	21.42452	27.75	- 0.050
21	23.22	25.40	- 0.0676
24	25.9617	22.42	- 0.063

The results in table 4.4 are presented in figure 4.15 a sixth order polynomial curve, in order to see the significance of the higher order terms. The dominant term is seen to be 'x' with a small contribution from x^2. In the analysis for the propagation of a time varying electromagnetic (EM) wave in Chapter 1 it was shown that the amplitude of its peak fell off as a function of $\frac{1}{r}$ where 'r' is the vector from the centre of the dipole to the point in question. The only condition on this criteria is that $r >> s$ where s is the separation between the two charges. Typically the charge separation is in the order of 20

– 70 Å, i.e. one angstrom (Å) = $1x10^{-8}$ m see (Chapter 1) and is a factor of 10^9 times smaller than the diagonal distance.

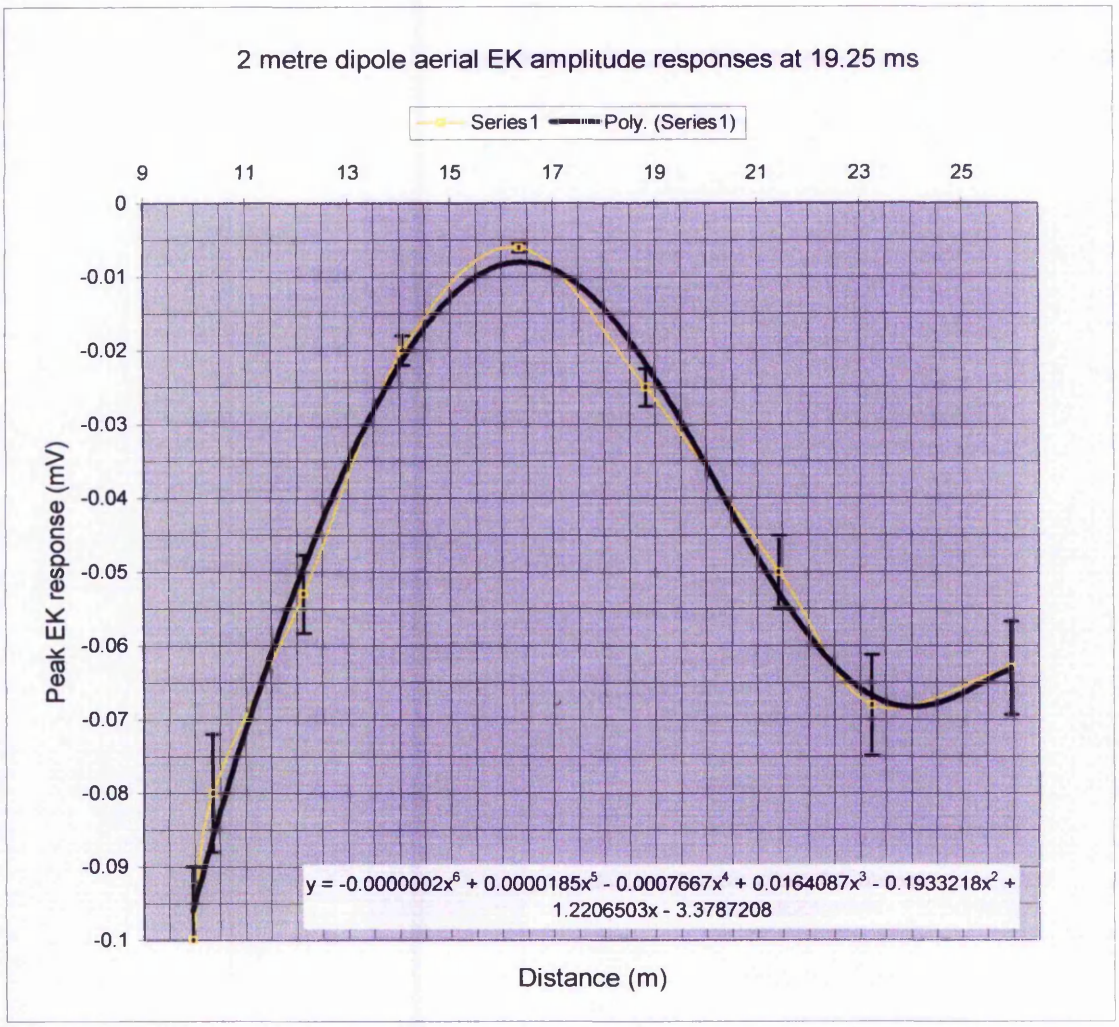

Figure 4.15 Plot of EK amplitude responses at 19.25 ms. Note the dominant terms in x^2 and x.

Further EK investigations were conducted in order to observe the effect on the EK response of rotating the dipole aerial clockwise through 90°, the results are shown in figures 4.16 to 4.18 for the EK responses from 19 metres to 24 metres.

As in the previous EK recordings the shot point was at borehole 33. Careful examination of the above figures 4.16-4.18 clearly indicate an increase in amplitude of the EK response with a 90 degree rotation angle and no EK move out with distance away from the shot point. This is due to the orientation of the dipole aerial in relation to the dipole electric field generated at its source. This is due to the dipole capture pattern becoming more preferentially aligned with the polarisation of the propagating EK wavefield. The extent of the electric dipole field can be seen by noting the decrease and then increase in amplitude of the EK response with distance away from the shot point.

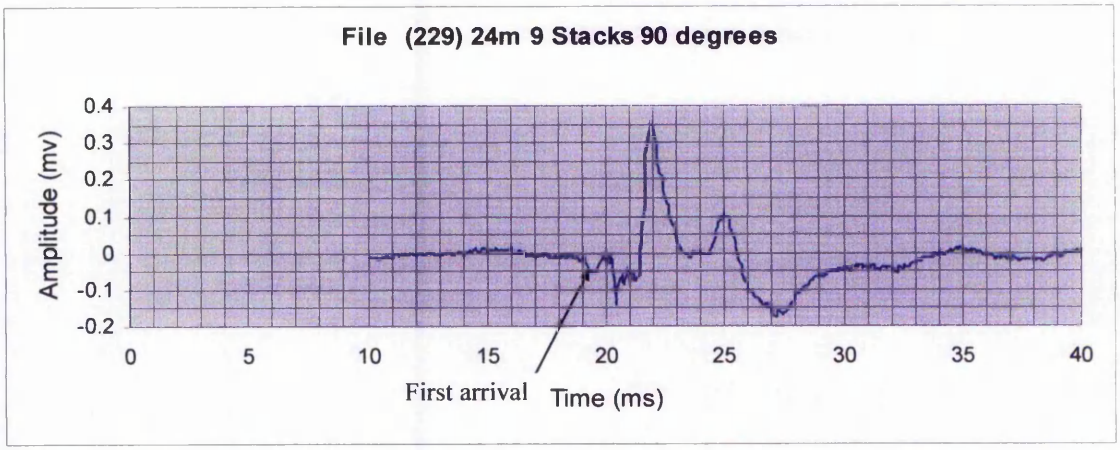

Figure 4.16 The amplitude distribution for the first EK response at 19.25 ms, at 24m from the shot point. The shape of the response clearly shows a dipole field.

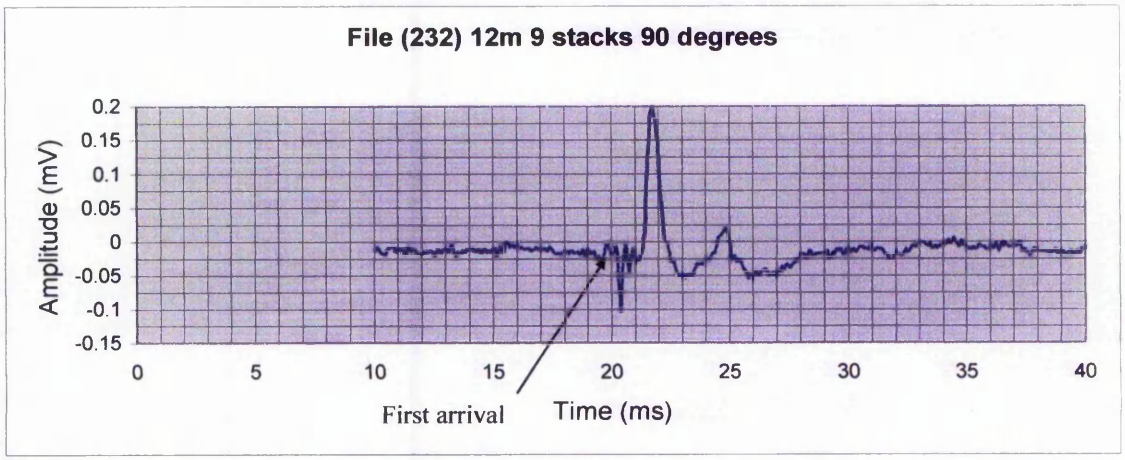

Figure 4.17 The amplitude distribution for the first EK response at 19.25 ms, at 12m from the shot point. .Note the small amplitude of the response at 19.25 ms

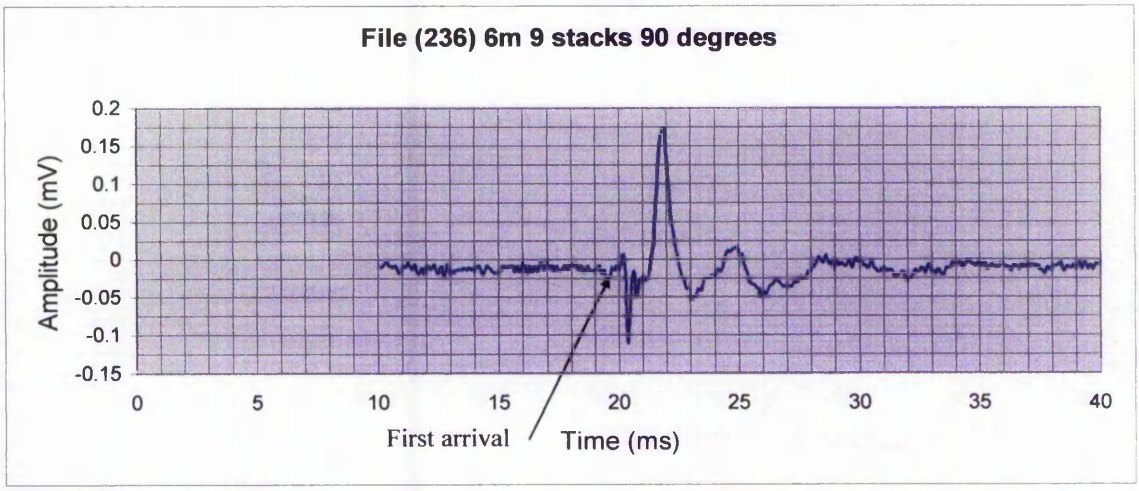

Figure 4.18 The amplitude distribution for the first EK response at 19.25 ms, at 6m from the shot point. Note the amplitude of the response at 19.25 ms

4.5.3 *New dipole aerial EK response profile.*

Before designing a new improved dipole aerial a test was carried out using two 3 metre lengths of standard 15 mm copper plumbing pipe. Figure 4.19 is the response of this test antenna. The region P1 to P2 is due to 50 Hz mains pick up. However, this can easily be removed by the noise removal program described in Chapter 8. Note the considerably increased amplitude response of the EK signal relative to figure 4.2. There is a two order of magnitude increase in the amplitude of the EK response and a significant improvement in the signal to noise ratio. By adding more one metre section pairs to the dipole the EK response would be increased in direct proportion to the increase in length.

The response obtained was considerable and an immediate decision was made to design an improved version that could be easily deployed in the field. This was described in Chapter 2.

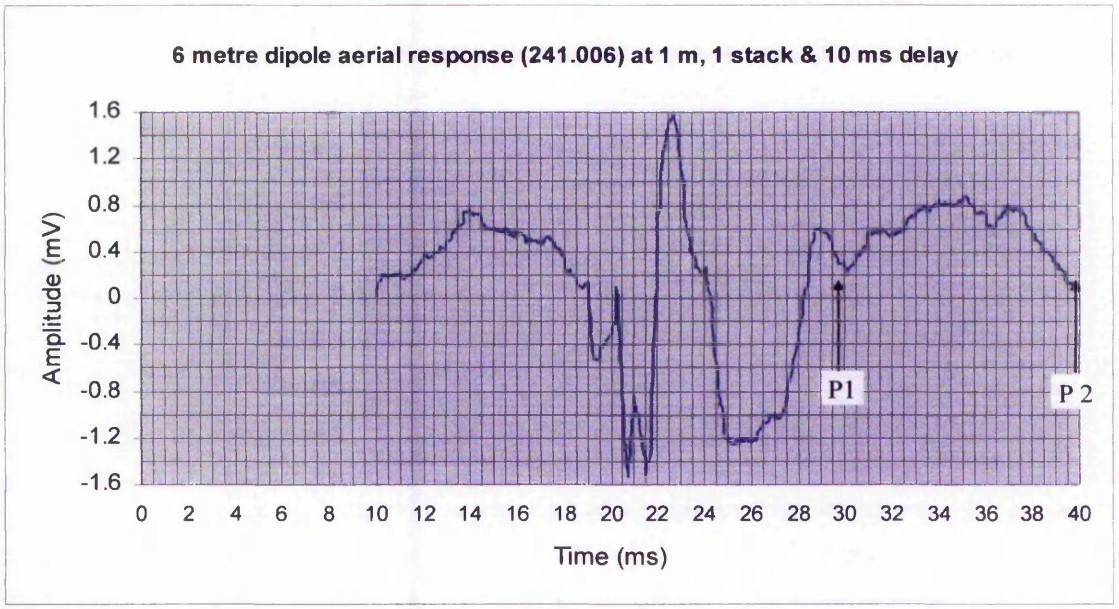

Figure 4.19 EK response of 6 metre 15 mm cu dipole aerial, 1 metre from the shot point.

In order to see if there were any further EK responses at greater depths the whole of the EK response profile for the recording period of 138 ms is shown in Figure 4.20. Careful observation of this response shows possible EK responses at 118ms, 58 ms and 48 ms.

Figure 3.3 in Chapter 3 shows the subsurface geology near to where these EK investigations took place. Calculations indicate these responses at 118 ms might come from the region shown at 320 m depth. However, it is realised that the seismic attenuation would be considerable and any seismic energy reaching these depths would

be very small indeed. Therefore this signal is unlikely to be from this depth.

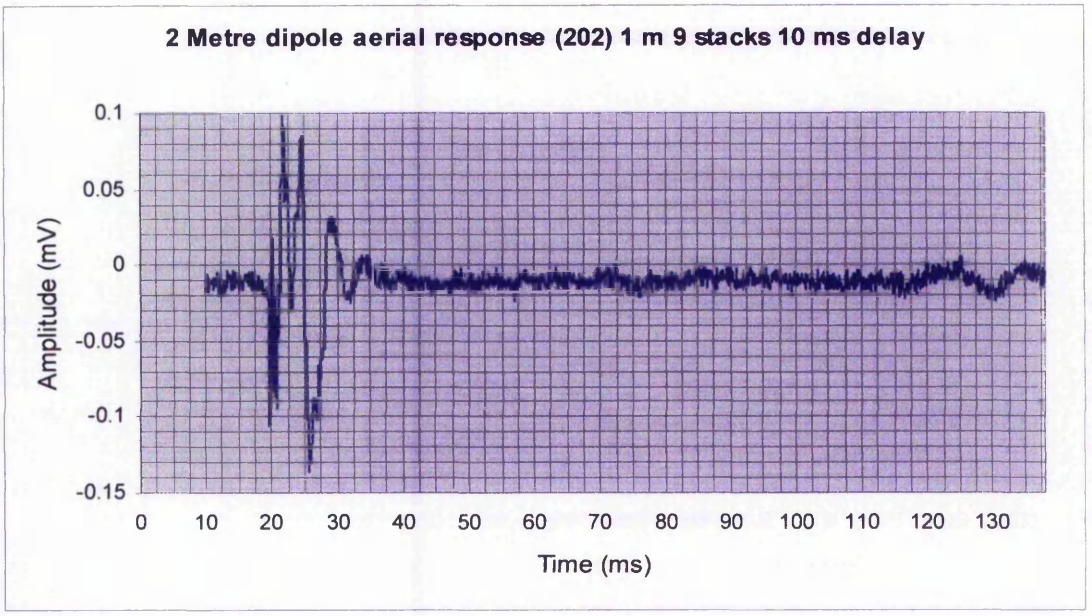

Figure 4.20 This figure is included to show details of the whole recording of 138 ms. Note the details in figure 4.23.

4.5.4 *Seismic refraction investigations.*

A seismic refraction survey close to borehole 32 was carried out in order to determine the seismic velocities down to at last 5 metres below the depth of the water table. This was to enable the travel times through the various layers down to the water table. This data would then be compared to the time of the of the EK responses in order to relate them to geological features. Details of the seismic survey are shown in graphical form figure 4.21. The data points for the first arrivals, shown in the coloured boxes, were picked form the wriggle trace shown in Appendix J. The slope of each line in figure 4.21 is $\frac{\text{Time}}{\text{Distance}}$ therefore the reciprocal of the slope will give the velocity. Linear trend lines have been applied to the data in order to determine the average velocities and time intercepts. The results are given in table 4.5.

For the direct wave the error bars are ± 10%, and the refracted wave ± 4%. The geophones were carefully laid out using a surveying tape. The geophone spacing error is estimated as no more than ± 0.5%, therefore this error was ignored.

It can be seen from the borehole log (Chapter 3 table 3.3) that the top 1.00 metre or so was composed of sandy loam with pebbles that extend down to 9 metres. The details of

the borehole log, in the range 9-13 metres, were absent from the records provided, unfortunately this coincides with the data in row 2 of table 4.5.

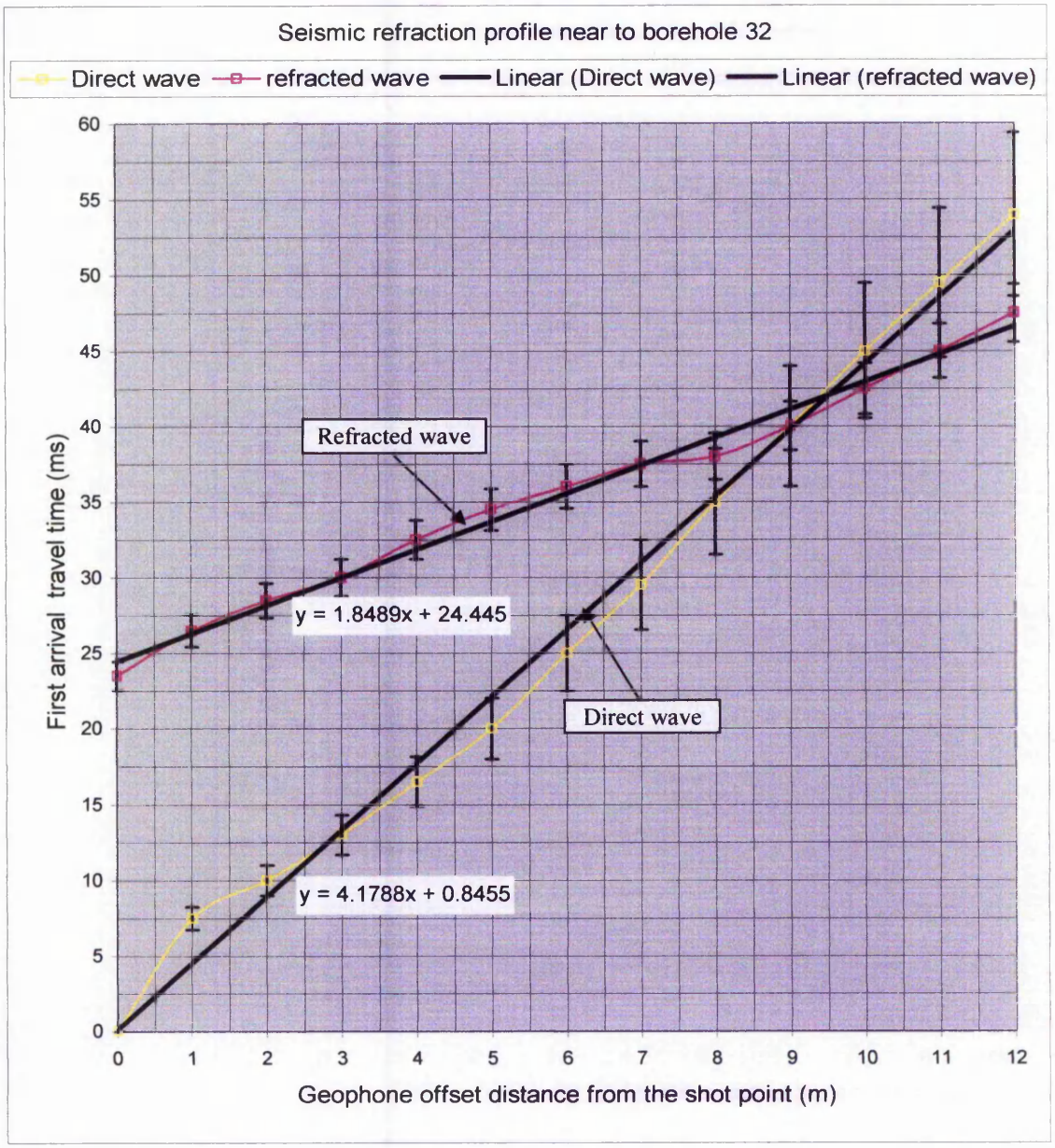

Figure 4.21 Graph of results of seismic survey. The geophone spacing for this data was 1 metre. The error bars for the direct wave are ± 10% and ± 4% for the refracted wave.

Table 4.5. Results of seismic velocities and related depth of layers obtained from figure 4.21.

Series	Slope of lines	velocity (v) m/s	Travel time through layers (ms)	Comments	Depth of layers (m)
1	4.1788	239.6	12.44	Topsoil with sand & pebbles	2.98
2	1.7733	541.0	24	First faster layer at 2.98 m	12.02
		Total travel time	33.94 ms	Total depth	15.00 m

The overall travel time down to the water table is 33.94 ms, table 4.5. The depth to the water table was also found from sampling the borehole.

The low seismic velocity of 239m/s in the top layer of 2.98 metres is not unusual for loose topsoil composed of loam mixed with sand and pebbles, Baker *et al.* (1999) reported seismic reflections from depths of less than two metres.

Using the time intercept equation to find the depth Z, $t_i = 2Z\frac{\sqrt{\left(V_2^2 - V_1^2\right)}}{V_1 V_2}$ .....(4.1)

$$\therefore Z = \frac{t_i V_1 V_2}{2\sqrt{\left(V_2^2 - V_1^2\right)}} = \frac{24.7\times10^{-3}\left(133840\right)}{2\sqrt{560^2 - 239^2}} = 2.98 \text{ m} \quad \text{.....(4.2)}$$

The time for the seismic wave to travel from the bottom of the top layers of 2.98 metres down to the water table, a distance Z_2, is found as follows:

$$Z_2 = \frac{(15.0 - 2.98)\text{m}}{560 \text{ m/s}} = 21.5 \text{ ms} \quad \text{..... (4.3)}$$

Total time to travel down to the water table is (12.44 + 21.45) ms = 33.94 ms.

4.5.5 *Determination of errors in the calculations in section 4.5.4*

The errors due to picking the first arrivals are contained within the error bars, shown on figure 4.21. However, the gradient $\frac{\text{time}}{\text{distance}}$ will vary as shown in table 4.6. The upper and lower level of the error bars where used to calculate the values shown.

Table 4.6. Results of calculations to determine velocity and intercept time errors

	+ 10 % error	- 10 % error	Error in intercept
Direct wave	$4.96\text{x}10^{-3}$ms	$4.29\text{x}10^{-3}$ms	N/A
Velocity	201.6 m/s	244.5 m/s	N/A
	+ 4 % error	- 4 % error	
Refracted wave	$1.71\text{x}10^{-3}$ms	$2.16\text{x}10^{-3}$ms	$0.46\text{x}10^{-3}$ms
Velocity	585.0 m/s	460.0 m/s	0

Using the velocities in table 4.6 to calculate the maximum and minimum errors in the arrival time of the seismic wave at the water table gave figures of:

Minimum time to water table = 32.39 ms..... (4.4)

Maximum time to water table = 40.2 ms.....(4.5)

Another factor which could also affect the above results was the possibility of a faster layer at a lower depth. This could only be verified by a seismic refraction survey over a greater distance. However, if this should be the case then it would have the effect of reducing the travel times in the results 4.4 and 4.5.

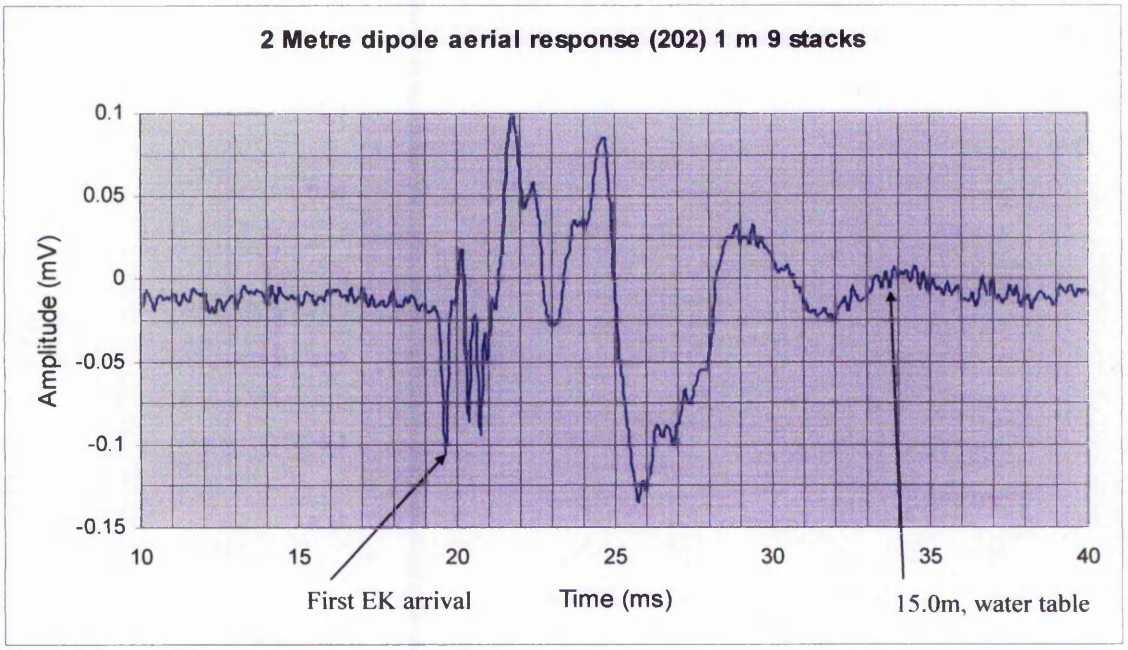

Figure 4.22 Location of main EK events relating to depth

Figure 4.22, with has the time scale expanded for clarity shows, shows the range of EK responses occurring up to 40 ms. It was not possible to correlate these responses with the data obtained from the seismic investigations due inability to resolve fine detail. The first arrival time is seen to occur at 19.25 ms. There are a number of EK responses following on from the first arrival and a faint EK is seen to exist in the vicinity of the water table response. However, allowing for an overall error of ± 10% and the possibility of a faster lower layer the EK response observed at 28.3 ms could be that arriving at the water table.

4.5.6 Summary of the EK investigation results for Mansfield.

The preceding results show not only virtually zero move out of the first arrival of the EK wave in all of the results for the EK response but also a possible correlation with other features such as fracture zones. However, although the responses are real, are unverified.

The depth of detection of EK responses has been shown to be more the original target of 20 metres (figure 4.20) where responses are evident out to 35.5 ms which corresponds to a depth of 28.5 metres. It is perfectly feasible that an EK response can be achieved at greater depths by increasing the number of stacks up to the order of 49 or more and by increasing the dipole length or both. However, it must be bourn in mind that approximately 65% of the seismic energy is lost due to the surface wave. For penetration of the seismic wave to greater depths a source which will impart more energy into the ground would be required, such as a drop weight or explosive charge.

During EK investigations at the Mansfield site it has been observed that the EK signal amplitude decreases with the number of rapid hammer blows. This was observed on more than one occasion. However, it was observed that is the rate of striking the hammer plate was reduced to once every 10 seconds this did not happen. It is likely to be due to electrical charge polarisation and depolarisation times within the double layer.

This can be explained by the movement of the ionic charges of the soil grains due to the passing seismic wave which have a finite drift velocity depending on the following:

1 The velocity of the disturbing source. Typically 300 to 5000 m/s

2 The viscosity 'η' of the medium.

3 Particle radius.

In general, when a particle is exposed to suddenly applied external force, a finite length of time is required for the particle velocity to reach that of the applied force. This can be compared to the case of the rise of the voltage across a capacitor when a suddenly applied voltage is applied across series capacitor resistance network, the rise of the voltage across the capacitor being governed by the following equation:

$$v = V_{max}(1 - \exp^{-t/cr}) \qquad (4.6)$$

where t = time, v is the voltage across c, r is the series resistance and V_{max} the maximum

applied voltage.

A point to note is that time constant of the series capacitance resistance circuit is defined to be the time it takes v to reach 0.5 V_{max}. Manipulation of equation 4.6 will show the time constant to be 0.69CR.

It is possible that the particle velocity will not have sufficient to reach the velocity of the applied force if the time the applied force is present is small compared to the ionic drift velocity. Similarly, when the applied force is removed the ion will take a finite time to return to its equilibrium state. The equation for the capacitance resistance network being in this case:

$$v = V_{max} \exp^{-t/cr} \qquad (4.7)$$

Figure 4.23 illustrates this effect.

Therefore, if the duration of the applied force << velocity polarisation time and the reapplication of the force << than the velocity depolarisation time of the particle then it is feasible the phenomena observed are due to the above mechanism as polarisation and depolarisation times in the order of seconds are not unusual (Dekker, 1967).

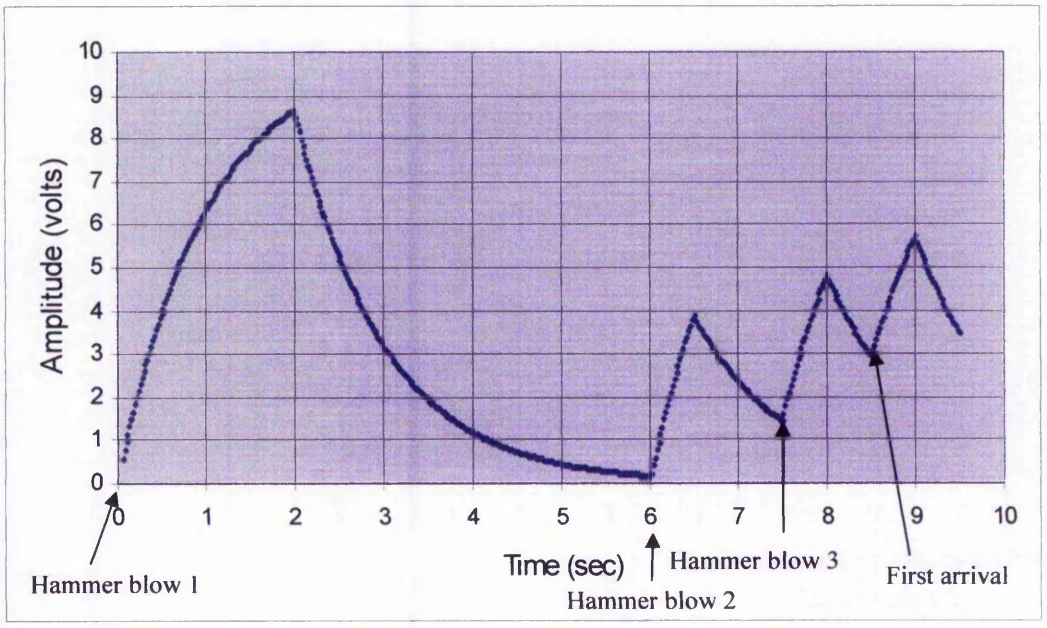

Figure 4.23 Effect of double layer charge polarisation and depolarisation on frequency of seismic hammer blows

Another observation while conducting these EK investigations was that as the number of hammer strikes increases, the signal amplitude increases, but the peak resolution appears to decrease, i.e., gets broader.

Although one day was spent carrying out these EK investigations a wealth of information was obtained. The success of these investigations has provided the led to a number of further possibilities for EK investigations including estimation of ground permeability and location of underground fractures. The location of fracture zones is particularly important when undertaking *in situ* permeability tests.

4.6 Ospringe in Kent

4.6.1 *Introduction to Ospringe EK investigations*

A geophysical and geotechnical survey was undertaken to assess the effects of compaction on Loess (brickearth) at Ospringe near Faversham in Kent. This section presents selected results of the EK investigations data collected from the various techniques used with a comparison of the different methods used and degree of correlation obtained. The site was originally chosen because of the significant loess deposit which lies on impermeable strata, the geological description of the site being given in Chapter 3 section 3.3.2. It also offered the opportunity to conduct tests with the new EK dipole aerial.

A number of geophysical and geotechnical investigations were conducted at this site over the period 9th to 12th October 2001. The techniques used were standard cone penetrometer test, German dynamic plate test, Prema dynamic plate test, a 'Geometrics' SM43 R24 seismic recorder was used for the seismic survey, using both horizontal and vertical geophones, and electro-kinetic measurements using the new adjustable length dipole aerial. In addition, a suite of other investigative tests were undertaken by the British Geological Survey (BGS) at this site. These included EM31/34 profiles, Standard Cone Penetrometer (SPT), small scale localised shear wave and resistivity. (Northmore *et al.* 2005 for details).

The investigations at the site were referenced to the location of the seismic hammer point (shot point) used during the geophysical surveys. A Global Positioning Satellite (GPS) reading was taken on the position of the seismic hammer plate, near to borehole

10 on the site map. The GPS reading was TQ 99592, BRG 61192 with an altitude of 42 metres. The boreholes marked out on the site map were no longer visible on the site, (Chapter 3, figure 3.5). It was noted there were no electricity pylons or overhead lines nearby. However, there was a railway line running east to west along the north side of the site, which was possibly electrified. This may be a possible cause of electrical interference.

4.6.2 Survey locations and additional details

As indicated on the sketch map of the site in Chapter 3 figure, 3.5 of the site, two main survey lines were used for all of the investigations in the quarry. The site was still very wet as a result of heavy rain a few days prior to the visit.

When initially appraising the site, and before commencing with the geophysical and geotechnical testing, a 30 metre strip of loess at the southern end of the quarry was chosen as being most suitable for compaction. The west-east survey line was selected for the main seismic survey, as this part of the quarry was most accessible and suitable for compaction. For comparison, a seismic survey on the SW-NE line was also performed. The seismic hammer plate (same point used for both surveys) was located at western end of the line. Plate 4.1 shows the west-east seismic line looking west.

Plate 4.1. Photograph of survey site taken from the edge of the quarry looking north-west. The author can be seen in the top left of the photo with the seismic recorder, orange box, and geophone spread. The yellow line in front of the author is the EK dipole aerial.

This line was laid out with shot point near to the location of BH10 and the line passing near to boreholes 14, 18 and 21. A sketch map of the borehole layout and the log data for boreholes 10, 14, 18 and 21 are provided in figure 3.5 and table 3.4, Chapter 3.

The samples taken for laboratory tests were taken from the pile of soil shown above middle left. Further soil samples were carefully dug out after the compaction and measurements were made. These were extracted halfway down the seismic line shown above in plate 4.1. A little more to the left of centre left, just off the edge of fig 3.5, is where the photograph, shown in plate 3.3. Chapter 3 was taken.

4.6.3 *Ground compaction*

The contractor engaged was unable, at the last minute, to supply a standard two-ton compaction rig. To carry out the work as planned, the ground was compacted, approximately 1.5 meters either side of the survey line, using an old cast iron pulley block system found on a nearby site, approximate weight 700 kg and a JCB, plate 4.2. The JCB was driven over the compaction area in order to level it and to consolidate the compaction. This led to inferior compaction being accomplished, than had been initially planned. Also of note is that the quarry floor surface had suffered considerable disturbance during the quarrying process, (plate 3.2 Chapter 3).

Plate 4.2. Photograph of the investigation site being compacted

However, compaction was exhibited to a depth of 0.8 m. Despite the problems with the method of compaction used sufficiently useful results were gained to demonstrate the success of the methods employed.

4.6.4 *Geophysical and geotechnical investigation methods employed*

(1) Shallow seismic refraction

Seismic surveys were conducted using both horizontal (shear-wave) and vertical (P-wave) geophones. These data were necessary in order to calculate the ground stiffness, shear wave data, P-wave data and under lying velocity profiles. The results for the P-wave data were used to correlate the EK responses with both pre and post compaction results. Data from such seismic surveys can yield information relating to the properties of the ground material, including seismic velocity, which is related to material density, shear modulus, and depth to various layers within the ground.

(2) 'Keros' Prima 100

The Prima 100 is a portable non-destructive test usually used for sub-grade assessments, involving the dropping of a weight onto a bearing plate. The force on, and deflection of the plate are measured, and a value for the stiffness (in effect the 'modulus of elasticity' or 'Young's modulus', E) of the ground calculated.

(3) German Dynamic Plate Test (GDP)

The German Dynamic Plate Test (GDP), also known as the Light Drop Weight Tester is a similar, but smaller, device to the Prima. The GDP differs from the Prima in the way ground stiffness is calculated.

(4) Dynamic cone penetrometer (DCP)

The DCP is a well established geotechnical device used for measuring the ground material resistance to the penetration of a metal cone, in terms of mm/blow, whilst the cone is being driven into the ground by a series of blows from a fixed weight dropped from a fixed height. An indication of soil strength and bearing capacity can be determined from DCP results.

(5) Laboratory tests.

Laboratory tests were carried to determine bulk density and moisture content and dry weight bulk density.

(6) Microscopic investigations

Microscopic investigations of the soil were carried out to determine the grain size distribution, other minerals presents and nature of chemical bonding.

4.7 Ground investigation results.

4.7.1 *Seismic*

The graphic results of the seismic profiles are presented in figures J1 to J5 Appendix M. The seismic velocities obtained from figures J1 to J5 are summarised in table 4.7

Table 4.7. Results of analysis of seismic profiles

Location	Wave type	Vel. m/s	Notes
Line 1	Pv_1	286 m/s	Uncompacted. Ground disturbed and uneven.
"	Pv_2	336 m/s	Uncompacted. Faster layer at a calculated depth of 0.58 metres.
"	Pv_3	465 m/s	Uncompacted. Faster layer at a calculated depth of 0.96 metres.
"	Sv_1	295 m/s	Uncompacted
"	Sv_2	699 m/s	Faster layer at depth of 4.47 metres
"	Pv_1	1.167 m/s	Compacted
"	Pv_2	235 m/s	Compacted slower layer at calculated depth of 0.697 metres
"	Pv_3	352 m/s	Faster layer at calculated depth of 0.96 metres
"	Pv_4	312 m/s	Slower layer implies hidden layer
Line 2	Pv_1	357 m/s	Uncompacted. Ground disturbed and uneven.
	Pv_2	791 ms	Uncompacted. Faster layer at a calculated depth of 2.03 metres

4.7.2 *Calculation of errors.*

Error bars of 3% are observed to encompass all variations on the slope of line y = 3.5x in figure J.2. Taking into account a ± 3% error, we have the percentage variation in slope given by:

$$\frac{3.5 \times 10^3}{100} \times 3 = \pm 0.0105 \times 10^{-3} \text{ s/m} \qquad (4.8)$$

∴ Maximum and minimum slopes are 3.5105×10^{-3} and 3.489×10^{-3} s/m with resultant velocities = 285 m/s and 287 m/s

Applying the same analysis to the slope given by 2.9786×10^{-3} s/m, a similar variation of ± 3% is observed

$$\therefore \left(\frac{2.9786 \times 10^3}{100}\right) \times 3 = \pm 0.089358 \times 10^{-3} \text{ s/m} \qquad (4.9)$$

maximum and minimum slopes are 3.068×10^{-3} and 2.88×10^{-3} s/m

Resultant velocities = 325 m/s and 347 m/s

Calculating the depth to the first layer taking into account these variations in velocity gives a depth variation of 0.715 m to 0.646 m

Mean depth = 0.681 m

These results will be used to compare the EK responses versus dynamic cone penetrometer results (page 89)

Table 4.8 Reciprocal of slopes for lines in table 4.6.

Pre-compaction results			
Slope of lines	velocity (v) m/s	Travel time through layers (ms)	Comments
3,5	286	2.164	First faster layer at 0.580 m
2.9786	336	0.655	Second faster layer at 0.22 m
2.12427	465	2.762	Bottom of loess 2.1 m
"	465	22.837	To fully saturated zone
Post compaction figure			
1.2649	1.167 ± 24	0.860	First fast layer 0.681
2.35	426 ± 11		To fully saturated zone
2.84	352		

The formulae 4.10 and 4.12 were used to calculate the depth to the various layers for the data in table 4.8

$$\text{Depth of the first layer } d = \frac{t_2 V_1 V_2}{2\sqrt{V_2^2 - V_1^2}} \quad \text{.....(4.10)}$$

$$\therefore d = \frac{2.5\times10^{-3}\times336\times286}{2\sqrt{(336^2 - 286^2)}}\ \text{m} = 0.681\ \text{m} \quad \text{.....(4.11)}$$

Depth of the second layer:

$$d_1 = \frac{t_3\times336\times465}{2\times\sqrt{(465^2 - 336^2)}} - \frac{0.68\times336\times\sqrt{(465^2 - 286^2)}}{286\times\sqrt{(465^2 - 336^2)}} = 0.65\text{m} \quad \text{.....(4.12)}$$

Thickness of second layer = 0.81 -0.58 = 0.23 m

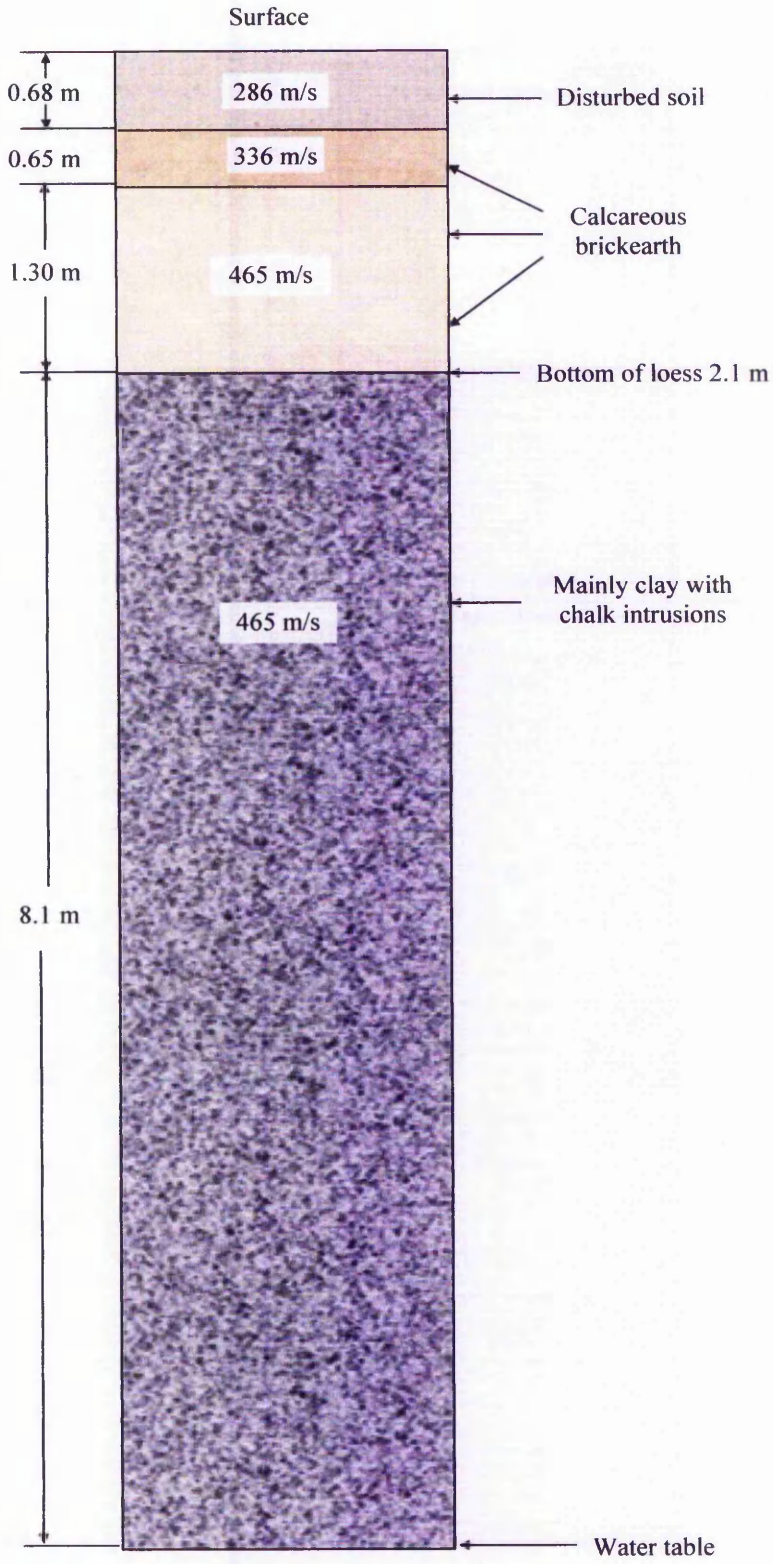

Figure 4.24 Diagram, scale 2cm = 1m, showing the calculated depths and seismic velocities down to the fully water saturated zone.

4.7.3 *Measurement of extent of compaction*

The extent of the compaction was determined using a dynamic cone penetrometer (DCP), figures 4.25 - 4.27, Prima 100 dynamic plate figure 4.28 and German Dynamic Plate, figures 4.29 & 4.30.

The results for all of the DCP locations and other details are listed in table F1 Appendix F with the results some of the DCP investigations are given in figures 4.25 to 4.27. These clearly show the effects of the compaction. Plots were made on all of the other DCP data which displayed similar results, but to save space, only a representative selection are shown here.

As can be clearly seen from figures 4.25-4.27, the depth of compaction is shallow. However, what has been clearly demonstrated is the ability to detect this shallow layer of compaction with a variety of geophysical and geotechnical methods including the new addition of the EK method. However, there needs to be further investigations conducted in differing geological profiles

4.7.4 *Dynamic cone penetrometer results*

A selection of representative graphs for the DCP are shown figures 4.25 to figure 4.27 inclusively.

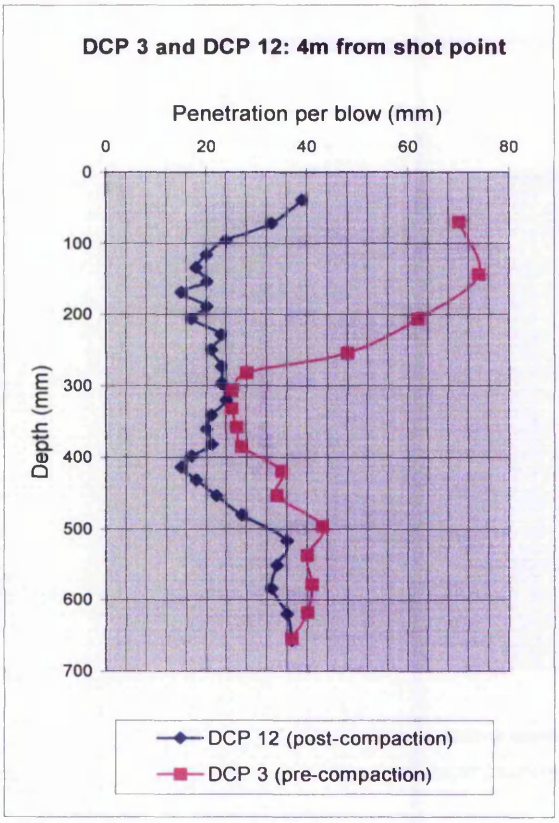

Figure 4.25 DCP 3 & 12 4 metres from shot point

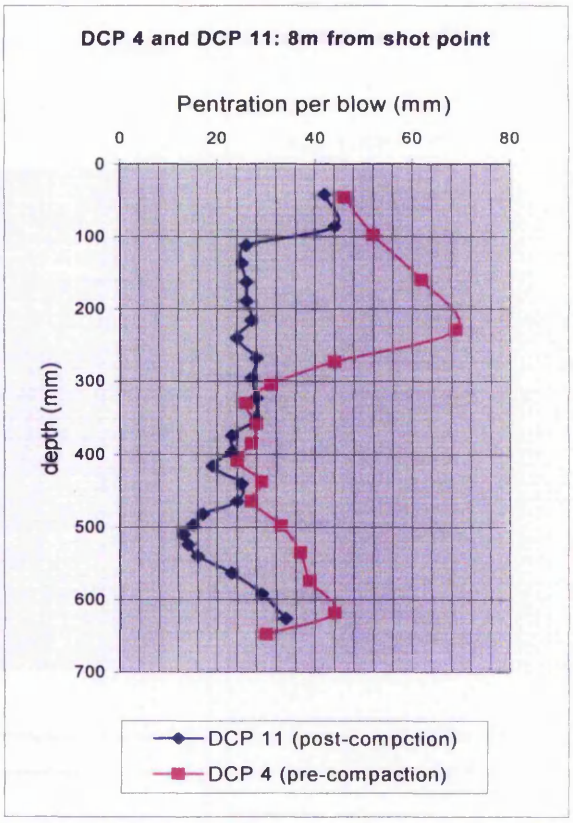

Figure 4.26 DCP 3 & 12 4 metres from shot point

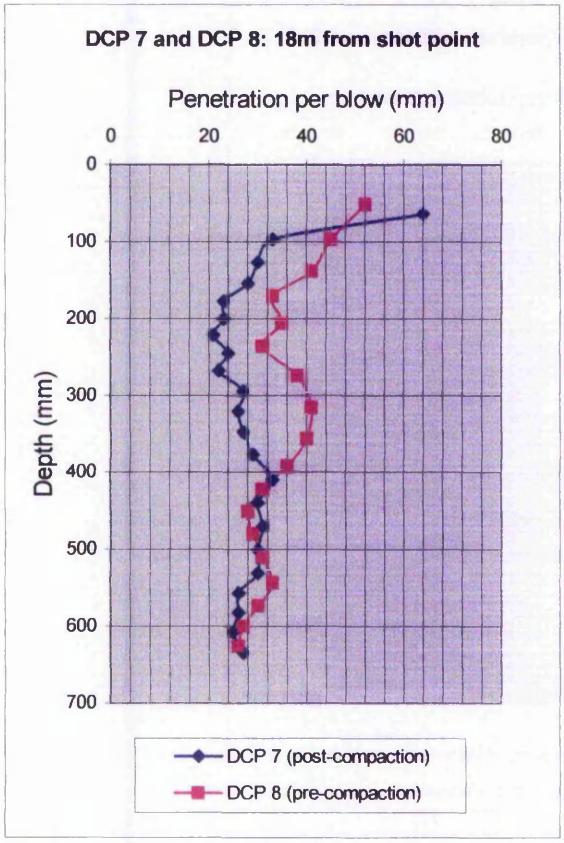

Figure 4.27 DCP 7 & 8 18 metres from shot point

4.7.5 *Prima 100 results*

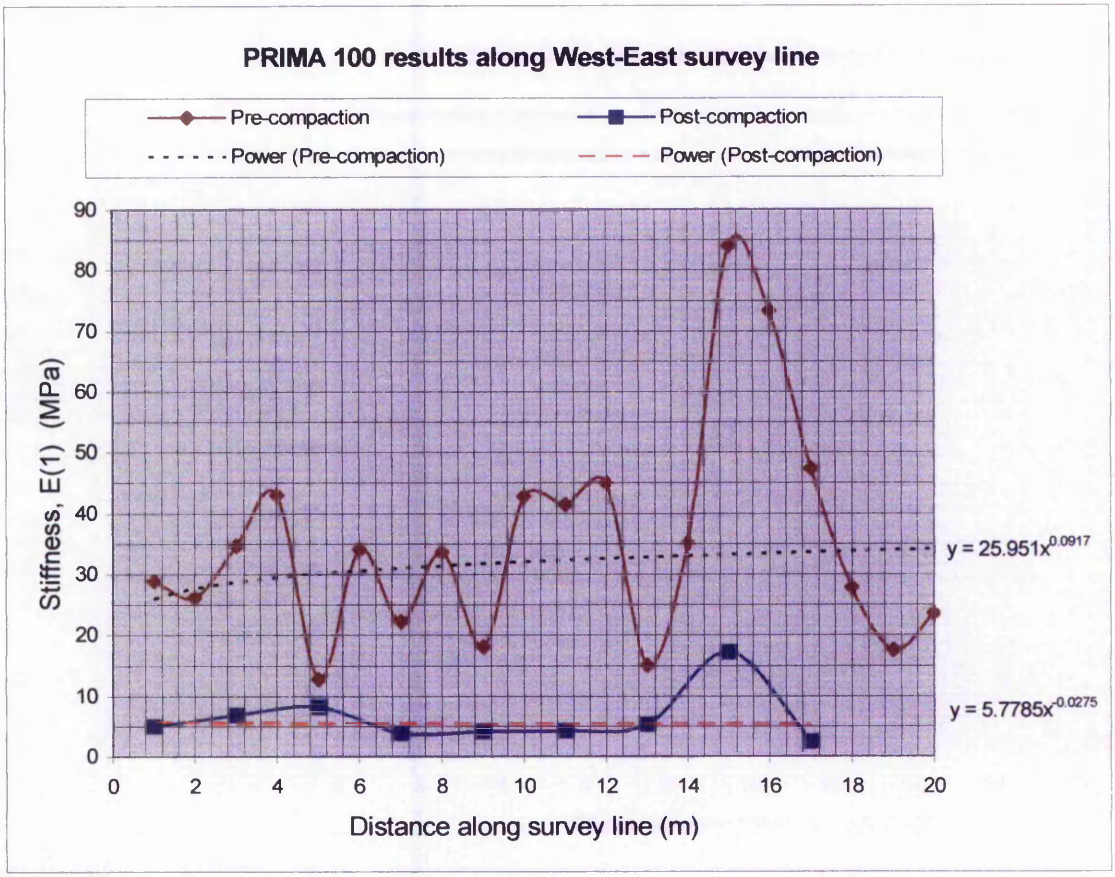

Figure 4.28 PRIMA results pre and post compaction, along west-east survey line

The result in figure 4.28, for the Prima, figure 4.29 and 4.30 for the GDP, clearly show the effects of the compaction although in both figures the stiffness is less after compaction than before. The reason for this is thought to be due to the shallow nature of the compaction, the variability of the compaction over the investigation area and the disturbed nature of the top 50 mm or so of the surface.

The pre-compaction data indicates a great deal of variability along the line of the survey, again this is indicative of the considerable disturbance due to the top layer of loess being removed for brick making purposes. The lower plot shows the effects of the compaction process in which most of the variability has been removed.

The point to notice is the presence of the large peak in the vicinity of 15 metres. This peak is seen to be present in both cases although its amplitude is reduced in the compacted case. One possible reason for the existence of these peaks is the weathered chalk outcrops, (see Chapter 9, P191).

4.7.6 *German Dynamic plate results*

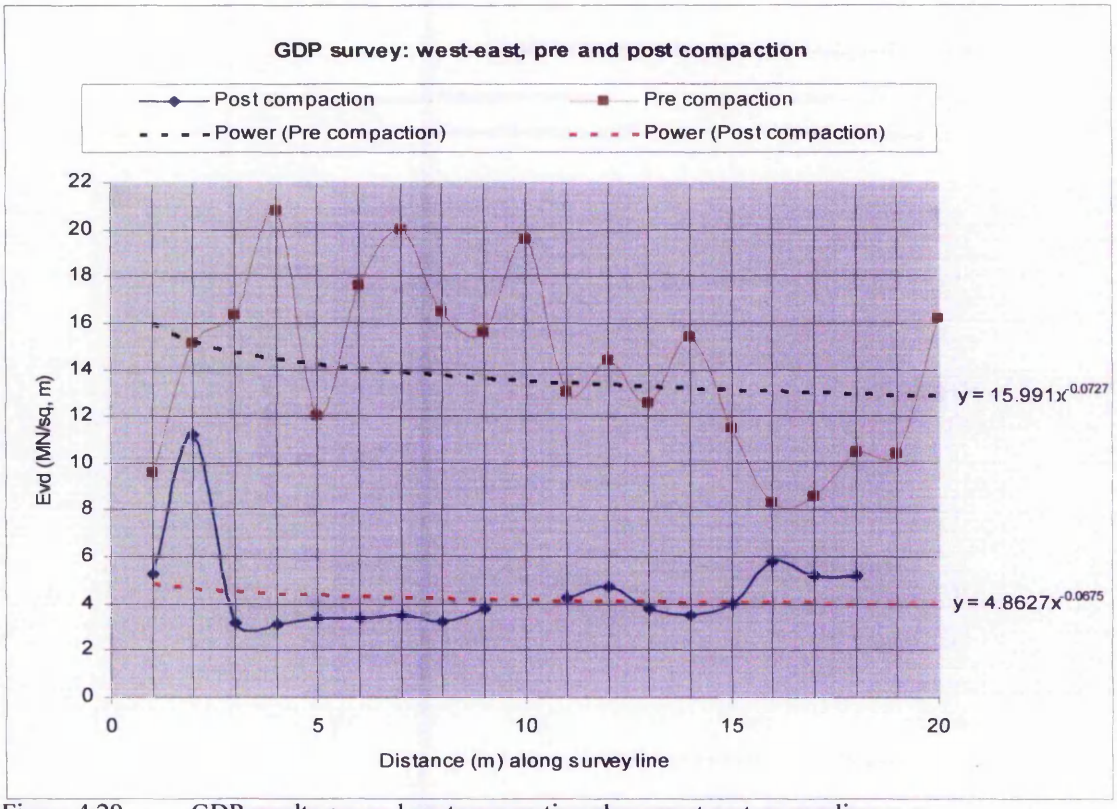

Figure 4.29 GDP results pre and post compaction along west east survey line

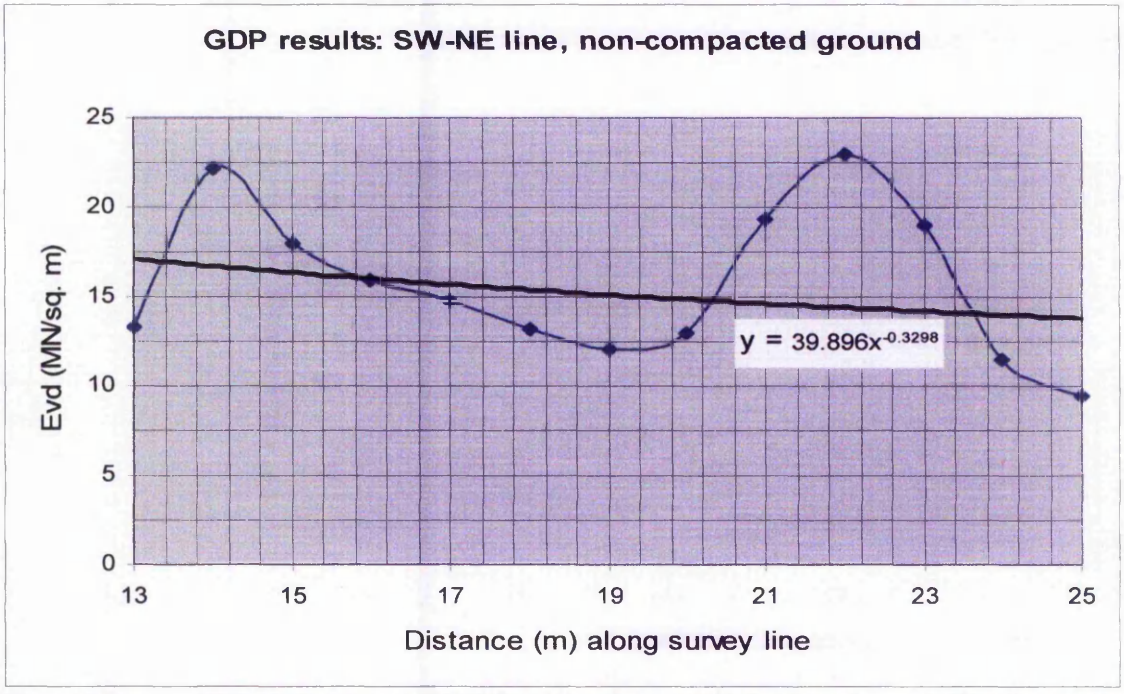

Figure 4.30 GDP results along a line 45° to the east west line. Due to a large puddle of water the results could only be obtained 13 metres from the shot plate.

For the Keros 'Prima 100' the system calculates the E-moduli by the following formulas:

$$E(\text{Centre}) = f \times (1-(\text{Poisson's ratio})^2) \times \text{Contact pressure} \times \frac{\text{load plate radius}}{\text{Deflection}} \qquad (4.13)$$

$$E(\text{Not centre}) = (1-(\text{Poisson's ratio})^2) \times \text{Contact pressure} \times \frac{(\text{load plate radius})^2}{(\text{Deflection radial distance})} \qquad (4.14)$$

At present the stress distribution factor 'f' is the default value of 2 and whilst the Poisson's ratio is preset at 0.35. It is not possible for the user to adjust this although this may be a possibility in a future software update. (Manufacturer's application note). The GDP is in effect an alternative method of determining ground stiffness

4.7.7 *Electro-kinetic*

The results of the EK survey along line 1 are contained in the records 1198 to 1229 Appendix H. An example is the noise recording shown in figure 4.31a and with high frequency noise removed figure 4.31b

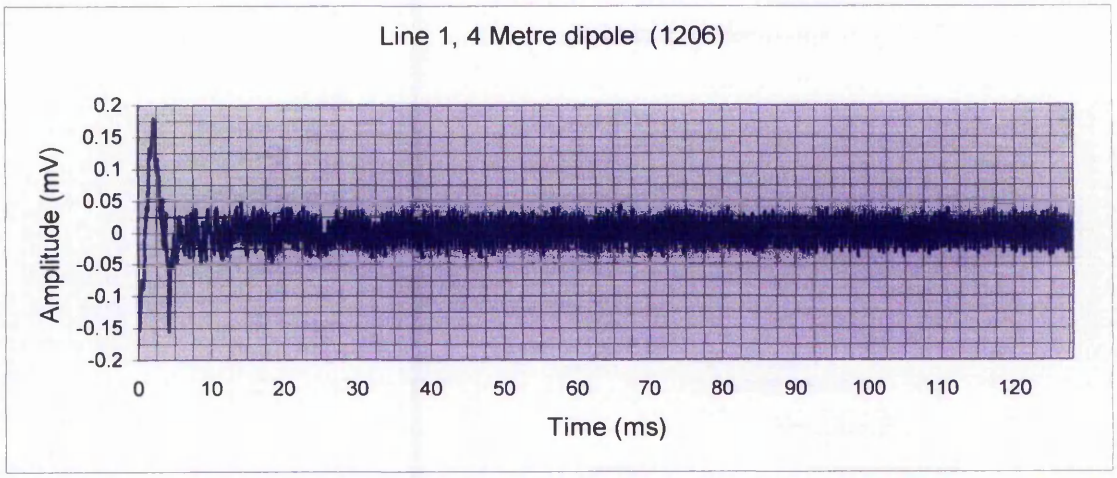

Figure 4.31 (a) Noise recording at 4 metres for the complete recording cycle of 128 ms.

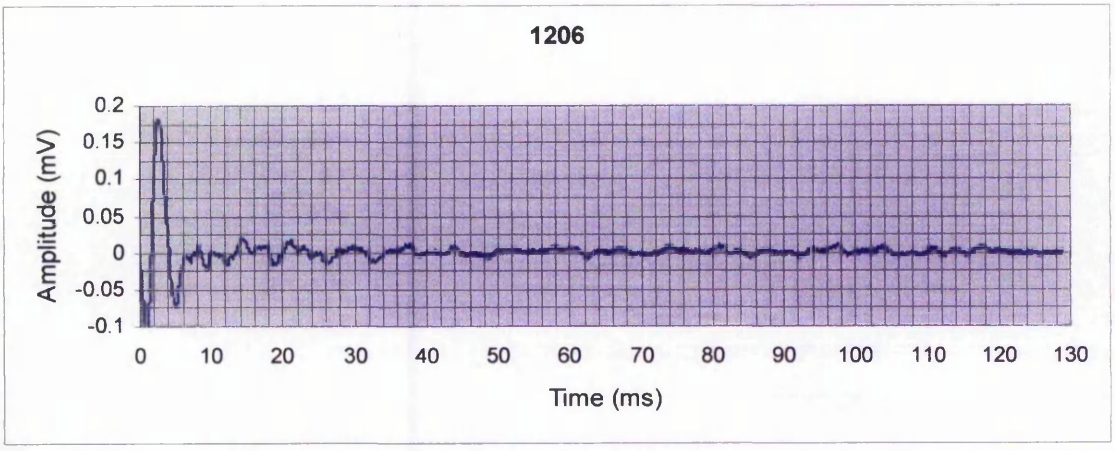

Figure 4.31 (b) Recording 4.32 with high frequency noise removed

The noise recording has a reasonably high frequency component at 1.938 kHz with a peak amplitude of 34 μV. These were determined by the noise removal software in which the frequency components were identified by applying a Fast Fourier Transform (FFT). As it appears to be coherent, it is most likely to be signal pick up from a circuit within the seismic recording system. This is the most likely cause as it was also found that channel three was not working and there was the possibility that other faults were present. The faulty channel was not in itself a major problem as only twelve channels were needed out of the twenty four available. As will be seen later there was additional noise on a number of the EK recording channels that could have come from this source. The response at the start of the recording is due to cross talk from the trigger geophone which was gently tapped by hand to obtain the noise recording.

The EK responses in figures 4.32 to 4.41 represent the pre-compaction state of the site and were taken on the east-west survey line along the edge of the quarry. The 4 metre dipole aerial was used in all cases. Most of the recorded EK responses are presented in order to discuss the some of the more problematic results. All of the EK response recording are raw data with no signal processing applied unless otherwise stated. All the filters on the Geometrics seismic recorder were disabled in order to ensure no distortion of the recorded waveform.

The unevenness of the site must also be taken into account when analysing the arrival times as should the very wet condition of the loess during data collection. All the records have the same time scale to simplify any comparisons made in relation to any EK response. The vertical amplitude scale may vary according to the nature of the EK response.

Recently reported results of an EM survey of the site shows an uneven base layer below the loess, (Northmore et al., 2004). These are data from a site investigation carried out by the British Geological Survey (BGS). It was only possible to include a map of the EM profile it in this thesis (See Chapter 9, section 9.4.7). The details provided by this EM profile have helped in explaining a number of anomalies such as the peak in figure 4.35 at 14 metres and in figure 4.39 at 22 metres.

There was no delay selected for these recording as was the case for the Mansfield data.

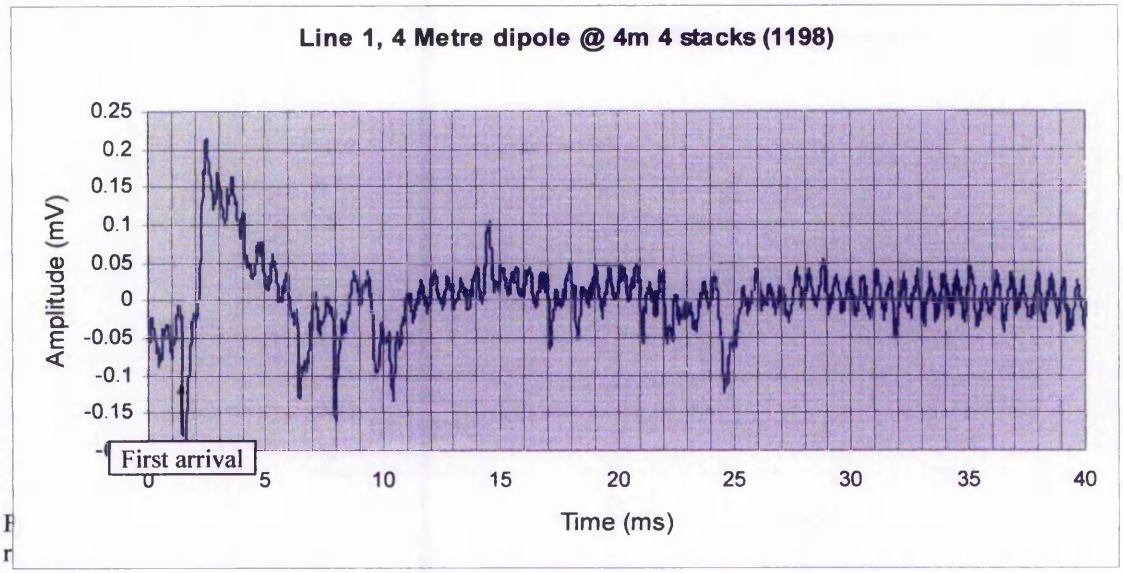

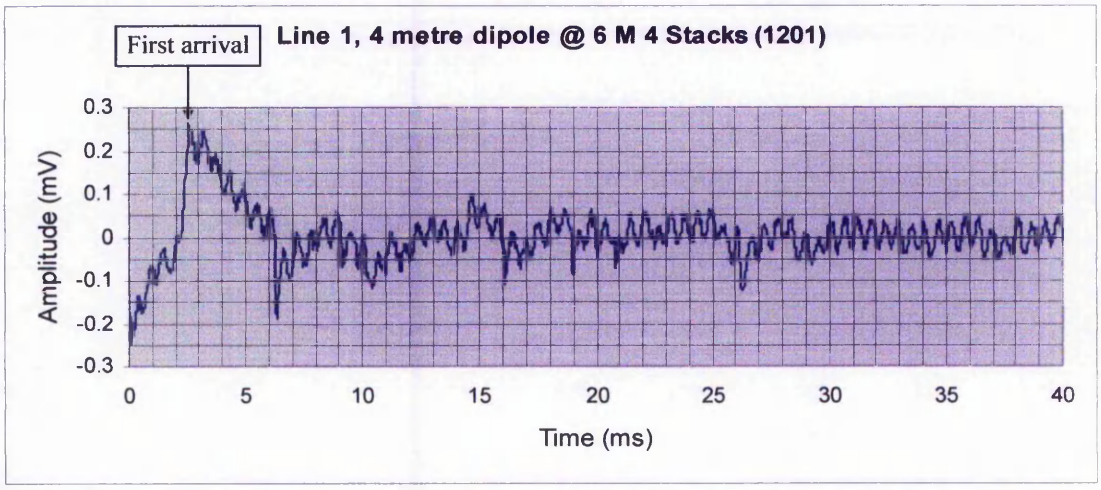

Figure4.33 EK response at 6m from the shot point. Note the first arrival at 2.5 ms and the EK responses following up to 35 ms, also the response at 6 ms and a shift in the response at 24.5 ms in figure 4.32 of + 0.75 ms.

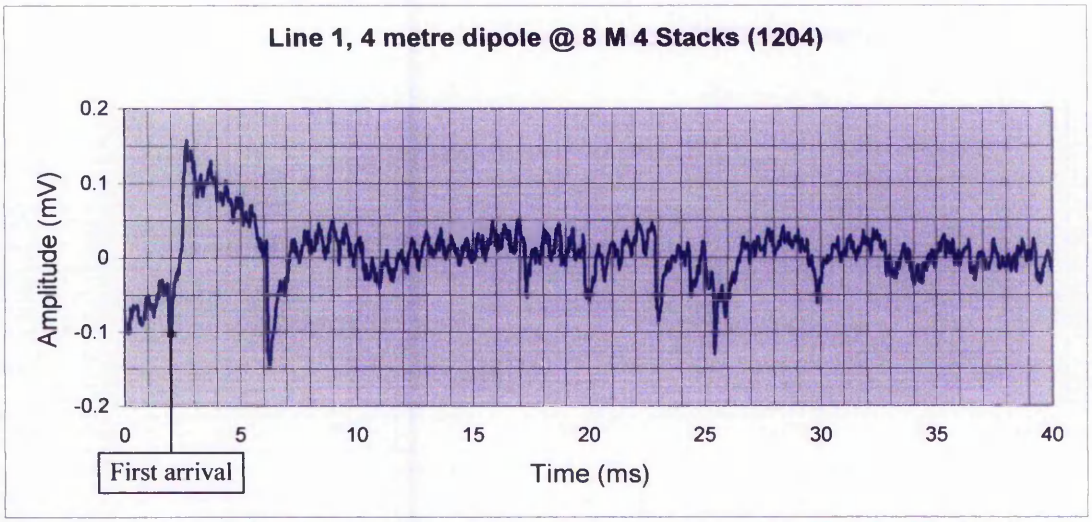

Figure 4.34 EK responses at 8m from the shot point. Note the first arrival at 1.5 ms and the EK responses following up to 32 ms and in particular the response at 6 ms and that at 24.25 ms.

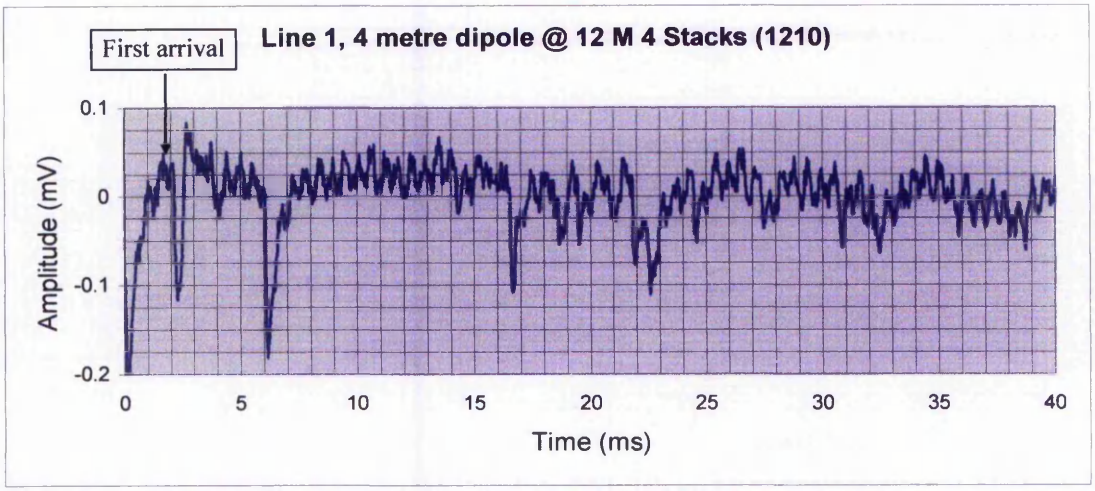

Figure 4.35 EK responses at 12m from the shot point. Note the first arrival at 1.5 ms and the EK responses following up to 32 ms and in particular the response at 6 ms and that at 24.25 ms.

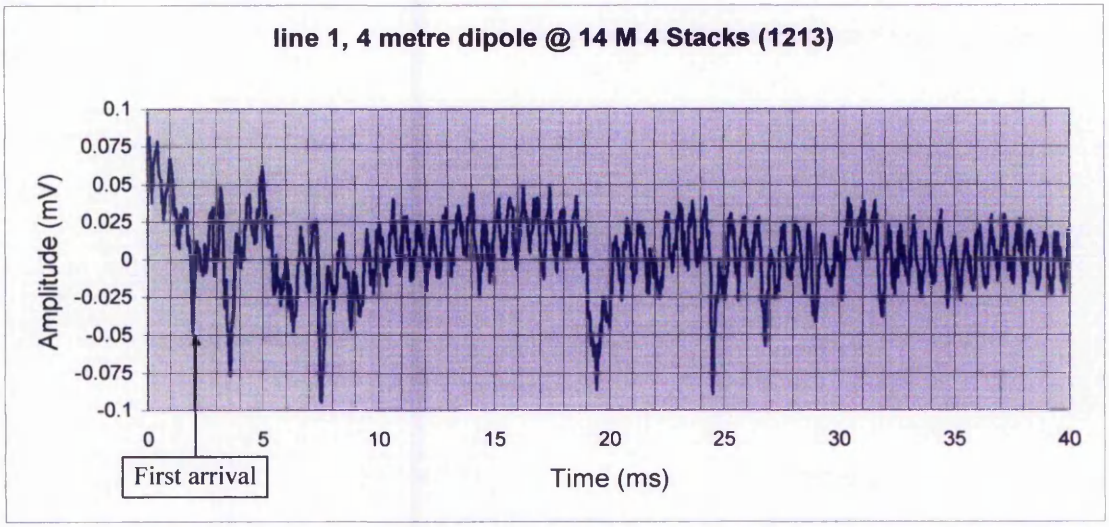

Figure 4.36 EK responses at 14m from the shot point. Note the first arrival at 1.5 ms and the EK responses following up to 32 ms and in particular the response at 6 ms and that at 24.25 ms.

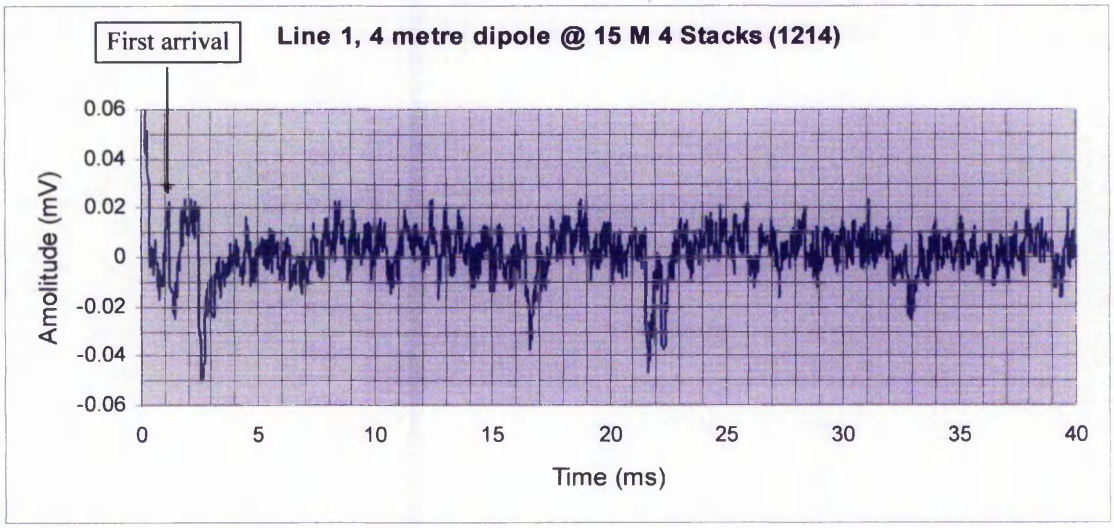

Figure 4.37 EK responses at 15m from the shot point. Note the first arrival at 1.0 ms and the EK responses following up to 35 ms and in particular the responses at 16.5 ms and 21.5 ms. In addition note the absence of the response at 6 ms and at 24.5 ms.

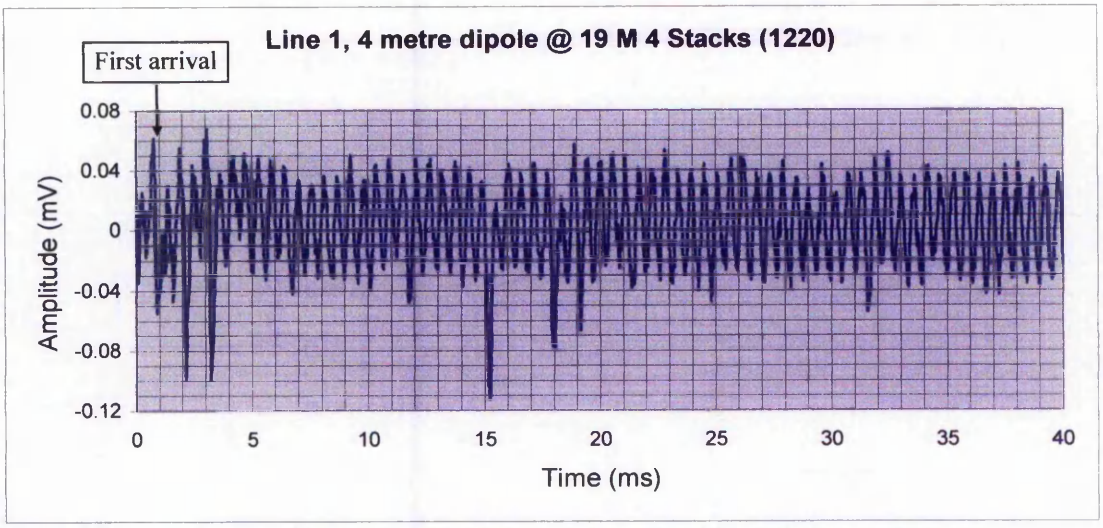

Figure 4.38(a) EK response at 19m from the shot point. Refer to figure 4.39 (b) for details.

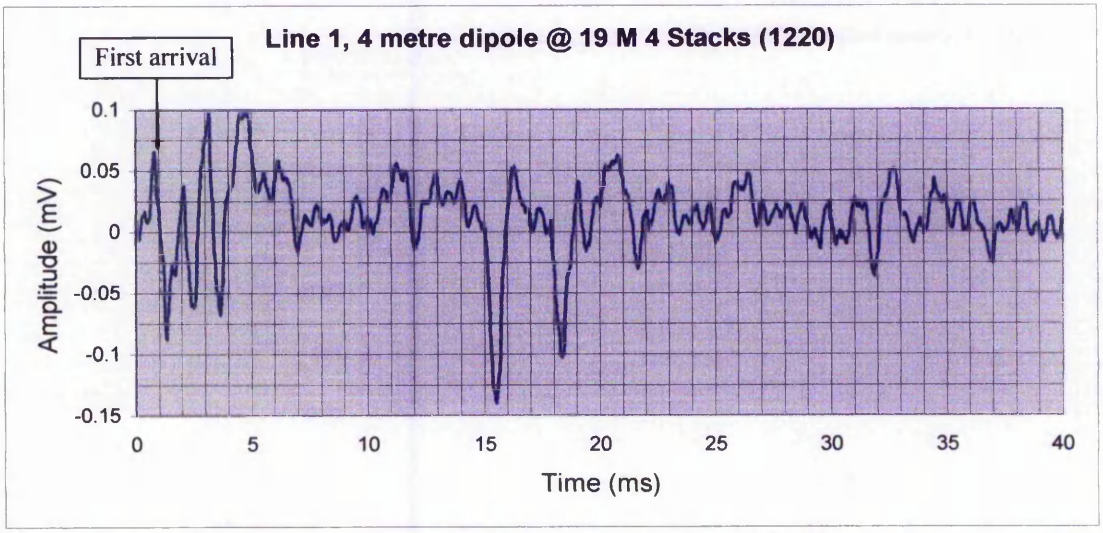

Figure 4.38 (b) EK responses at 19m from the shot point, refer to figure 4.39(a) with noise removed. Note the first arrival at 0.5 ms and the EK responses following up to 38 ms and in particular the response at 15 ms and that at 21.5 ms.

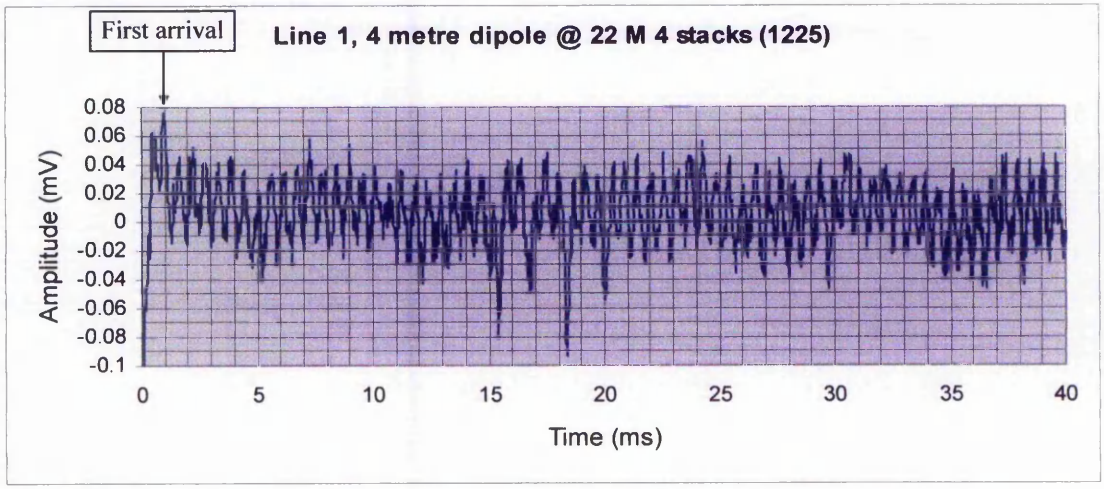

Figure 4.39 EK responses at 22m from the shot point. Note the first arrival at 1.05 ms and the EK responses following up to 38 ms and in particular the response at 15 ms and that at 18.25 ms.

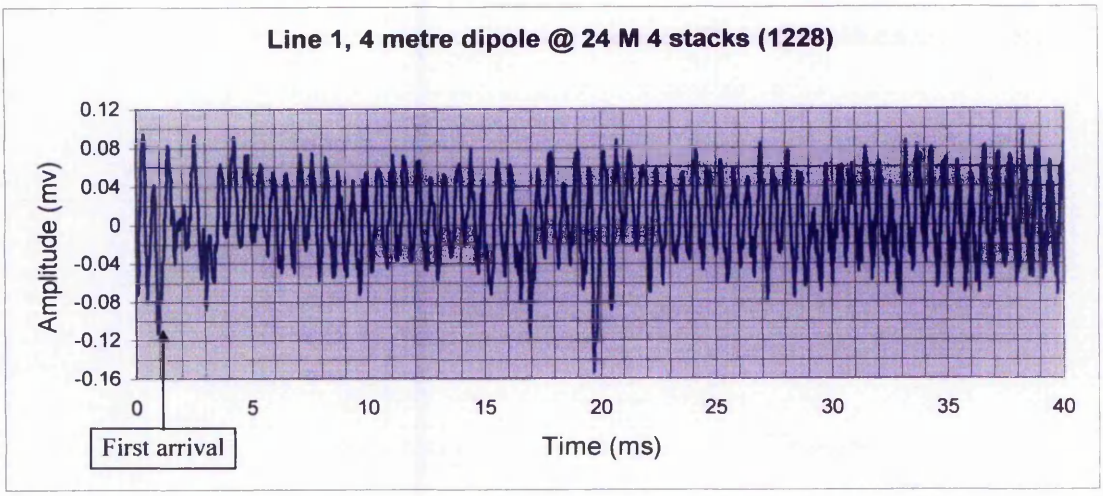

Figure 4.40 (a) EK response at 24m from the shot point; refer to figure 4.41(b) for details.

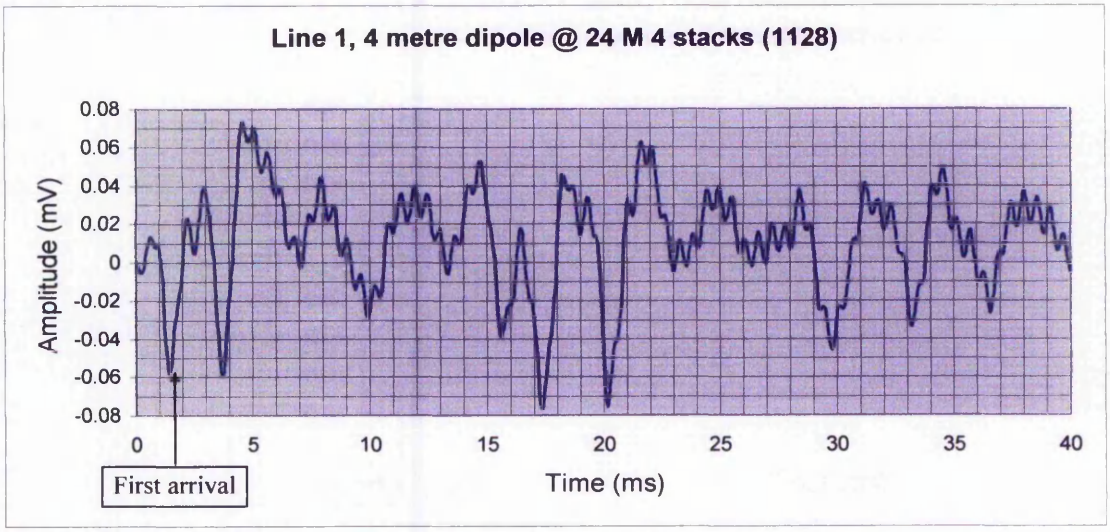

Figure 4.40 (b) EK responses at 24m from the shot point, figure 4.40(a) with noise removed. Note the first arrival at 1.25 ms and the EK responses following up to 38 ms and in particular the response at 29.8 ms.

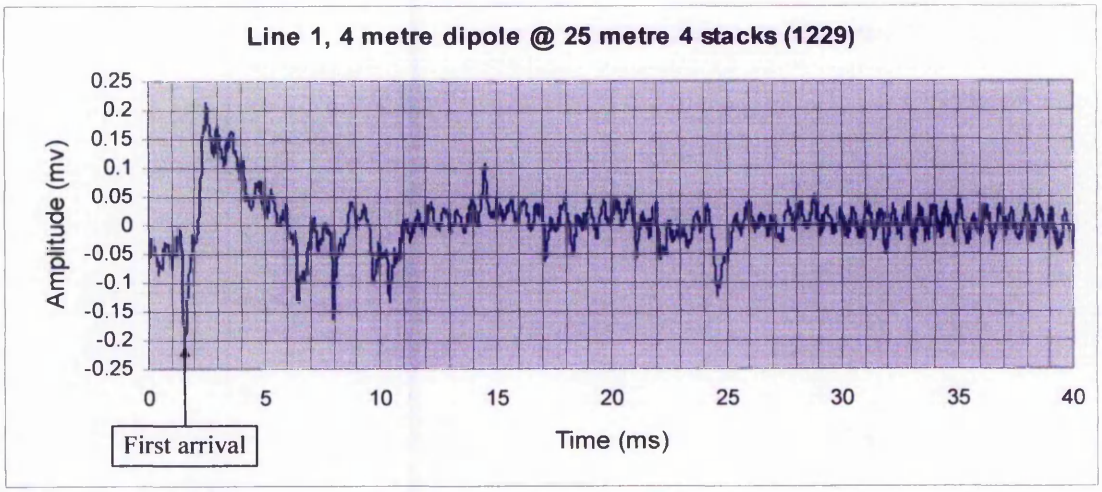

Figure 4.41 EK responses at 25m from the shot point. Note the reappearance of the response at 6 ms and a weak response at 24.5 ms.

4.7.8 *Survey line 2 (no compaction)*

Only a small selection of traces are shown as no compaction had taken place over the area this line covered. However, it is seen that there is no EK moveout and there is symmetry at 45^0 thus meeting criteria 1 and 2 as described in Chapter 2.

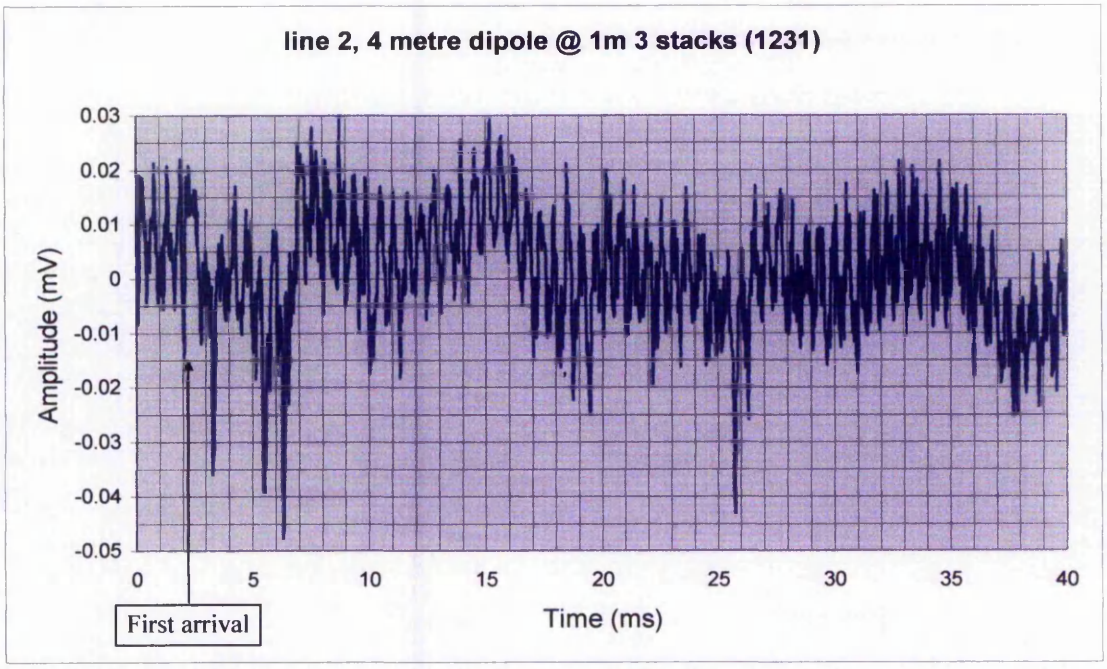

Figure 4.42 EK responses at 1m from the shot point. Note the first arrival at 2.0 ms and the EK responses following up to 38 ms, and in particular the response at 25.75 ms.

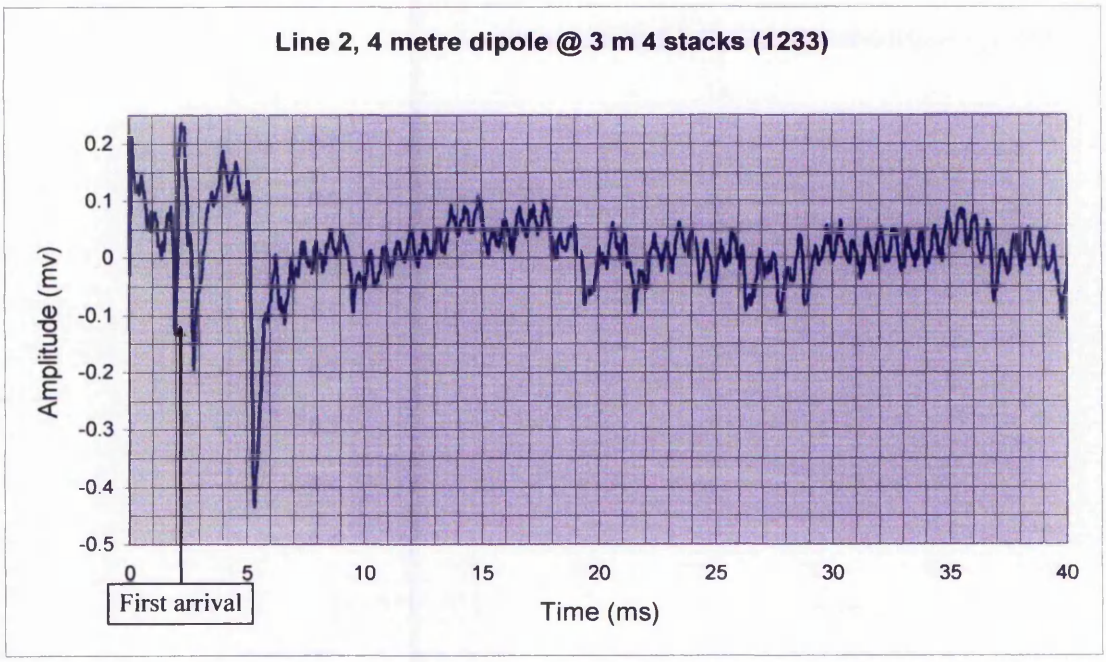

Figure 4.43 EK responses at 3m from the shot point. Note the first arrival at 2.0 ms and the EK responses following up to 38 ms and in particular the response at 5.0 ms and that at 26.0 ms. In addition note the increase in the amplitude of the EK response and the improvement in signal to noise level

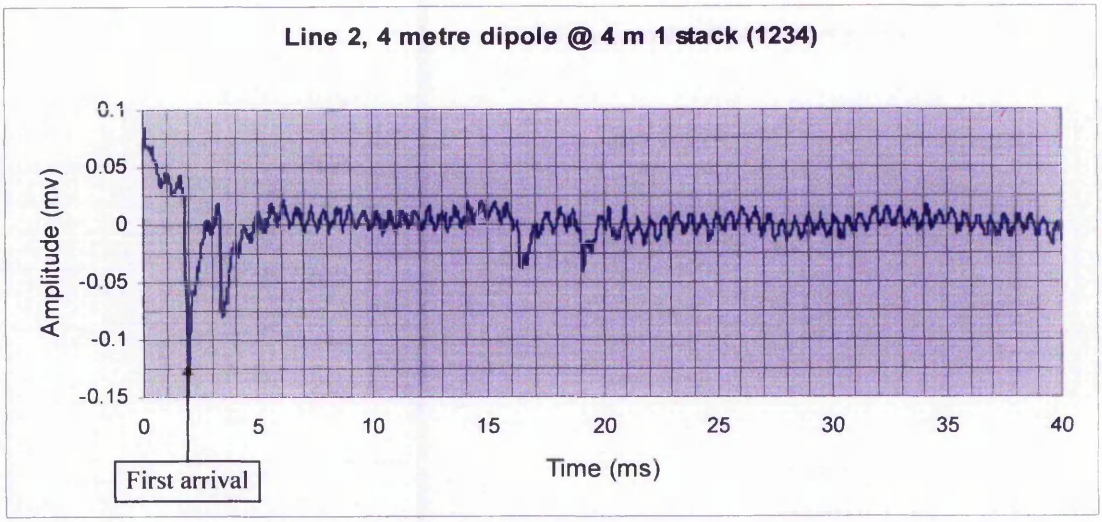

Figure 4.44 EK responses at 4m from the shot point. Note the first arrival at 2.0 ms and the EK responses following up to 38 ms and in particular the response at 15.0 ms and that at 19.0 ms. In addition note the increase in the amplitude of the EK response and the improvement in signal to noise level

4.7.9 Survey line 1 (post compaction)

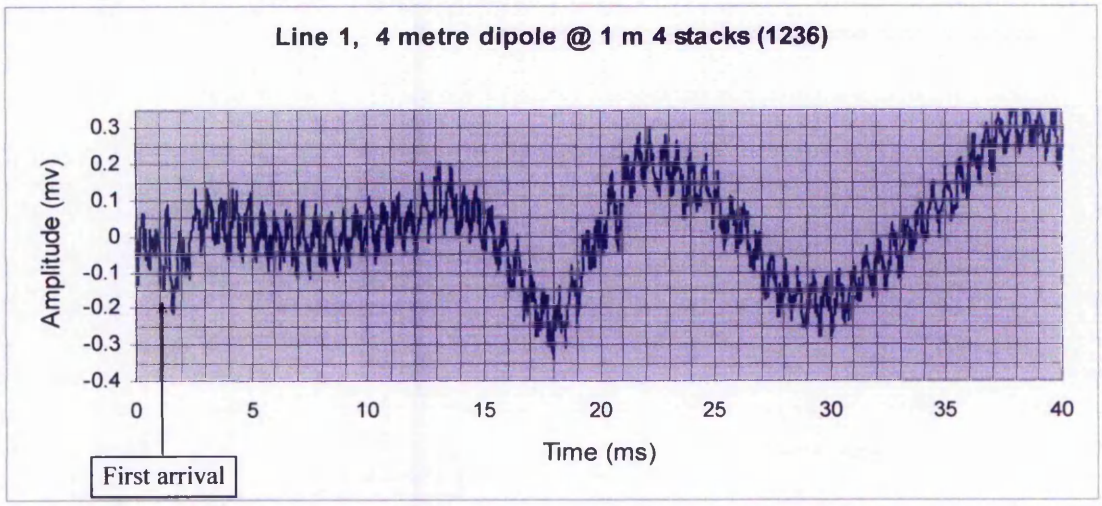

Figure 4.45 EK responses at 4m from the shot point. Note the first arrival at 1.0 ms and the EK responses following up to 38 ms. Note the small EK response at 2ms and the presence of 50 Hz noise.

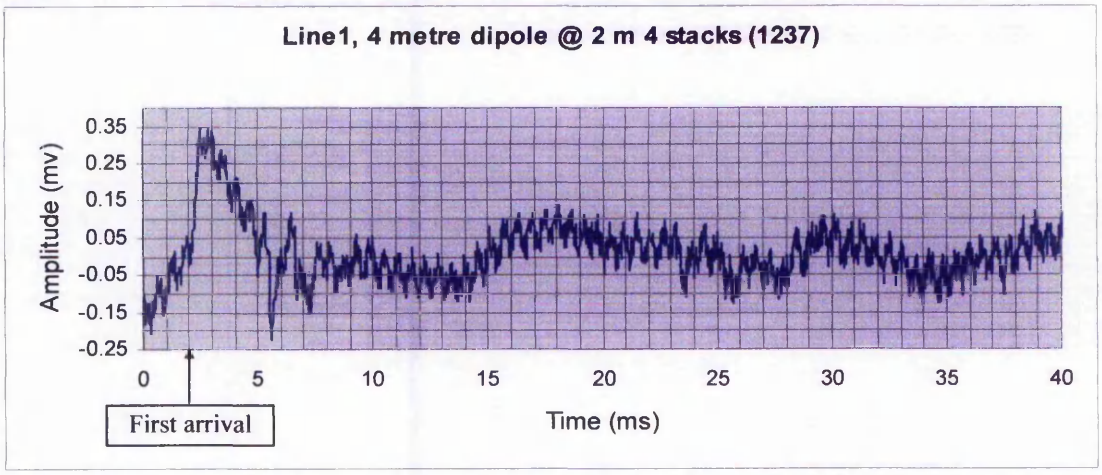

Figure 4.46 EK responses at 4m from the shot point. Note the first arrival at 2.0 ms and the EK responses following up to 38 ms and in particular the response at 5..5 ms and that at 23.5.0 ms.

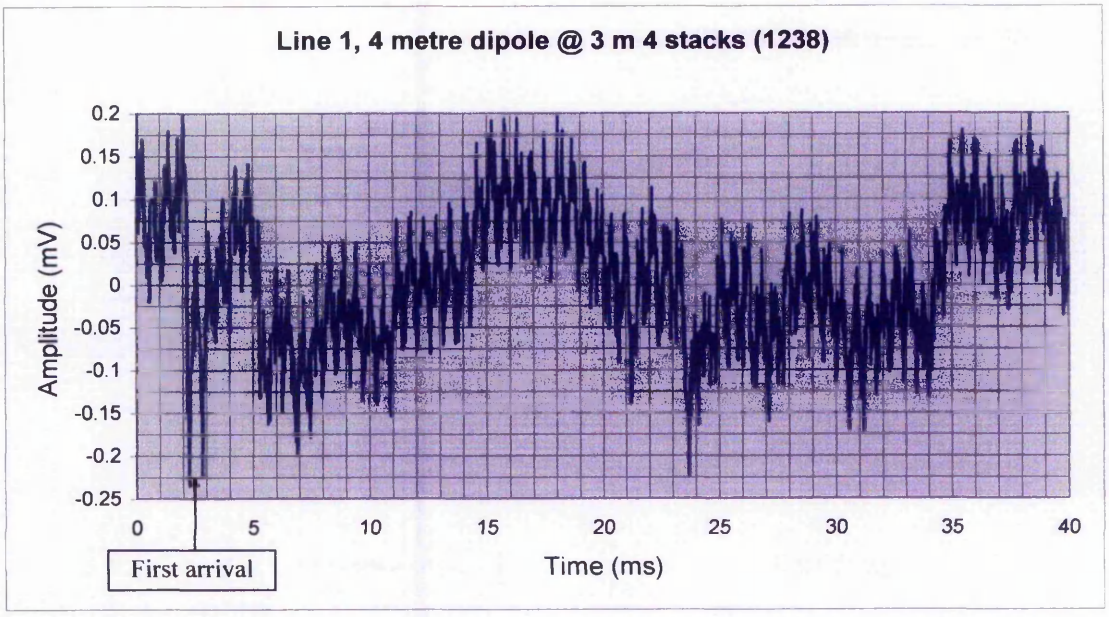

Figure 4.47 (a) EK response at 3m from the shot point. Note the increase in amplitude for the 2 ms response compared to figure 4.6.

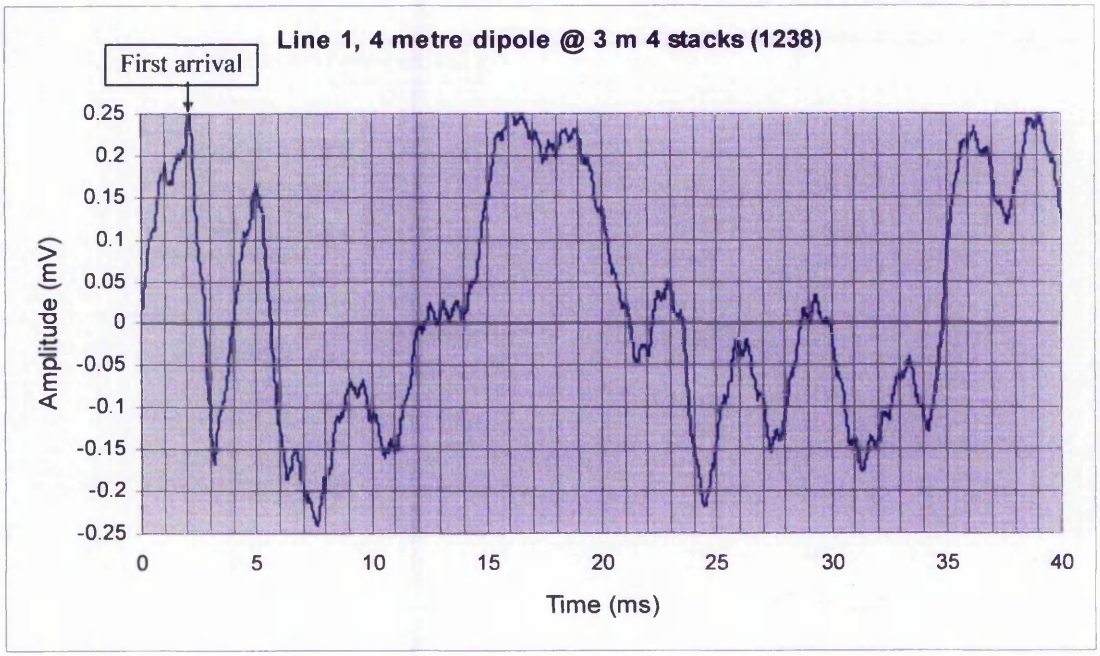

Figure 4.47 (b) EK responses at 4m from the shot point. Note the decrease amplitude for the 2 ms response compared to figure 4.46.

4.7.10 *Comparison of EK and DCP results*

The EK data are compared to the results obtained from the DCP, Prema and GDP. The data for DCP 3 and 12 has been redrawn in order to make the comparison with the EK response data easier to view. The results in figure clearly show that the post compaction ground is stronger.

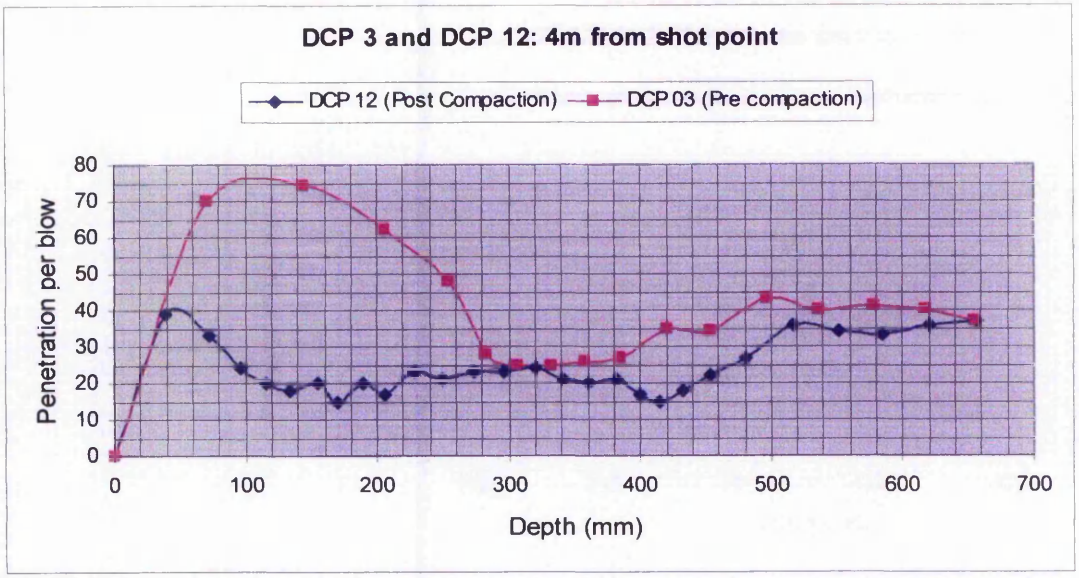

Figure 4.48 Cone penetrometer results along west-east survey line. The drop weight was 8 kg and the drop height was 585 mm. The zero points are shown for completeness; however, in some cases they are omitted.

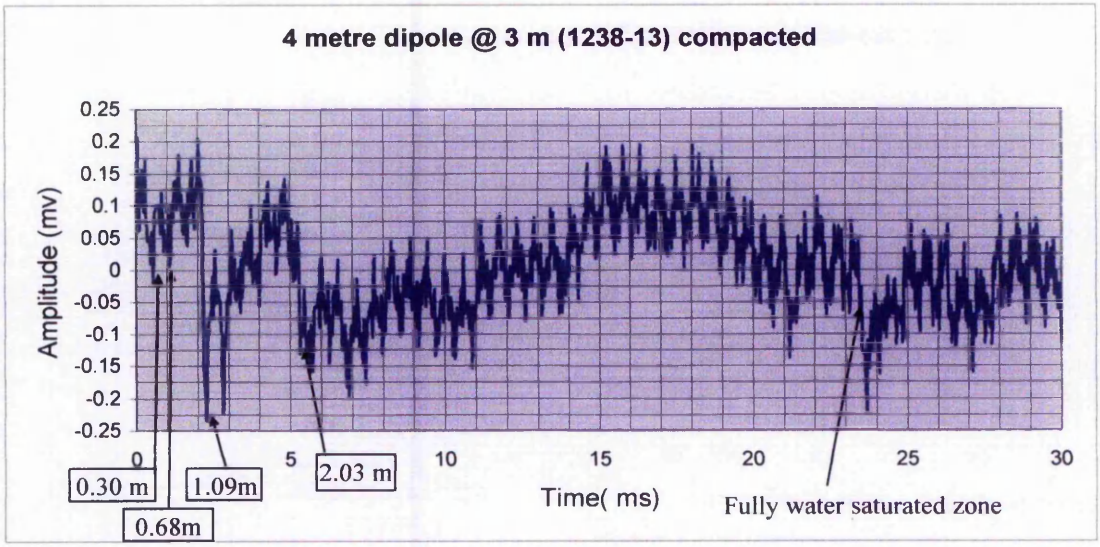

Fig. 4.49 Comparison of DCP and EK data at the 4-metre point on the west east survey line.

4.7.11 *Discussion on comparison of the results.*

The EK responses at 0.30 and 0.68 metre correlate with the change in compaction at the same points for the DCP profiles. The rising stepped response of the EK waveform after 1.08 meter or 2.12 milliseconds is suspected to be due to the change of the moisture content in the ground due to compaction. The response at 1.90m or 2.18ms are the bottom of the lower layer of the calcareous quality brickearth. There is evidence of 50 Hz mains and high frequency, approximately 2 KHz, pick up on the above data. Examining the first EK data (Figure 4.50) there are EK responses noted at 0.36 ms, 0.68

ms, 1.12 ms, 2.1 ms, 5.18 ms as well as 24.25 ms in the full data. These correspond to depths of 0.30, 0.68, 1.09, 2.03 m and 10 meters, again in good agreement with the other data. The response at 24.25 ms corresponds to the depth of the water table which was confirmed by the Kent water authority to be at 40 feet (12.2 m), allowing for the fact that the quarry floor was 1.5 m below this would put the water table, relative to the quarry floor, at 10.7 metres. In addition allowing for the exceptional rainfall during the month September 2001 the water table could have risen in the order of 0.5 m, not an unreasonable assumption. However, it was not the object of this exercise to detect this.

An expanded view of the data in figure 4.50 is shown in figure 4.51

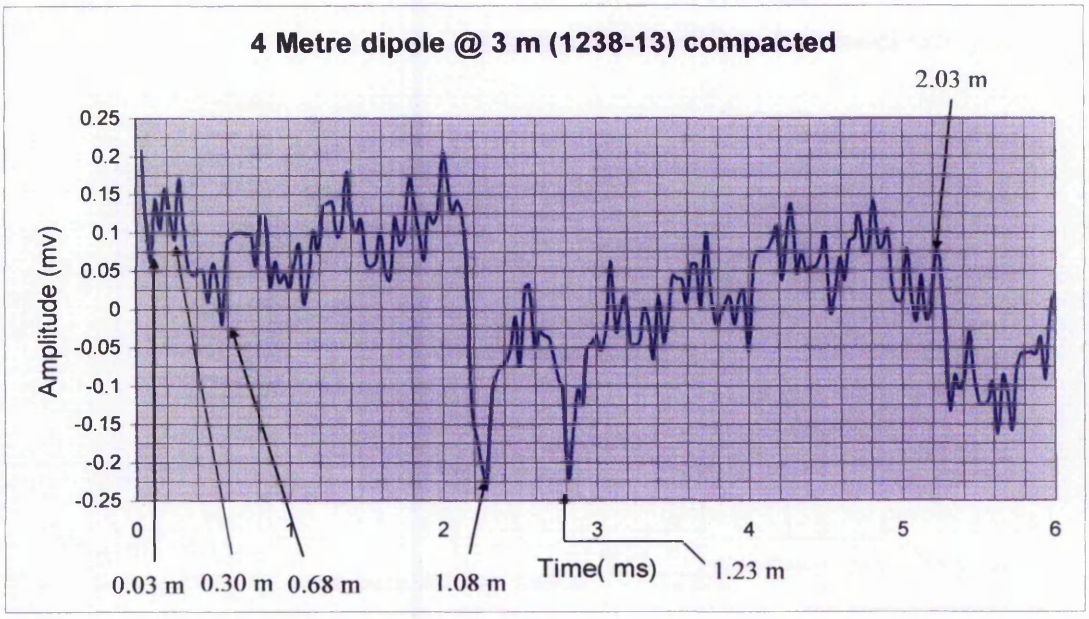

Figure 4.50 Expanded view of data in figure 4.50.

It should be noted that the EK data shown are raw data as recorded. However, where appropriate, figures 4.31, 4.38 and 4.40, high frequency noise has been removed from the data. The broad response beginning at 2 ms (0.6m) and settling at 6.2ms (1.8m) is due to third harmonic distortion from the 50 Hz mains pick up. The EK data was obtained in 1 metre steps from the shot point and no move out was observed, thus showing beyond any doubt the responses are electro-kinetically generated.

The calculated water table level from the EK results is 10.7 metres ± 0.35m. This is a perfectly reasonable figure allowing for the arguments above. This was checked with the local water authority who confirmed the water table to be at 12.20 meters. The one metre difference is simply by the measurement being taken approximately 1.5 metre

down on the quarry floor. The DCP data as given in Figures 4.25 to 4.27 indicate the depth of compaction to cover the range approximately 280 to 300 mm. Taking in account that the ground was disturbed by the compaction process and experimental errors the DCP, Prima and GDP results agree remarkably well. The results also agree very closely with the seismic and EK data.

4.8 Summary.

The EK results for the Mansfield investigations have been summarised in section 4.36 and will not be repeated here. However, one observation while conducting these investigations is worthy of mention.

The results of the Ospringe EK investigations in a loess geological profile where pre and post compactions studies were conducted using a range of geophysical and geotechnical techniques. Good correlation was obtained between cone penetrometer (DCP), Prima 100, German dynamic plate, seismic and EK data.

The seismic data were analysed and used to assist in the location of EK responses to results obtained from the other investigation techniques and to determine the ground stiffness using the 'S' wave data for the geotechnical investigations.

The results of the EK investigations were very encouraging indeed as results were observed at very shallow depths, < 1 metre, figures (4.48 and 4.49). The water table was shown to be at 10.7 metres which agreed with the data obtained from the local water authority. Finally the results support and enhance those obtained from the Mansfield site investigations.

4.8.1 *summary/conclusions*

The EK results obtained for both the Mansfield and Ospringe sites clearly show that the EK responses recorded are genuine. These EK responses also they meet the criteria provided for the detection of EK responses. It has been demonstrated that the EK data, from both the Mansfield and Ospringe sites, correlate with features such as the water table and fracture zones in the Mansfield case and with compaction results and also detecting the depth of the water table at the Ospringe site.

Chapter 5 | Laboratory investigations of EK

endeavours to ascertain the unknown causes of processes from their visible effects; it seeks to comprehend them according to the laws of causality. ... Theoretical natural science must, therefore, if it is not to rest content with a partial view of the nature of things, take a position in harmony with the present conception of the nature of simple forces and the consequences of this conception. Its task will be completed when the reduction of phenomena to simple forces is completed, and when it can at the same time be proved that the reduction given is the only one possible which the phenomena will permit.

Herman Ludwig Ferdinand Helmholtz 1821- 1894

5.1 Laboratory studies of the EK effect in rock-water systems.

To date there have been a number of papers describing laboratory studies of the EK effect. Of these the majority focussed on laboratory studies of EK effects in rock-water systems and have mainly focused on the double layer, the most notable being the work of Ishido *et al.* (1981). Their laboratory apparatus consisted of a glass sample 'U' tube, which held a crushed rock sample, with two platinum electrodes across the ends fed by two glass vessels, holding held an aqueous solution. Nitrogen gas was passed through the assembly to measure the streaming potential across the electrodes. Measurements were made on a number of minerals and the experiments were based on measurements of the zeta, (ξ) and streaming potentials. Later Lorne *et al.* (1999) used streaming potential measurements on crushed rock samples to investigate the properties of the double layer. A laboratory method of determining the electro-kinetic coefficients of porous media was described by Hang *et al.* (1998), the experimental technique described used an electrochemical cell.

The above papers did not however, address the issue of EK signals generated by an acoustical wave. Haartsen *et al.* (1995) described the generation of seismoelectric signals at ultrasonic frequencies of 100 kHz in a contrasting two layer sandstone model.

Later, Zhena and Toksöz (2001) described seismoelectric measurements in borehole models with fractures. The data gathered from their electrode arrays were stacked 128 times. The work of Haartsen *et al.* (1995) and Zhena and Toksöz (2001) are more in line with the laboratory investigations discussed later in this thesis.

The laboratory experiments discussed in this thesis were conducted in order to gain a better insight into the exact nature of the generated EK signal when crossing a well-defined contrasting boundary. A simple two-layer model was used to represent three main types of geological profiles the Sherwood sandstone, a saturated limestone and a boulder clay. Details of these are described and discussed in Chapter 3.

5.2 Experimental details

The method used to determine the EK response at a sandstone-water table interface made use of two ultrasonic transducers operating at a frequency of 150 kHz. These were used to simulate the field conditions, one transducer acting as the transmitter and the other as the receiver. These transducers are similar to those used as echo sounders in small boat echo sounder systems and are easily available at a modest cost. In the final experiments 50 kHz ultrasonic transducers were used as these provided a greater power output. An electronic driving source had to be designed in order to drive the transducers. The design had to produce a high voltage pulse in the order of 800 volts peak amplitude with adjustable pulse duration of 1 to 10 μ-seconds and a variable repetition rate of 1 to 100 pulses per second (PPS) in the range 1-10 and 10–100 PPS. A one shot facility was also incorporated. For all of the experiments conducted the transmitting transducer was pulsed at 100 Hz rate with a 5 μ sec width pulse, giving a mark space ratio of 2000:1, so to enable the received signal to be stacked. This was done in order to get a clear representation of the signal above any noise. Two electromagnetic detectors were used to detect any EK response, one being a dipole aerial to detect the electric field and the other a ferrite rod coil aerial to detect the magnet field of the EM wave. By simultaneously measuring the responses from both detectors valuable information was gained on phase shift and relative signal amplitudes.

In order to eliminate any electromagnetic interference from the ultrasonic transmitter the specimen was selected to be long enough to allow the ultrasonic wave to still be travelling up the specimen after the electronic exciting pulse had ceased. It would then

arrive at the interface, where an EK response was expected, long after the cessation of this pulse. The exciting pulse applied to the source transducer was 5.0 μ- seconds long with amplitude of 800 volts with 30 volts dc applied to the input of the transmitter circuit. The amplitude of the exciting pulse could be adjusted by varying the input voltage.

The velocity of the induced ultrasonic wave was typically in the order of 2000 m/s for sandstone therefore, the time taken to travel 500mm would be 1000 μ-seconds or 1 ms. It was decided that specimens should be at least 500 mm in length and approximately 100 mm square or in the case of a core sample 76 mm diameter, thus allowing a minimum period of 1000 – 5.0 μ-seconds, i.e., 995 μ-seconds after the cessation of the generating pulse. It was appreciated that the velocity in different sandstone samples could vary but not however, to an extent that would affect the above argument.

With a sandstone sample of length 315mm, which was acquired from a company called 'Realstone' in Derbyshire it was observed that the water level rose by capillary action to the height of the specimen with only 30 mm of water around its base. Care was taken when conducting the experiments to make sure the sandstone specimens were fully saturated. This was checked by measuring the electrical conductivity across two faces of the specimen. Figure 5.1 provides a diagrammatic view of the experimental arrangement.

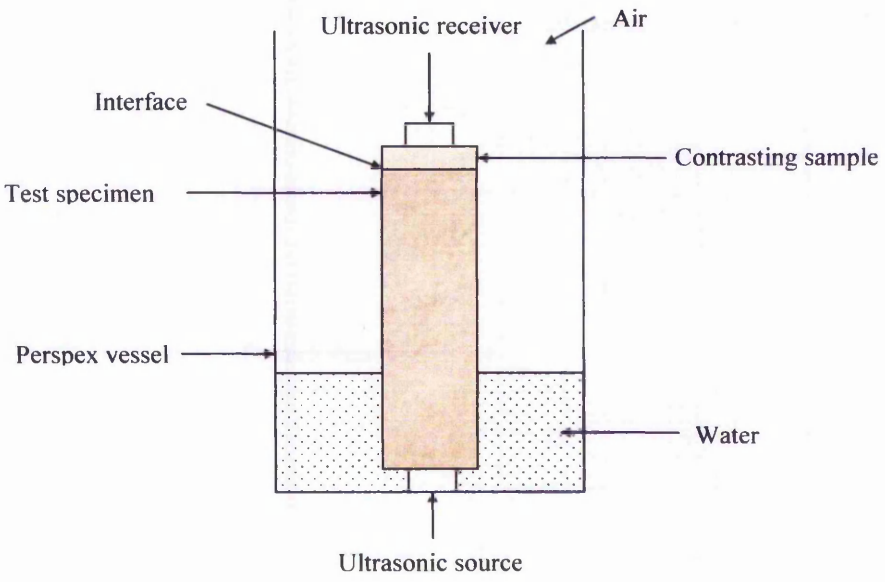

Figure 5.1. Diagrammatic view of experimental arrangement. See plate 5.1 for further details of the experimental vessel.

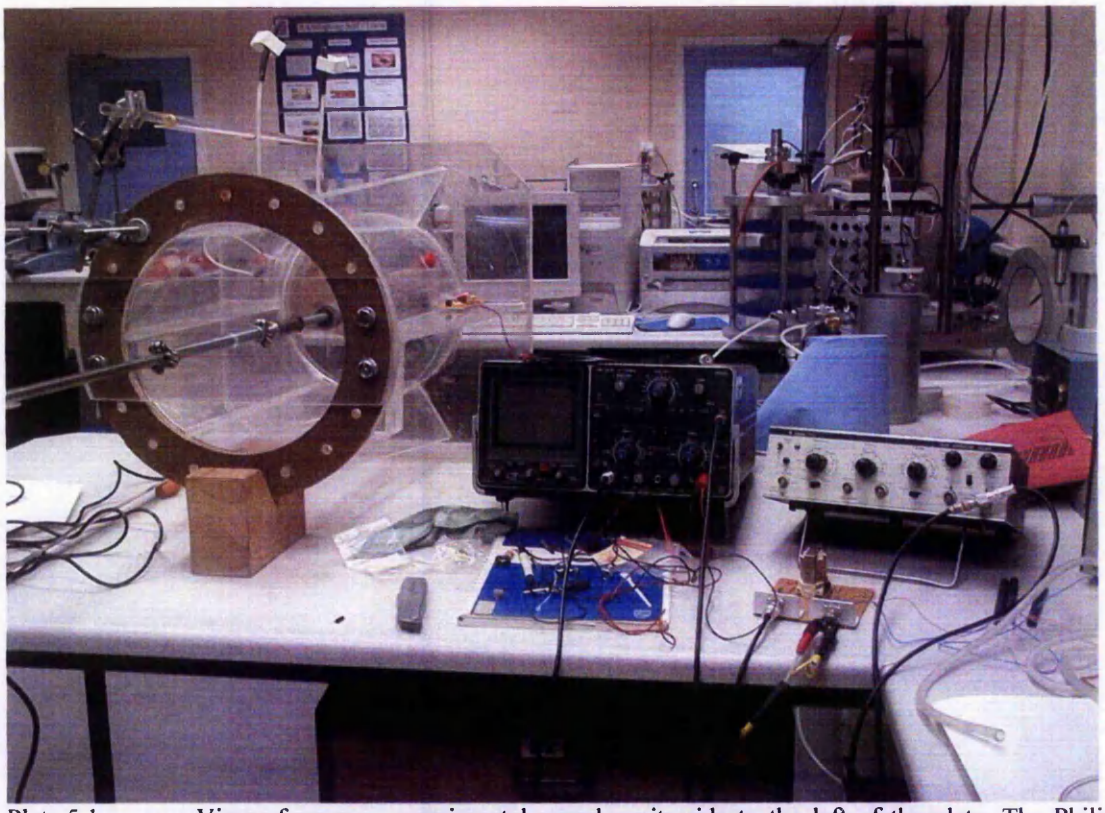

Plate 5.1. View of perspex experimental vessel on its side to the left of the plate. The Philips storage oscilloscope can be seen in the middle with the pulse generator on the right. The ultrasonic transmitter module can be seen below the pulse generator.

A cylindrical perspex tube was used to carry out the experiments. One of the ultrasonic transducers was inserted in the base with a waterproof seal; this can be clearly seen in plate 5.2. The remaining ultrasonic element was fitted to a sliding stainless steel tube that was supported via a Perspex bridge across the top of the vessel. This provided the ability to adjust the height of the device. A vertical glass tube, with a calibrated scale, was fixed to the outside of the vessel via a connection through to the base of the vessel in order to measure to mean water level, (see Plate 5.2). Plate 5.1 shows the experimental vessel, lying on its side, with the supporting instrumentation. The adjustable support mounted on the perspex bridge for the receiving transducer can be seen in plate 5.1 protruding from the top of the cylinder.

In testing the experimental vessel and its associated components, loose sand was used as this was readily available in the laboratory. From this it was found that the amplitude response of the signal on the receiving transducer decreased after a few hours. After checks were made to make sure there was no system fault it was discovered that pressing down on the vertical transducer tube gave a significant increase in signal amplitude. A weight platform was designed to take a standard split weight and was

attached to the top of the tube. By experiment it was found that a weight of 10N gave a significantly improved response, increasing the weight beyond this gave no significant increase in the signal amplitude. Importantly, therefore the change in arrival time of the ultrasonic response is a measure of change of stress. This new arrangement also has the advantage of supplying a constant contact pressure during the experimental measurements.

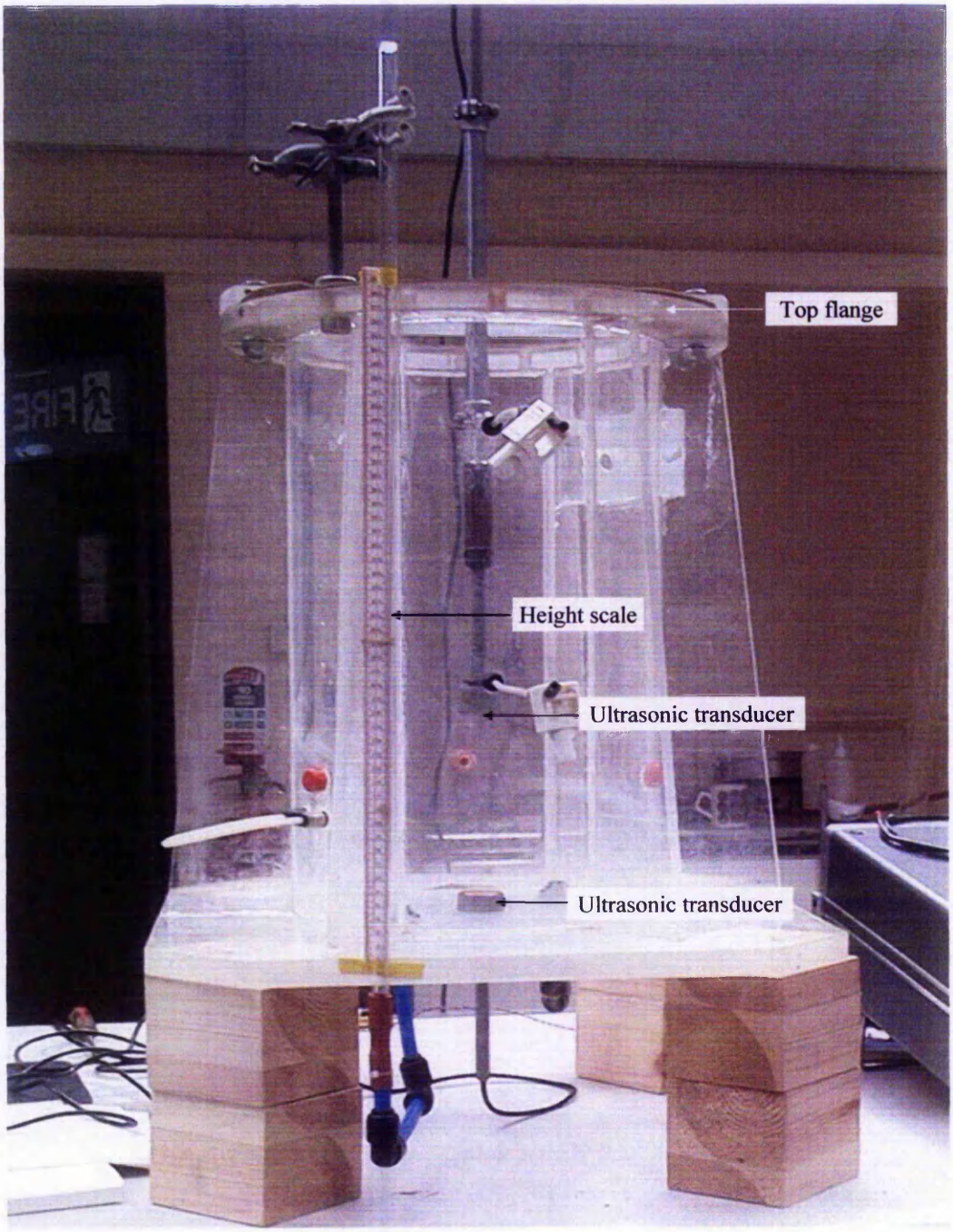

Plate 5.2 View of the experimental vessel in its normal upright position. One of the ultrasonic transducers can be seen mounted centrally in the base plate. .Cylinder diameter 300mm, height 490 mm base to top flange.

Additional it was observed that was made when the lower layer of sand was placed in the vessel and a measurement taken of the vertical transit time, the velocity of the ultrasonic wave was 312 m/s. On making the same measurement a day later the velocity had increased to 500 m/s, thus suggesting there is a settling factor to be taken into account. One possibility is that settlement takes place due to the force exerted by the 10N weight acting down from the top transducer. Another possibility in addition to the force of the weight could be due to the applied high frequency action of the ultrasonic transducer.

5.3 Details of the measuring system

A schematic layout of the experiment is shown in figure 5.2. The transmitting ultrasonic transducer was driven by a purpose designed pulsed high voltage driver circuit which steps up the circuit voltage supply by a factor of 30. The circuit is shown in Appendix L. The output drive voltage is fully isolated by means of the pulse transformer. The voltage driver circuit was powered by a standard dc power supply with an adjustable output voltage of 0 to 30 volts. The driving signal was obtained from a commercially available pulse generator, Gould Advance Electronics PG58A, the pulse width being set at 5 μ-seconds with an output voltage of 2 volts from a 50 ohm source impedance. A Philips PM3234 0-10MHz dual channel storage oscilloscope was used in the initial tests in setting up the experiment, for the subsequent EK experiments a Tektronix TDS3032, recording digital oscilloscope was used for the observation and measurement of the EK signal, it has a 200mHz bandwidth, a 1GHz/s sampling rate and a dual input channel. It also has the facility to record the recorded data onto a floppy disk, a hard copy print out and a general purpose interface buss (GPIB) output facility.

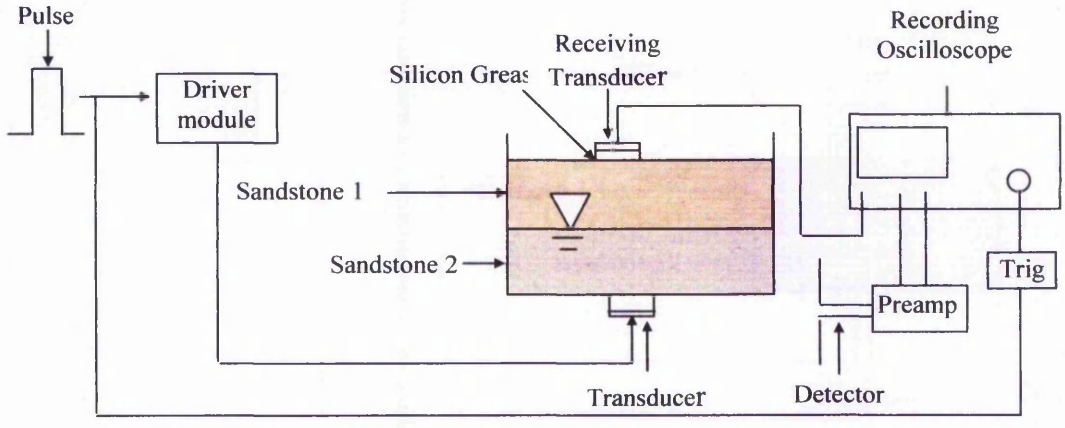

Figure. 5.2. Schematic layout of the experiment. Sandstone 1 has a lower acoustic velocity than sandstone 2.

5.4 EK detection devices

The typical velocity of the seismic impulse in the field is in the order of 500 m/s below the top surface layer hence for a source of 100 Hz the wavelength λ would be 5 m. However, the wavelength of the EM field will vary at the acoustical frequency which propagates at a velocity near to the speed of light, i.e. $3x10^8$ m/s. In the field the length of the dipole aerial was typically 6 m, the dominant frequency of the acoustical excitation was 100Hz therefore in this case the wavelength of the EM wave would be $3x10^6$ m. Thus the dipole aerial length is many times less than the wavelength of the EM wave being in the order of a factor of $5x10^5$ less. However, the dipole aerial was still able to reliably detect the radiated EK signal over a range of 1 to 24 metres from the source with the help of a low noise amplifier, as seen by the results in Chapter 4.

For the laboratory measurements the 150 kHz ultrasonic transducer generates an acoustical signal with a typical wavelength in sandstone of 13.3mm. However, the wavelength of the EM wave is $2x10^3$ m. The dipole aerial was designed with a basic length of 200 mm which could be extended in increments of 200 mm. Again the dipole length is less than EM wavelength by a factor of $1x10^4$, which is within a factor of approximately two when compared to the field condition. The EK detection devices were designed to mimic as far as possible those used in the field, the principle detection devices being a dipole aerial and coil.

5.4.1 *Ferrite rod aerial*

A ferrite rod aerial was designed based on a ferrite rod of length 125 mm and diameter 10 mm as this is available as a standard size. The electrical permeability of the ferrite rod was not known, so a coil of 525 turns was wound onto the ferrite rod using enamelled copper wire 0.10 mm diameter, this would also necessary to form the aerial. A measurement of the inductance was carried out from which a value of the permeability of the ferrite rod was calculated. Table 5.1 gives details of the measurements carried out on the ferrite rod coil for the frequencies of 100 Hz and 1 kHz. The measuring bridge used, Racal-Dana LCR Databridge model No. 9341, was not able to carry out measurements at 150 kHz.

Table 5.1 Measurement of ferrite rod coil characteristics at two frequencies.

Frequency (Hz)	Resistance (ohms)	% Error (ohms)	Inductance (mH)	% Error (mh)
1000	44.00	0.5	17.45	0.5
100	39.36	0.5	19.21	0.5

It was realised that the permeability of the ferrite rod could vary with frequency. Figure 5.3 shows the extent of the variability of the permeability over the range 0.1 to 10 MHz. However, for the region of interest in the investigations in this thesis, 50 kHz to 150 kHz, the permeability is seen to be 100 H/m at 150 kHz and < 10 at 50 kHz. Bearing in mind the highest measuring frequency of the Racal component bridge was 1.0 kHz the calculated value of $\mu_e = 0.85$ H/m is not unreasonable.

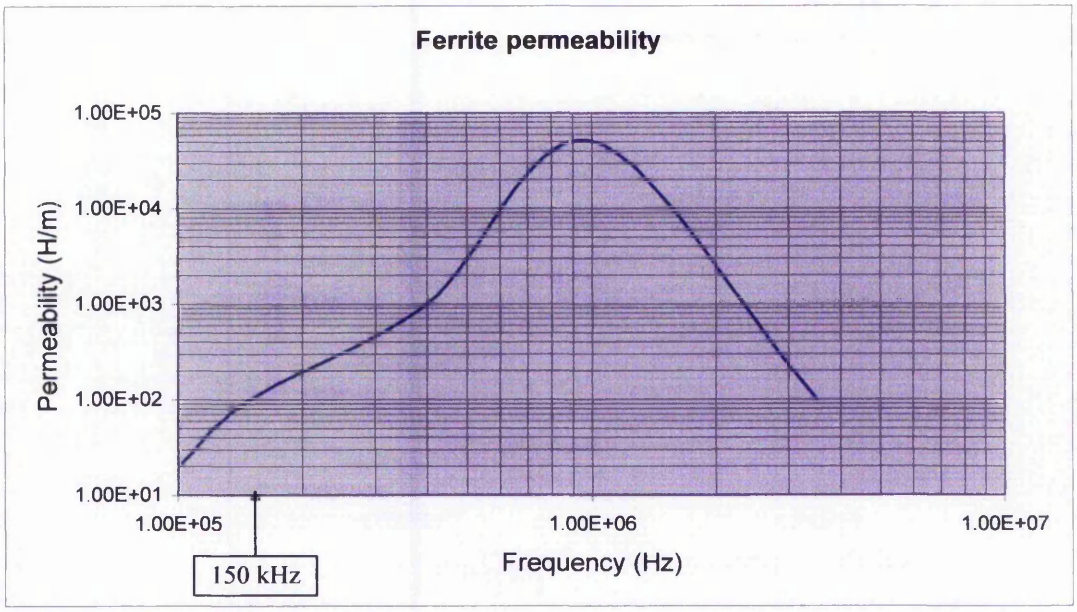

Figure 5.3 Variation of permeability with frequency. Redrawn from manufactures data sheet

Using the formulae $L = \frac{\mu_e \mu_0 n^2 a}{l}$ H, is used to calculate μ_e (5.1)

where L = inductance of the coil measured in Henry's 'H'

μ_e = effective permeability of the ferrite rod

μ_0 = permeability of free space = $4\pi.10^{-7}$ H/m

n = number of turns, in this case 525

a = diameter of ferrite rod = 9.5 mm

l = length of ferrite rod = 120 mm

Calculating $\mu_e = 120.4/4\pi.10^{-7}.(525)^2.\pi.(9.5)^2$ thus $\mu_e = 0.85$ H/m ± 5% (5.2)

5.4.2 *Calculations to determination the value of capacitance at a resonant frequency of 150 kHz for the ferrite rod aerial.*

The standard formula for the resonant frequency of a parallel LC circuit is given by equation 5.2

$$\therefore \quad \text{Resonant frequency '}f_0\text{' of aerial} = \frac{1}{2\pi\sqrt{LC}} \text{ Hz} \qquad (5.3)$$

$$\therefore \quad (2\pi f_0)^2 = \frac{1}{LC} \qquad (5.4)$$

Where f_0 is the resonant frequency of the circuit

L the inductance

C the parallel capacitance

$$\therefore \text{ from (5.2)} \quad C = \frac{1}{L(2\pi f_0)^2} = \frac{1}{(17.45\times10^{-3})\times(2.150.10^3)^2} = 64.5.10^{-12} \text{ farad or 64 pf.}$$

The coil, L1 figure 5.4, was shunted by a fixed capacitor of 33pf in parallel with an adjustable capacitor of 5-60 pf and tuned on test. The test circuit to achieve this is shown in figure 5.4. The final value of the tuning capacitor at resonance was measured and found to be 32 pf.

5.4.3 *Measurement to determine the resonant frequency of the ferrite rod aerial*

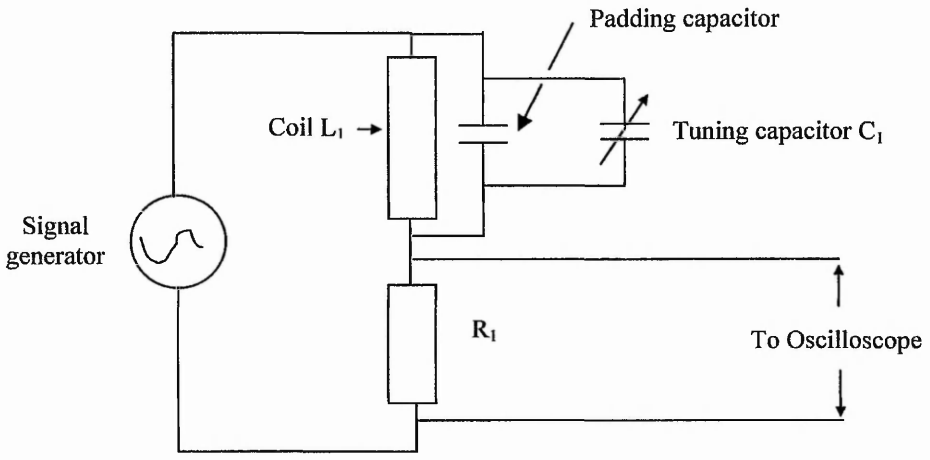

Fig. 5.4 Schematic diagram of the circuit to determine the resonant frequency

Using this value of the permeability and the value of the parallel tuning capacitor a set of readings were taken to determine the resonant point of the circuit in figure 5.4. In order to determine the resonant frequency of the coil aerial a sine wave signal of amplitude 5 volts was applied to the input of the circuit in figure 5.4 starting at 50 kHz

below the resonant frequency of 150 kHz and slowly increased to a level of 50kHz above 150 kHz in steps of 5 kHz noting the amplitude response on the oscilloscope connected across resistor R_1, 4k7 ohm. Table 5.2 lists the results.

Table 5.2. Results of frequency versus output volts for ferrite rod aerial.

Frequency (kHz)	Output (Volts)	Comments Range on oscilloscope	Frequency (kHz)	Output (Volts)	Comments Range on oscilloscope
100	2.000	Y amp range 0.5 V/div	155	0.240	0.05V/div
105	1.700	"	160	0.390	"
110	1.400	"	165	0.440	0.1 V/div
115	1.200	"	170	0.590	"
120	0.900	"	175	0.640	0.2 V/div
125	0.700	"	180	0.680	"
130	0.500	0.2 V/div	185	0.850	"
135	0.300	"	190	0.900	0.5V/div
140	0.190	"	195	1.000	"
145	0.042	0.02 V/div	200	1.100	"
150	0.150	"			

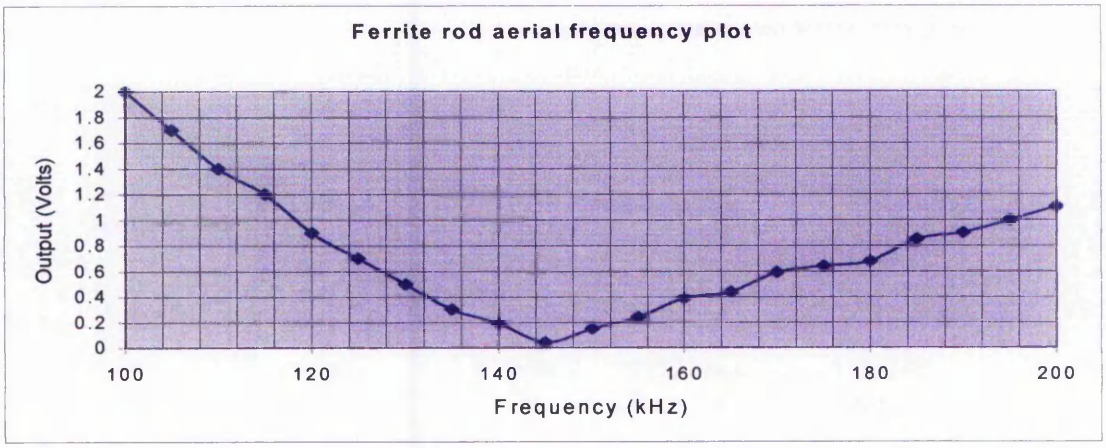

Figure 5.5. Observing that the resonance point is very close to the desired frequency of 150 kHz, indicates that the permeability of the ferrite rod is as determined above, equation 5.2.

The ferrite rod aerial is shown mounted on Vero Board. Plate 5.3

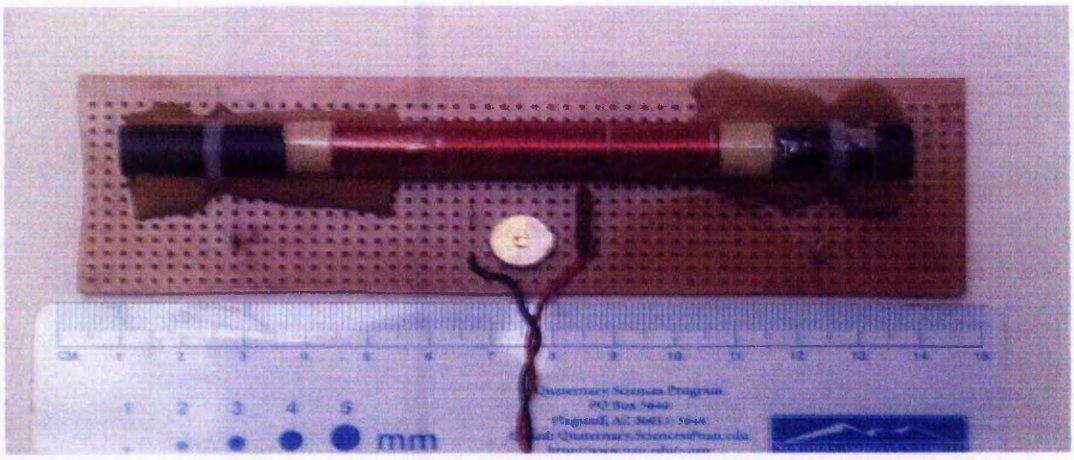

Plate 5.3 The completed ferrite rod aerial with a plastic rule below it to show the scale. Note the tuning capacitor, lower centre. To the right of the tuning capacitor is the silver mica fixed capacitor

5.4.4 *Dipole aerial detector*

The dipole aerial detector was made up of two 97.5 mm lengths of 4 mm diameter copper tube which can be joined by a brass collar as seen in plate 5.4. The dipole aerials

sections the ends which were threaded in order to extend its length were mounted on a nylon holder, which was design to enable it to be fixed to a mounting frame in order to orientate it to investigate the direction and strength of the electric field. The dipole aerial is shown in Plate 5.4

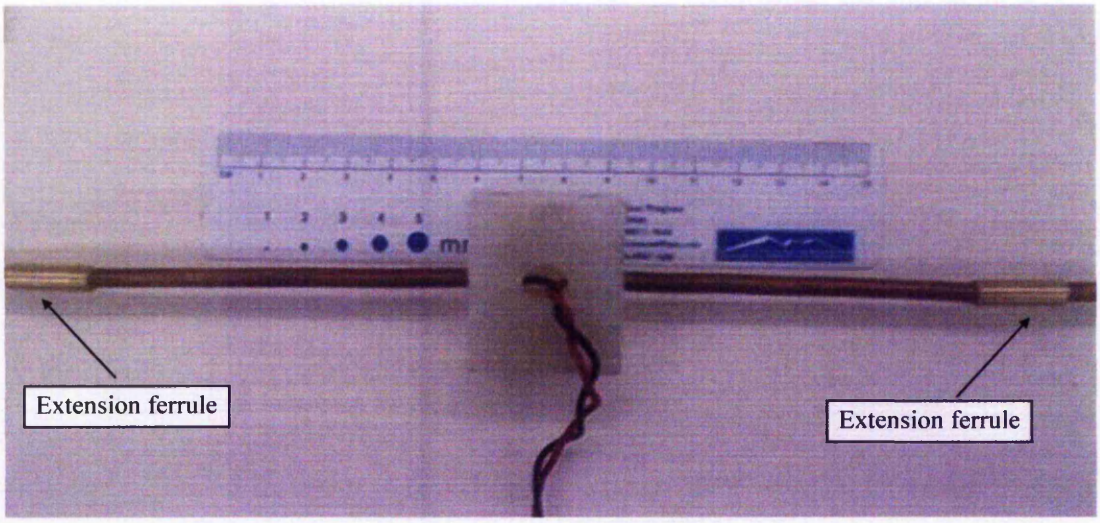

Plate 5.4 Dipole aerial. The brass extension ferrules can be seen to the right and left of the plate.

5.5 Experimental results

Most of the data gathered in the laboratory were recorded using a Tektronix TDS3032 two channel Colour Digital Phosphor Oscilloscope. The recorded details of the laboratory experiments are noted in tables 5.3 to 5.7 (see section 5.5.3). Recording details for Tektronix 3032 digital oscilloscope shown in plate 5.5 are described in section 5.5.1.

5.5.1 *Tektronix recorded data format*

The Tektronix data file structure has two extensions one being the internal file format ISF and the other in Microsoft Excel format CSV. The ISF file was recorded as this has the date and time of each recording, the time-base and 'Y' amplifier channel settings and trigger details.

The data for both files were recorded onto a floppy disk as it may be necessary in the

future to play back a file into the oscilloscope. Each floppy disk only holds thirteen files and when a new disk is put into the oscilloscope its software interprets this as the beginning of a new set of files and records the first entry as data as Tek000000, Tek000001, etc. Careful labelling of the disks and entry of details into a laboratory notebook was therefore required.

For these experiments 50 KHz transducers, that were part of a Pundit flaw tester, were used as more energy could be introduced into the specimen than from the 150 KHz transducers.

5.5.2 *Calibration checks*

Prior to starting the experiments, a check was made on the accuracy of the travel times of the ultrasonic wave through a precision ultrasonic calibration bar. The result is shown in figure 5.6. The travel time for the calibration bar is given as 26.3 μs. whereas from the graph it is seen that the rise of the ultrasonic pulse is 25.0 μ-sec, a discrepancy of 1.3 μs. There were two possible explanations for this:

a) An error in the calibration bar
b) An error in the oscilloscope time-base.

A Bradley Electronics oscilloscope calibrator was used to check the oscilloscope time-base which would be used for the experiments. The time resolution accuracy of the calibrator was < 1ns, i.e. < 1 part in 10^{-9} seconds. The Tektronix TDS 3032 oscilloscope time-base calibration was checked on a range identical to that used in the calibration check for the ultrasonic calibration bar (figure 5.7). The oscilloscope time-base was found to be well within its quoted accuracy. Therefore the calibration figure stamped on the ultrasonic reference bar was deemed incorrect.

The calibration of the standard was checked by carefully lapping the end of the calibration bar with a 1 micron lapping paste to remove any minute burrs or scratches and similarly for each end of the ultrasonic transducers. The two ultrasonic transducers were mounted onto each end of the calibration bar using silicon grease for the couplelent. A force of 10N was applied to the ends of the two ultrasonic transducers to assure a good contact.

Pulses were then applied to the transmitting ultrasonic transducer and the received pulses recorded and stored on the oscilloscope (figure 5.6). The averaging facility, applied to 16 traces, on the oscilloscope was used to remove any small variations in the amplitude. Careful examination of the recording shows the ultrasonic response starting at 25.00 μs ± 1%.

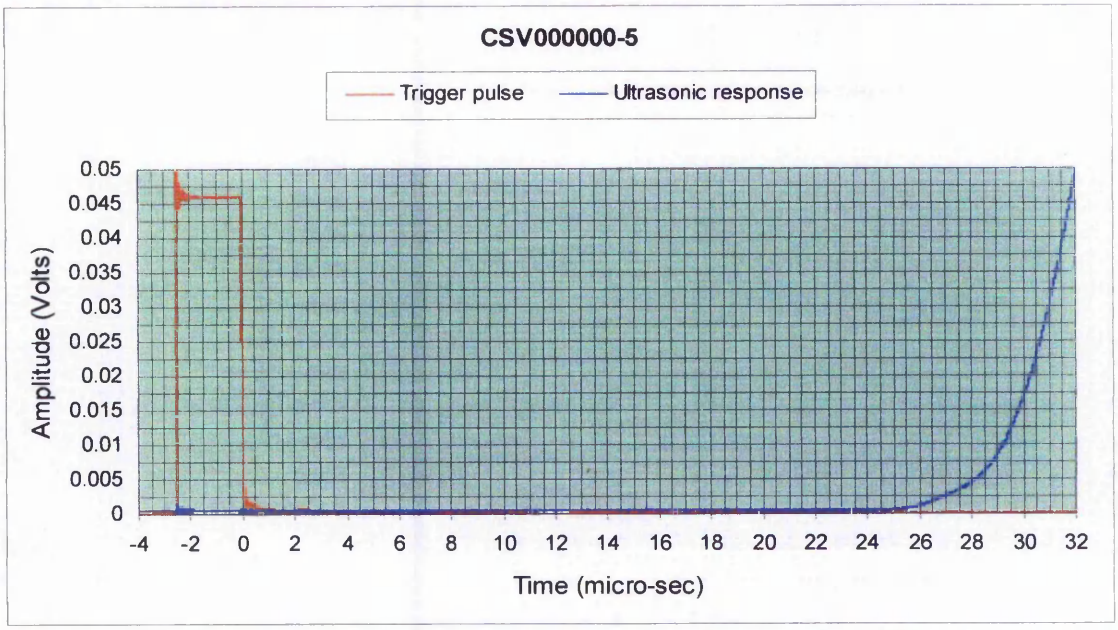

Figure 5.6 Ultrasonic driver trigger pulse (red) and corresponding ultrasonic response after traversing calibration bar. Note the drive signal is triggered on the trailing edge of the pulse.

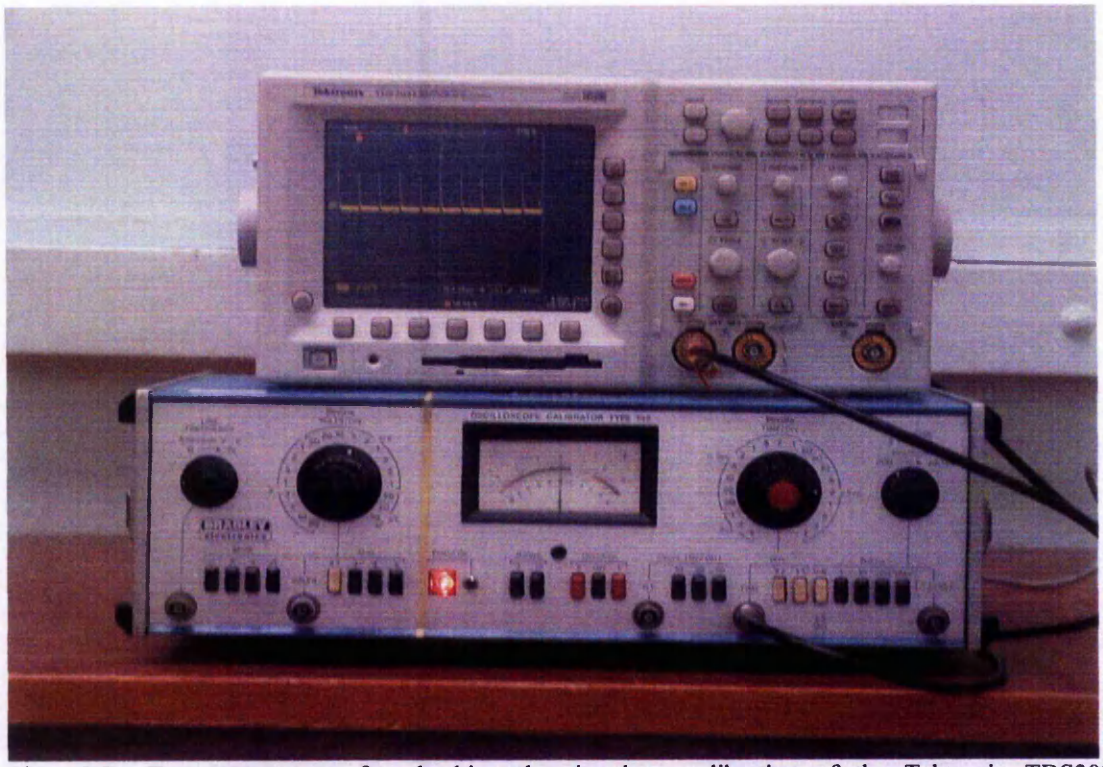

Plate 5.5 Test arrangement for checking the time-base calibration of the Tektronix TDS3032 oscilloscope. The calibration pips can be seen on the screen of the oscilloscope.

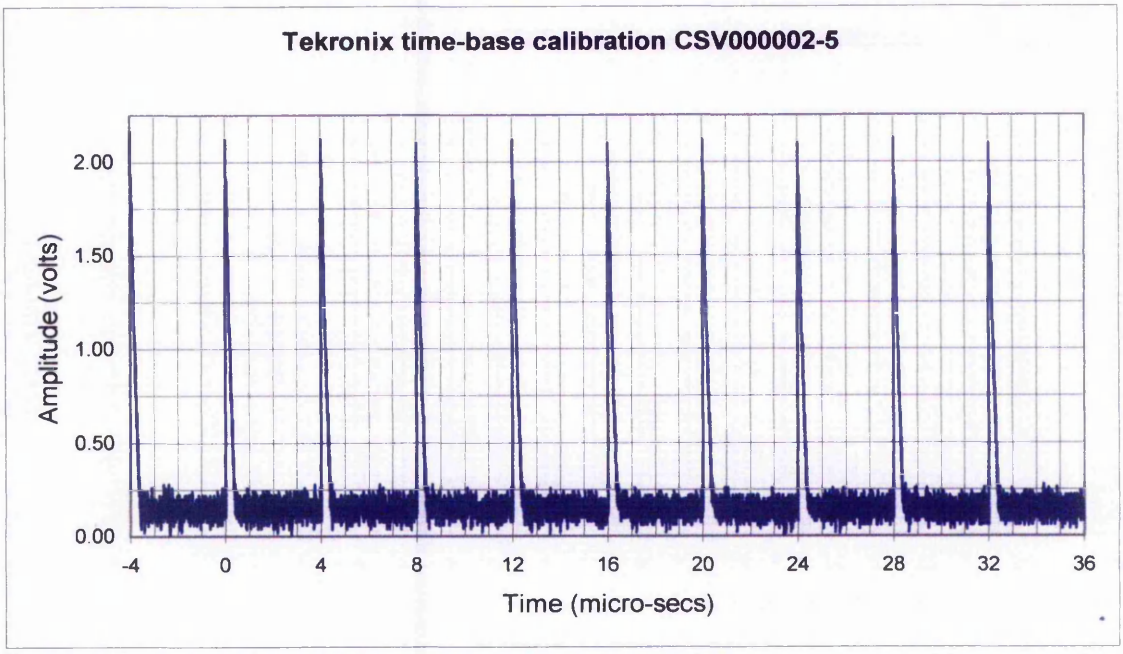

Figure 5.7 Screen record of the calibration. Calibration markers from Bradley electronics calibrator shown as displayed on the screen of the Tektronix TDS 3032 oscilloscope. Note the precise alignment with the screen graticule.

5.5.3 *Details of experimental specimens*

The following characteristics of the possible samples used in the experiments are noted in table 5.3. The samples were water saturated at the time when they were selected for the experiment.

Table 5.3. Dimensional details of specimens used in experiments and their acoustic velocities.

Specimens used in the laboratory experiments						
Sample Ref	Height mm	Width mm	Length mm	Ultrasonic travel time through the height μs	Velocity m/s	Comments
SS0	317.0	101.6	109.0	149.20	2125	Buff coloured sandstone
FSS1	13.32	103.0	180.9	4.90	2718	Fine Red cove
CSS2	11.9	100.47	190.4	9.00	1322	Coarse Red cove
ALS3	20.19	103.6	180.89	4.90	4120	Ancaster limestone
NYL4	49.66			22.60	2200	Irregular off-cut
FSS5	10.288	103.24	188.8	4.00	2630	Fine Red cove
CSS6	12.40	105.0	190.12	9.20	1350	Coarse Red cove
FSS7	15.3	142.7	Dia	6.17	2480	Fine Red cove
FSS8	15.5	142.4	"	5.94	2610	Fine Red cove
NYL9	26.28			12.50	2100	Irregular off-cut
NYL10	16.20	114.8	Dia	7.70	2100	"

5.5.4 *Details of experiments*

A table of all of the EK laboratory experiments is shown in tables 5.4 to 5.7. Because of the limited space for files on the 1.4 mbyte floppy disk only six data sets could be held. Hence, disk 1, 2 etc noted in the tables. Also note that when a new floppy disk is

inserted into the oscilloscope the listing reverts back to 00000. The abbreviation nu under Ch2 represents not used

Table 5.4. Laboratory experimental results for the date shown

Data for the Friday 30th April 2004								
Tek. File No		TB	Y gain		Trig	Sample	V_T	Comments
00000?	Ext	Time div.	Ch.1	Ch.2	%		10	
0	ISF	2.0 µs	1.0 V	nu	50	SS	22.5	Delay between transducers 3.6 µs
0	CSV	"	"	"	"	"	"	"
1	ISF	40µs	200 mV	"	"	"	"	Transit time end to end 152 µs
1	CSV	"	"	"	"	"	"	"
2	ISF	"	20 mV	"	"	"	"	"
2	CSV	"	"	"	"	"	"	"
3	ISF	2.0µs	50 mV	"	"	FRSS 1	"	Transit time 6.2 µs
3	CSV	"	"	"	"		"	"
4	ISF	"	"	"	20	CRSS 2	"	Transit time 10.3 µs
4	CSV	"	"	"	"		"	"
5	ISF	"	"	"	"	ALS 3	"	Transit time 6.2 µs
5	CSV	"	"	"	"	"	"	"
6	ISF	4.0µs	2.0 mV	"	"	Nylon 1	"	Transit time 20.4 µs
New floppy disk (2)								
0	CSV	4.0µs	2.0 mV	nu	20	Nylon 1	22.5	"
0	ISF	"	"	"	"	Nylon 2	"	Transit time 11.2 µs
1	CSV	2.0 µs	1.0 mV	"	"	"	"	"
1	ISF	"	"	"	"	Nylon 3	"	Transit time 8.0 µs
2	CSV	"	"	"	"	"	"	"
2	ISF	20.0µs	1.0 mV	1.0 mV	10	N4 +SS	25	Dipole aerial on ch.1
3	CSV	"	"	"	"	"	"	"
3	ISF	"	"	"	"	"	"	Ch 2. Ultra sonic response 170 µs *1
4	CSV	"	"	"	"	"	"	"
4	ISF	"	"	"	"	"	"	Dipole aerial Ch.1
5	CSV	"	"	"	"	"	"	"
5	ISF	"	"	"	"	N1+SS	"	Ch 2. Ultra sonic response 170 µs
New floppy disk (3)								
0	CSV	20.0 µs	1.0 mV	2.0mV	10	N1+SS	"	"
0	ISF	"	2.0 mV	2.0 mV	"	N2+SS	"	Coil aerial respnse
1	CSV	"	"	"	"	"	"	"
1	ISF	"	1.0 mV	"	"	N3+SS	"	Ch 2. Ultra sonic response 170 µs
2	CSV	"	"	"	"	"	"	"
2	ISF	"	"	"	"	N4+SS	"	Dipole aerial Ch.1
3	CSV	"	"	"	"	"	"	"
3	ISF	"	"	"	"	"	"	Ch 2. Ultra sonic response 160 µs
4	CSV	"	"	"	"	"	"	"
4	ISF	"	"	"	"	"	"	Dipole aerial Ch.1
5	CSV	"	"	"	"	"	"	"
5	ISF	"	"	"	"	"	"	Ultra sonic response 160µs
6	CSV	"	"	"	"	"	"	"

Table 5.5. Laboratory experimental results for the date shown

Data for the Tuesday 4th May 2004								
New floppy disk (4)								
Tek. File No		TB	Y gain		Trig	Sample	V_T	Comments
00000?	Ext	Time div.	Ch.1	Ch.2	%		10	
0	ISF	4.0 µs	1.0 V	nu	10	USCB	22.5	Transit time through bar µs
0	CSV	"	"	"	"	"	"	"
1	ISF	4.0µs	5.0 mV	5.0	"	"	"	Trigger pulse in relation to CSV000 µs
1	CSV	"	"	"	"	"	"	"

Table 5.6. Laboratory experimental results for the date shown

Data for the Wednesday 5th May 2004								
Tek. File No		TB	Y gain		Trig	Sample	V_T	Comments
00000?	Ext	Time div.	Ch.1	Ch.2	%		10	
2	ISF	4.0 µs	1.0 V	NU	10	NA	"	Calibration
2	CSV	"	"	"	"	"	"	"
3	ISF	1.0µs	"	"	"	"	"	"
3	CSV	"	"	"	"	"	"	"
4	ISF	0.4 µs	"	"	"	"	"	"
4	CSV	"	"	"	"	"	"	"
5	ISF	20.0 µs	1.0 mV	2.0 mV	"	ALS 3	"	SSO + ALS Transit time 154.10 µs
5	CSV	"	"	"	"	"	"	"
6	ISF	4.0µs	2.0 mV	"	"	Nylon 1	"	Transit time 20.4 µs
New floppy disk (2)								
0	CSV	20.0µs	1.0 mV	2.0 mV	20	Nylon 1	22.5	"
0	ISF	"	"	"	"	Nylon 2	"	Transit time 11.2 µs
1	CSV	2.0 µs	1.0 mV	"	"	"	"	"
1	ISF	"	"	"	"	Nylon 3	"	Transit time 8.0 µs
2	CSV	"	"	"	"	"	"	"
2	ISF	20.0µs	1.0 mV	1.0 mV	10	N4 +SS	25	Dipole aerial on ch.1
3	CSV	"	"	"	"	"	"	"
3	ISF	"	"	"	"	"	"	Ch 2. Ultra sonic response 170 µs *1
4	CSV	"	"	"	"	"	"	"
4	ISF	"	"	"	"	"	"	Dipole aerial Ch.1
5	CSV	"	"	"	"	"	"	"
5	ISF	"	"	"	"	N1+SS	"	Ch 2. Ultra sonic response 170 µs

Table 5.7. Laboratory experimental results for the date shown

Data for Thursday 25th May 2004								
Tek. File No.		TB	Y gain		Trig	Sample	V_T	Comments
00000?	Ext	Time div	Ch.1	Ch.2	%		30	Transducer response
0	CSV	1 ms	1 mV	1 mV	10	SS0 + ALS 3	"	"
0	ISF	"	"	"	"	"	"	Dipole aerial
1	CSV	"	2 mV	2 mV	"	"	"	"
1	ISF	"	"	"	"	"	"	"
2	CSV	20.0 µs	1 mV	1 mV	"	"	"	"
2	ISF	"	"	"	"	"	"	"
3	CSV	"	"	"	"	"	"	"
3	ISF	"	"	"	"	"	"	"

A recording of the ultrasonic transducer response when transmitted through the length of specimen SS0 (sandstone) is shown in figure 5.8a which clearly shows the effects of transducer ringing. However, as the high voltage exciting pulse is very short, < 5µs, the oscillation slowly dies away. Figure 5.8b is an expanded view of the same recoding. The signal from receiving ultrasonic transducer was fed directly into the 'Y' amplifier channel of the oscilloscope without any prior amplification.

The actual passage through the specimen is 149.2 µs as observed from table 5.3. However, the main point to note is the amount of ringing that occurs after the cessation of the exciting pulse. This was why the lengths of the various soil samples were chosen to be at least 500 mm in length. The effects of this post ringing can be seen in figure 5.9. There are no noticeable effects due to reflections of the ultrasonic wave from the

walls of the specimen.

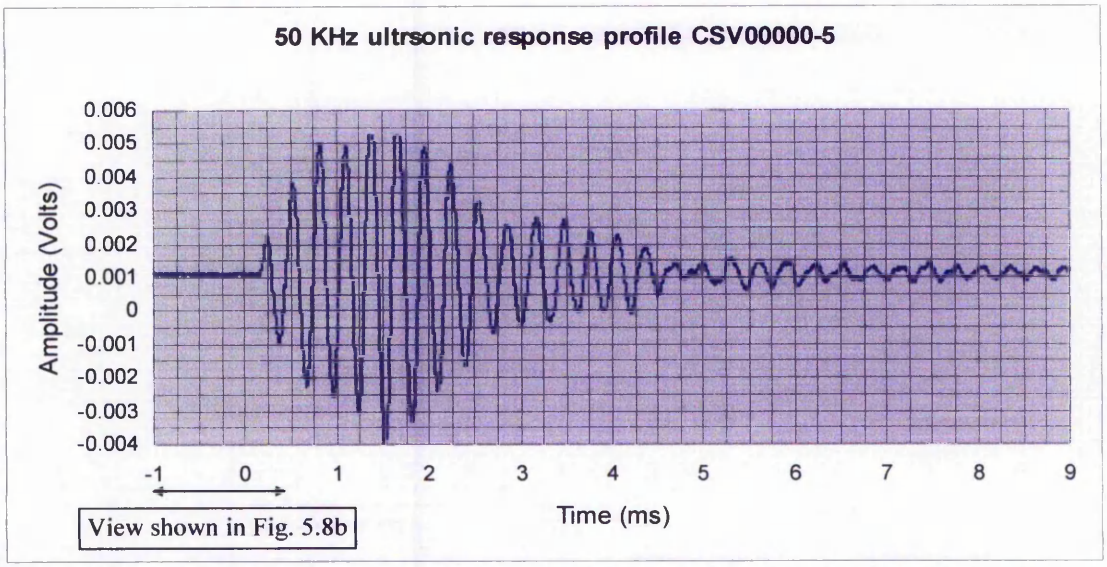

Figure 5.8a. Ultrasonic response profile to show ringing. Careful examination of the recording will show the delay between the application of the excitation pulse the ultrasonic transducer and the arrival of the ultrasonic wave after passing through the specimen. The oscilloscope was set to record 10% pre-trigger detail.

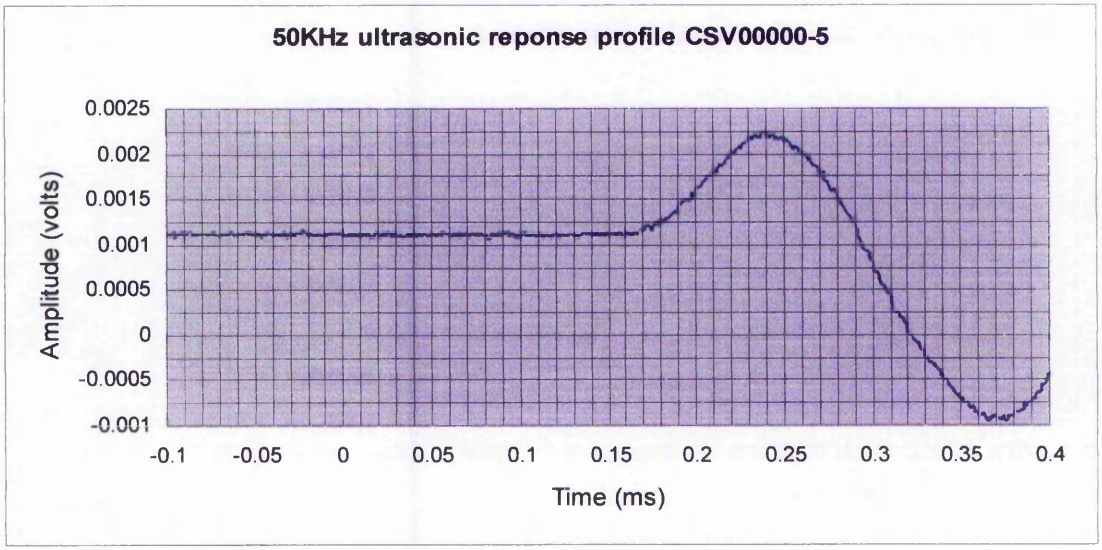

Figure 5.8b. Expanded view of figure 5.8a. This shows the rising edge of the response of the receiving ultrasonic transducer. The time is seen to correspond with that given in table 5.4.

5.5.5 *EK response experiments with SSO sandstone sample.*

To aid the coupling between the specimen SS0 and Ancaster Limestone sample (ALS3) a tissue wetted with a saline solution was placed between the two. The sample ALS3 was selected to create a velocity contrast at the sandstone-limestone interface. The EK response shown in figure 5.9 was observed when conducting setting up experiments. Both the dipole aerial response and that of the ultrasonic transducer are shown. Silicon

grease was used to improve the coupling between the ultrasonic transducers and the specimens. The sample SSO was partially water saturated. The responses in figure 5.10 were with the specimen SSO fully saturated.

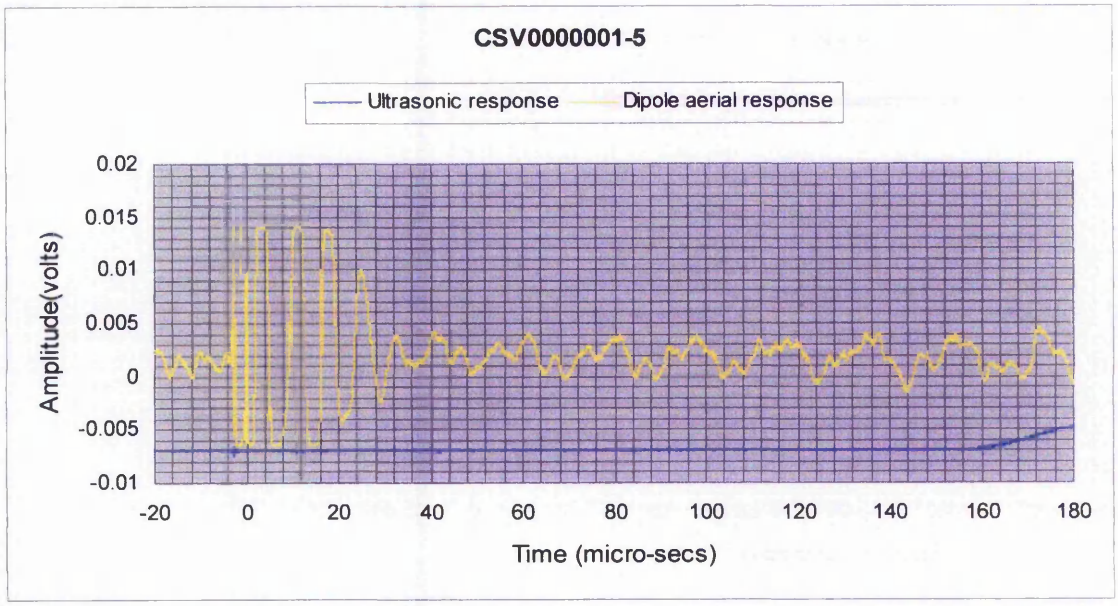

Figure 5.9. Dipole aerial response. Note the large response at the beginning over a period of 28 μ - seconds. This is due to ringing in the driving circuit. The remaining part of the waveform shows small EK responses generated as the ultrasonic wave traverses the specimen. Note the period of 20 μs, i.e. 50 kHz

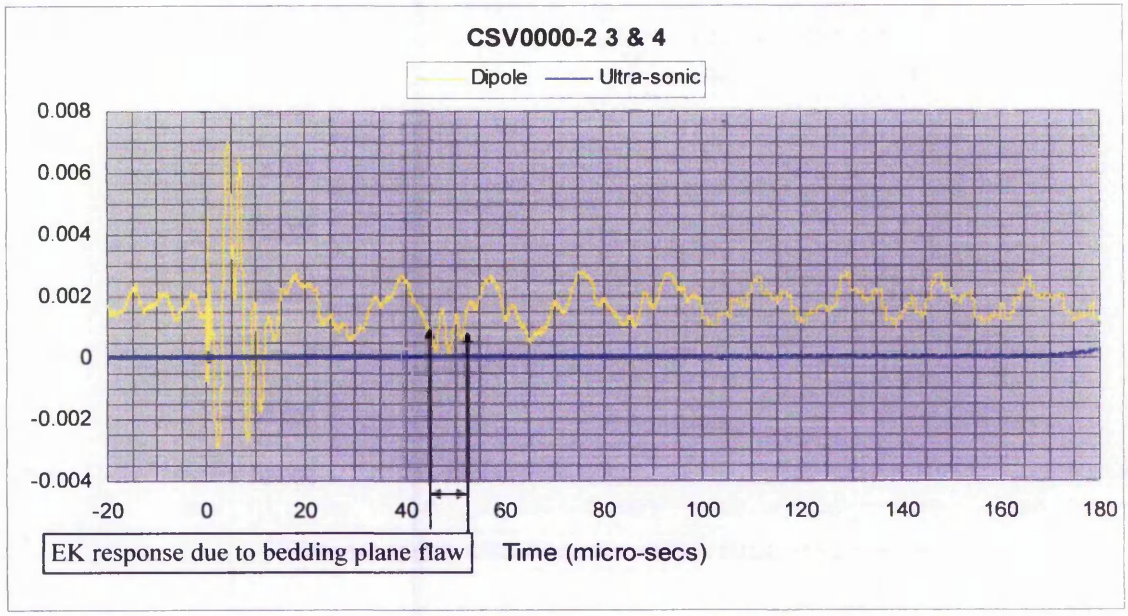

Figure 5.10. Dipole aerial response with ultrasonic response shown for timing purposes

It was considered important to see if similar EK responses could be obtained by turning the specimen upside down and repeating the experiment. The position of the EK responses would be noted and compared with the EK previous responses. If these responses correlated with the data as shown in figure 5.10 this would be conclusive

proof that they occurred at the interface with the bedding plane flaw. The recording shown in figure 5.11 is the result obtained by turning the specimen upside down. However, high frequency noise was removed from the original recording using the noise removal software described in Chapter 8 in order to clearly reveal the two main EK responses.

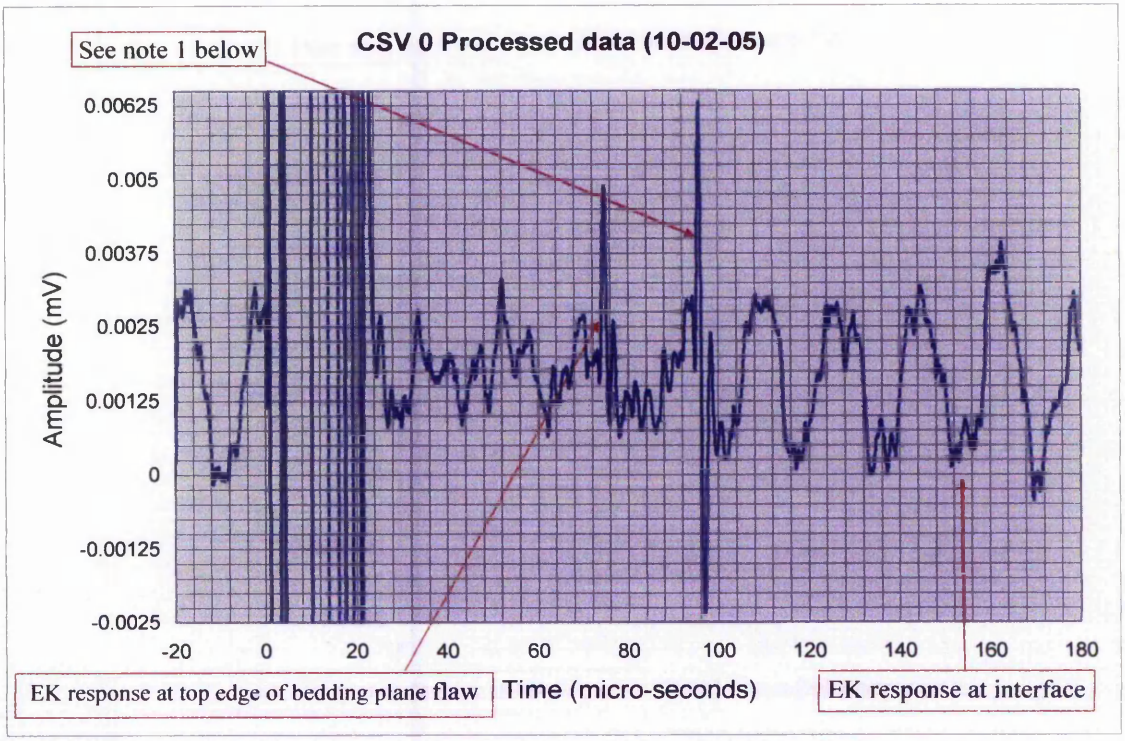

Figure 5.11 Dipole aerial response with specimen reversed from top to bottom.

The response seen at 45 – 55μs, figure 5.10, is due to a noticeable diagonal flaw in specimen SSO, a side view of the specimen is shown in plate.5.6.

Note 1. The response at 96μs figure 5.11 is due to the arrival of the ultrasonic wave at the bottom part of the bedding plane fault shown on the lower left hand side of plate 5.6 at 210mm, i.e., 150 + 60 mm.

The extended EK response in figure 5.10, between 4 and 50μs, and is due to the leading edge of the ultrasonic wave taking a finite time to traverse the bedding plane flaw. The length of the response is seen to be in the order of 8μs, the sloping height of the bedding plane, across the view shown, was measured to be 60 mm. However, on the left hand face it sloped down another 25 mm from its lowest point on the front view.

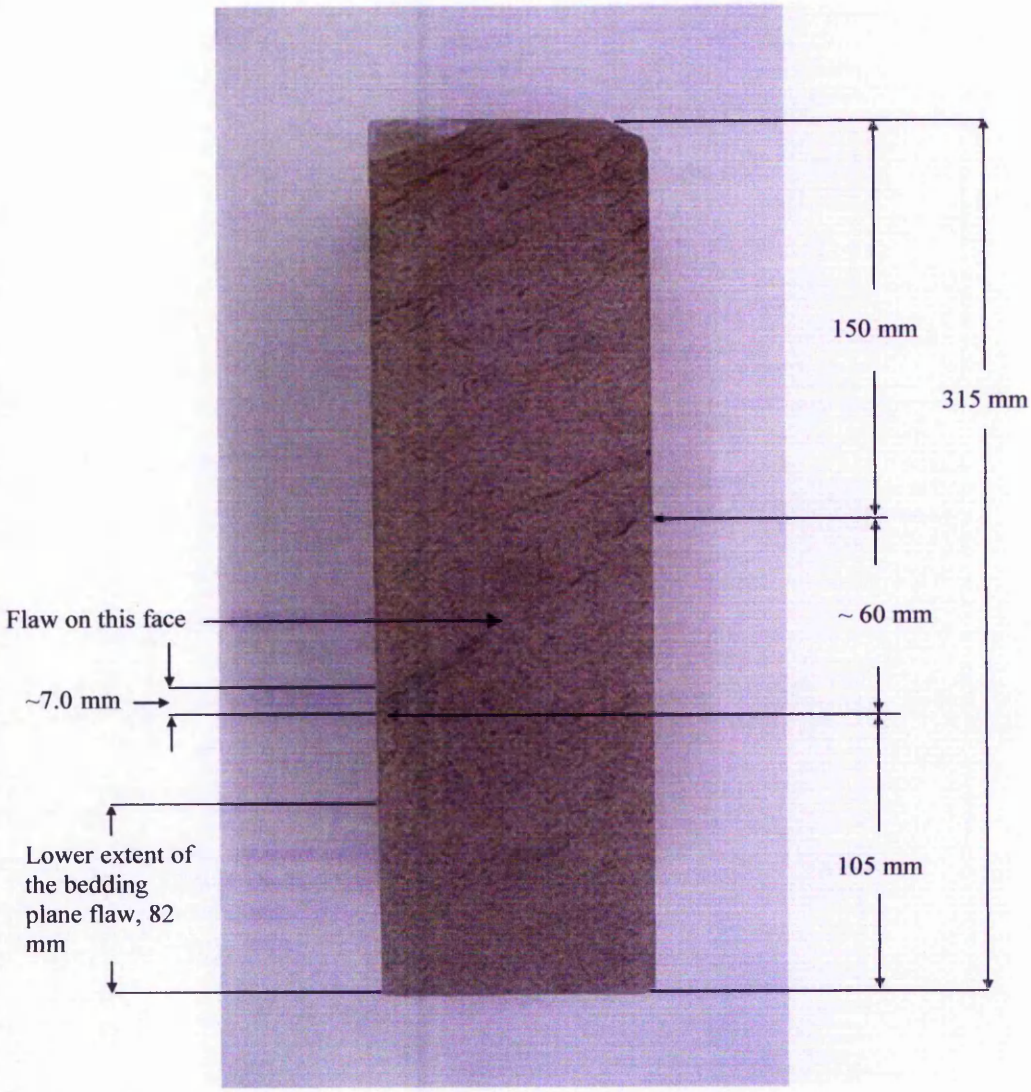

Plate 5.6 The diagonal bedding structure of the specimen 'SSO'.

An isometric view of the bedding plane flaw is shown in figure 5.12

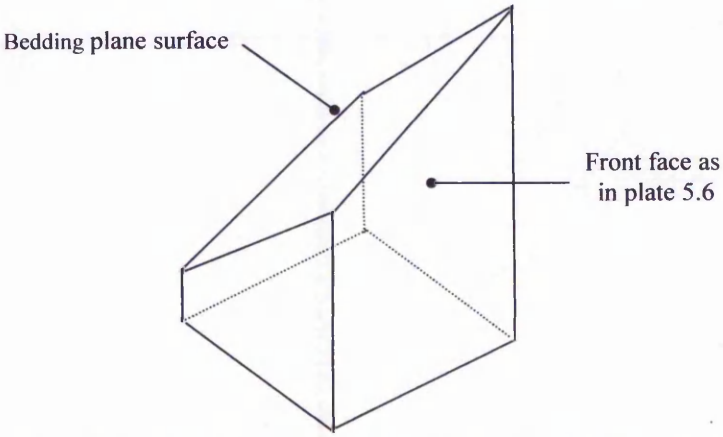

Figure 5.12 3D isometric sketch of the bedding plane in Plate 5.6, not to scale. The top half of the specimen has been removed for clarity

The travel time from the base of the specimen to the lowest edge of the bedding plane flaw is:

$$\frac{\text{Distance}}{\text{Velocity}} = \frac{0.082\text{m}}{2.125\times10^{3}\text{m/s}} = (38.6 + 1.6)\mu\text{s} = 40.2\ \mu\text{s} \pm 10\% \qquad (5.5)$$

1.6 μs must be added to the above result to compensate for the delay time when the two ultrasonic transducers are placed face to face.

Therefore the time to traverse the bedding plane fault from its lowest point on the left hand side face to the top edge shown on the front view is:

$$\text{Time} = \frac{0.023\text{m}}{2.125\times10^{3}\text{m/s}} = 10.8\ \mu\text{s}. \qquad (5.6)$$

This value agrees, within 10%, of the observed wave form in figure 5.10 of 10 μs.

The travel time with the sample turned upside down to the top edge of the bedding plane is:

$$\text{Time} = \frac{0.150\text{m}}{2.125\times10^{3}\text{m/s}} = (70.6 + 1.6)\mu\text{s} = 72.2\ \mu\text{s} \pm 10\% \qquad (5.7)$$

The travel time from the first response to the bottom of the sample turned upside down is:

$$\text{Time} = \frac{0.06\text{m}}{2.125\times10^{3}\text{m/s}} = (27.1 + 1.6)\mu\text{s} = 28.7\ \mu\text{s} \pm 12\% \qquad (5.8)$$

Time of second response is the sum of the two times result in equations 5.7 and 5.8.

$$\text{These are } (72.2 + 28.7)\mu\text{s} = 100.9\mu\text{s} \sim 101\mu\text{s}$$

The second EK response can be seen to occur at 96 μs. However, when compared to the result above at 101μs there is a discrepancy of 5μs. This can be explained by the broad nature, ~7 mm (Plate 5.6), of the bedding plane flaw at the lower position, for the EK

response to occur at the start of this flaw would give rise to a difference of 3.3μs, e.g., $\frac{0.06\text{m}}{2.125\times10^{3}\text{ms}}$. This difference when subtracted from the value of 101μs is within the 10 % error quoted for the result.

The thin bedding plane is approximately 7 mm thick as far as can be estimated from the surface features. The wavelength of the ultrasonic wave is;

$$\frac{2.125\times10^{3}\text{m/s}}{50\times10^{3}\text{Hz}} = 42\text{ mm} \qquad (5.8)$$

Widess (1973) states that a thin bed is one with a thickness of $\lambda_b/8$ where λ_b is the predominant wavelength as found in (5.8). Therefore, as

$$\lambda_b/8 = 5.25\text{ mm}$$

the bedding plane flaw can be justifiably classified as a thin bed.

5.6 Summary of laboratory EK investigations

5.6.1 *Sources of experimental error*

Although the ultrasonic transducer driving circuit worked as designed there were problems with radiated EM interference from the pulse generator and also the ultrasonic high voltage driving circuit. In fact when the driver circuit was switched off there was still evidence of a signal radiating from the Advance Electronic pulse generator, figure 5.13.

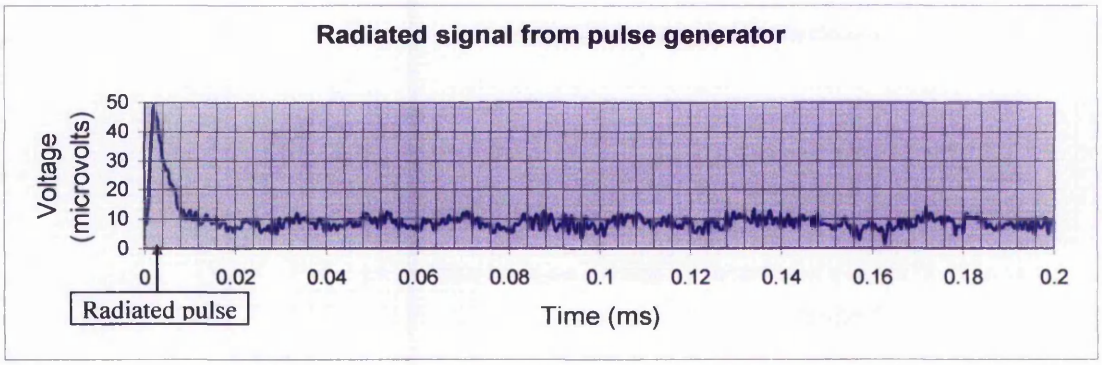

Figure 5.13 The radiated pulse is clearly seen at the start of the recording and has a peak value in the order of 50 μV. The ultrasonic transducer driving circuit was switched off, all other conditions being as normal. The small dc offset is due to a problem within the pulse generator. However, the peak-to-peak background noise is seen to be 10 μV.

5.6.2 *Experimental observations.*

Most of the EK responses were obtained with the dipole aerial as the coil aerial did not detect any EK responses. However, it is intended to carry out further investigations into this with the application of a shear wave source, possibly a bender element.

With a stacking arrangement and signal processing applied to remove the non-EK noise the very small amplitude EK signals will be more easily resolved. It is intended to carry out the noise remove process in real time with use of a digital signal processing integrated circuit such as the Texas Instruments TMS320C64x DSP. It would also considerably aid future investigations with the shear wave source.

The observed increase in ultrasonic velocity with the settlement of loose sand, due to the application of a weight to ultrasonic transducer in the experimental vessel, agrees with the results of the compaction studies described in Chapter 4.

5.6.3 *Concluding comments*

This part of the research took a considerable amount of time bearing in mind the amount of problems encountered and overcome. After some considerable effort positive results were obtained and have pointed the way forward for future EK laboratory investigations. All of the current problems have been identified and solutions found. However, the design and construction of a number of EK laboratory reference standards has been noted as a high priority for any future research.

Chapter 6 EK Spectrometer hardware design

"In science we can aspire to accomplish something
...every discovery, however small, is a permanent gain."

Pierre Curie to Marie, 1894, urging her to
join him in "our scientific dream."

6.1 Introduction.

Due to economic constraints it was decided to consider the design and construction of a purpose made instrument, which when not in use could be used for other applications in addition to the EK investigations (such as shallow ground seismic investigations and the Prima dynamic plate ground testing apparatus). In addition when used as an EK spectrometer it could also be used to analyse EK and seismic data in the field.

6.2 Main factors taken into account for the design of the EK spectrometer.

This chapter will discuss the cost, ease of operation, and development time. The cost of a conventional seismic recorder is in the order of £25,000, by using a ruggedised laptop computer and a purpose designed interface a considerable cost could be achieved.

6.3 Design outline

For the reasons outlined above, the design was based on a portable ruggedised laptop computer with a plug in PCMIA card and a purpose-designed low noise preamplifier module. A block diagram of the EK spectrometer is given in figure 6.1. In addition to the specifications outlined in 6.2 the more technical requirements features are listed below:

(1) To have a continuous operating time in the field of at least ten hours

(2) To store recorded data files on a floppy disk in SEGII format, these would also be backed up on the hard disk and on 1.4 Mb floppy disc or on a 16 Mb or larger memory pen.

(3) To be compatible with SEGII seismic and radar data format, Pullen (1993)

(4) Ease of incorporating modifications

(5) Reliability.

(6) To have a minimum of 12 EK data input channels.

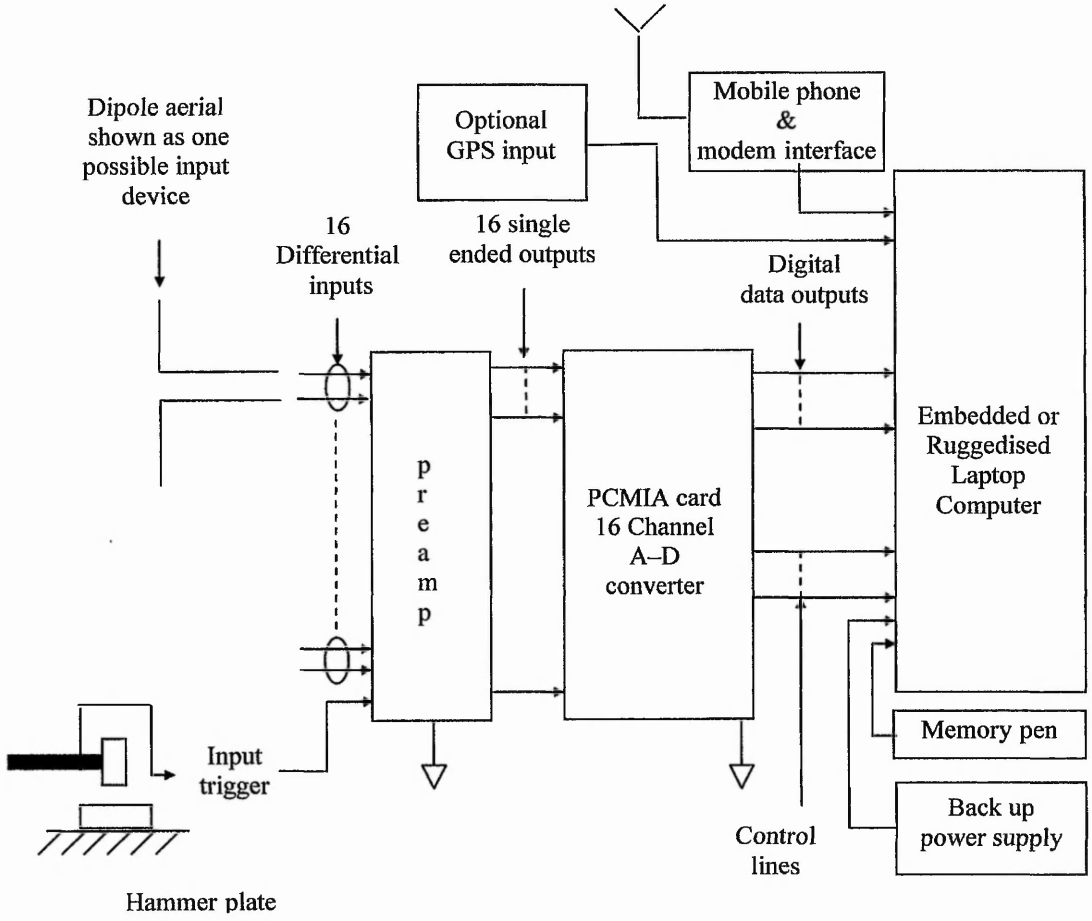

Figure. 6.1 Block diagram of EK Spectrometer

The PCMIA card comprised a 16-channel 16-bit A-D converter with self-contained timers and an external-internal trigger facility. A circuit diagram and notes are shown in Appendix Q. A low noise preamplifier system was constructed to act as a front end to the PCMIA card. Previously, a two-channel version of the preamplifier had been designed, built and successfully evaluated for an earlier EK project. The 16 channel pre-amplifier system was housed in a die cast waterproof case mounted underneath the laptop computer and contained all of the sockets for the connection of the geophones, EK aerials and trigger cable. The preamplifier housing was designed to be easily demounted from the laptop computer.

Also shown in figure 6.1 are options to add a mobile phone data link and a Global Positioning System 'GPS' receiver module. A back up power supply is shown which will provide ten hours continuous use in the field. An additional power supply option has already been designed, which will run off a car cigarette lighter socket. Allowance was made for the attachment of a 64 Mb memory pen to the USB port as an alternative data storage device to a floppy disk. A larger capacity memory pen can be used if it is required. However, a 64 Mb unit is more than sufficient for the results of three to four days field work.

In the field, a temperature variation of 30^0C can be encountered, therefore a temperature monitoring 'K type' thermocouple was permanently assigned to channel 16 of the A-D converter and was mounted on the die cast box as this would be at the temperature of its surroundings. This would enable temperature corrections to be applied to the data as the in house calibrations were conducted at 23^0C.

The seismic hammer is a conventional 4.5 kg sledge hammer fitted with a piezo-electric trigger element. The seismic hammer plate was made from a 50 mm thick Ultra High Molecular Weight (UHMW) polypropylene sheet, being cut to 254.0 mm diameter. An 8 mm hole was drilled in the side of the plate and a 4 mm thick polypropylene rope made into a loop was fixed into the hole to assist removal form the ground.

A photograph of the pre-amplifier board (looking down onto its component side) is shown below in plate 6.1. The multi-pin connector socket seen on the right of the plate is the connection to the laptop computer. The green connector block on the left of the board is the input connections from the two Amphenol 27 pin fixed plugs connectors, for the input the signals from the geophones or EK aerial. The 16 black sockets house the Burr-Brown 1N118 low power, low noise input amplifiers.

The specifications for the laptop computer and PCMIA card are given in appendices A and B. Specifications for electrical and mechanical details of the pre-amplifier are given in Appendices D and E.

Plates 6.2 to 6.5 provide various views of the key elements of the EK spectrometer.

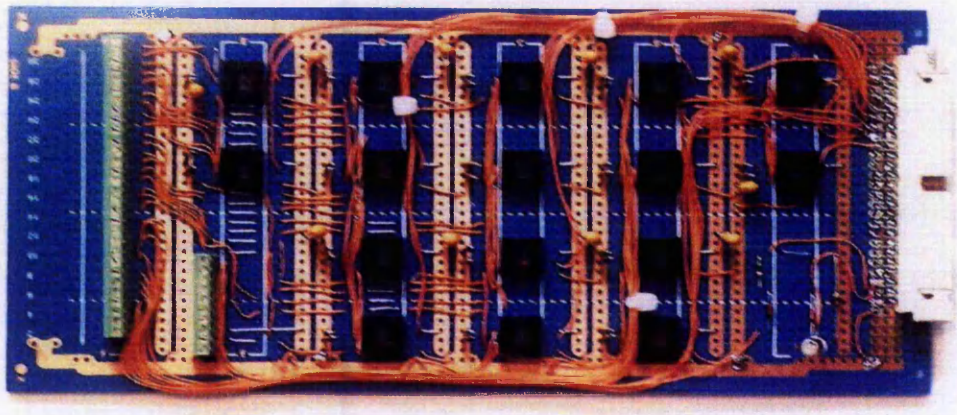

Plate 6.1. Left hand side shows the printed circuit board input connector BC1 in green. The sixteen black sockets are where the 1N118 integrated circuits are mounted. On the RHS is the 50 way insulation displacement connector by means of which the pre-amp board is connected to the DAS 16/16 A/D card. In the lower right hand corner is where the trigger circuit is housed.

Plate 6.2. Is a view of the pre-amplifier card mounted in the die cast box and plate 6.3 shows the laptop computer mounted on the preamplifier box. Finally, in plate 6.5., an angled view of the die cast pre-amplifier housing is provided which clearly shows the quick release bracket in the foreground.

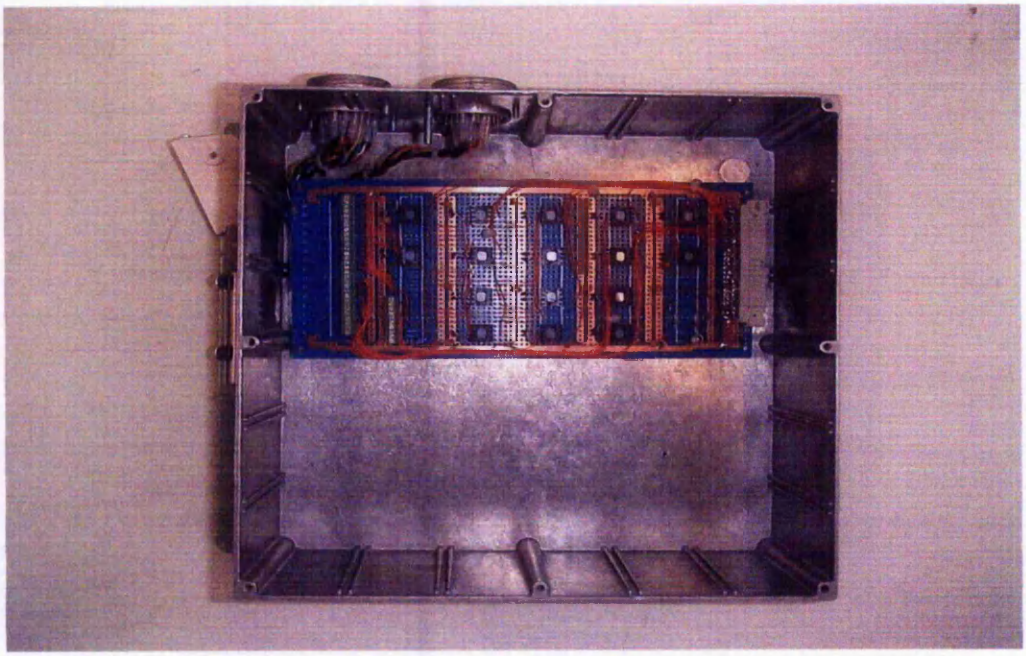

Plate 6.2 View of pre-amplifier card mounted in the die cast box housing

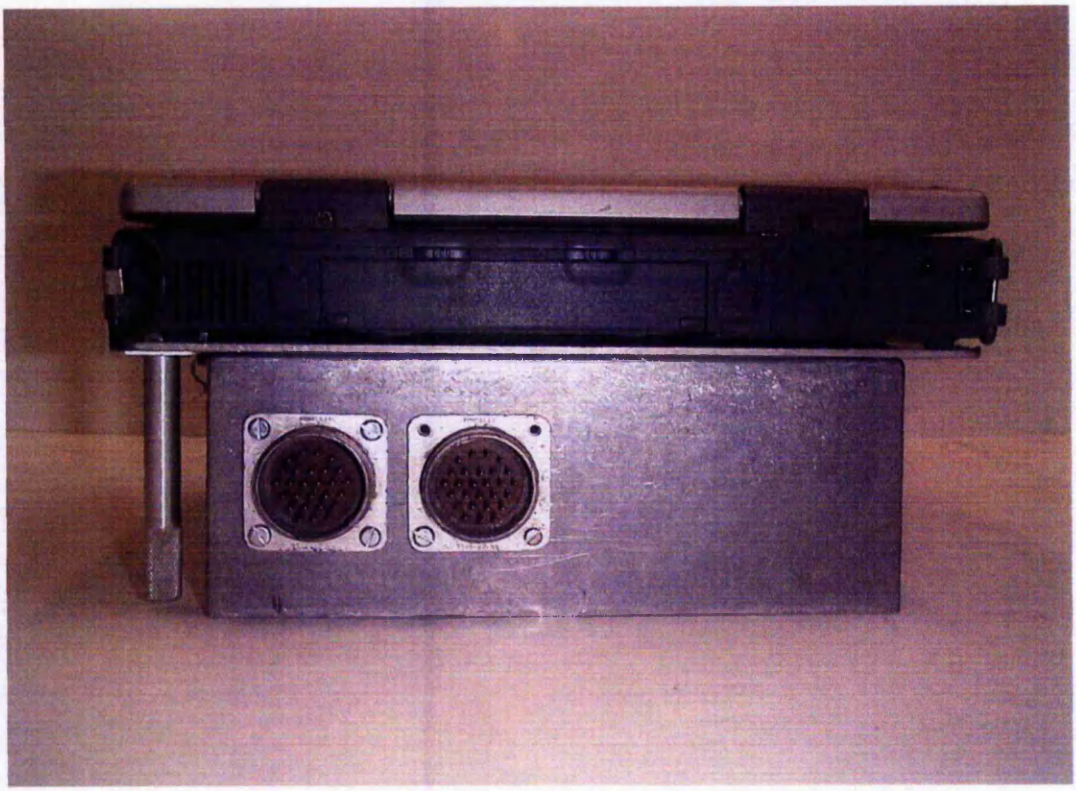

Plate 6.3. Rear view of pre-amplifier housing with the laptop computer mounted above. The two NK 27-S data input sockets are clearly visible. The bracket, lower right, is the quick release fixing to the laptop computer. Note the fixing screw on the same side held in position by two 'Terry clips'.

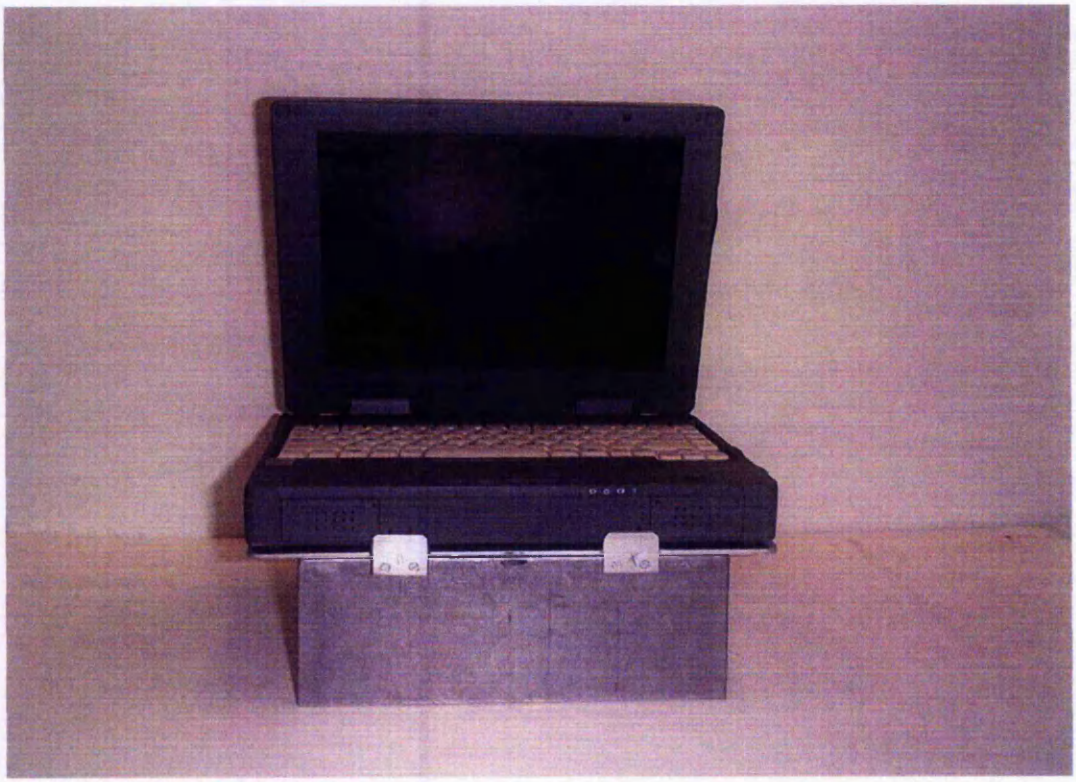

Plate 6.4. Front view of EK spectrometer. The two brackets shown at the top of the die cast box are the quick release 'claws' which locate into two slots in the laptop computer.

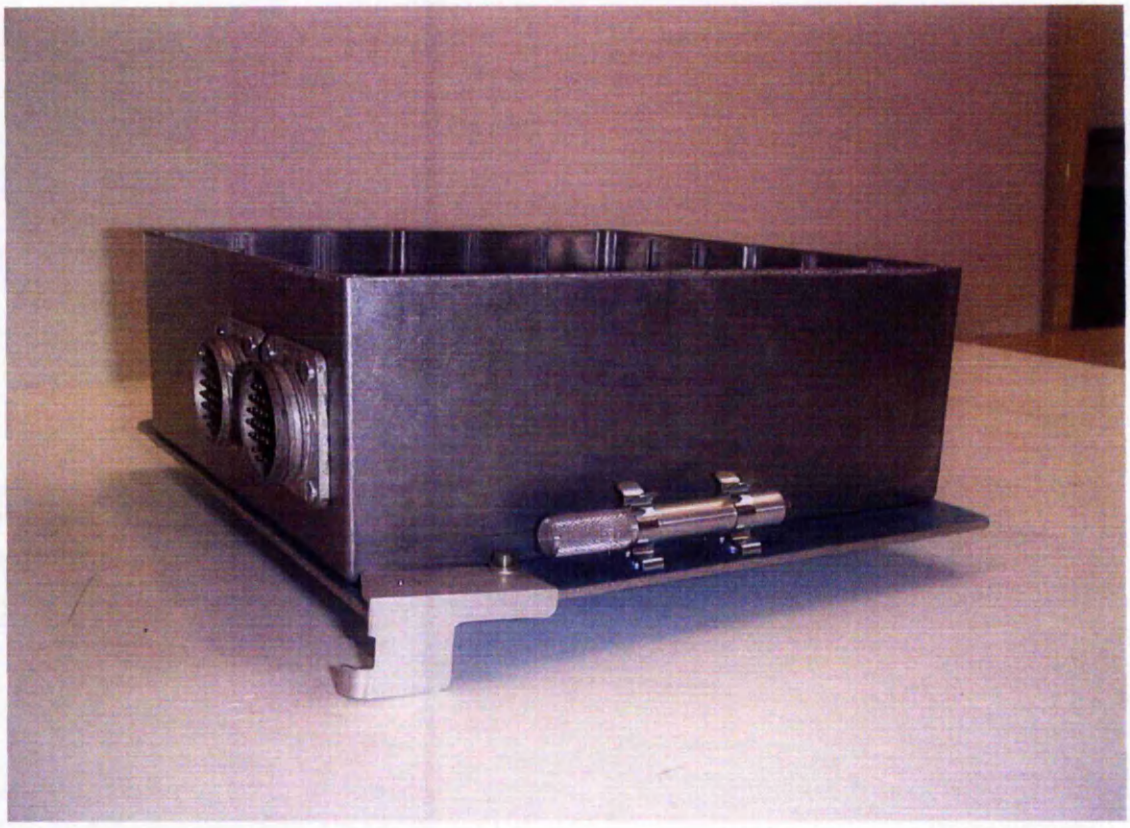

Plate 6.5. An angled view of the die cast pre-amplifier box clearly showing the quick release bracket in the foreground. The clamping screw pillar is shown in its storage position.

6.3.7 *Software for laptop operation.*

It was decided to use 'AGILENTVEE' for the software development for the following reasons:

(a) It was available within the University

(b) It contained MATLAB script which was used for the data processing

(c) Software drivers were available for A-D card.

(d) The application programme can be used as a compiled stand-alone subset of the main development package, which has a free license.

The software for the operation of the laptop data gathering, manipulation and display was developed using the full development package but downloaded to the laptop as an embedded application. This saves considerably on computer hard disk space and RAM memory, ensure that the software cannot be altered by a user and has the advantage that it does not require any licence. Any modifications have to be done on the main development package and then downloaded as a patch. This also has the advantage that it is not possible to interfere with the embedded software. At this stage the 50 Hz and its

harmonics noise removal programme has not been included purely due to the constraints of time, however it is available on the desktop processing system using 'MATLAB', (see Chapter 8).

6.3.8 *Technical details*

The maximum sample rate of the A-D converter was 100kHz, therefore given 16 channels the individual sample rate for each channel would be 100kHz/16 = 6.25kHz. This would give a Nyquist sampling frequency which corresponds to 3.0 kHz per channel Nyquist (1928). The minimum sample rate based on these figures was set at 0.25 milliseconds. The range of sample rates was set to be 0.25, 0.50, 1.00, 1.25, 2.5, 5.00 and 10 ms, all controllable via software. The option to extend the range and number of samples to 1024, 2048, 4096 or 8192 samples per shot was maintained to provide extra flexibility, should this be required.

The trigger circuit was designed to operate either from a seismic hammer contact closure or trigger pulse of minimum amplitude 0.20 volts. For calibration or noise monitoring purposes, it would be internally triggered on a repetitive basis via the software. An analogue 50/60 Hz notch filter was not included in the design as this can lead to signal distortion and phase shift of the received signal, a very important consideration when detecting very low level signals and analysing their arrival times and other features. For similar reasons high and low pass filtering was not included. The digital noise filtering process, high and low pass digital filters available on the desktop computer do not give rise to these problems.

As an addition a facility to record on one channel, and extend the recording time, e.g. for a sample rate of 0.125 ms and record length of 8196 samples and using one channel a total recording time of 8196 x 16 x 0.000125 = 16.392 seconds was incorporated.

A 12-volt battery pack was designed for use with the laptop computer in order to extend its operating life in the field to ten hours. The design was based on a 12 volt sealed lead acid battery with a capacity of 7.0 ampere hours.

6.4 Design of preamplifier.

The design of the pre-amplifier is based on a Burr-Brown, (See TI), precision low

power instrumentation amplifier type 1N118. The minimum voltage resolution of the A-D converter is $1.25/2^{16}$ volts, which is 19.07 μ volts. To provide a higher resolution the gain of the preamplifier was designed to be 1.907, 3.81 and 19.07, to give resolutions of 10, 5 and 1.0 μ-volts. At these gain levels the frequency response is flat to 12 KHz. The voltage noise figure for the 1N118 is quoted as 0.28 nano-volt at a gain of 1000 over a frequency range of 0.1 to 1 kHz, with the source impedance (R_s) being zero. The current noise is quoted as 80 pico-amps peak-to-peak under the same conditions. The noise contribution from sources external to the main amplifier have been kept to a minimum by using high quality precision metal film resistors, see section 6.4.5 on resistor noise below.

The circuit diagram of one of the preamplifier channels is given below with the trigger circuit shown as well. The complete unit is completely self-contained with an internal power supply based on four AA batteries.

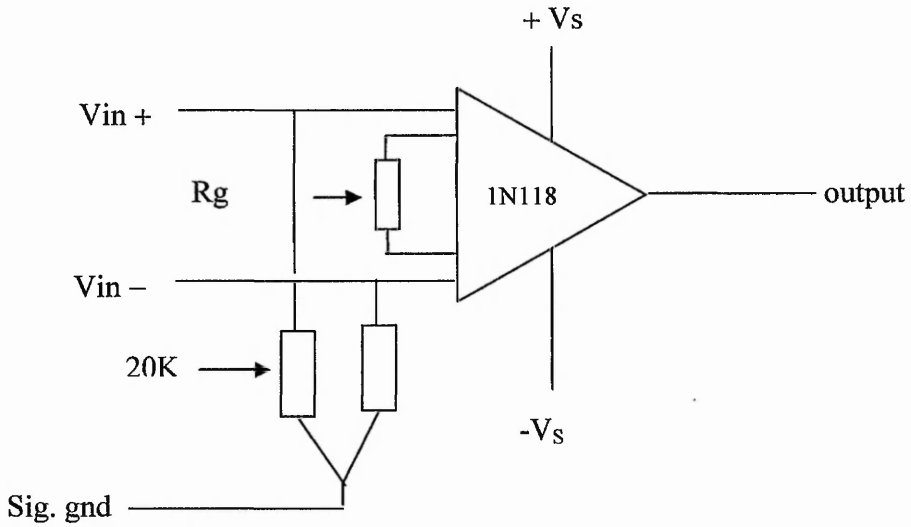

Figure 6.2. Circuit for preamplifier. The complete specification, data sheets, parts list and drawing for the above are given in Appendices. E and F.

The total current consumption is typically 6 mA, which would give a total operating time in the field of 33 days based on 9 hours use per day. It is easily detached from the laptop computer making servicing and testing a straightforward process.

6.4.1 *Preamplifier details*

The full technical details of the low power instrumentation amplifier used in the pre-amplifier can be downloaded from the TI website in PDF format. It has the ability to run from a supply range of ± 1.35 volts to ± 18 volts. In this

application it was decided to have the power supply set to ± 3.00 volts which comprised two sets of standard AA batteries as these are available worldwide at a low cost. The total current drain was 6.0 ma giving the batteries a continuous operating life of 100 hours used on an intermittent basis say 8 hours a day. This would provide at least 12 days use.

6.4.2 *Gain equation of 1N118 instrumentation amplifier*

The gain of the input amplifier is important to detect very low amplitude EK responses, typically in the range 1μ-volt to a few tens of millivolts with a lower noise level as possible. The least significant bit (LSB) of the A-D converter is 19 μ-volts, therefore signals below this level need to be amplified

The gain 'G' is given by the following equation

$$G = 1 + 50k\Omega/R_G \qquad (6.1)$$

Rearranging to give equation 1 in terms of R_G we have

$$R_G = 50k\Omega/G\text{-}1 \qquad (6.2)$$

Example: To amplify a 0.5 μ-volt signal to 19.07 μ-volt a gainof 19.07/0.5 is needed, which is equal to 38.14. From eq.6.2 above.

$$R_G = 50{,}000/(38.14\text{-}1) = 1346.25 \text{ ohms or } 1K346.25 \text{ ohms} \qquad (6.3)$$

6.4.3 *Effects of resistor tolerance on gain.*

For analysis of the EK data it is important that the gain of the input pre-amplifier is as stable as possible, or to know what the possible gain variation is for a given resistor tolerance. As an example take a precision metal film resistor with a tolerance of 0.5% as in the above example. 0.5% of 1346.25 ohms is 6.73 ohms

Take the upper limit of 1346.25 + 6.73 = 1352.98 ohms substitute this in eq'n. 6.1 above

$$\therefore\ G = 1 + 50000/1352.98 = 37.96 \qquad (6.4)$$

This gives rise to a gain error of 0.47%. Taking the lower limit of 1346.25 – 6.73 = 1339.52 ohms again substitute this in eq.6.1 above

$$\therefore G = 1 + 50000/1339.52 = 38.33 \qquad (6.5)$$

This gives rise to a gain error of 0.50%. Thus the overall gain variation is ± 0.5%.

To reduce this gain variation further, 0.1% resistors were used. For most applications these errors are acceptable, however, the effects of the temperature coefficient of the resistors must also be taken into account, this is discussed in section 6.4.4.

6.4.4 *Effects of the resistance temperature coefficient on gain.*

For the resistors considered above, the temperature coefficient is quoted as ± 50ppm/^{0}C over an operating temperature range of –55^{0}C to 155^{0}C.

For the resistor value of 1346.25 ohms used in the above examples, a ± 1 ^{0}C change in temperature will change the resistance by 1346.25 x 50 x 10^{-6} ohms = 6.73 x 10^{-2} ohms. In the field, a working temperature range of 0^{0}C to 40^{0}C would not be uncommon. The resistance values are normally quoted at 23^{0}C so in this case have a range –23^{0}C to + 17^{0}C exists which would result in a resistance change of –1.55 ohms to +1.13 ohms.

To reduce the temperature coefficient variation metal film resistors with a resistance tolerance of 0.1% and a temperature coefficient of ± 15ppm/^{0}C were chosen as they only added a small amount to the overall cost and would reduce both the effects of resistor tolerance and temperature coefficients described above to an acceptable level.

6.4.5 *Theoretical noise in resistors.*

The effects of noise and sources of noise are complex and it is not intended to go into this subject area in any depth: further information of electronic noise is provided by Callen (1951). However, a brief outline of the different sources of noise is provided in order to clarify the noise that is being discussed below. Thermal noise is caused by the thermal motions of electrons within a conductor that has resistance, R. Shot noise results from the fact that current is not a continuous flow but the sum of discreet impulses in time, each corresponding to the transfer of an electron through the conductor.

In contrast to thermal noise, shot noise cannot be reduced by lowering the temperature of the resistance. Flicker or pink noise (otherwise known as 1/f noise) is noise whose power spectrum is a function of the frequency range being considered. It behaves like $P(f) = \frac{1}{f^2}$ where a is very close to 1. If 'f ' is mapped onto a logarithmic scale it has an even distribution of power, e.g. there is as much power in the octave 200 – 400 Hz as there is in the octave 2kHz – 4kHz. There are other sources of noise that are not relevant to the noise voltage referred to below, which is thermal.

The noise power, P_N, in a resistor is given by

$$P_N = k.T.\Delta f \text{ watts (der Ziel, A. 1954)} \qquad (6.6)$$

Where k = Boltzman's constant 1.38×10^{-23} joules K

T = Absolute temperature –273.15 K

Δf = system bandwidth Hz.

$$\text{Therefore the noise voltage } V_{noise} = \sqrt{4.k.T.\Delta f.R} \text{ volts} \qquad (6.7)$$

The noise voltage for the resistor used in the examples above, see section 6.3.4, would be

$$V_{noise} = \sqrt{4 \times 1.38 \times 10^{-23} \times 296.15 \times 5000 \times 1346.25} \text{ volts} = 3.33 \times 10^{-7} \text{ volts} \qquad (6.8)$$

The important fact to be aware of is that this noise is random and is due to the physical movement of thermal electrons within the resistor.

The input bias current return path resistors of 20k ohms were chosen to match that of most seismic recorders. The noise contribution from these will be calculated:

$$V_{noise} = \sqrt{4 \times 1.38 \times 10^{-23} \times 296.15 \times 5000 \times 2 \times 10^{4}} \text{ volts} = 1.26 \ \mu \text{ volts.} \qquad (6.9)$$

As the noise is random it will not cancel out in the differential input. The noise contribution from the integrated circuit must also be added to the resistor noise above. The quoted noise over a bandwidth of 1KHz is $10nv/\sqrt{Hz}$.

Figure 6.3 is a recording of the output noise for a pre-amplifier gain of 32 with its input shorted out. The result was recorded on a Tektronix 3032 digital oscilloscope.

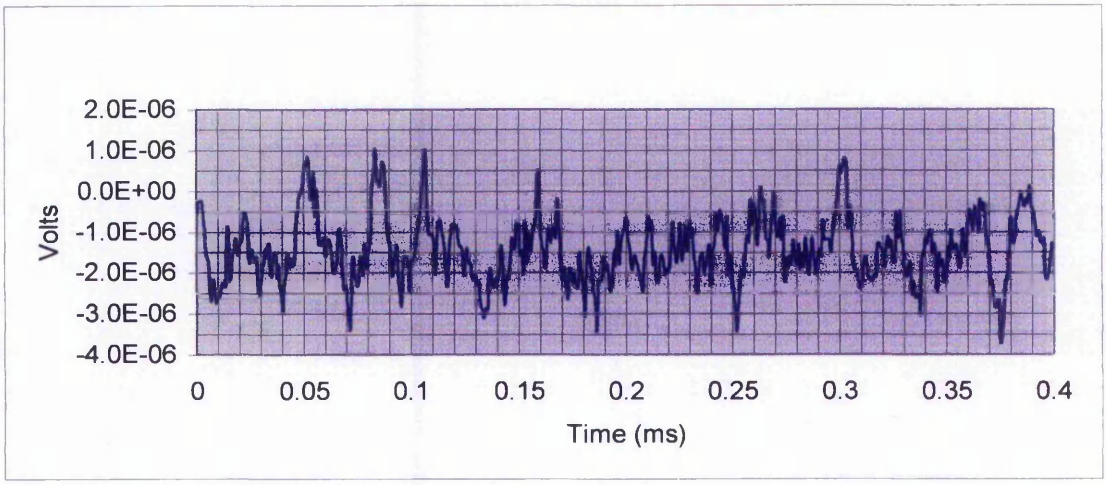

Figure. 6.3. Pre-amplifier noise recording. The rms output noise pp is 3.0 μ-volts. Referred to the input, the noise is 0.09375 μ-volts. Note the amplitude scale on the left of the graph. This also includes the noise contribution from the oscilloscope. This result is very close to the theoretic calculation for the noise level, taking into account resister noise + pre-amplifier noise + oscilloscope noise.

For comparison, a recording of the oscilloscope noise on channel 1 is shown in figure 6.4. The 0.49mv offset is due to an offset adjustment error in the vertical channel of the oscilloscope.

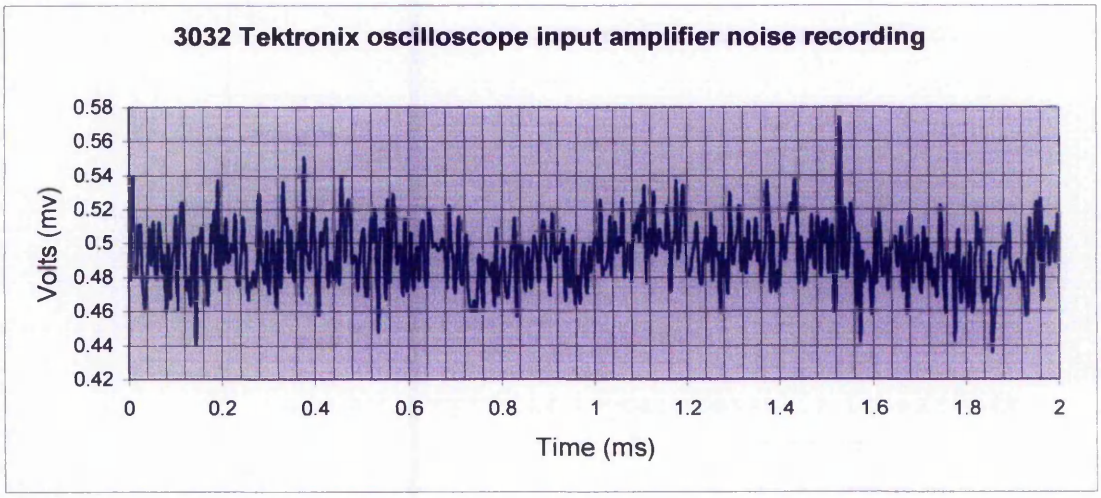

Figure. 6.4 The input amplifier sensitivity was set at 1 milli-volt per division with the time-base set at 200μ-sec per division.

The noise level seen in figure 6.4 is higher than that shown for the pre-amplifier however, this is not serious as the recorded EK signals are processed within MATLAB or Excel. The oscilloscope is mainly used for testing and fault finding and as such has no influence on the field recorded data. For the laboratory recording of the EK

responses a single channel version of the pre-amplifier was used with its gain set to 32 as a front end to the oscilloscope

6.4.6 *Frequency response of pre-amplifier*

The frequency response of the pre-amplifier, figure 6.2, is shown up to the point where frequency roll off occurs (at approximately 200 KHz in figure 6.5). However, the frequency range of interest for EK field investigations is 0 to 5 KHz see section 6.3.8. This is therefore much higher than our recording equipment.

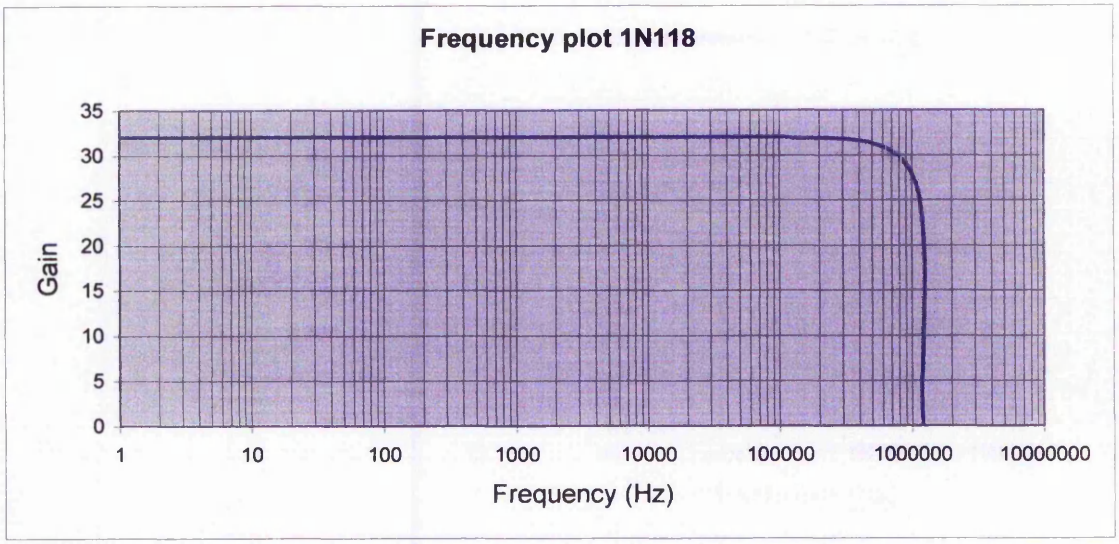

Figure 6.5. From an operating viewpoint the main frequency range of interest is 0 to 5 Khz.

6.4.7 Pre-amplifier input connections

Details of the input connections to the pre-amplifier module and other related wiring are provided in Appendix G

6.5 Input trigger circuit

The input trigger circuit was designed to work with a seismic hammer, a relay contact closure or piezo electric trigger. An optical isolator chip, able to withstand a 3000 volt transient, was included in the design to provide input protection against any misuse, should a mishap occur a replacement integrated circuit is easily fitted. The input connector for the trigger circuit is a 'Bendix' fixed socket part number PT 06F 08. 04SN, this is standard for most seismic recorders.

The circuit shown in figure 6.6 is contained on the preamplifier printed circuit board. Input 1 is for the signal from the piezo electric element on the seismic hammer and

input 2 is a relay contacts.

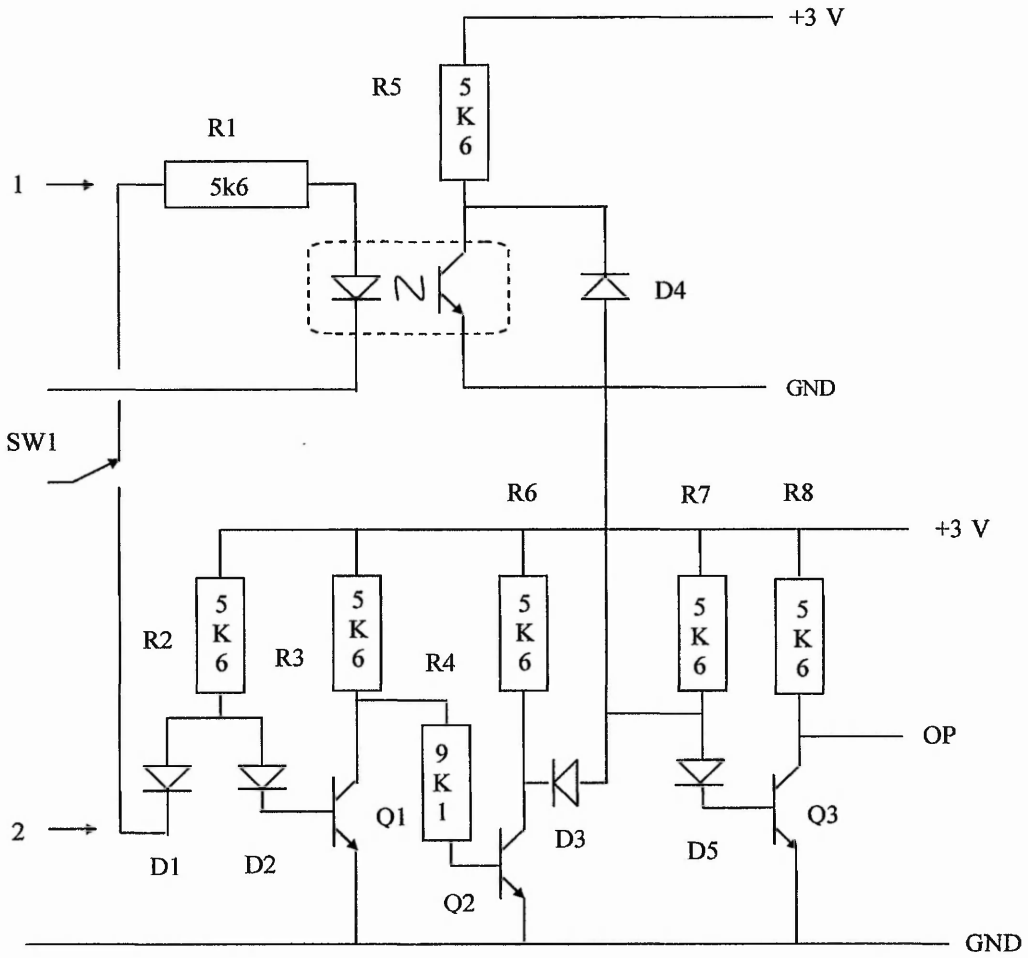

Figure 6.6 Input trigger circuit for seismic hammer with relay contacts or piezo electric device

6.5.1 Description of circuit operation.

Switch SW1, (figure 6.6), selects either the relay contact closure, or piezo electric device or a seismic hammer. For input 1, an impulse is received from the piezo electric element on the seismic hammer with the positive going transition of the impulse causing current to flow through R1 and the light emitting diode in the opto-isolater assembly. In turn a current will flow in the collector circuit of the light sensitive transistor and hence the voltage across the collector to emitter circuit will decrease down to a low value. This will cause current to flow through D4 and R5 thereby reverse biasing D5 and turning off the current flow in Q2. The voltage across Q2 will rapidly rise causing the recording system in the laptop computer to start its recording programme.

Similarly, for input 2 with no input applied transistor Q1 is turned on by the current

flowing through R2 and D2 resulting in diode D3 being reverse biased and thus allowing current to flow through D7 and R5 therefore causing the voltage across Q3 to fall close to zero volts. When the relay contacts on the seismic hammer close due to plate impact, D1 is shorted to ground causing Q1 to switch off resulting in the voltage across Q3 to rise causing the recording system in the laptop computer to start its recording programme. A typical response from a piezo electric actuator in a seismic hammer is shown in figure 6.7.

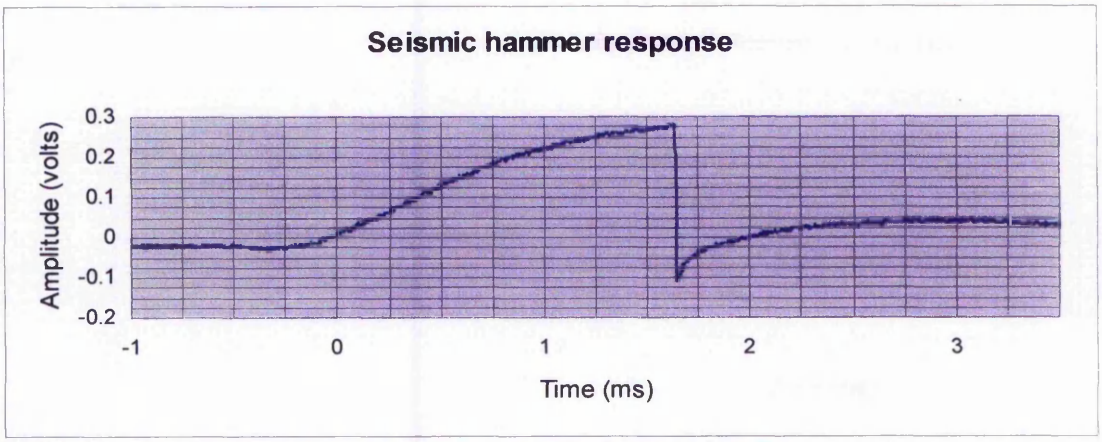

Figure.6.7. Response from the piezo electric element on the seismic hammer.

Another possible trigger device is a geophone place near to hammer plate. The output signal from this can be fed into the piezo electric input.

6.6 Test and calibration module

For the purposes of testing both in the laboratory and field, a unit was designed for use in both situations, (it would also help to locate faults in the EK spectrometer should they arise). Again, cost was one of the main considerations. The specification decided upon was as follows:

1 In view of the need for field use, it was required to run on standard 'AA' batteries and to have low power consumption.

2 Make available simultaneous signals for all sixteen channels with the capability to switch signal in and out in any combination.

3 Output signal to be either an adjustable width pulse or a differentiated pulse

4 An adjustable pulse delay of 1 to 20 ms

5 An adjustable pulse width of 1 to 10 ms

6 One shot facility to be available

7 Trigger output for EK spectrometer.

8 A precision stepped voltage output for amplitude calibration purposes.

A circuit diagram is shown in figure 6.8. The unit was designed to operate both in the field and laboratory and to be simple in operation. The digital integrated circuits IC1 & 2 were low power C-MOS with IC3a and b being low power operational amplifiers. It was therefore designed to be powered by two sets of AA alkaline batteries to provide ± 3.00 volt supplies. The batteries are available worldwide and are reasonably cheap.

The output functions have been kept to a minimum in order to facilitate easy and straightforward operation while at the same time providing meaningful signals. The whole unit takes a total current of + 3.0 ma and -1.0 ma which will enable it to function for 125 hours. The power supplies are not shown in order to simplify the circuit diagram in figure 6.8. However, they are controlled by a shutdown circuit to conserve power. There is also a normal off-on switch to isolate both power supplies.

6.6.1 *Description of operation of calibration module*

The bistable circuit formed by IC1 is to eliminate switch bounce from SW1, a biased toggle switch. In its normal, position the output of the upper logic element is in the low state, however, when SW1 is depressed its output goes high and triggers the monostable IC2a which has an on time set to 5ms, (adjustable by means of R3 which is a variable resistance). When IC1a returns to its stable state, it triggers the monostable IC1b which generates a positive going pulse of duration 8ms, which is adjustable by means of the variable resistance R5, on its Q output (which is buffered by transistor Q_1 and the output from its emitter driving a CR circuit of IC2b). The leading edge of the pulse from IC2Q is integrated by the CR network with the expression for the voltage being given by equation 6.10:

$$v = V_{max}(1 - \exp^{-t/cr}) \qquad (6.10)$$

where t = time, v is the voltage across R and V_{max} being3.0volts in this case.

The trailing edge of the pulse is differentiated by the CR network and the expression for the voltage is given by equation 2, the discharge case for a CR circuit.

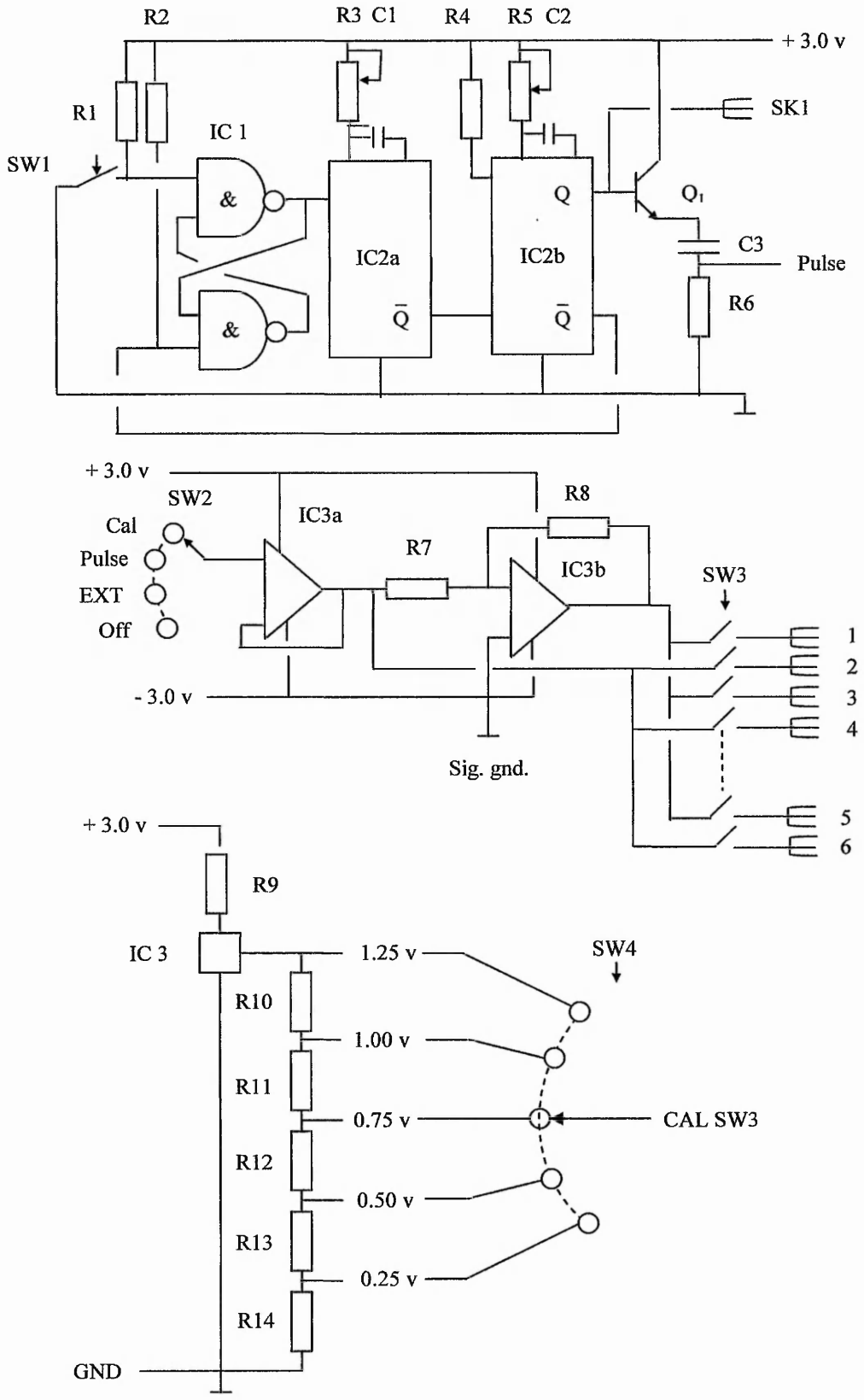

Figure. 6.8 Circuit diagram for calibration module. For further details consult drawing and parts list in Appendix

$$v = V_{max}exp^{-t/cr} \qquad (6.11)$$

The $\bar{Q}$ output from IC2b is used to reset the bistable IC1. IC4 is a 1.25 volt low noise voltage reference across which is a voltage divider made up of precision metal film resistors to give a range of output voltages as shown in figure 6.8.

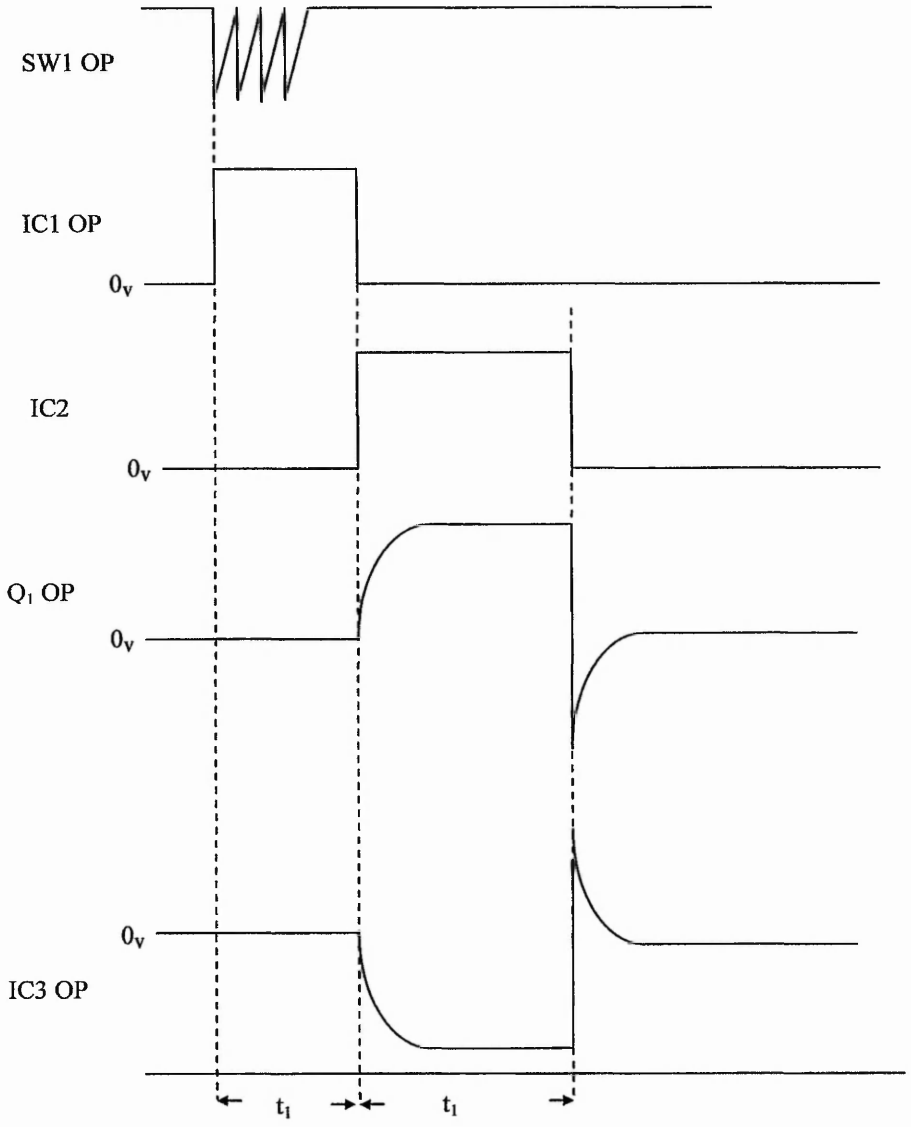

Figure 6.9 Operating sequence and input/output waveforms of IC1, IC2a and IC2b.

The voltage outputs are selected by SW4 which is buffered by IC3a to avoid loading them and possibly affecting the voltage output. IC3a is a voltage follower providing a high input impedance, > 10^{10} ohms, and unity gain. The output from IC3a is fed into the input of IC3b which has a voltage gain of unity, determined by the ratio of R6 and R7, with its input signal inverted. The waveforms for figure 6.8 are provided in figures 6.9

6.7 Concluding remarks on EK spectrometer system.

One further development could be a single channel version designed solely for EK investigations. This would eliminate the expense of a multi channel A-D PCM1A plug in board, typically £800. However, a single channel high resolution 24 bit sigma delta A-D converter would be needed such as the Crystal Corporation's CS5321/2. This unit is available on a development board at a modest cost therefore saving time and effort to design, and construct a printed circuit board. Very minor changes would be needed to the software to accommodate such a unit. With the multi-channel version already designed built and tested the single channel version could readily be deployed due to the modular design of the system.

Three further advantages of the single channel system are:

(1) The faster sampling rate that could be employed limited only by the characteristics of the CS5321/2.

(2) The wider dynamic range of the unit, i.e. 24 bit. This is equal to a gain of 16,777,216.

(3) The unit would also be suitable for laboratory investigations

Very late in the day DAS16/16 was found to have become faulty. It was replaced by the PMD1603FS unit described in Chapter 7 sections 7.2.1 c and 7.2.2.

Chapter 7

EK Spectrometer Software Design

Who taught the raven
in a drought to throw pebbles
into a hollow tree,
where she espied water,
that the water might rise
so as she could come to it?

Francis Bacon (1561-1626)

7.1 Introduction

There were two stages to the software design:-

1. The design of the software to control the laptop computer and its data gathering function. This made use of the AGILENT HPVEE software package in which there is MATLAB script programming language embedded. This is described in this Chapter. The more technical details of the system are described in Chapter 6 and will be referred to as necessary. For reasons of time the system does not incorporate a graphical user interface (GUI). The use of 'Borland C or C^{++} and Visual Basic were both considered for this application but with more experience of MATLAB it was decided to use software based on this.

2. The design of the software to process and analyse the data gathered in the field by the EK spectrometer. This is described in detail in Chapter 8.

7.2 General description.

In designing the software for both of the two applications listed above the SEGII seismic data format was adhered to, this is described in more detail in Chapter 8. This would ensure compatibility with most other seismic systems apart from some of the earlier systems. The data available from various seismic recorders appears as binary or ASCII formats, this may not be the case for some very old designs. Provision has been made to set the data input routine to accommodate either of the above two formats, if in very rare cases it is needed to input data from one of the older seismic recorders the

programme can be modified to do this. Once the data was placed in a file the data display routine simply displays the data in a strip chart format, (see figure 7.3), together with timing lines. Individual channel gains are shown at the top of each trace in decibels (db's).

$$\text{Gain in db} = 20\log\frac{V_2}{V_1} \qquad (7.1)$$

where V_2 and V_1 are the output and input voltages of the a-d system respectively. In practice the input and output impedances across which V_1 and V_2 are obtained must be the same.

There is a fill routine that fills all of the positive or negative going waveform transitions with a colour, normally black, this aids the determination of break points and calculation of seismic velocities. There is a facility to enables the determination of the seismic velocity for a given set of first arrivals. It is possible to invert one or more of the displayed traces as sometimes when shear geophones are used it is possible that one has been placed in the ground the wrong way round i.e. 180 degrees resulting in an inverted waveform. Signal processing and wavelet analysis toolboxes are used to provide, energy spectrum analysis, digital filtering and phase information of the recorded waveform among other things.

The software has been designed to allow other functions to be incorporated at a later date if required.

7.2.1 *EK Spectrometer software*

The EK spectrometer is composed of three main modules:

a) The ruggedised laptop computer.
b) The preamplifier module.
c) The analogue to digital converter module, PMD1603FS.

The preamplifier module is a low noise front end to the system and is not under software control. The analogue to digital converter requires software control of its various functions as does the laptop computer in which it is housed. Reference was

Very late in the day DAS16/16 was found to have become faulty. It was replaced by the unit mentioned in 7.2.1 c. This replacement unit feeds into the USB port making the interfacing easier. However, it has 8 single ended channels as against the 16 in the previous module. It is possible to have two of the new modules running in tandem but for reasons of cost a second module was not purchased as this can be retrospectively fitted at a later date if required. For further information refer to the PMD1603FS users guide revision 1, 2004.

7.2.2 *Design of overall operational process*

The starting point was to design a flow chart of the functions required in the data collection process. The flow chart for these is shown in figures 7.1, 7.2, 7.3 and 7.4.

For some of the boxes shown to figure 7.1 there will be a separate flow chart for the function they perform (see figures 7.2, 7.3 and 7.4). After selecting the EK spectrometer control program, a series of prompts appears such as set sample rate, set sample period, etc., as shown by the boxes on the left hand side of the flow chart. The date and time are inserted automatically from the computer date and time clock.

These data are compiled in SEGII format and stored as header information. When the system is switched on, a prompt appears asking for either the recording mode or the monitoring mode. The monitoring mode allows the display to continuously monitor all incoming signals from the all of the selected channels. This is useful in seismic investigations in setting up each channel gain for the geophone signals. Also, if the EK aerial is placed on channel 13, channels 1 to 12 being used for seismic geophone inputs, the gain will need to be set to allow optimisation of the received EK signal. If a data sample period of say 100ms seconds is selected at a sample period of 0.125 ms then 800 samples are recorded for one data sample.

Having set up the recording parameters the system is then placed in the recording mode. The trigger circuit is automatically set to the external trigger mode and waits for an external trigger signal. The trigger circuit defaults to trigger on the positive edge of a signal. However, it is possible to set the system to trigger on the trailing or negative edge of a signal. With receipt of a trigger signal the system records the input signal data for all of the parameters selected and stores the data in a register on the 'c' drive.

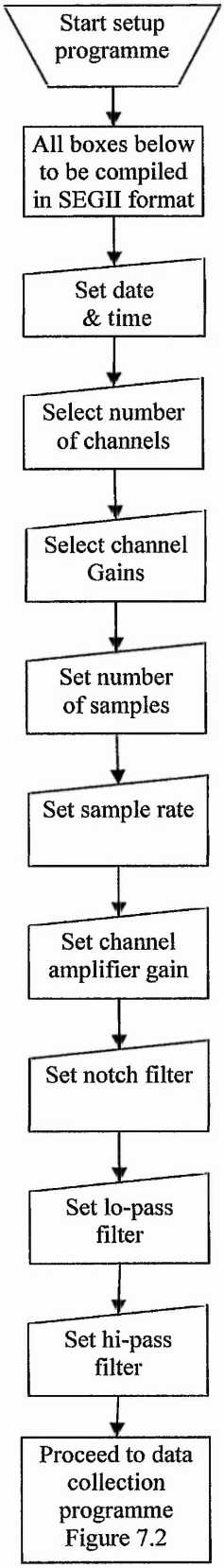

Figure 7.1 Initial setting of EK spectrometer

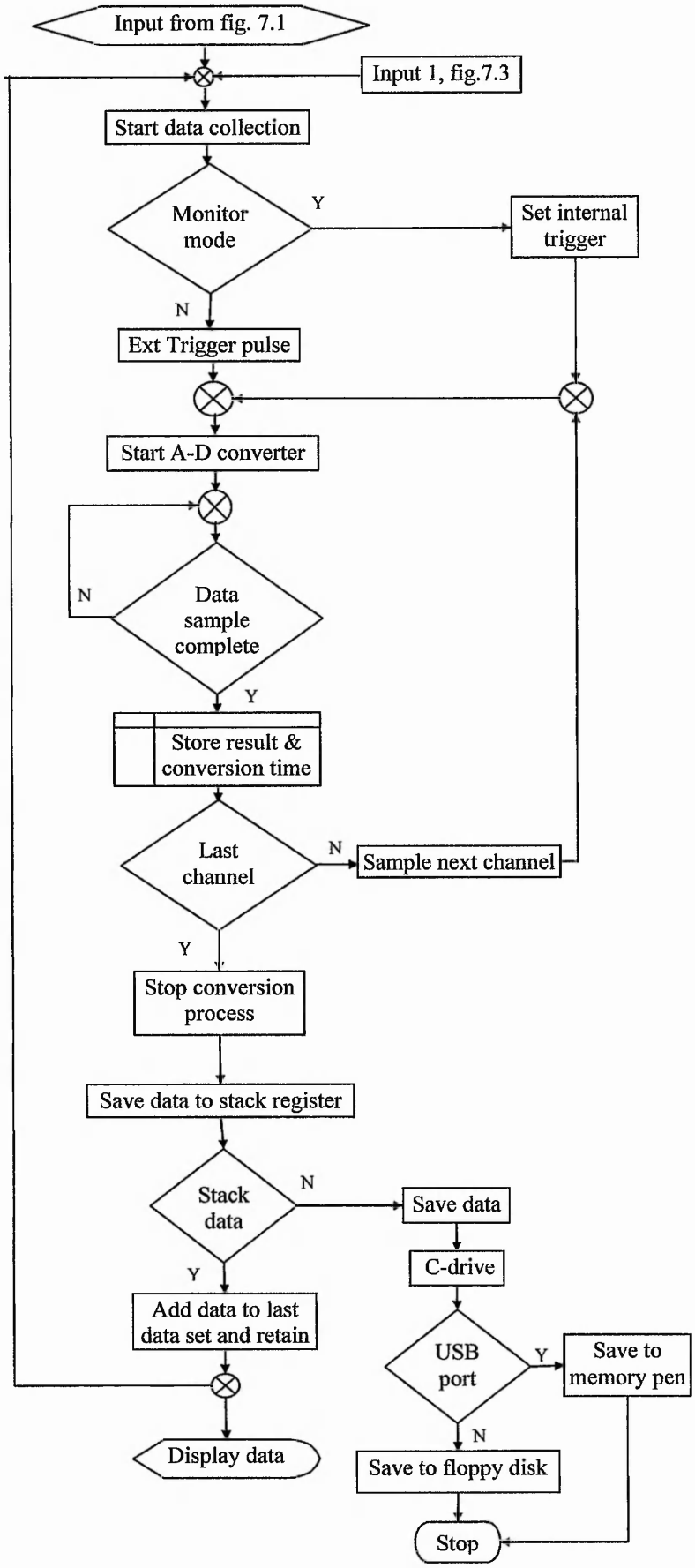

Figure 7.2 Flow chart for data collection process.

A screen display of the data is presented with a prompt to stack data. If the stack data are selected, the software will activate the system on the next trigger pulse and repeat the data gathering algorithm adding the new data set to that saved from the previous data cycle. The most recently stacked data are shown on the screen. It is important note that the original data are lost in the stacking process. This stacking process can be continued up to a maximum of 128 stacks. The number of stacks is stored and will appear in the header information. A more detailed description of the stacking routine is provided below in 7.2.3.

7.2.3 *Description of stack control flow diagram.*

Figure 7.3 is the stack control flow diagram showing the more detailed working for the stacking process.

If the monitor function is selected then no stack operation takes place. The monitor is a rolling display, which can be paused manually and is normally used for setting up a survey and for noise monitoring It is also useful when setting up for a seismic survey as a faulty, or incorrectly sited, geophone can be easily identified by the shape of its response. In the pause mode the channel gains can be adjusted manually in order to optimise the gains for each channel. When normal operation is selected a new data cycle commences, the stack register and the stack counter are set to zero. On receipt of a trigger pulse a new data cycle is started and after the first a-d conversion takes place, the number of data samples for each channel are stored in channel data storage register, the size is being dependent on the data sample rate and data sample period. At the end of the first data sample period, the stack counter is set to 1. A prompt to stack the data are presented and if selected, the data is displayed and another data recording cycle commences. This process continues until the data stack prompt is not selected. The number of stacks is stored as required in the SEGII format recommendations. Normally the number of stacks is selected to give an integer solution to $\sqrt{n}$ where 'n' is the number of stacks.

A further point to be aware of is that in most of the 'Geometrics' series of seismic recorders if a high or low pass filtering function is applied to recorded data then the original raw data set is lost. The current stage of development does not include the use of 50 Hz notch filter, low and high pass digital filters. However, these can be incorporated into the design at a later date.

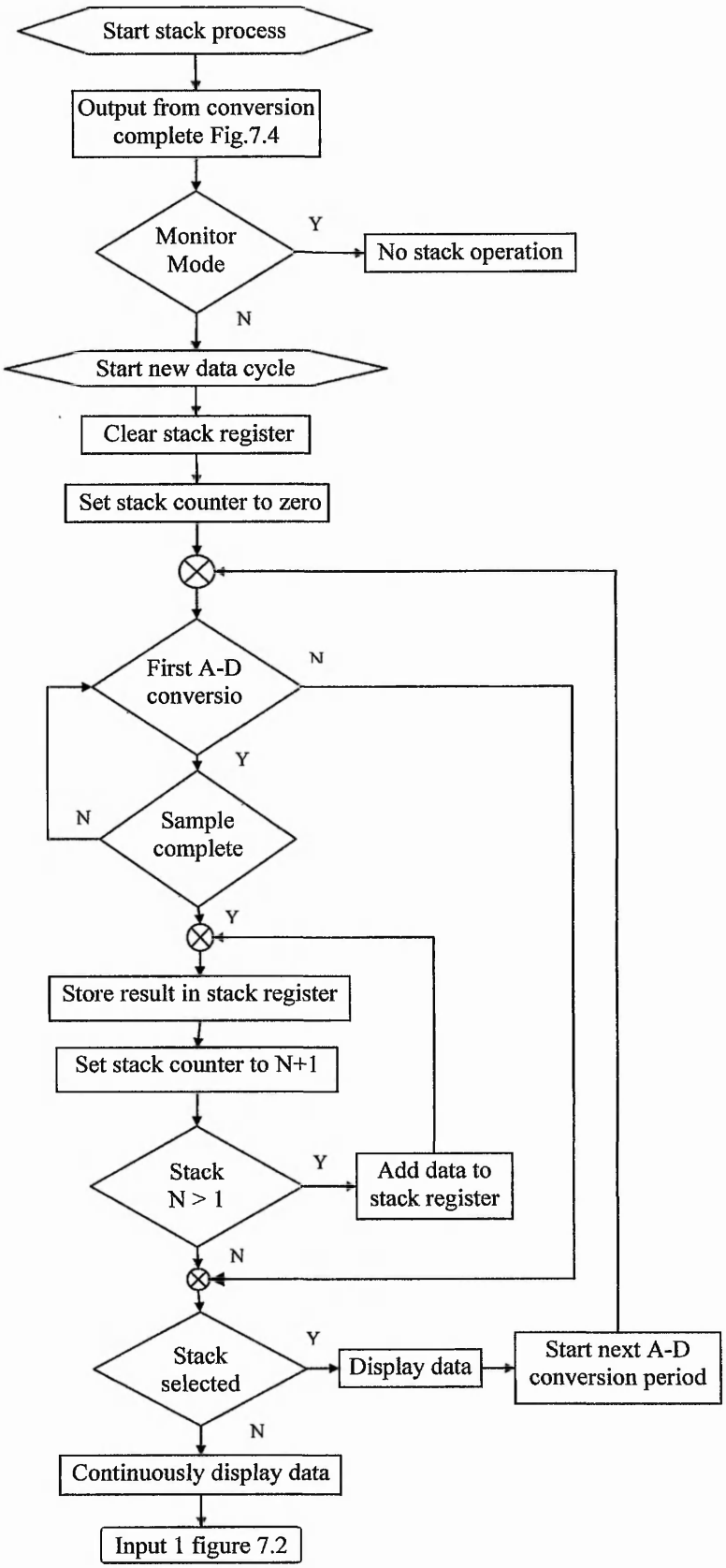

Figure 7.3 Stack data process, study in conjunction with figures 7.1 and 7.2.

7.2.4 *Description of analogue to digital conversion flow chart*

A flow chart of the analogue to digital conversion sequence is shown in figure 7.4. The description of the flow chart process follows after figure 7.4.

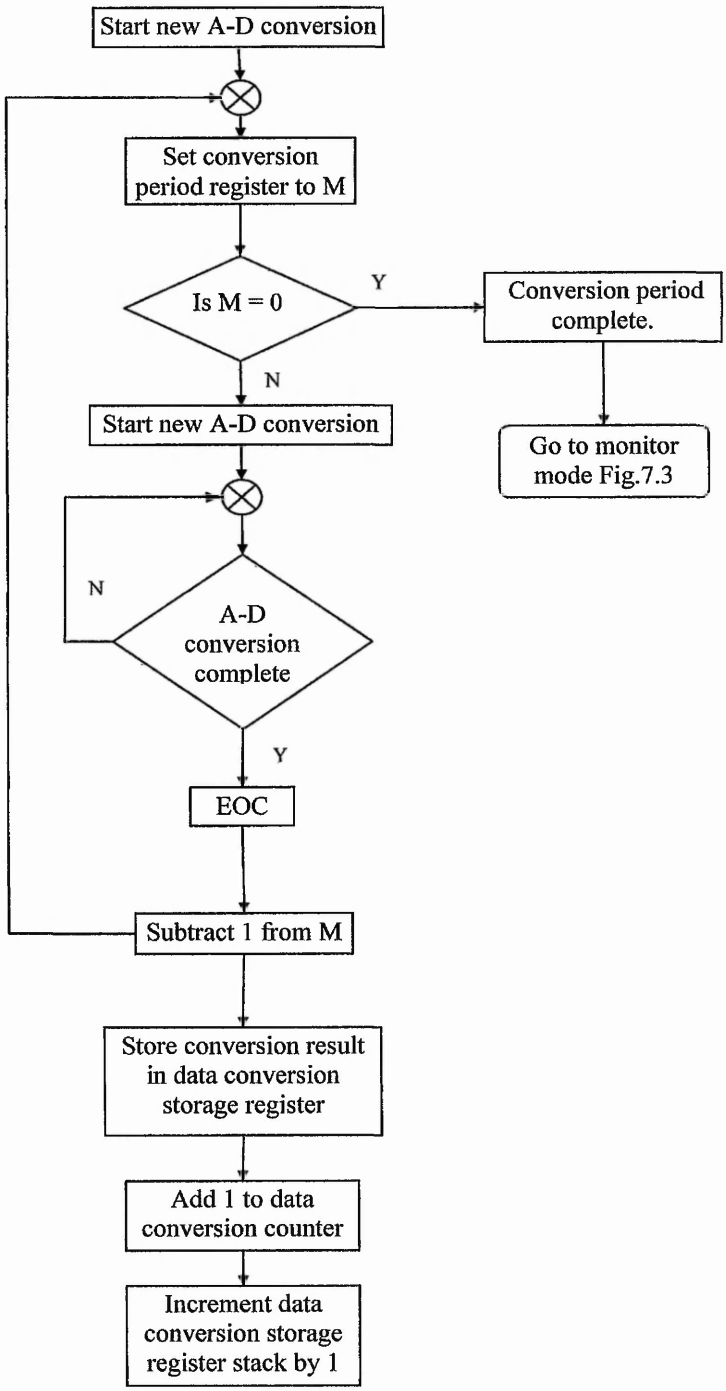

Figure 7.4. Flow chart for A-D conversion process.

Prior to the receipt of a trigger signal the conversion period register is loaded with the number of samples 'M' required for the conversion period, e.g., 1024. With the receipt of a trigger pulse the A-D converter starts its conversion cycle, see figure 7.2. At the end of the first conversion cycle an end of conversion signal (EOC) is generated the conversion period register is decremented by 1, resulting in M now becoming 1023. The data from the A-D conversation is stored in the data conversion register stack. A check is made to see if M = 0, if M ≠ 0 the A-D conversion cycled is repeated until M = 0 when the process is terminated. The system is then returned to the display mode where the result is displayed.

(5) *Graphical display of EK and seismic data*

The display of data in MATLAB was achieved by the use of the subplot command, which is described in Chapter 8. Figure 7.5 is the programme listing for the test programme used in its development. Five dummy functions v, w, x, y, and z were created in order to confirm the correct display of data. In practice the data stored from each channel would be displayed. The form of the data is shown in figure 7.5. In practice the display would be on a larger screen than an A4 page. Currently data are shown for the all 'x' axis labelling. In the final version only the lowermost 'x' axis, which represents time in milliseconds, will be labelled. The 'y' axes are normally automatically scaled. A facility to be included will be to display as many traces as desired, with one trace being typical when fine detail of the recorded trace is required.

However, additional software needs to be written in order to enable the 'y' axes scale factor to be adjustable manually. The functions v, w, x, y and z would be replaced by C1, C2, C3 etc, where these represent the data held in channels 1, 2, 3 etc, in the final version.

The programme listing is shown in figure 7.5

```
t=0:0.001:0.6;
x=sin(2*pi*50*t);
y=x+2*rand(size(t));
z=x+rand(size(t));
w=x+0.5*rand(size(t));
```

Figure 7.5 Test programme for the display of seismic and EK data. (continued below)

```
v=x+0.25*rand(size(t));
Subplot(16,1,1),plot(x);
subplot(16,1,2),plot(y);
subplot(16,1,3),plot(z);
subplot(16,1,4),plot(w);
subplot(16,1,5),plot(x);
subplot(16,1,6),plot(y);
Subplot(16,1,7),plot(x);
subplot(16,1,8),plot(z);
subplot(16,1,9),plot(x);
subplot(16,1,10),plot(w);
subplot(16,1,11),plot(x);
subplot(16,1,12),plot(z);
subplot(16,1,13),plot(x);
subplot(16,1,14),plot(y);
subplot(16,1,15),plot(x);
subplot(16,1,16),plot(x);
```

Figure 7.5 Test programme for the display of seismic and EK data

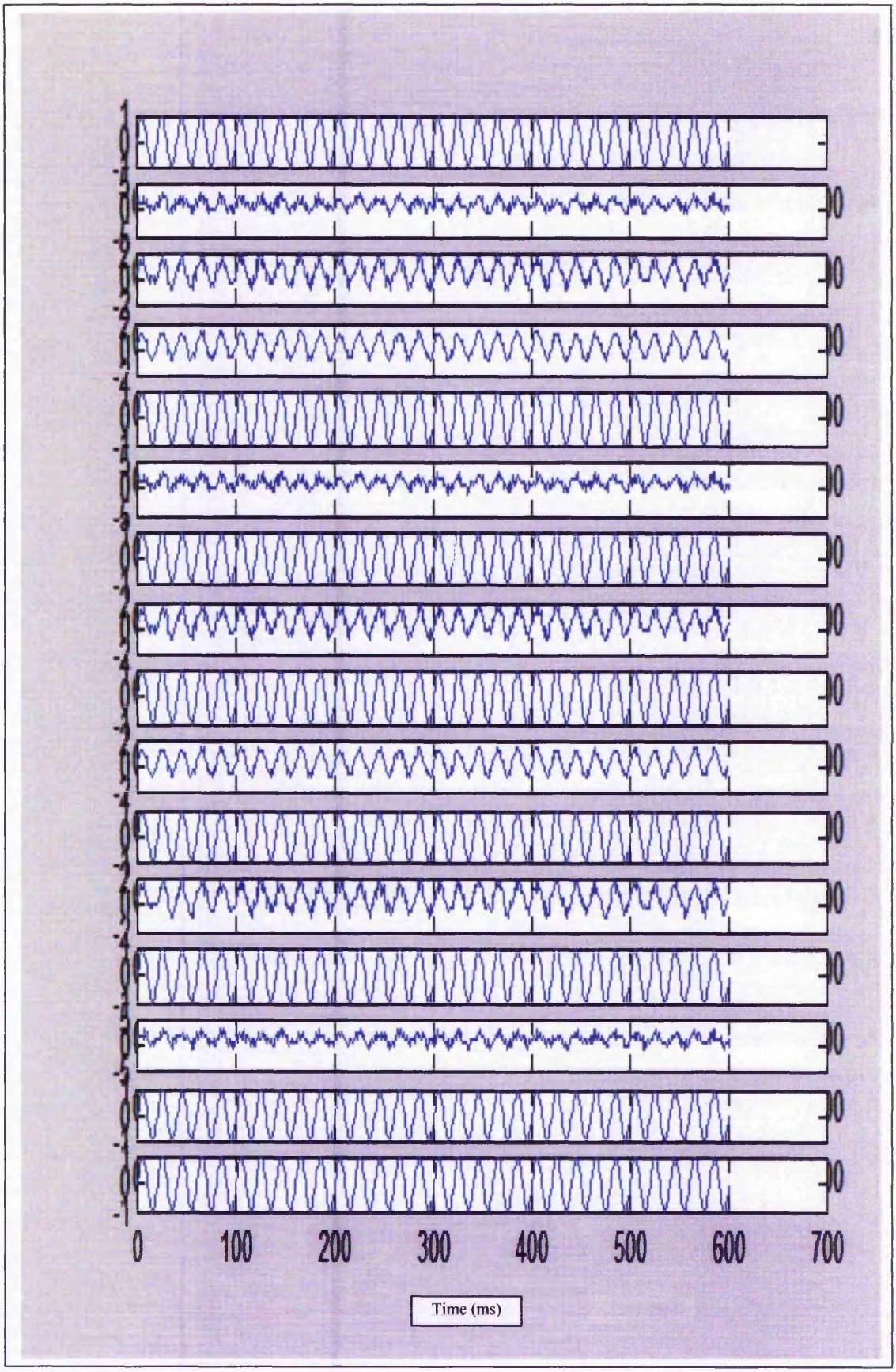

Figure 7.6 Display of data plot for 16 channels

7.3 Mains generated 50 Hz and its harmonics noise removal programme

This process is described in Chapter 8 and the software will be incorporated in the laptop computer at a later date. For the EK recordings there is a noise removal routine based on the Butler and Russell (1994). The main problem with EK signals is their low amplitude, normally in the order of micro-volts. Even with the new dipole aerial system described in Chapter 3 the peak levels are at the best in the hundred milli-volt range.

The main source of interference is mains borne noise consisting of 50Hz and its harmonics. The normal field procedure is to take a noise reading at each location of the dipole aerial. This noise recording has a Fourier transform applied to it which converts it from the time domain into the frequency domain. The appropriate frequency components are then selected and then a least squares routine applied of the newly selected data to create a new noise waveform. An inverse Fourier-transform is applied to convert it back to the time domain and is convolved with the original waveform in A to subtract it. This process is shown below in figures 7.7 and 7.8:

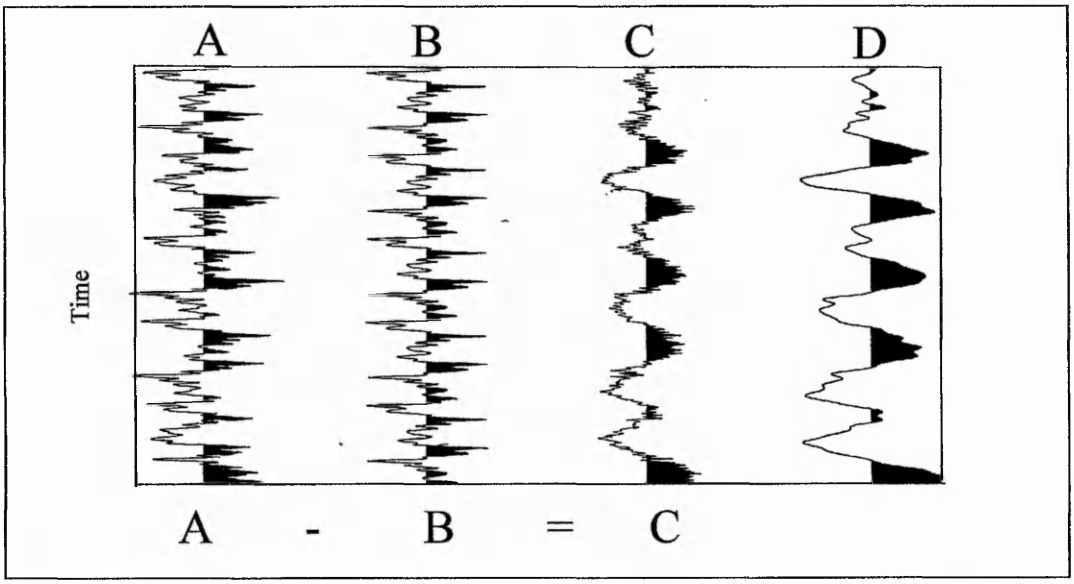

Figure 7.7 Steps in the removal of mains noise from a recoded waveform, (A) the recorded waveform. (B) the reconstituted noise waveform with the fundamental of 50Hz, 3rd harmonic 150 Hz, 5th harmonic 250 Hz and 8th harmonic 400 Hz selected. (C) the result of subtracting (B) from (A) and (D) Low pass filter applied to (C)

The low pass filter applied to the waveform in figure 7.7D is mainly to improve its appearance.

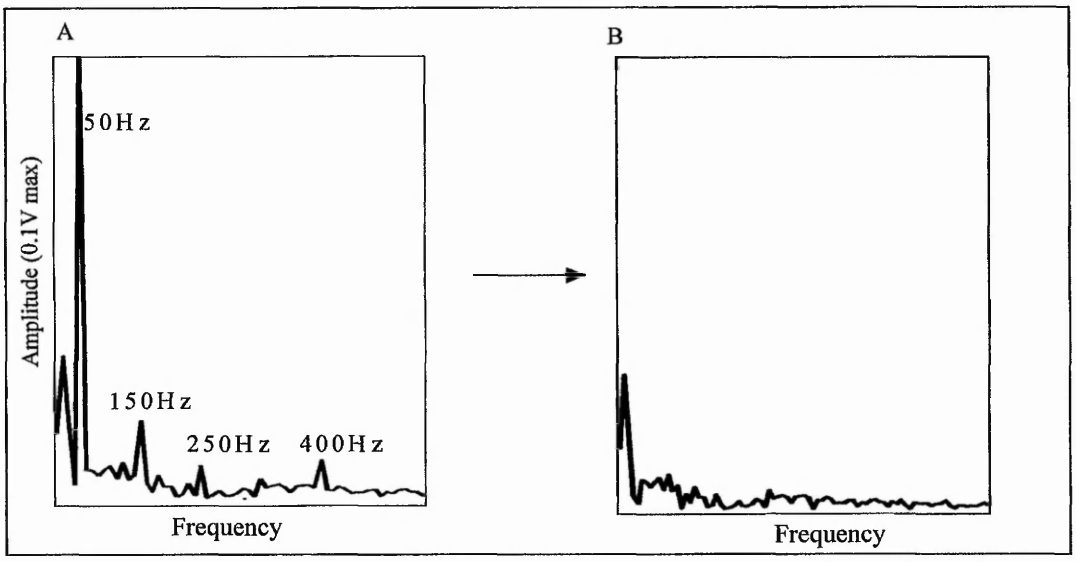

Figure 7.8 The result of applying a fast Fourier transform to the waveform in figure 7.6A. (A) the result of Fourier transform of the recorded waveform noise into the frequency domain. (B) the result of removing the mains frequency components from the recorded waveform.

A more detailed description of the above process is given in Chapter 8, section

7.4 Summary

7.4.1 *Problems encountered*

During the development of this software a fault appeared in the A-D converter, which disabled it when trying to access it in HPVEE. The fault was confirmed when the card was tested in a software package 'Instacal' which was supplied with the card for testing and calibration purposes. The cost of replacement was beyond the budget available so the development had to be put on hold. Owing to the high replacement cost of the DAS16\16 card a more realistic approach would have to be adopted.

7.4.2 *Solutions to problems encountered*

After a search of various manufacturers literature an 'Analog Devices' AD7655 4 channel 16 bit analogue to digital converter was chosen. Three of these linked together would make up a 12 channel recording system which could be expanded to a greater number of channels if required. For a short-term solution a 'Measurement Computing' PMD 1608FS 8 channel 16 bit data acquisition module was purchased.

Chapter 8

PC Based Signal Processing Software

To see a World in a Grain of Sand
And a Heaven in a Wild Flower,
Hold Infinity in the palm of your hand
And Eternity in an hour.

Auguries of Innocence
by William Blake
(1757 -1827)

8.1 Introduction

Initially EK field investigations were undertaken before development of the field data processing software required for use on a desktop personal computer (PC). As an interim measure a freely available program from 'Geometrics' was used to view the results. This program converted the binary SEGII data into ASCII format Pullen (1993), ANSI. (1997). Data could then be read into Microsoft EXCEL, Corel Word Perfect Quattro Pro, MATLAB or Mathcad where a graph of the data can then be drawn.

The problem was that following a recording from a 12 channel survey, e.g., such as seismic or EK, each of the 12 channels had to be converted separately. This would consume a considerable amount of time as 12 separate plots would have to be made in EXCEL and each one of these lined up carefully to locate break points or other features. In the case of 24 channels the time to process the seismic or EK data would become prohibitive.

After careful investigation of the available software, it was decided to use MATLAB as the development platform for a suitable seismic and EK data processing package, as it had, in addition to the basic package toolboxes for various applications such as signal processing, image processing and wavelet processing. The signal processing toolbox was used in the development of the 50/60 Hz mains noise removal software. The wavelet toolbox is to be used for developing a power spectrum analysis routine as it is more suited to processing impulse type waveforms and is ideal for EK analysis.

8.2 Details of analytical software

Before proceeding to the description of the data processing software developed in MATLAB a description of the conversion process described above in section 8.1 is given. The Geometrics ASCII software runs in DOS so it is necessary to select the command prompt if running in any of the following Windows 98, Windows ME and Windows 2000. With Windows XP it is necessary to carry out the following steps, as it was not possible to access the windows temp directory:

1 Select programme, Accessories and command prompt

2 A line similar to the following should appear C:\Documents and Settings\DBXXXXXX.ADS where DBXXXXXX.ADS is the user name and ADS the domain name.

3 Now type in CD Windows return. The following will appear C:\Documents and Settings\DBXXXXXX\Windows\ADS\windows. Now type in 'MD temp' return, the following should appear:
C:\Documents and Settings\DBXXXXXX.ADS\Windows\temp.
If a previous temp directory still exists then the following message will appear: A subdirectory or file temp already exists. If this does not appear type in CD Temp – Ret.

With XP service pack 2 the following message may appear: unzip DBXXXXX.ADS Local~1.Temp. Return to windows and unzip and copy seg2asci to windows/temp. Check this location to make sure the file is there.

4 Now copy in to 3 above the file seg2asci. If the seg2asci file is already in the system there is no need to do this. Once the above procedures have been completed asc2asci will remain in the temp file with any conversions.

5 The system is now ready to use.

It is assumed that the recorded ASCII data have a file extension ".DAT" and are less than 133 channels with a file length of less than 8K. However, the file length can be set by the user if it is greater than 8K. An ASCII file with header and data information in

millivolts is generated for each channel. On the screen it will show the processed trace number and its maximum and minimum values.

Before starting to convert an ASCII file select the command prompt and type in CD/windows/temp, note the comments above for Windows XP. Put the disc with the extension DAT files on it, as recorded in the field, into the appropriate drive. For example were the data is on a floppy disk, normally in drive 'A', type in seg2asci A:\999\240 where 999 is the directory, the 'Geometrics series of seismic recorders insert a directory automatically, where the file is held and 240 is the file number.

The programme converts the data file to ASCII and gives readings for the channels of the maximum and minimum peak readings. It saves each channel as say Trace #1 for channel 1, Trace #2 for channel 2 etc. An example of how the DOS screen appears after a file has been processed is shown in figure 8.1. File 1234 had thirteen channels selected.

```
TOTAL NUMBER OF CHANNELS IS 1
TRACE # 1 -- 4096 SAMPLES, MAX VALUE    0.10058 mV, MIN VALUE   -0.15323 mV
FILE CONVERSION COMPLETE!
TOTAL CPU TIME 7 SECONDS

C:\DOCUME~1\DBXXXXXX.ADS\WINDOWS\temp>seg2asci a:\6801\1234
SEG2ASCI v1.3   TYPE SEG2ASCI FOR HELP

TOTAL NUMBER OF CHANNELS IS 13
TRACE # 1 -- 4096 SAMPLES, MAX VALUE   73.69838 mV, MIN VALUE  -76.33080 mV
TRACE # 2 -- 4096 SAMPLES, MAX VALUE   39.24720 mV, MIN VALUE  -68.44568 mV
TRACE # 3 -- 4096 SAMPLES, MAX VALUE    0.23738 mV, MIN VALUE   -0.31178 mV
TRACE # 4 -- 4096 SAMPLES, MAX VALUE   76.73678 mV, MIN VALUE  -61.82070 mV
TRACE # 5 -- 4096 SAMPLES, MAX VALUE   19.44900 mV, MIN VALUE  -21.98775 mV
TRACE # 6 -- 4096 SAMPLES, MAX VALUE   25.58490 mV, MIN VALUE  -42.40140 mV
TRACE # 7 -- 4096 SAMPLES, MAX VALUE   16.05428 mV, MIN VALUE  -19.85340 mV
TRACE # 8 -- 4096 SAMPLES, MAX VALUE   11.91638 mV, MIN VALUE  -12.88455 mV
TRACE # 9 -- 4096 SAMPLES, MAX VALUE   11.40728 mV, MIN VALUE  -13.54313 mV
TRACE #10 -- 4096 SAMPLES, MAX VALUE    7.18230 mV, MIN VALUE  -10.61678 mV
TRACE #11 -- 4096 SAMPLES, MAX VALUE    6.72158 mV, MIN VALUE   -8.61532 mV
TRACE #12 -- 4096 SAMPLES, MAX VALUE    5.99085 mV, MIN VALUE   -6.89760 mV
TRACE #13 -- 4096 SAMPLES, MAX VALUE    0.08430 mV, MIN VALUE   -0.12173 mV
FILE CONVERSION COMPLETE!
TOTAL CPU TIME 14 SECONDS

C:\DOCUME~1\DBXXXXXX.ADS\WINDOWS\temp>
```

Figure 8.1 Illustration of data converted in the DOS to ASCII 'Geometrics' program.

It should be noted that the way data are presented from various seismic recorders can vary, even if it is formatted as SEGII, i.e. the Geometrics 2401 will present data as either 16 bit, 20 bit or 32 bit depending on the internal set up. These data are presented in floating point format and appears under a four digit file number followed by .DAT.

e.g. 1234.dat.

Figure 8.2 shows how data will appear when one channel is processed in EXCEL.

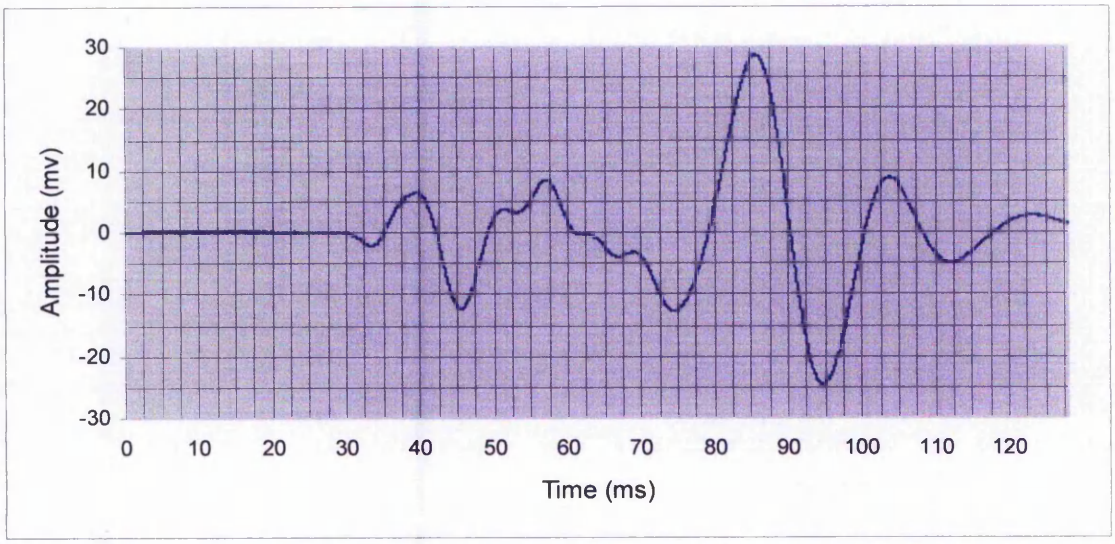

Figure 8.2. Data processed in the DOS programme seg2asci and subsequently displayed in Microsoft Excel. Displayed wave form is typical of a geophone response.

Data from the later versions of Geometrics seismic recorders, such as the Smartseis again varies. However, data are normally saved in binary format, on a standard 3.5" floppy disc. Table 8.1 shows the amount of data that can be stored on a standard high density 1.4 m-byte floppy disc for differing system parameters.

Table 8.1 File storage size for a HD 3.5" floppy disk

Representative file sizes				
No. of Channels	Record Length	File size K	Files per 1.44 Mb floppy	Files per Gigabyte
12	2048	106	12	9400
12	4096	204	7	4900
12	8192	394	3	2500
12	16396	794	1	1250
24	2048	212	6	4700
24	4096	410	3	2400
24	8192	800	1	1250
48	2048	423	3	2300
48	4096	816	1	1200
48	8192	1600	0	600
60	2048	528	2	1900
60	4096	1020	1	1000

To conserve floppy disc space, the screen save function was switched off together with any unused channels. Failure to do this can reduce the data floppy disc capacity by 60% or more. In some cases where there are 24 channels active, only one file can be saved.

For other makes of seismic recorders the data format may be different to that described even though it is SEG2 format.

Most data can be viewed in Excel after converting the original files with the seg2asci DOS programme. However, some of the details may be missing such as date and filter settings, the data appears in five columns and the appropriate number of rows. If data are read into Excel prior to the ASCII conversion these are read in from left to right then down to the start of the next row and left to right, etc. It is not recommended to use Excel other than to view the header information prior to conversion.

For some of the earlier data processed on a programme called Nucleus the data were saved 1234.TDF, for example, where TDF stands for 'Trace Descriptor File'. These files can be read in MATLAB or EXCEL.

8.3 The development of the software in MATLAB

For this application, the programme was written noting the recommendations as suggested in a special report by Pullan (1990) for seismic/radar data files for use in the personal computer environment. Pullan's report contains a detailed description of the SEGII file structure. All current Geometrics seismic recorder present their data in the recommended SEGII format.

A print out of the ASCII data are shown in figure 8.3, a few lines of data are shown for completeness. There are some minor amendments made to enable the plotting of these data in Microsoft Excel. This is described as follows:

1 Insert 2 columns to the left of the data column.
2 In the first column starting at the first data entry insert 1 then use the edit fill function to insert numbers into the column to list all of the data entries. The second column is used to scale the time axis on the plotted graph. For example in the header information in figure 8.3 it will be observed that the waveform sample time is 0.00003125 seconds or 31.25 μ-seconds with a total of 4096 samples. This gives an overall sampling period of 128 ms. Therefore to convert the data to read directly in milliseconds the equation editor is used in column 2 to multiply the values in column 1 by 0.03125. (e.g. for the 1024 sample the

time would be 32ms). This effectively gives the scale on the graph in ms; this process may need to be adjusted for other sampling rates.

```
ACQUISITION_DATE 10/OCT/2001
ACQUISITION_TIME 13:51:15
INSTRUMENT GEOMETRICS StrataView F
TRACE_SORT AS_ACQUIRED
UNITS METERS
NOTE
 BASE_INTERVAL 1.00
 SHOT_INTERVAL 0.00
 AGC_WINDOW 0
 DISPLAY_FILTERS 12 0

CHANNEL_NUMBER 2
DELAY 0.000
DESCALING_FACTOR .000075
LINE_ID 00-00
LOW_CUT_FILTER 0 0
NOTCH_FREQUENCY 0
RAW_RECORD 1233.DAT
RECEIVER_LOCATION 1001.00
SAMPLE_INTERVAL 0.00003125
SKEW 0.00004454
SOURCE_LOCATION 997.00
STACK 4
NOTE
 DISPLAY_SCALE 36

-0.19943
-0.20243
-0.20693
-0.20333
```

Figure 8.3 Details of the header information as seen on a print out of a recording on the 'Geometrics Strata viewer' in Excel

8.3.1 *Programme listing*

A listing of the 3rd version is given below, see figure 8.4, earlier versions had modifications incorporated to include problems mainly encountered the data structure:

```
function  [TRC,NumberOfTraces,NumberOfSamples,FILE_STRING,TRACE_STRING]
= seg2_r(filnam);

global TRC
global NumberOfTraces
global NumberOfSamples

% seg2_r.m read SEG2 seismic files
%
% [TRC,NT,NS,F_STR,T_STR] = SEG2_R('filename');
% TRC(i,j) contains the seismogram; i=samples; j=traces
% NT       NumberOfTraces in file
% NS       NumberOfSamples in on Trace
```

Figure 8.4 Programme listing (cont)

```
% F_STR     File String (ascii) Header
% T_STR     Trace String (ascii) Header
%
% v.1.1; 12.10.2000; read all information from trace headers; "key-
word" must be specified
% v.1.2; 15.04.99; read File header and all trace headers and store in
File_STRING and TRACE_STRING
%
% reference: Pullan, S.E., 1990, Recommended standard for seismic
% (/radar) data files in the personal computer enironment:
% Geophysics, Vol.55, No.9, pp 1260-1271
%
%
% ============================================================
% File Descriptor Block
% ============================================================

[FID,MESSGAGE] = fopen(filnam,'r');
[HH1,COUNT1] = fread(FID,16,'char');

M = HH1(5) + HH1(6)*256;       % Size of trace pointer sub-block
N = HH1(7) + HH1(8)*256;       % Number of traces in this file
TC = HH1(10);                  % First String Terminator character

DUMMY = fseek(FID, 32, 'bof');

TPS = fread(FID,N,'int32');    % Pointers to trace descriptor blocks

F_STRING = fread(FID,TPS(1)-32-4*N+1,'char');
FILE_STRING = char(F_STRING');

clear TRC
% ============================================================
% Read Trace description block
% (TID must be 17442dec = 4422hex)
% ============================================================

for j = 1:N                                                    %      loop
over traces

      DUMMY = fseek(FID, TPS(j), 'bof'); % adress of trace description
block
      TID = fread(FID, 1,'int16');         % trace descriptor block ID
      TX  = fread(FID, 1,'int16');         % size of this block
      TY  = fread(FID, 1,'int32');         % size of corresponding data
block
      TNS = fread(FID, 1,'int32');         % number of samples in data
block
      DFC = fread(FID, 1,'uchar');         % data format code

      DUMMY = fseek(FID, 32+TPS(j),'bof'); % adress of beginning of
string in trace descriptor block
      STR = fread(FID, TX-32+1, 'char'); % read string
   TRACE_STRING(j,:) = char(STR');

      %SEARCH_TRC_HEAD('SAMPLE_INTERVAL',STR, TC);
      %SEARCH_TRC_HEAD('HIGH_CUT_FILTER',STR, TC)
      %SEARCH_TRC_HEAD('LOW_CUT_FILTER',STR, TC);
   %SEARCH_TRC_HEAD('NOTCH_FREQUENCY',STR, TC);
%SEARCH_TRC_HEAD('DESCALING_FACTOR',STR, TC);

% ============================================================
```

Figure 8.4 Programme listing (cont).

```
% Read Data
% ============================================================

DUMMY = fseek(FID, TPS(j) + TX, 'bof'); % adress of beginning of data

%disp(sprintf('%d %d %d',TPS(j),TX,TPS(j) + TX))

%..DataFormatCode = 1; data is 16bit fixed point format if DFC == 1

      TRC(:,j)  = fread(FID, TNS, 'int16');


%..DataFormatCode = 2; data is 32bit fixed point format
   elseif DFC == 2

      TRC(:,j)  = fread(FID, TNS, 'int32');


%..DataFormatCode = 3; data is 20bit floating point format;
%..conversion from 20bit floating point format to MatLab format
   elseif DFC == 3

      if mod(TNS,4) ~= 0 disp('number of samples per trace must be
      divisible by 4')
      break
      end

%  TEMP(:,j) = fread(FID, 5*TNS/4, 'int16');
      for k = 1:1:TNS/4 TEMP(k*5-4,j) = fread(FID, 1, 'uint16');
% Exponents of 4 samples TEMP(k*5-3:1:k*5,j) = fread(FID, 4, 'int16');
% Mantissas of 4 consecutive samples
      end
      isam = 0;
      for ipac = 1:5:5*TNS/4-4;
         EXPONENT(4) = bitand(TEMP(ipac,j), hex2dec('f000')) / 2^12;
         EXPONENT(3) = bitand(TEMP(ipac,j), hex2dec('0f00')) / 2^8;
         EXPONENT(2) = bitand(TEMP(ipac,j), hex2dec('00f0')) / 2^4;
         EXPONENT(1) = bitand(TEMP(ipac,j), hex2dec('000f')) / 2^0;
         %disp(sprintf('%d                    %d                    %d
%d',EXPONENT(1),EXPONENT(2),EXPONENT(3),EXPONENT(4)));
         for inpac = 1:4;
            TRC(isam + inpac,j) = TEMP(ipac + inpac,j) *
2^EXPONENT(inpac);
         end
         isam = isam + 4;
      end

%..DataFormatCode = 4; data is 32bit floating point format;
   elseif DFC == 4
TRC(:,j)  = fread(FID, TNS, 'float32');


%..DataFormatCode = 5; data is 64bit floating point format;
 elseif DFC == 5

TRC(:,j)     = fread(FID, TNS, 'float64');

else


      disp('Format is not recognized')
      disp('supported formats:')
```

Figure 8.4 Programme listing (cont).

```
      disp('01h = 16-bit fixed point')
      disp('02h = 32-bit fixed point')
      disp('03h = 20-bit floating point')
      disp('04h = 32-bit floating point')
      disp('05h = 64-bit floating point')
      break
end
end

ST = fclose(FID);

disp(sprintf('Number of traces = %i', N));
disp(sprintf('Number of samples/trace = %i', TNS));

NumberOfTraces = N;
NumberOfSamples = TNS;


% Subroutine SEARCH_TRC_HEAD : looks for 'target' in traceheader and
returns 'value'

function [value] = SEARCH_TRC_HEAD(TARGET,STR, TC);

STRI = char(STR');
ind = findstr(TARGET,STRI) + length(TARGET);
% index of start of 'value'
ine = findstr(char(TC),STRI(ind:length(STRI))); % index of termination
character after value
value = STRI(ind:ind+ine(1)-1);
% read 'value' of 'Target'
%disp(value);
```

Figure 8.4. Programme listing for the reading in of SEGII formatted data

8.4 Noise removal software

The noise removal software was primarily developed for use with the EK responses as the dipole aerial would be more prone to pick up local 50Hz mains noise if it was close to electricity pylons or overhead power lines. In other countries, where the frequency of the mains supply is 60Hz, the software will function equally well. In most cases the EK signal received by the dipole aerial was strong enough to observe the EK response. In the case of the laboratory experiments, (Chapter 5) the EK signals were very difficult to see due to background noise and for these data the software proved to be extremely useful.

The programme was written in MATLAB script and is designed to input a data file from either MS Excel or a MATLAB 'M' file. It is possible to also input other file formats such as Mathcad, if required.

The technique is to take the recorded EK data in its raw form and then identify any 50 hertz mains induced interference and harmonics by applying a fast Fourier transform (FFT) to the data set. A cursor has been programmed to appear on the screen when the FFT is activated. A rifle sight cursor can be moved over the peak of interest and by clicking the left hand mouse button the data, peak position Hz and amplitude, will be loaded into a file. If higher harmonics of the interfering wave are present these can also be loaded into a file and the process is terminated by clicking on the last peak of interest with the right hand side mouse button. The data file with the information from the FFT data set is then convolved with the original data set to remove the offending 50 Hz noise and its harmonics. In addition to removing unwanted noise the programme can be used to characterise EK response data.

8.4.1 *Test and demonstration programme for noise removal*

A test program has been written to demonstrate the above process using two software generated sine waves of 50 Hz and 120 Hz. The text following the percentage sign is non-executable thereby permitting comments to be added to the programme lines to aid debugging. The original programme was written on the date shown. However, additions have been made more recently. The listing for the programme is provided below (see figure 8.5).

```
Date "Tue 04/Sep/2001 time 15:37:50
MATLABSCRIPT

t = 0:0.001:0.8;% Interval for t, i.e. 0-800
x = sin(2*pi*50*t) + sin(2*pi*120*t);% Adds two sine waves of 50 & 120
Hz
% y = x+2*randn(size(t));% Adds randon number to x.
subplot(5,1,1),plot(x(1:800));% Plots 5 graphs in one column
Title('Time series ms');
xlabel('Time ms');              % Positions 'X' axis label.
ylabel('Amplitude mv');         % Positions 'Y' axis label.
Y = fft(x,512);
Pyy  = Y.*conj(Y) / 512;        % Makes the FFT positive
f = 1024*(0:255)/512;           % 1024 point discreet Fourier transform.
subplot(5,1,2),plot(f,Pyy(1:256));
Title('Frequency spectrum');
xlabel('Frequency Hz');
ylabel('Amplitude');
u = [ ];                        % Start of programme to get mouse data.
a = [ ];
n = 0;
but = 1;
while but == 1;
[a,u,but] = ginput(1);          % Get data from the position selected by
the mouse
```

Figure 8.5 Test noise removal programme listing

```
gtext(s);
s =sprintf('x = %6.2f, y=%6.2f\', a,u);
n = n+1;
u(n,1) = u;
a(n,1) = a;
Z = ifft(a,u);                  % Inverse Fourier transform.
l = length(Z);
h = line(400,100);
subplot(5,1,3),plot(l);
c = conv(x,Z);                  % Convolve x and Z data
subplot(5,1,4),plot(c);
G = fft(c,512);
Pyyi = G.*conj(G)/512;
k = 1024*(20:255)/512;
subplot(5,1,5),plot(k,Pyyi(20:255));
semilogy(k,Pyyi(20:255));
end                             % End of programme.
```

Figure 8.5 Test noise removal programme listing

Figure 8.6 shows the effect of removing the 120 Hz component of the signal

(a) The first graph (a) is a plot of the software generated signal, note it is difficult to see what signals are present.

(b) The second graph (b) is the discreet Fourier transform of the signal clearly showing the two frequency components of 50 and 120 Hz.

(c) Careful examination of the third graph (c) shows a point above 1 on the x axis. This is the result of applying the inverse FFT or IFFT to the selected peak from graph. The signal is seen to be 120 Hz with matching amplitude.

(d) Graph 4 (d) shows the result of convolving the original data with the result of the IFFT which removes the unwanted signal.

(e) Graph (d) To check on the process the FFT is applied to the new data clearly showing the complete absence of the 120 Hz peak, and the presence of the 50Hz signal.

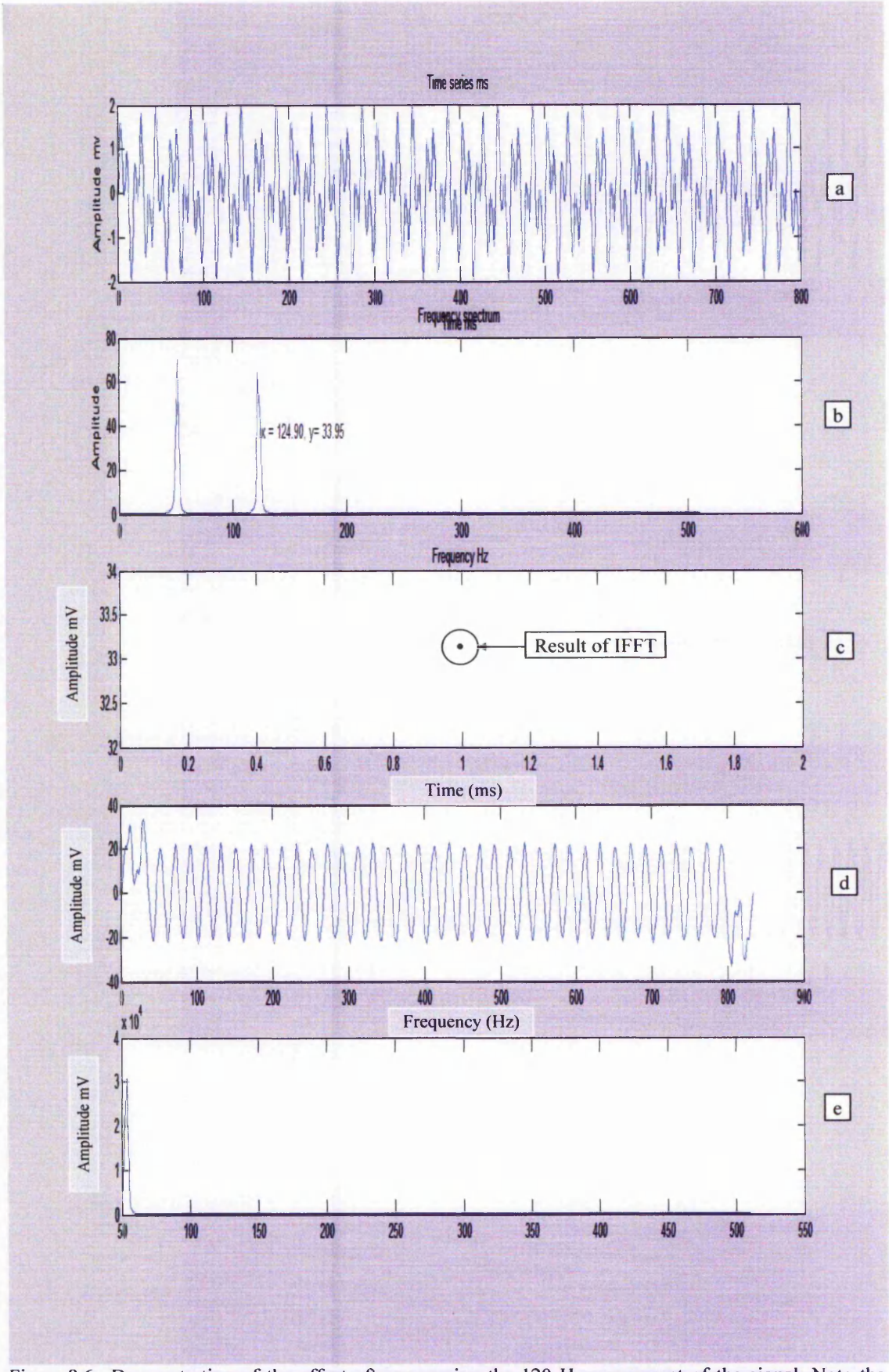

Figure 8.6 Demonstration of the effect after removing the 120 Hz component of the signal. Note the presence of the 50Hz signal in the last graph and the absence of the 120 Hz signal.

Care has to be taken when aligning the cross wires on the signal it is wanted to be removed, as the IFFT is very sensitive to the selected frequency and its amplitude. An option to have a logarithmic 'Y' scale for the display of FFT and IFFT data has been included in the operational programme.

The application of the FFT can also be used to examine the EK data in order to identify the characteristics of the EK response.

8.4.2 *Demonstration of the noise removal software on real data*

Two files have been selected to demonstrate the working of the software so far. The first file is number 1220 from the Ospringe site in Kent. The second file is number 202-013 from the Mansfield site. These two files are raw data with no filtering applied in the recording device.

8.4.2.1 Ospringe data

As a check on the working of the newly developed noise removal software the original recording of file 1220(a), shown in figure 8.8, was expanded in the horizontal axis. The vertical scale was adjusted in order to identify the nature of the high frequency noise observed on the waveform (see figure 8.7).

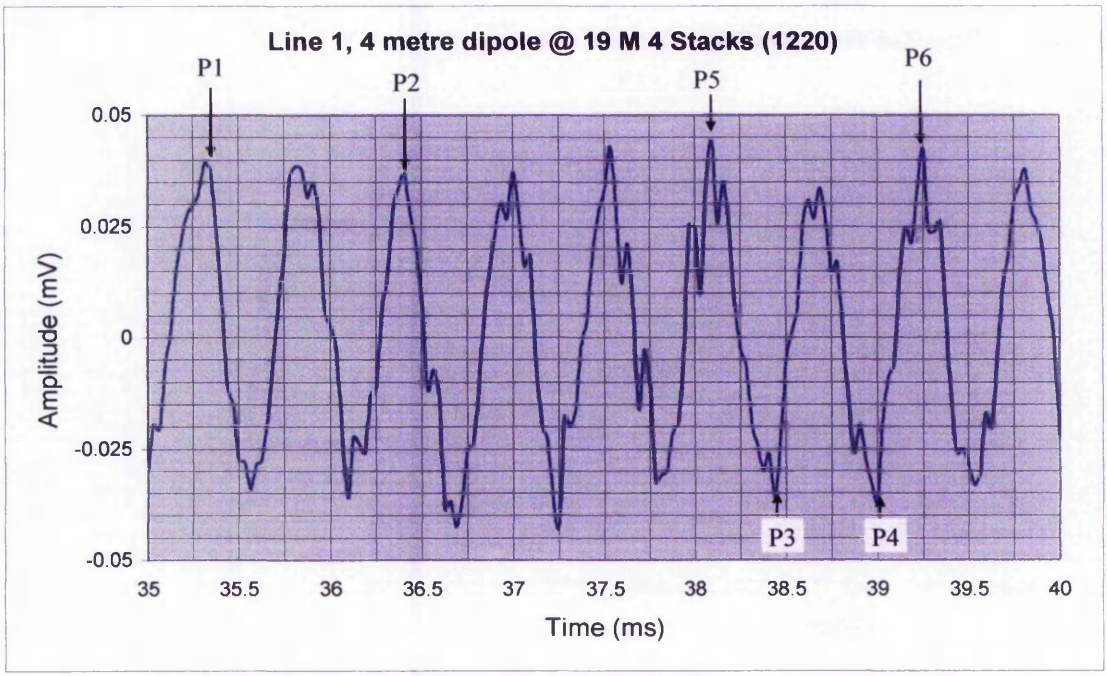

Figure 8.7. Section from the original EK recording, Ospringe, Kent. P1 to P2 is the time of 2 cycles, P3 to P4 the time of 1 cycle and P5 to P6 the time of two cycles. These times are used to calculate the frequencies listed in Table 8.2.

For the points P1, P2, P3, P4, P5 and P6 the resulting frequencies were calculated, using the relationship $f = \frac{1}{t}$, the results being shown in table 8.2.

Table 8.2 Times and corresponding frequencies for the points shown on figure 8.5

	Time P2 – P1	Time P4 – P3	Time P5 – P6
Time ms	1.09375	0.5625	1.15625
Frequency (kHz)	1.8285	1.778	1.73

From the results in table 8.2 there appears to be a frequency modulation of the waveform about a centre frequency of 1.778 kHz.

In figure 8.8 a fast Fourier transform (FFT) has then applied to the data set to convert the recorded data into the frequency domain the lower graph, the top graph being the recorded unprocessed EK data. The peak at 1022.35 Hz has been selected and is in a file ready for later processing. The small peaks between 1600 to 1800 Hz are due in part to the high frequency interference seen figure 8.8(a). The peak in figure 8.9 (b) at 1723.50 Hz is in reasonably close agreement with the value shown in table 8.2.

Other parts of the frequency spectrum were examined in more detail to identify other dominant frequencies. Improved resolution of FFT data was achieved by plotting the FFT over a restricted frequency range. These results are shown in figures 8.9, 8.10, 8.11 and 8.12 for the frequency ranges indicated. These figures illustrate the complex nature of the noise recording. The software allows for manual selection of frequency range of the FFT, if required.

The FFT data seen in figure 8.10 (b) has no peak at 50Hz, thus there is no mains frequency pick up. However, there are dominant peaks at 9, 39 and 77Hz. One of the more interesting results is shown in figure 8.12(b) a peak centred on 1935.51 Hz and two small amplitude sidebands. The data for figure 8.12 (a) is plotted over a range of 200 ms.

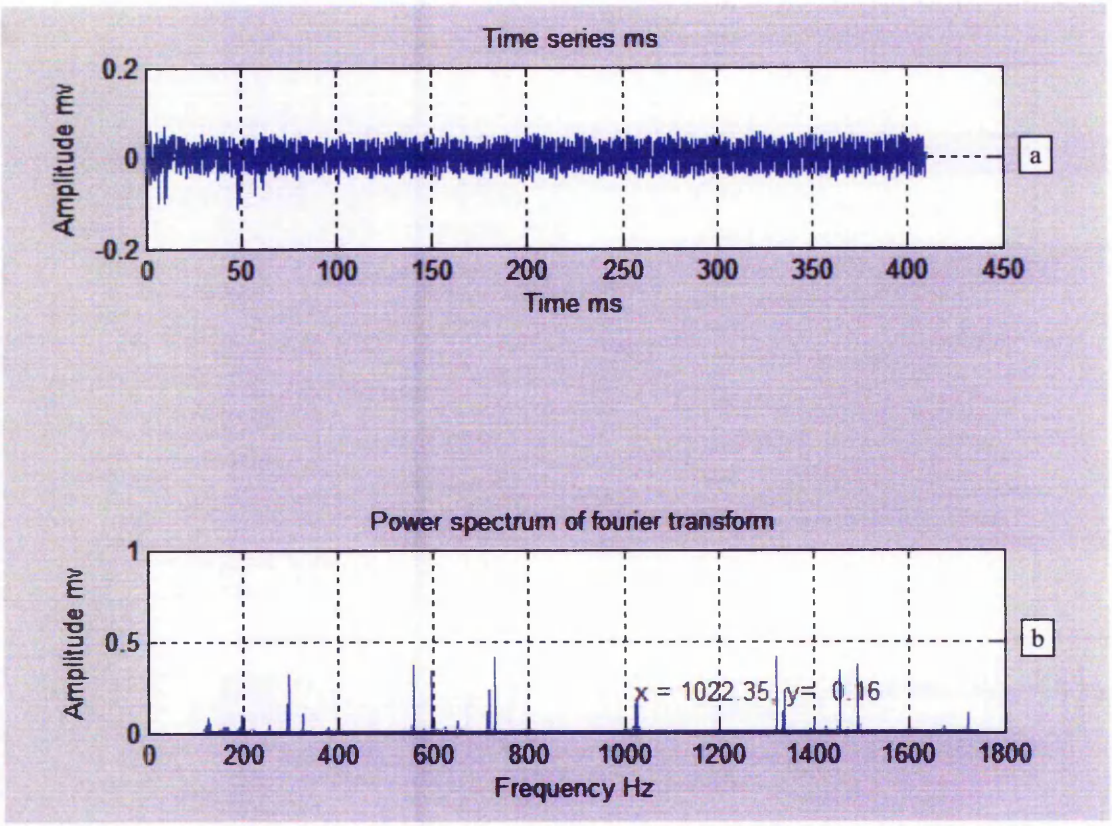

Figure 8.8 Original data for noise recording 1220, top trace (a), and its Fourier transform in the lower trace (b) for the frequency range shown of 0 to 1800 Hz .

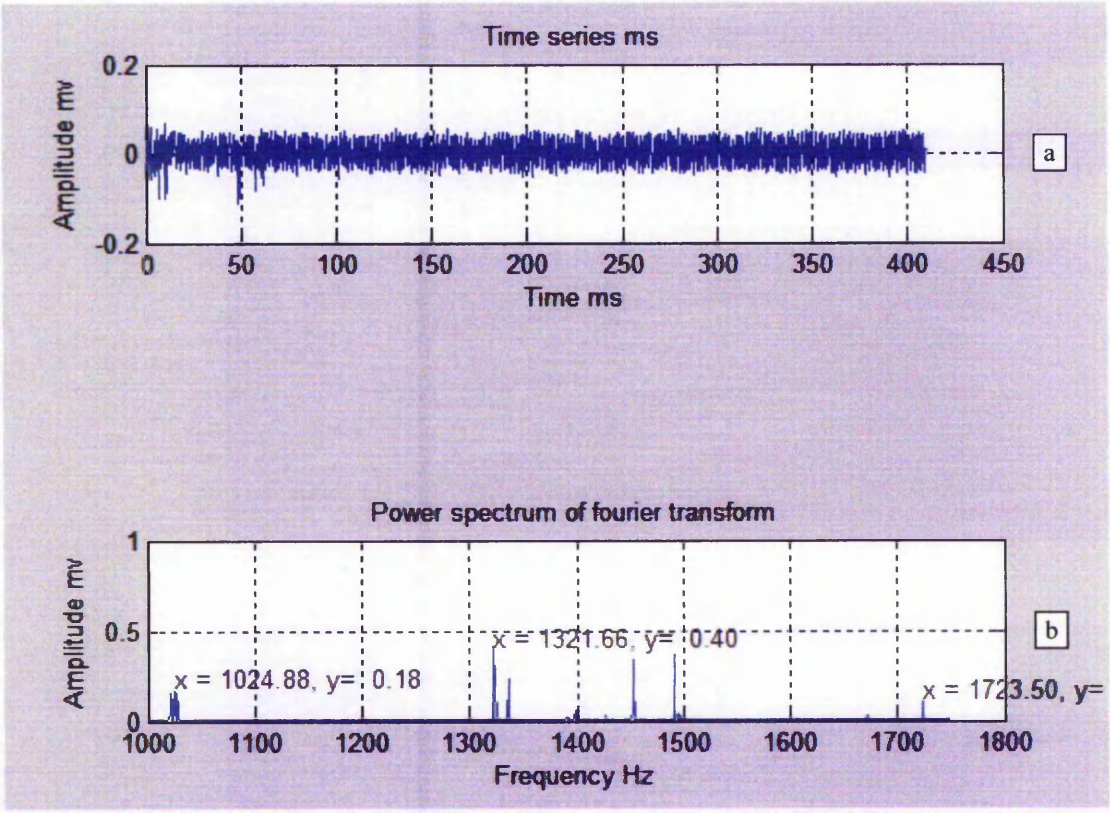

Figure 8.9 Original data for noise recording 1220, top trace (a) and its Fourier transform in the lower trace for the frequency range 1000 to 1800 Hz.

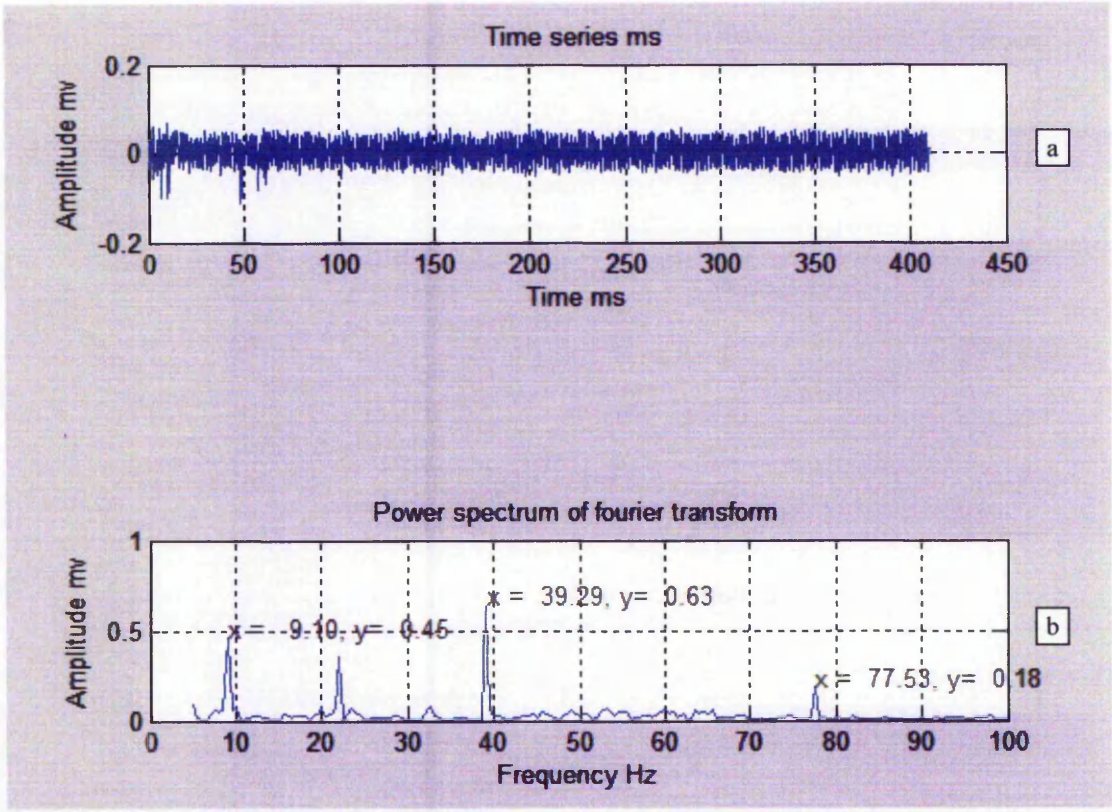

Figure 8.10 Original data for noise recording 1220, top trace (a) and its Fourier transform in the lower trace for the frequency range 0 to 100 Hz.

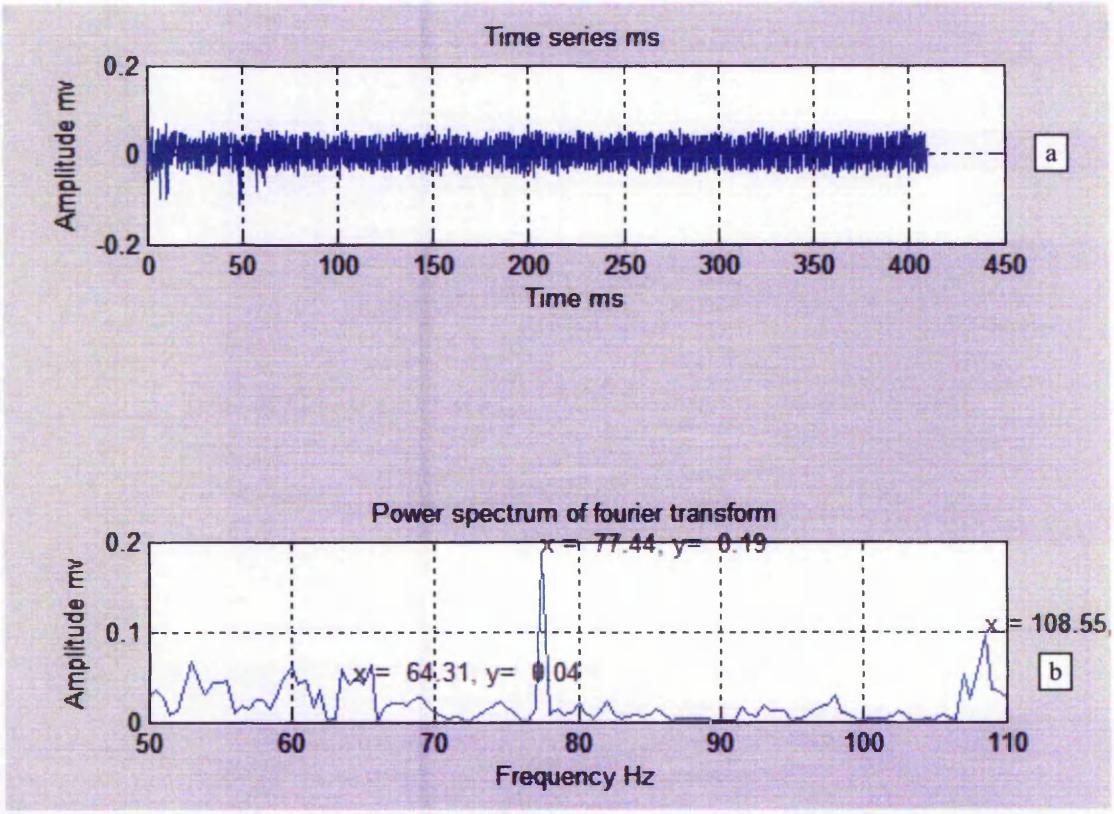

Figure 8.11 Original data for noise recording 1220, top trace (a) and its Fourier transform in the lower trace for the frequency range 50 to 110 Hz.

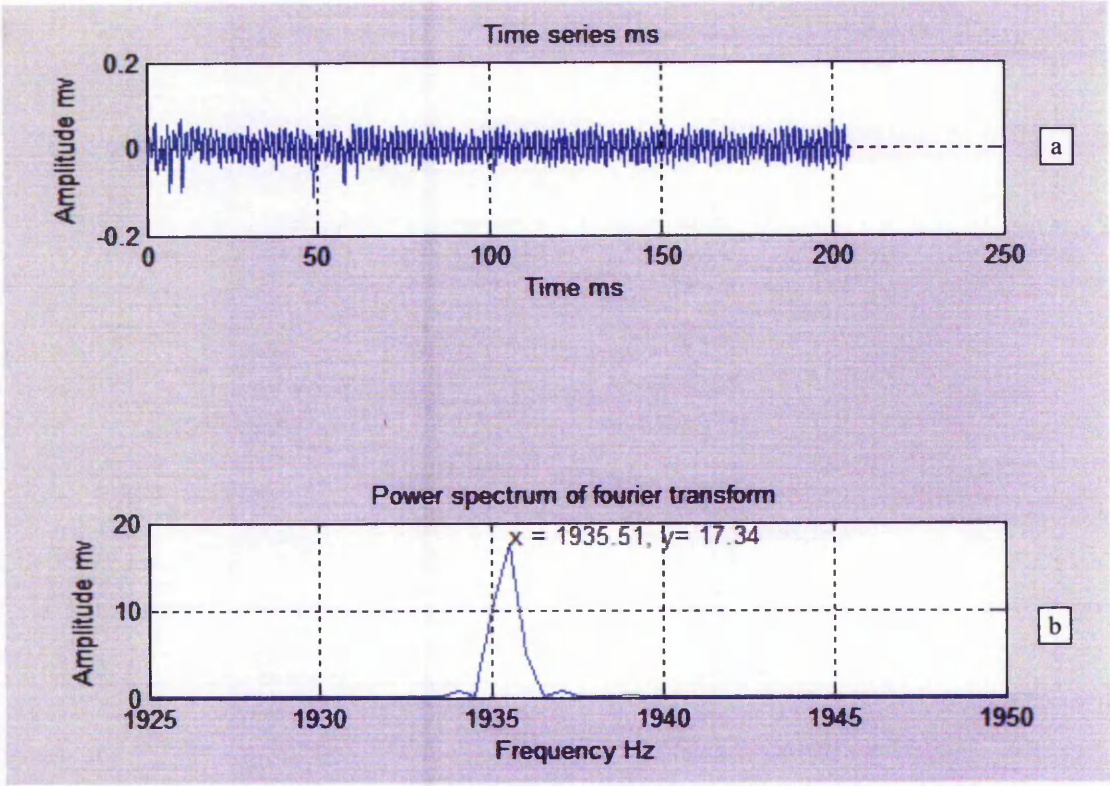

Figure 8.12 Original data, top trace, and its Fourier transform in the lower trace for the frequency range 1925 to 1950 Hz.

Reference is made to Chapter 4 figures 4.31, (a) & (b) in which the latest version of the noise removal software has been applied to remove the high frequency noise shown in figure 8.8 (a).

4.4.2.2 Mansfield data (file 202 – 013)

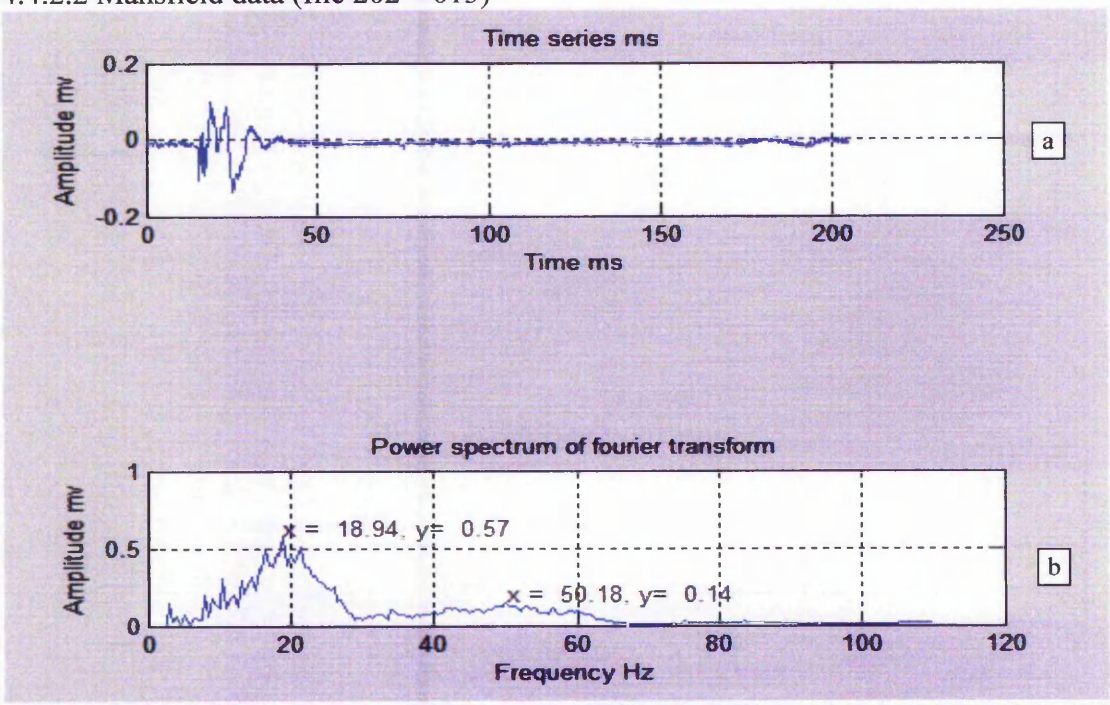

Figure 8.13 Original data, top trace, and its Fourier transform in the lower trace for the frequency range 1925 to 1950 Hz.

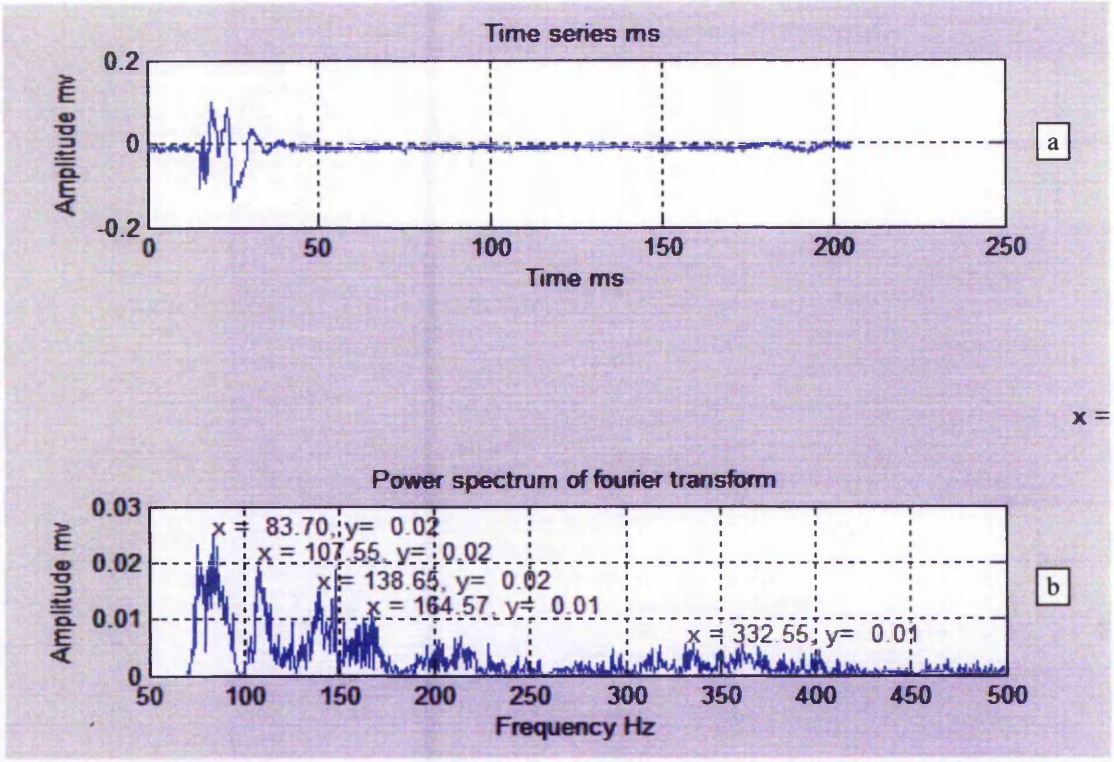

Figure 8.14. Original data, top trace, and its Fourier transform in the lower trace for the frequency range 50 to 500 Hz.

The data in figure 8.14 (a) & (b) has been shown to demonstrate the more dominant components in the EK recording taken from the Mansfield investigations. The two broad peaks, in graph (b), selected at 83.7 and 107.55 Hz show the frequency components due to the hammer source (see Keiswetter & Steeples, 1995). Other frequencies of interest are seen in the remaining peaks that have been selected

8.5 Noise removal programme listing

```
y = data(1:2048,3);
f = y*1;
x = data(1:2048,2);
m = x;
subplot(5,1,1),plot(m,f);% plots y over the range 1 to 1000
grid on;                 % Places a grid on the graph.
Title('Time series ms');
xlabel('Time ms');
ylabel('Amplitude mv');
Y = fft(f,4096);         % performs a fast fourier transform on y
Pyy  = Y.*conj(Y) / 64; % makes the fft data positive
w = 1024*(70:4096)/2048;
subplot(5,1,2),plot(w,Pyy(70:4096));
grid on;
Pyy = [ ];
```

Figure 8.15 FFT programme listing

```
title('Power spectrum of fourier transform');
xlabel('Frequency Hz');
ylabel('Amplitude mv');
u = [ ];
a = [ ];
n = 0;
but = 1;
while but == 1;
[a,u,but] = ginput(1);
s =sprintf('x = %6.2f, y=%6.2f\', a,u);
gtext(s);
n = n+1;
u(n,1) = u;
a(n,1) = a;
%Pyy(n,1) = Pyyi;
%f(n,1) = fi;
Z = ifft(a,u);
%subplot(4,1,2),plot(z,Pyyi);
c = conv(f,Z)/200;
%Pyy = Z.*conj(Z)/512;
k = 128*(1:2048)/4096;
Subplot(5,1,3),plot(k,c(1:2048));
grid on;
B = fft(c,2048);        % performs a fast fourier transform on c
Pyyj  = B.*conj(B) / 64; % makes the fft data positive
w = 1024*(70:2048)/2048;
subplot(5,1,4),plot(w,Pyyj(70:2048));
grid on;
g = [ ];
h = [ ];
n = 0;
but = 1;
while but == 1;
[g,h,but] = ginput(1);
end
s =sprintf('x = %6.2f, y=%6.2f\', g,h);
gtext(s);
n = n+1;
g(n,1) = g;
h(n,1) = h;
F = ifft(g,h);
%subplot(4,1,2),plot(z,Pyyi);
d = conv(c,F)/1024;
k = 128*(1:2048)/4096;
Subplot(5,1,5),plot(k,d(1:2048));
grid on;
end
```

Figure 8.15 FFT programme listing (cont)

8.6 Summary.

8.6.1 Current state of the noise removal software development.

The software for both the display and noise removal routines has been developed to the point where it is now useable. Noise peaks can now be selected and removed as demonstrated in figure 8.6. The amplitude and frequency of the noise peaks are displayed. Data can be read in from a number of differing formats

This programme has been successfully deployed to remove noise from a number of the EK recordings obtained at Ospringe. The ability to select and display frequency ranges for the FFT has proved to be very useful. This will prove to be very useful in characterising EK responses in both laboratory and field investigations

8.6.2 Improvements

Some of the problems have been outlined following the software listing such as the display of an individual data traces, have an automatic scale selection on the vertical axis relating to the gain set for that channel and accessing any one trace from a data set.

For the noise removal programme exploring different frequency ranges the parameters in the line $w = \frac{1000*(16:50)}{1024}$; has to be adjusted manually within the lines of code. A Graphical User Interface (GUI) will make this task alone much easier eliminating the risk of making a mistake. Another feature that could be included at a later date is to have a box attached to the data selection cursor showing the position of the cursor prior to selection of the peak.

One further observation was that the Fourier transform has a spread of frequencies, as seen in figure 8.13 around 20Hz. Taking one of the obvious peaks and removing it has little effect on the original trace. One possible solution to this is to take a least squares fit of the data either side of the peak and use this result to subtract from the original recording.

Chapter 9 | Discussion of field and laboratory EK results with comparisons to previous research

Yet what are all such gaieties to me
Whose thoughts are full of indices and surds?
x.x + 7x + 53 = 11/3
But something whispered "It will soon be done:
Bands cannot always play, nor ladies smile:
Endure with patience the distasteful fun
For just a little while!"

I of four riddles
Lewis Carol (1832 – 1898)

9.1 Introduction

In this Chapter main emphasis is on the field results, on the generation of the EK response and correlation, where appropriate, with the additional tests conducted in the field such as seismic refraction surveys and the Dynamic Cone Penetrometer (DCP), which is not easily simulated in the laboratory. No previous EK investigations involved the use of a dipole aerial, which is the novel feature around which this thesis is based. All previous investigations involved the use of metal stakes, or in some cases porous pots, placed in the ground, which pose a number of problems as described in Chapter 2.

The results of the laboratory investigations of EK will be discussed purely on the basis of comparison of an EK response with the travel time of an ultrasonic pulse through a selection of samples representative of the field environments investigated in order to gain further insight into the EK generation process in laboratory controlled conditions. In particular one sample was used for the more important investigations. The 50 kHz ultrasonic transducers used for the EK investigations represents a scaled up version of the seismic hammer impact used in the field investigations, which has a dominant frequency of 100 Hz and generates a 'P' wave. These experiments were all related to 'P' wave responses only.

9.2 Field EK investigations

The results of the analysis of the field investigations are presented in Chapter 4 and reference will be made to these in the following discussion. There are four key questions that arise from this thesis or in fact for any EK investigation whatever detection method is employed. However, this Chapter will only consider the use of an adjustable length dipole aerial for the detection of EK responses. The four key points are:

(1) Is there any moveout of the EK response with regard to a change in position from the seismic impact point?

(2) Is there a correlation with a known feature such as a water table or knowledge of depth to the fully water saturated zone?

(3) Is there an EK response symmetry, relative to the shot point, at a position diametrically opposite to an EK survey line? This is to be expected if one considers the line rotated through 180°. Diametrically opposite symmetry should be maintained.

(4) Is there a predicable fall off in the amplitude of the EK response with distance?

To provide the answers to these four key questions reference will be made to the results presented in Chapter 4 of this thesis.

The important point to note is that if the EK response is electromagnetic in origin then there will be no moveout of the EK response arrival time with distance from the shot point when compared with the seismic moveout.

However, there will be a fall off in the amplitude of the EK response with regard to distance from the shot point. The fall off in the amplitude of the EK response is indicative of the dipole nature of the electromagnetic field, e.g. the strongest electric field lines exist near to the dipole source.

The headings on all of the EK responses have the following format; Survey line number, distance from the shot point in metres, number of stacks and record number in

brackets. However, for simplicity of appearance only the file number is shown in figures 9.1 to 9.6

The EK recordings were taken over a total sampling period of 128 ms with a 62.5 μs sample interval. No high pass, low pass or notch filters were used. All data shown are without any signal processing being applied.

9.3 Discussion of the EK results from the Mansfield site

In all of the EK records it was found after the investigation that a 10 ms delay had been present in the seismic recorder. This delay has been accounted for in all figures showing an EK response by the blank portion at the start of the recording. The delay of 10 ms was considerably less than the estimated arrival time of the 'P' wave at the water table. Data are not recorded during this delay period.

The negative offset seen on the original EK amplitude response data has been corrected by adding +12.5 mV offset to the data set to make sure the responses varied about a zero voltage point. This offset may have been due to the self-potential in the ground or possibly a drift on the channel of the seismic recorder. For future reference a measurement of the self-potential of the ground will be made as part of any EK field investigation. If there is a correlation between the recorded EK response and millivolt offset and the measurement of ground self-potential then this needs to be noted. A simple modification to the software enables this possible self potential to be measured.

In respect to the four key questions:

(1) Is there any moveout of the EK response with regard to a change in position from the seismic impact point?

For the EK investigations conducted at the Mansfield site, which was predominantly a sandstone environment, the EK responses were remarkably good. The EK responses shown in figures 4.6, 4.9 and 4.14 clearly indicate that there is no perceptible moveout of the EK responses such as would occur in a seismic survey. In practice there is a small amount of move out due to the finite propagation velocity of an EM wave, 2.99×10^{8} m/s. This moveout would be in the order of a few tens of nano-seconds i.e. 1×10^{-9} s,

which would not be resolvable on a millisecond scale.

Therefore this lack of moveout with respect to distance from the shot point is clear proof that the source of the EK response is electromagnetic in origin. What is considered here is that with the seismic source in a fixed position, the travel time of a seismic or acoustic wave down to the water table is fixed, the detection of the refracted wave is dependent on the distance of the detector away from the seismic source, e.g. the further away it is the longer it will take to receive the refracted wave due to the finite travel time of the seismic wave. However, when an electromagnetic wave is generated at a conducting boundary the resultant radiation is transmitted at close to the speed of light, 2.99×10^8 m/s, and no seismic move out will be apparent. Therefore this satisfies the criteria in (1).

Another important feature to note is the EK response is clearly visible in each of the figures 4.6 to 4.14 and these show the raw data without any signal processing being applied to any of the records. All of the records in figures 4.6 to 4.14 were the result of 9 stacks in order to enhance the EK response. However, a one-stack recording was also taken for comparison purposes with figures 4.6 to 4.14. This is shown in figure 4.20 and again the EK response is clearly visible despite the signal to noise ratio being a lot worse. An interesting point to observe is that the EK response in figure 4.6 is 9 times that of figure 9.1 thus clearly demonstrating the improvement due to stacking.

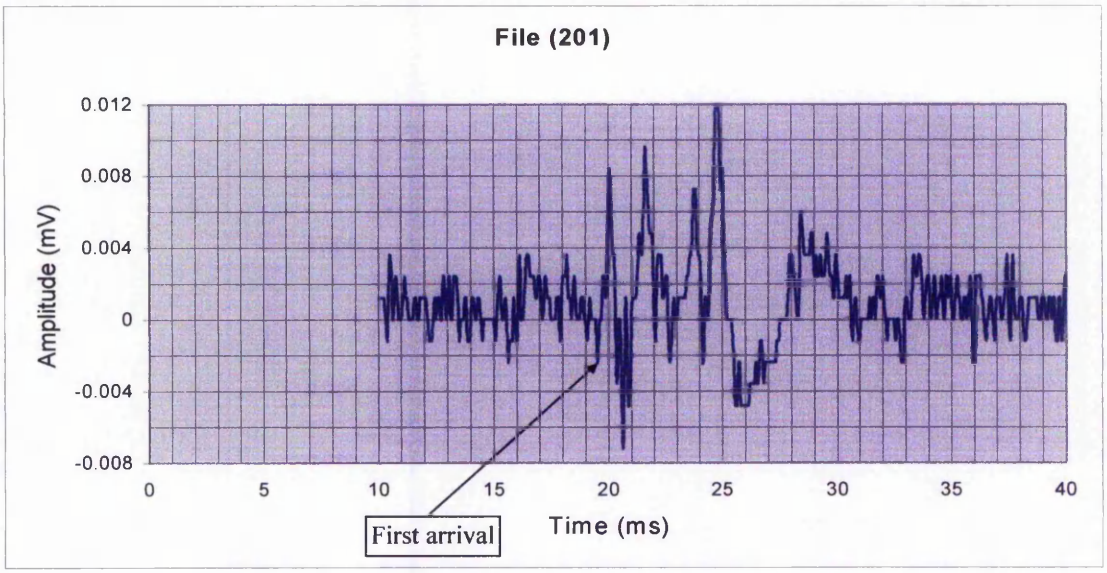

Figure 9.1 2 metre dipole aerial EK response at 1 metre from shot point, 1 stack... Note first arrival at 19.5 ms and a possible weak EK response at 15.5 ms.

(2) Is there a correlation with a known feature such as a water table or knowledge of depth to the fully water saturated zone?

There were a number of accessible boreholes and the ones near to the area of investigation were dipped to determine the depth to the water table. The depth was found to be 15 metres. As there had been a considerable amount of rain over a number of weeks prior to the investigation and ground water would have been seeping down over this time making the underlying sandstone moist. As these investigations were conducted in early February with the weather being very cold the effects of surface evaporation would have been minimal.

Examination of the EK response data, figure 4.6 shows a first arrival occurring at 19.25 ms. This is possibly due to a fracture zone. Unfortunately, there were no log details for the region 9 to 13 metres (see borehole log Chapter 3, Table 3.3). However, for the log that was available there was observed to be a considerable number of fracture zones at various depth therefore the probability of one being at this depth is reasonably high. The large response at 31 ms has a correlation with the capillary zone, which would extend up above the water table for some two metres Buckingham(1907). There is evidence of EK responses out to 33 milliseconds. Further stacking, e.g. 36 would have enhanced these signals and enhanced the feature seen to start at 30 ms. However, this was not realised until the data had been analysed.

Reference to the borehole log accurately shows most of the fracture zones and certain other features over the range of interest. However, some further analysis of the whole data set indicated other EK responses possibly due to fracture zones.

These results clearly indicate is it possible to locate the water table and possibly fracture zones above the water table, in certain instances, or fully water saturated zone.

(3) Is there a symmetry at a position diametrically opposite to an EK survey line?

The survey clearly shows a phase reversal when conducted symmetrically at 180° about the shot point. This has also been observed on all earlier EK surveys, (See Chapter 9), and was done as a matter of routine. For future EK investigations a radial survey with an angular spacing of 45° should be taken about the shot point. This will measure if any

anisotropy is present. This result is to be expected. Examination of figure 2.5 Chapter 2, shows the electric lines of force emanating from the dipole are symmetrically opposite either side of the dipole.

(4) Is there a predicable fall off in the amplitude of the EK response with distance?

Inspection of the EK response in figures 4.1 to 4.14 show a distinct reduction in the amplitude of the EK response with move out from the shot point. In fact the graph, figure 4.15 Chapter 4, illustrates this very well and the equation for the curve showed dominant terms in both x and x^2 which is consistent with the theory for an oscillating dipole field, Lorrain and Corson (1962), see also Chapter 2, section 2.4.2.

Thus for EK results the data obtained have proved to be highly significant after taking into account the wavelength of the EM wave produced as a result of the seismic wave traversing a fluid contrasting boundary. For a seismic hammer response, with a dominant frequency of a 100Hz, would result in very long wavelength of 2.99 $x10^6$ m. This explains why the signal received on the dipole aerial is in the order of millivolts or less.

By increasing the length of the dipole aerial in increments of two metres the detection sensitivity can be increased in direct proportion to the increased length. Stacking, as demonstrated, will also improve the signal to noise ratio and also its amplitude. Therefore it should prove feasible to locate EK responses down to at least 80 metres or more.

However, one of the objectives for this thesis was to demonstrate the detection of EK responses down to 20 metres or so, which has been achieved. In fact it has been shown that it is possible to obtain EK responses down to at least 80 metres or so in the right conditions. Further experiments are needed to confirm this. The site at Mansfield has a borehole with a logged depth of 82 metres and would be suitable for these investigations. However, it is intended to conduct future EK investigations at another site with a different geological profile with an accessible borehole of at least 40 metres, together with a detailed geological log. This would enable comparison of EK data with that already obtained.

9.4 Discussion of the EK results from the Ospringe field site.

The investigations conducted on this site were to study the effects of compaction of loess using a range of geophysical and geotechnical investigation techniques which are described in detail in Chapter 4. Two survey lines were undertaken, one along the south edge of the quarry site and the other at 45° NNE relative to the shot point. The main three main differences compared to the Mansfield site are:

(1) The geological profile was different, in this case being loess. The underlying geology was also different and much closer to the surface.

(2) The EK responses relate to very much shallower profiles, in the order of one metre for the compaction studies and eleven metres for the location of the fully water saturated zone.

(3) No borehole was available to determine the depth to the water table either on or near to the site.

As for the Mansfield results the four key questions are:

(4) Is there any moveout of the EK response with regard to a change in position form the seismic impact point?

For the EK investigations conducted at the Ospringe site, which was predominantly a loess or brickearth environment. The EK responses, figures 9.2 to 9.4 clearly indicate that there is no perceptible moveout of the EK responses seen to occur at 2 ms such as would occur in a seismic survey, for these investigations the time shown is real, i.e. no delay present as for the Mansfield results. The changes in occurrences and time of the EK responses over the length of the survey line will be discussed after the remaining questions have been addressed.

(5) Is there a correlation with a known feature such as a water table or knowledge of depth to the fully water saturated zone?

The water table depth was estimated at 11.7 metres. This is seen as the EK response at 24 milliseconds on most of the records. The water table depth was confirmed with the

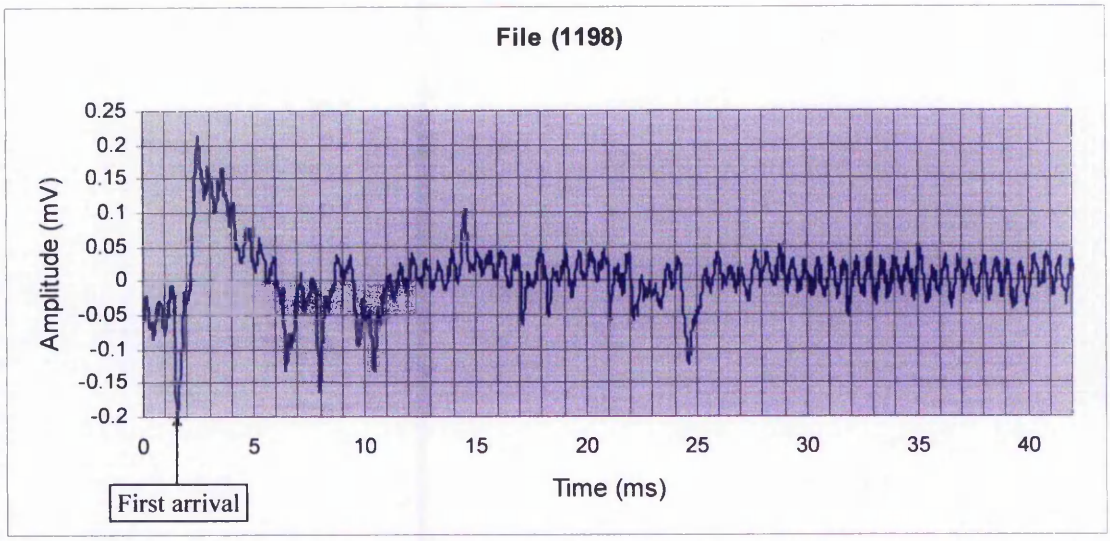

Figure 9.2 EK response at 4 metres, Line 1, 4 Metre dipole at 4 m, 4 stacks

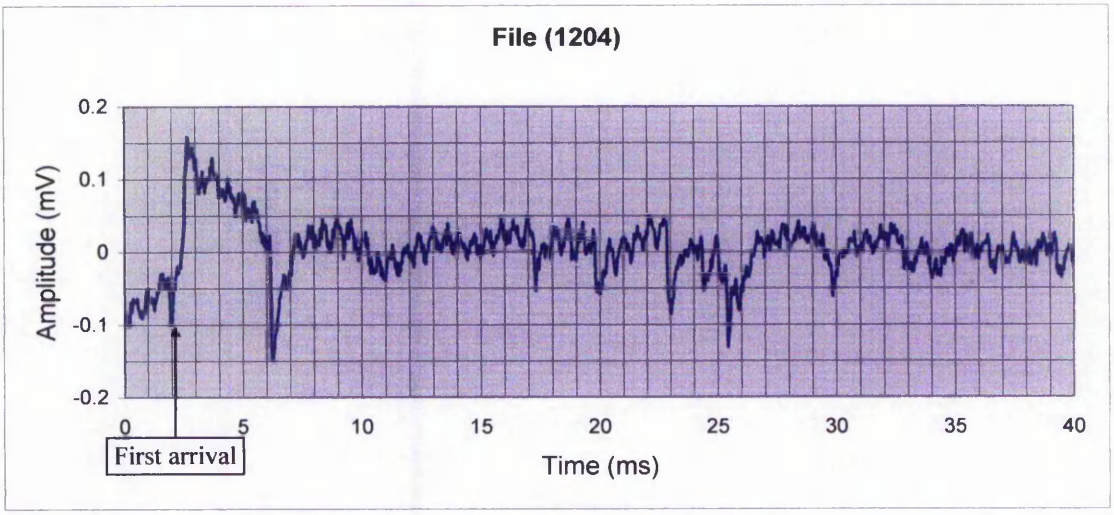

Figure 9.3 EK response at 8 meters, Line 1, 4 metre dipole at 8 m 4 Stacks

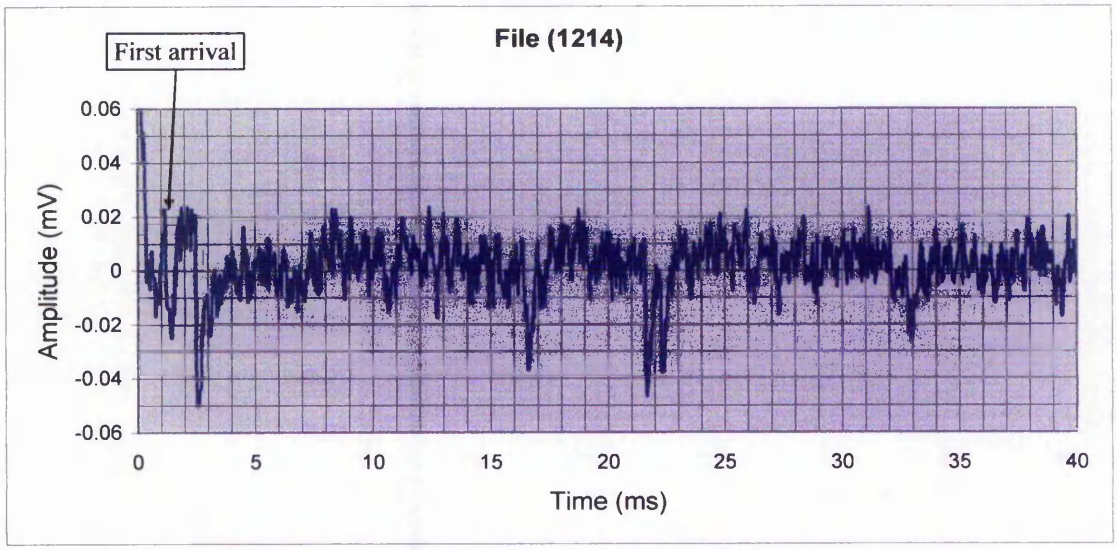

Figure 9.4 EK response at 15 metres, Line 1, 4 metre dipole at 15 M 4 Stacks

water authority to be at 13 metres one year before. However, the depth where the EK survey was conducted was 1 metre below the ground level, which made the water authorities estimate at 12 metres. Allowing for seasonal variations in rainfall and measurement errors this is a very good correlation with proven data.

(6) Is there a diametrically opposite symmetry at a position to an EK survey line?

Due to the very disturbed condition of the ground and taking the diametrically opposite line would have meant going up a slope, which was another entrance to the site. For these reasons this survey geometry was not possible. However, a survey recorded at 45° to survey line 1 was taken as the best compromise to having no results at all.

Comparing the pre-compaction results for survey line 2 with survey line 1 at 4 metres, (figures 9.2 and 9.5, respectively) the responses occurring at 2 ms are seen to be similar. However, the negative spike at 2.75 ms on the EK record for figure 9.4.is thought to be due to the hammer plate becoming heavily embedded in the ground. Although this was realised, it was left in situ to avoid any effect on the results as the whole of the investigation was referenced to this point.

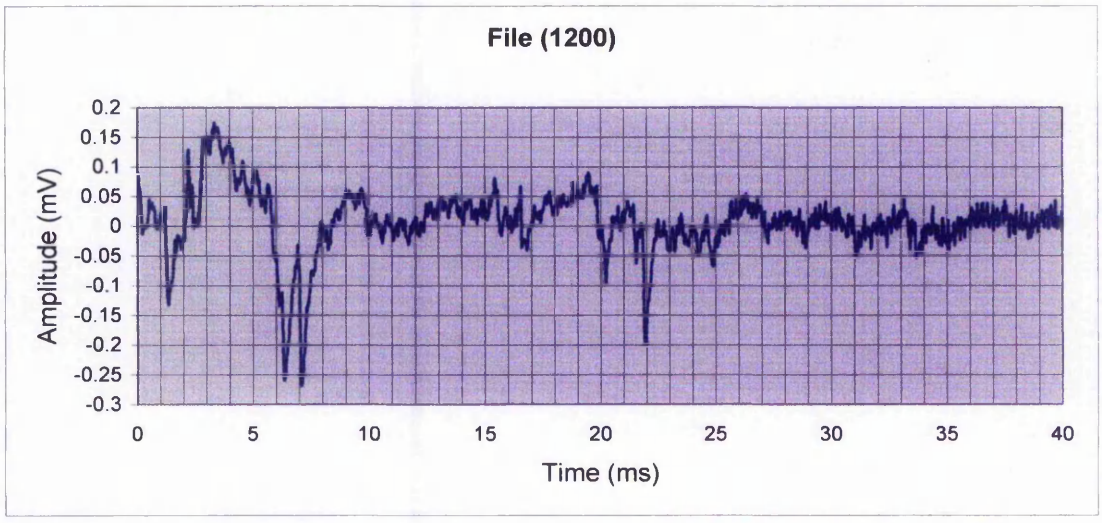

Figure 9.5. 4 metre dipole at 5 m, EK response, line 1, and 4 stacks. Pre-compaction.

(7) Is there a predicable fall off in the amplitude of the EK response with distance? Inspection of figures 9.2 to 9.4 show a distinct decrease in the amplitude of the EK response with distance. From figures 4.39, Chapter 4 onwards noise is seen to obscure

any EK responses. However, figure 4.51 shows a much clearer EK response. This is most likely due to the distribution of the dipole electric field. The noise problems and differences in the EK response at various offsets is due to the very disturbed surface and the presence of chalk pinnacles and solution pipes. These are seen on figure 9.7, after Northmore *et.al.* (2003), together with the variability in the ground conductivity over the whole area of the investigation site and, in particular, where the EK survey was conducted.

These results clearly illustrate the need for careful interpretation of geophysical data and where appropriate, to have data from more than one geophysical technique available such as the EM profile in figure 9.6.

9.5 Laboratory investigations

The EK laboratory results for the Mansfield site were conducted on a sandstone sample that was obtained close to the site. The results in Chapter 5 show weak EK responses at the interface of the main sample and lime stone sample. This provided a velocity contrasting layer effected. In addition, an EK response was noted at the location of a fine bedding fault. This was unexpected considering the challenges in getting these experiment working. The main observation was that an EK response as theory predicted.

9.6 General discussion

These will take the Mansfield results followed by the Ospringe pre and post-compaction EK results. Reference will be made to some earlier EK investigations that were conducted with the original dipole aerial at the Mansfield site in the early part of 1998.

9.6.1 *Mansfield results: Past and present*

Earlier EK investigations conducted at Mansfield in early January 1998 were conducted in order to investigate the dipole field distribution. A survey was laid out along the upper part of the site near to borehole 26 (see figure 3.2 Chapter 3 page 52) which was approximately six metres above the height where the investigations described in Chapter 4 took place. Therefore, the depth to the water table was in the order of 21 metres, allowing for the increase in height above borehole 32. The 2 meter dipole aerial

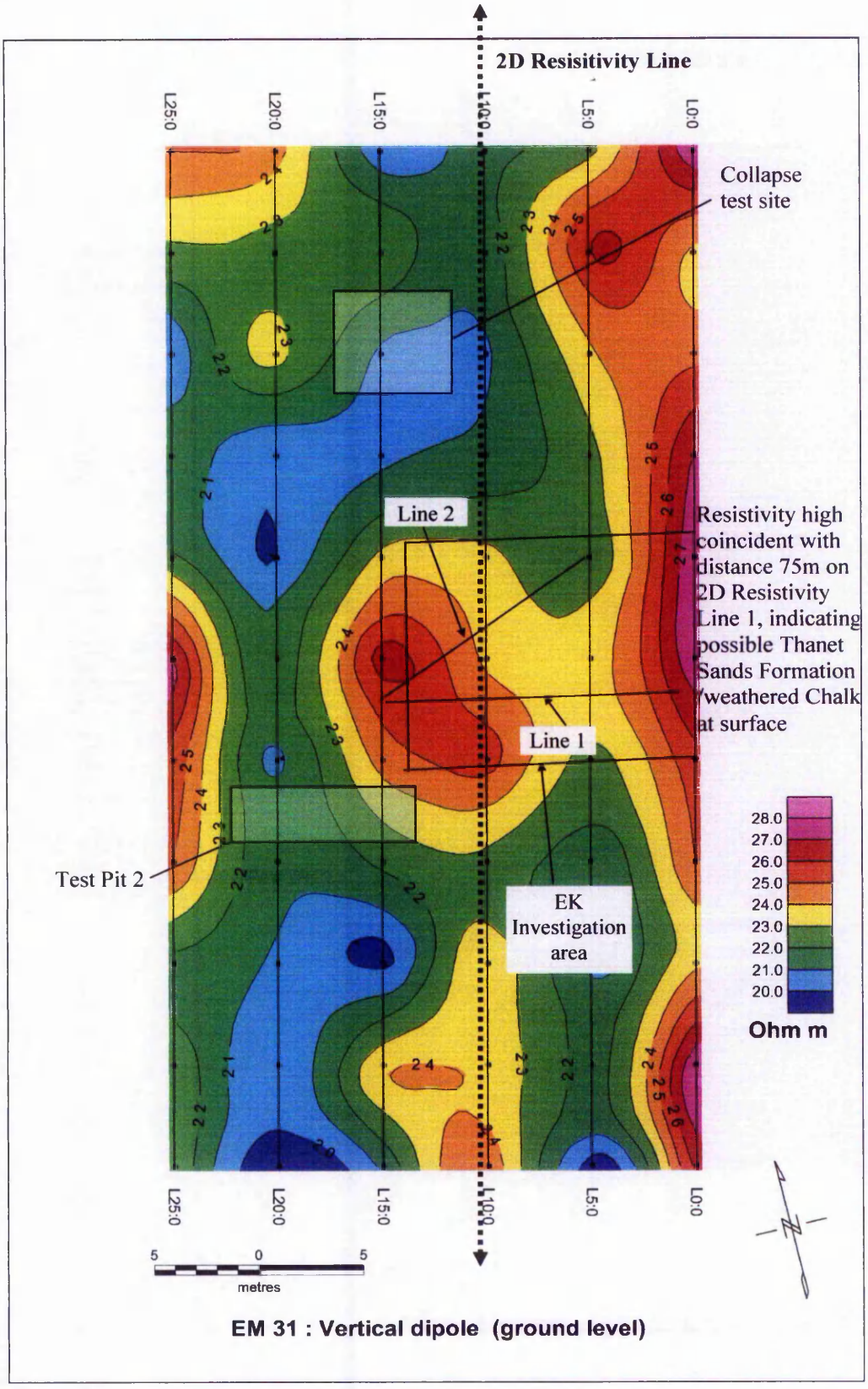

Figure 9.6 EM31 survey data for the Ospringe site. After Northmore *et.al.* (2004) Lines 1 and 2 are those referred to in this thesis.

was laid out in 1metre increments to a range of 20 metres then in 2 metre intervals up to 40 metres either side of the hammer plate. The results are shown in figures 9.7 and 9.8 for the survey lines due west and east of the hammer plate. The East survey line is similar to the west survey line with phase reversal and identical peak amplitudes. From figure 9.7 and 9.8 the EK responses seen at 1 or 2 milliseconds are due to hammer plate reaction with the ground. The EK response seen at 5 ms is due to a layer of landfill debris. Figure 9.8 shows EK responses at 33 ms and the water table at 45 ms. These results were all obtained with the original 2 metre dipole aerial and are 9 data stacks.

The results shown in figures 9.7 and 9.8 are as expected as the nearer the source the larger the EK response is likely to be.

The results of another EK investigation where the dipole aerial was lowered down borehole 32 in 1 metre steps from the surface to the water table are shown in figure 9.9. The centre of the dipole aerial was used as the reference point. Some of the records have been omitted for the sake of clarity.

2 Observations

(1) The peak amplitude is seen to occur at 14 metres. The responses seen at the start of the recording is due to the hammer plate reacting with the ground.

(2) The absence of EK response moveout with distance

(3) The increase of the EK response as it gets close to the water table.

(4) The increase in background noise as it gets near to the water table

(5) The almost total lack of an EK response at the water table.

An explanation for the above observations and in particular 9.6.1.5 is provided in section 9.7.

Finally, the results of an EK survey close to borehole 32 are shown in figure 9.10. The survey was conducted out to 20 metres in 1 metre steps up to 12 metres and then in 2 metre steps from 12 to 20 metres. Not all of the individual EK responses are shown.

However, the depth to the water table is again seen to be in close agreement with that obtained from dipping the borehole. The small EK responses at 17.5 and 27 milliseconds are due to the fracture zones. This was not realised at the time of these investigations.

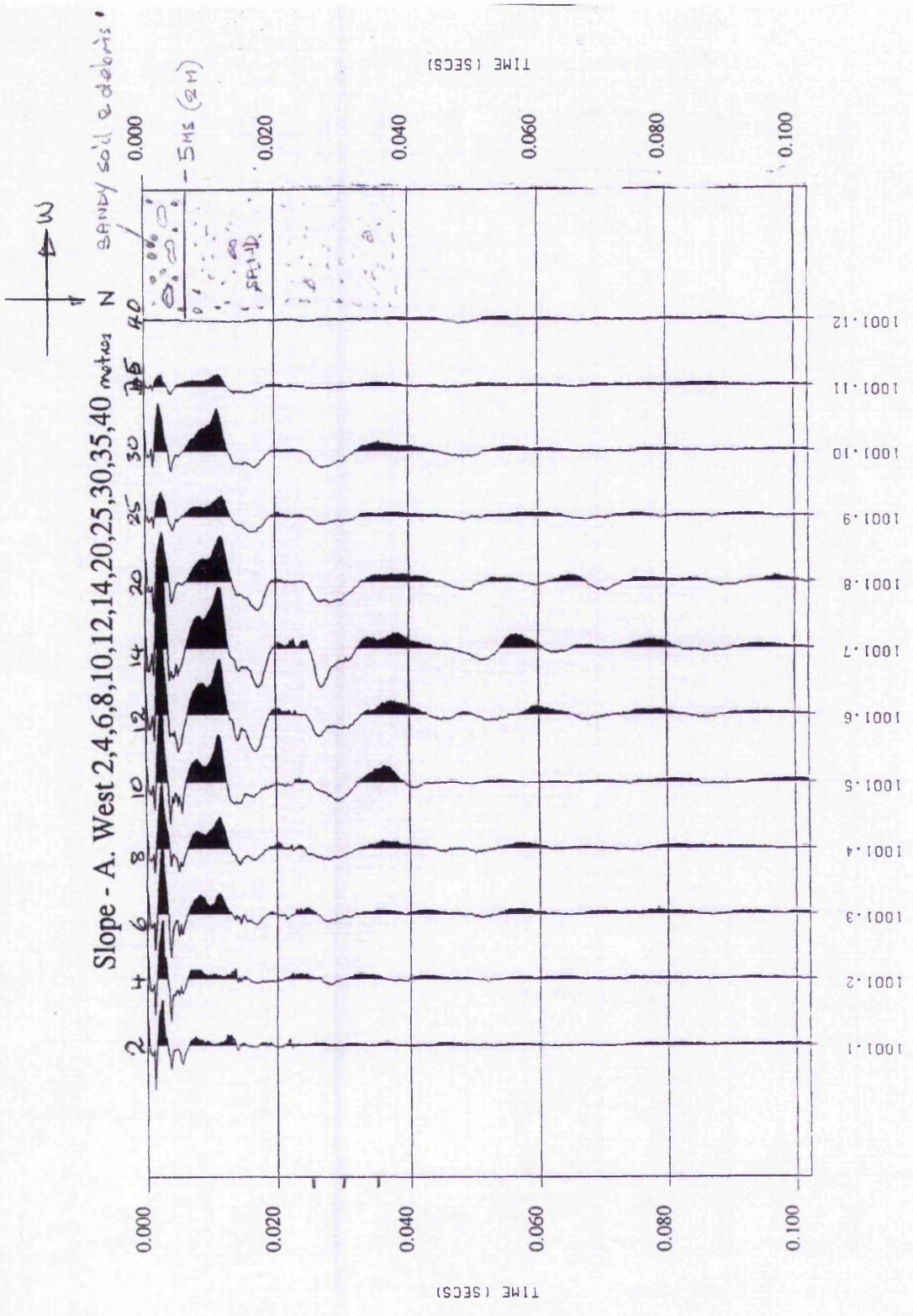

Figure 9.7 EK survey line due west of shot point. at borehole 26

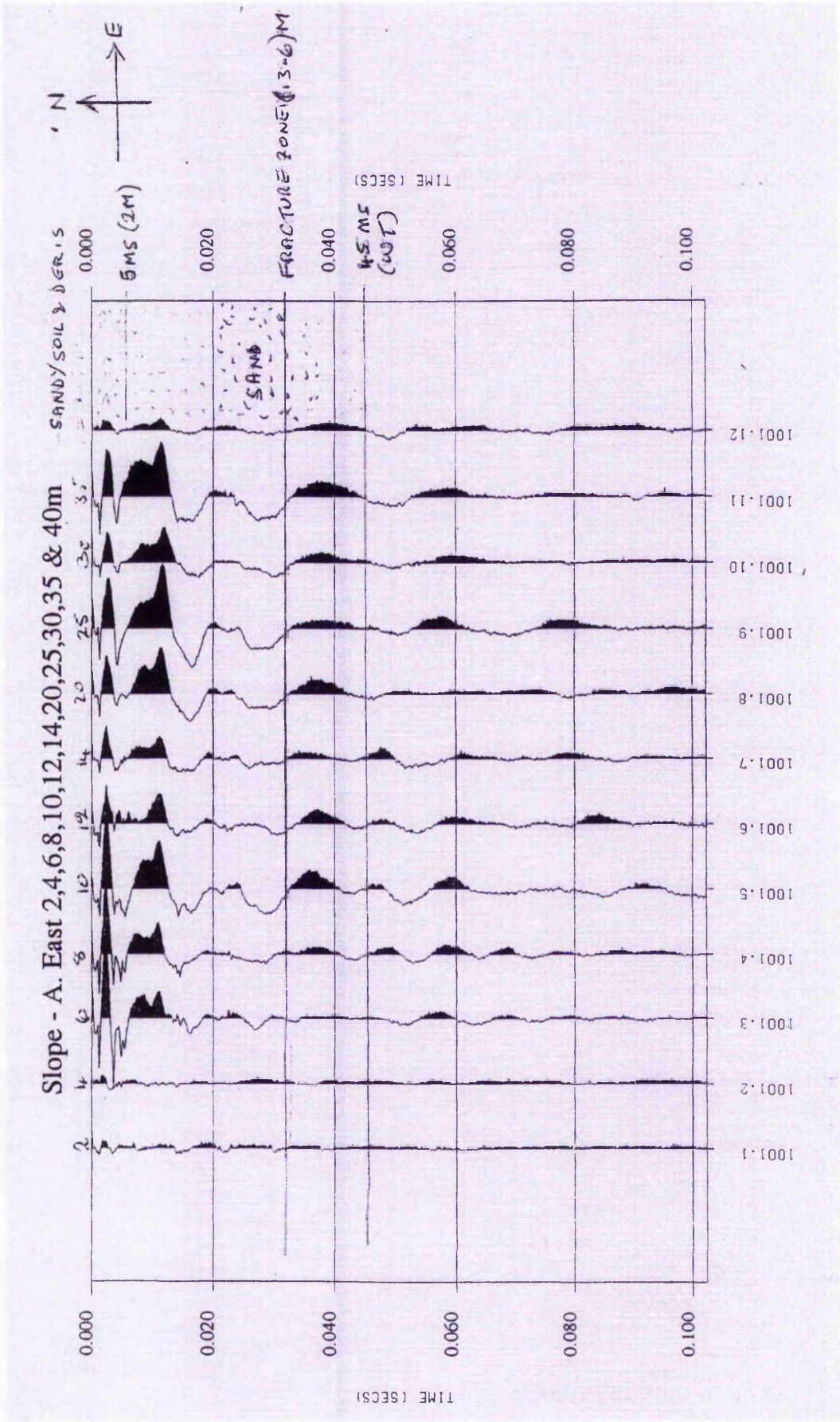

Figure 9.8 EK survey line due east of shot point at borehole 26. Complementary to figure 9.7.

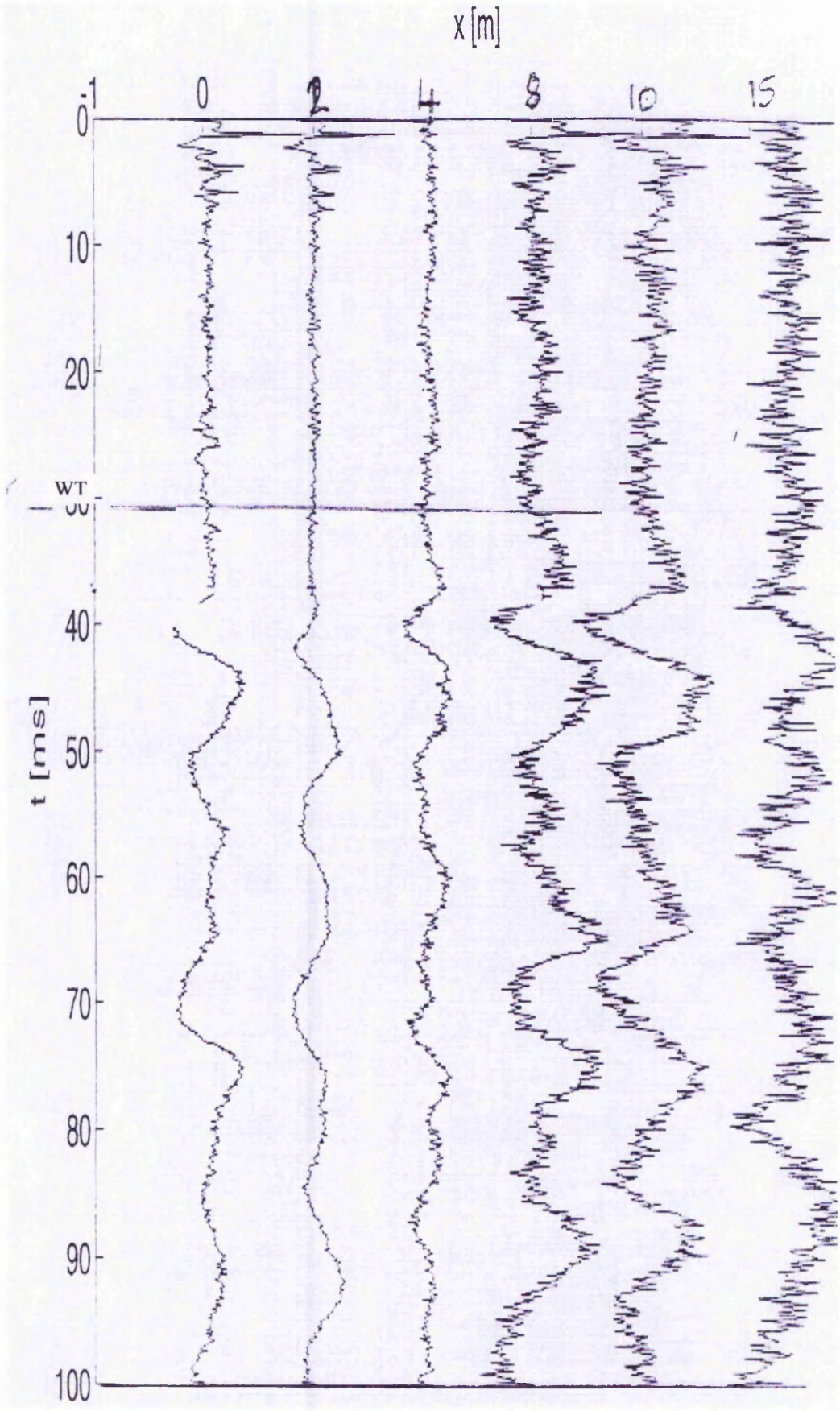

Figure 9.9 EK response from the surface down to the water table

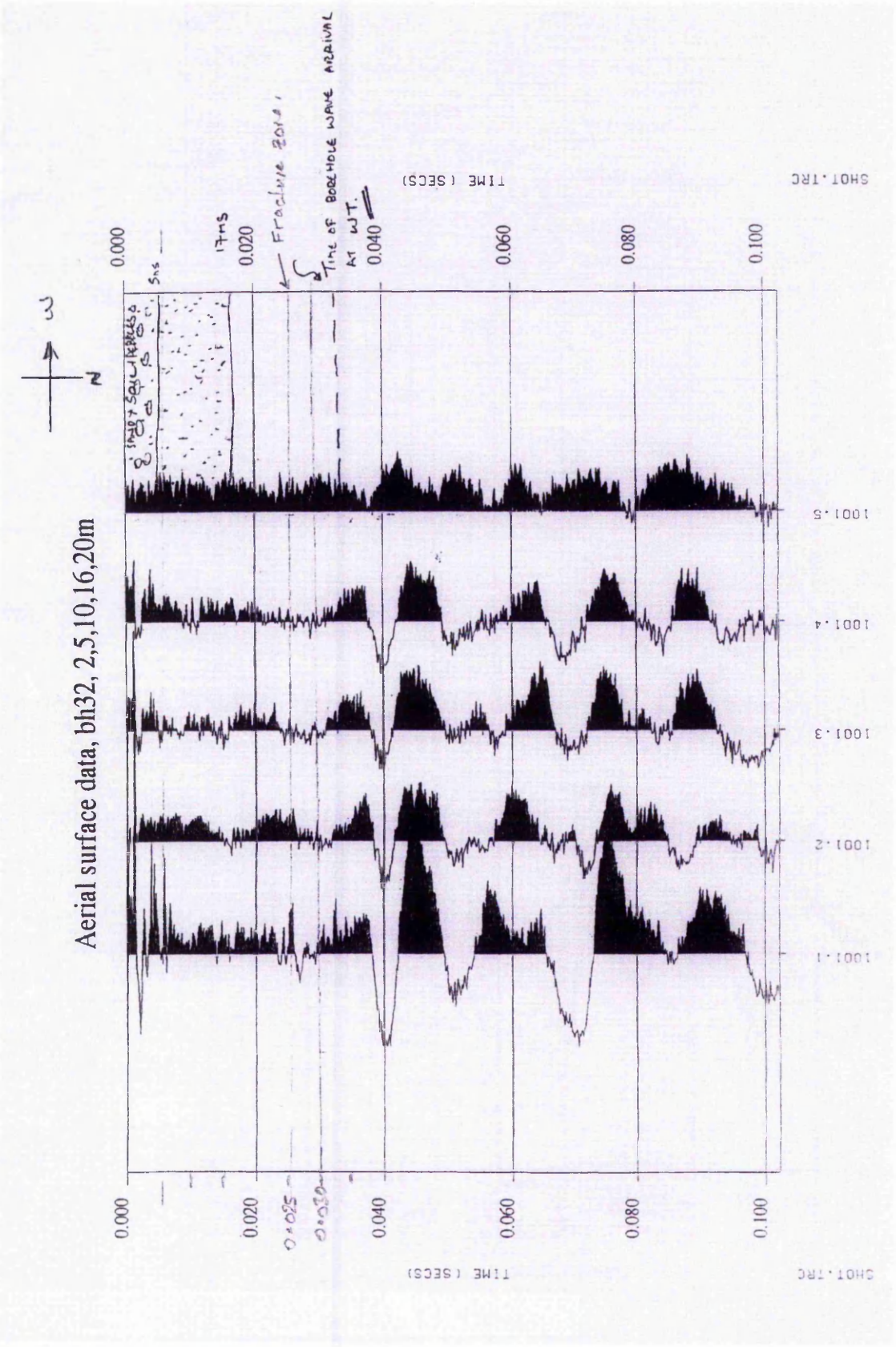

Figure 9.10 EK response for survey carried out at borehole 32

9.7 Final comments..

The results of the EK investigations conducted at the Mansfield site and contained in this thesis were compared with the results of earlier EK investigations conducted at the same site by the author. The two sets of results compare very favourably and showed very clearly the repeatability of the results over a two year period between the investigations.

The results described for figures 9.7 and 9.8 show both the EK response symmetry and the nature of the dipole field distribution about the shot point. Also observed are responses due to fracture zones and the water table.

One of the more interesting results of the earlier EK investigation was the down hole detection of the dipole field distribution and the cancellation of the EK signal when the dipole aerial was placed midway between the source of the electromagnetic generated dipole-field, the source of the electro-kinetic electromagnetic radiation being generated at the interface of the strata with the water table. The reason for the cancellation of the EK signal is best explained by reference to figure 9.10. The dipole electric field lines move in opposite directions away from the source and either side of the dipole aerial as in figure 9.16, thus the induced voltage on the dipole aerial is zero.

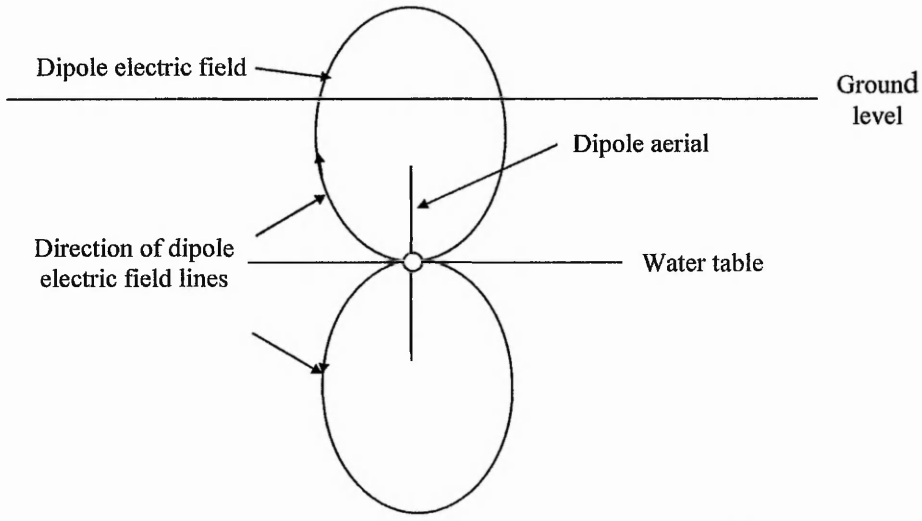

Figure 9.11 Model of dipole electric field lines as seen by the dipole aerial.

The signal has a maximum amplitude at 14m, this id due to the proximity of the dipole aerial to the dipole source.The EK results shown in figure 9.11 are for an EK surface investigation carried out near to borehole 32. There are a number of EK responses in

the region 6 to 25 ms these are due to the fracture zones the arrival of the seismic wave at the water table is seen to occur at 30 ms which is close agreement with the later EK data obtained as discussed in Chapter 4. The data shown are without any signal processing applied.

The EK results obtained from the geotechnical investigations at the Ospringe site show the possibility of resolving very fine detail, < 1 metre, in the right circumstances. However, this site proved to be a very noisy environment, although despite this very acceptable results were obtained. For compaction studies the use of EK proved to be very beneficial.

The ability to detect water tables has been demonstrated in two different geological environments with the added bonus of being able to locate fracture zones. The ability to locate fracture zones would aid the positioning of a packer unit for borehole investigations.

The results of the laboratory research have made clearly identified some of the problems in conducting EK investigations in the laboratory and results obtained have been very promising and point the way to further investigations one important line of research being outlined below in 9.8.

9.8 Future work and applications of the work in this thesis.

9.8.1 *Determination of ground permeability using EK*

The determination of permeability using EK is very difficult due to the limited research having taken place in this area and the problems outlined below. A number of borehole EK investigations were carried out by Miller and Clark (1995). They claim to relate ground permeability to the rise time of the EK signal. There is only limited data from other authors.

If an estimation of permeability can be achieved by the use of EK, then that would be extremely useful in the built environment and hydrology, the widely varying range of geological profiles presents additional problems to address, (see Chapter 10.3). A general analytical approach is considered below, with suggestions for the field and laboratory investigations.

To consider how a measure of permeability may be achieved, refer to the equations given below. It has been shown, , that the EK effects due to piezoelectric effect are equal to zero and is therefore ignored for the analysis considered below, Pride (1994).

The transport and porous continuum governing equations, Pride & Haartzen (1996) state that:

9.8.1 Transport equations

$$J = \sigma E + L(\varpi)\cdot(-\nabla p + \omega^2 \rho_f u(\varpi) + f) \qquad (9.1)$$

$$-i\omega w(\omega) = L(\omega)\cdot E + \left(\frac{k(\omega)}{\eta}\right)\cdot(-\nabla p + \omega^2 \rho_f \quad u(\omega) + f) \qquad (9.2)$$

Where $\omega = 2\pi f$, 'f' being the frequency of the seismic disturbance.

$-i\omega w(\omega)$, the filtration velocity, represents the volume of the fluid traversing unit area in unit time

J is the current density

k is the fluid flow permeability

L is the Electrokinetic coupling coefficient tensor

E is the Electric field

σ = electrical conductivity

p = fluid pressure

η = fluid shear viscosity

f = f_f fluid force

i = the complex operator

$\nabla p = (\partial p/\partial x)i + (\partial p/\partial y)j + (\partial p/\partial z)k$ i, j & k being unit vectors

Note that in equations 9.1 and 9.2 the coupling is due to the electro-kinetic coupling tensor L. If the electro-kinetic coupling tensor is made equal to zero then equation (1) reverts to Maxwell's equation for current density and equation (2) becomes Biot's equation, Biot (1956). There is a limitation on the upper frequency at which these equations will hold true. The condition being that the wavelength of the acoustical wave must be much greater than the grain size under consideration. Typically for sand a range of grain size would be 2.0 – 0.06 mm, silt 0.06 – 0.002 mm and clay < 0.002 mm.

Gravel has a distribution of grain size much larger than those above and has been ignored for the purpose of the analysis considered here.

At a frequency of 1MHz and an acoustical velocity of 3000 m/s the wavelength would be $3x10^{-3}$ metres or 3mm. Thus, 1MHz would be a safe upper limit for a wide range of geological grain sizes < 0.02 mm. For laboratory EK investigations, a frequency of 150 KHz and 50 KHz was used as the ultrasonic transducers in the experimental vessel typically have this frequency. In the field, seismic frequencies are in the range 30Hz to 3 KHz with corresponding wavelengths of 100 to 1 metre. For a seismic velocity of 3000 m/s, the maximum resolution being $\lambda/4$ or 250mm to 25m. For gravels, the above equations would apply at these frequencies.

Dynamic equation

$$\nabla\cdot\tau = -\omega^2[\rho u(\omega) + \rho_f w(\omega)] - \mathbf{F} \qquad (9.3)$$

Where F = the bulk force

Poroelastic equations

$$\tau = [K_G\nabla\cdot u + C\nabla.w]I + G[\nabla u + \nabla u^T - \frac{2}{3}\nabla\cdot uI] \qquad (9.4)$$

$$-P = C{:}\nabla\cdot u + M\nabla\cdot w \qquad (9.5)$$

where τ is the bulk stress tensor

C current source density

P the pore-fluid pressure

M an applied magnetic force

W is related to the porosity

K_G Gassmann's bulk modulus See table 9.1

I the identity tensor

τ The bulk stress tensor

G Stiffness, shear modulus of the framework of the grains

μ Magnetic permeability

A full discussion of Gasman's equations, Gassman (1951) is not possible here owing to the time available. However, table 9.1 provides information of Gassman's constant for

some minerals.

Table 9.1: Properties of sediment mineralogy, water, gas and pure hydrate.

Substance	Bulk Modulus [GPa]	Shear Modulus [GPa]	Density [g/cm^3]
Calcite	76.8	32	2.71
Clay	20.9	6.85	2.58
Quartz	36	45	2.65
Water	2.5		1.032
Pure Hydrate	5.6	2.4	0.9
Gas	0.1		0.235

The primary source for the electromagnetic field is the current source density C.

NB. If $u_f(r)$ and $u_s(r)$ are defined as the average displacement of the fluid and solid phases within an averaging volume with V_A positioned at point r (V_A being larger than the grains but much smaller than the wavelengths), then the u and w in Eq's. (9.1) to (9.5) are defined as:-

$$u \equiv u_s \tag{9.6}$$

$$w \equiv \phi(u_f + u_s) \tag{9.7}$$

where ϕ is porosity.

As most of the investigations where carried out with a 5Kg sledgehammer impacting on a composite plate, it can therefore be reasonably assumed that most of the seismic energy is centred around 100 Hz, Keiswater and Steeples (1974). Therefore the term $\omega = 2\pi f$ equals 628f radians.

To obtain an equation for k, the fluid flow permeability

From equation 9.2 $$(k(\varpi) = -\eta\{(\varpi w(\varpi) - L(\varpi)\cdot E)/(-\nabla p + \omega^2 \rho_f u(\varpi) + f)\} \tag{9.8}$$

To simplify the equation (9.8), a substitution for the term $(-\nabla p + \omega^2 \rho_f u(\varpi) + f)$ is made by rearranging eq'n (9.1)

$$J - \sigma(\varpi)\cdot E/L(\varpi)\cdot = (-\nabla p + \omega^2 \rho_f u(\varpi) + f)$$

Substituting for the term $(-\nabla p + \omega^2 \rho_f u(\varpi) + f)$ in (8) gives

$$k(\omega) = -\eta\{(\omega w(\omega) - \frac{L(\omega)\cdot E)\cdot L(\omega)\}}{J} - \sigma(\omega)\cdot E \qquad (9.9)$$

The term $(-\nabla p + \omega^2 \rho_f u(\omega) + f)$ has now been eliminated which makes the determination of $k(\varpi)$ dependent on the terms η, J and E

All of the above would require carefully controlled laboratory experiments, in addition to fieldwork using where possible using some of the results in this thesis. In addition mathematical modelling using the above derivation in equation 9.9 for the fluid flow permeability employing 'MATLB SIMULINK'.

In order to carry out the field investigations the following development of the software already available would be needed as it will be necessary to use more sophisticated signal processing techniques in the analysis of the data related to the permeability studies.

9.8.4 *Further enhancement of the MATLAB desktop data processing software*

The programmes developed for the purposes of analysing data for this thesis were sufficient to accomplish the task in hand. However, there are many improvements that could be made to the existing software. Some of which are more related to this research topic are listed below:

(1) To apply a fill to the positive transition of the seismic waveform. This would aid the identification of first arrivals.

(2) To enable the software to communicate with a USB port directly. Data from field experiments will be stored on a USB 2 64 m-byte, or larger, memory pen.

(3) To provide an accurate voltage calibration to the amplitude response. This is necessary in order to compare subtle differences in voltage amplitude responses.

(4) Incorporation of the 50Hz and its harmonics noise removal routine.

(5) Incorporation of an interactive digital filtering routine for both a high and low pass filter.

(6) Use of Graphical User Interface, GUI. Use of this facility would make the use of the software more user friendly as the functions would be placed in a windows type environment.

9.8.5 *Laboratory investigations*

Chandler (1981) of Schlumberger showed via laboratory experiments showing that the permeability of rocks can be determined by measuring the electro-kinetic (EKS) signal or "streaming potential". These results, figure 9.13 shows a good fit between the core plug and calculated EKS permeability values, both expressed in Darcies, Darcy (1969).

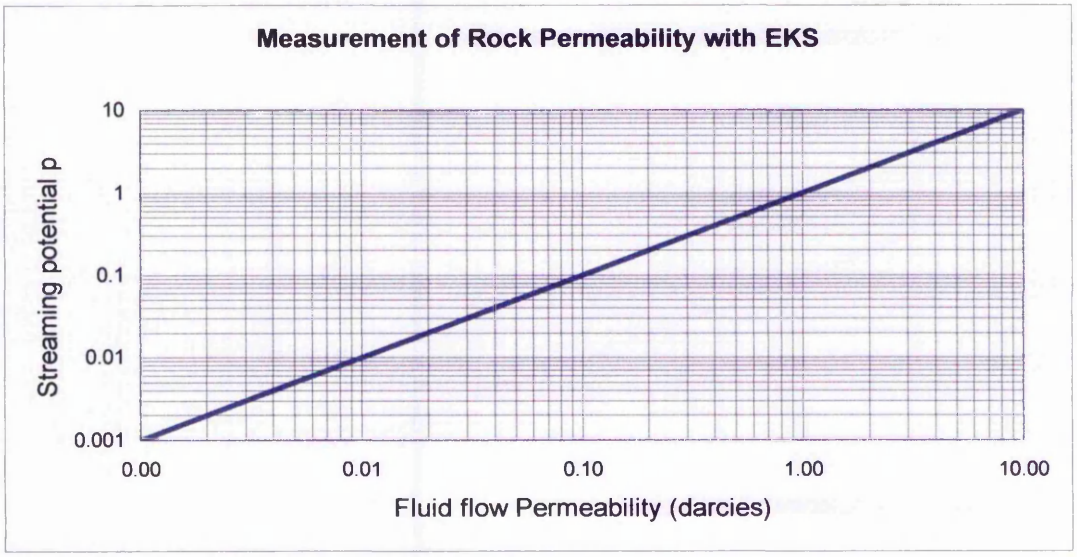

Figure 9.12. After Chandler (1981)

These experiments appeared to confirm that when a sharp pressure pulse is applied to a rock sample the rise time of the electrical signal is inversely proportional to the rock sample's permeability. However, the rise time of an EK response is governed by a number of other factors such as the ground dielectric constant, ground moister content and the characteristics of the recording system, all of which can significantly affect results. Further investigation and detailed analysis coupled to laboratory experiments are needed to confirm this and would involve carrying out detailed experiments for a wide range of ground permeabilities. This would require making modification to the existing apparatus, either that used for the EK response investigations or more preferably the GDS ADVTTS triaxial cell system, in order to allow water to flow through the sample in a controlled and measurable way.

Samples will have to be obtained from the area of interest would be prepared and mounted in the experimental apparatus The water flow rate adjusted to the required level and a measurement taken of the EK response taken when an ultrasonic pulse is injected into the specimen. This process would need to be repeated for a range of flow rates and permeabilities. An ultrasonic transducer with a heavily damped response would be required, to minimise spurious EK responses would be generated after the transition of the ultrasonic wave. Although this reduces the available power output from an ultrasonic transducer, this is not so crucial where ultrasonic path lengths are in the order of 500mm Medina *et.al.* (2003).

A two layer model would be designed based on consolidated sand to provide a significant velocity contrast between the two layers. The intention is to use this model as an EK reference standard.

(6) *Field work*

Carefully controlled field EK investigations on one new site with a consolidated limestone environment, similarly for a clay environment and further seismic and EK measurements on the Mansfield site. The investigations would also include taking samples from each location to correlate results with the laboratory studies, as was the case with the sandstone specimen in Chapter 5 section 5.5.

Chapter 10 Conclusions and recommendations for future research

Knowledge does not mean mastering a great quantity of information
but understanding the nature of the mind.
This knowledge can penetrate each one of our thoughts
and thus illuminate each one of our perceptions

Matthieu Ricard

Buddhist Monk

10.1 Introduction

As specified in the introduction the aim of the thesis was to demonstrate the use of EK as a non-destructive shallow ground investigation tool. The use of EK for this application has been demonstrated to be an effective means of geophysical ground investigation, complementing other methods such as seismic refraction and resistivity. In addition, other potential applications have been realised some of which are listed under recommendations for future research.

The much improved detection of seismically generated electro-kinetic signals has been made possible by use of the novel dipole aerial. This particular development of the antenna is new and exciting breakthrough in the detection of EK responses opening up a whole new area of research. Careful inspection of the EK results provided in Chapter 4 clearly demonstrate the detection of these signals from depths of 40 metres or so, revealing the depth to the water table and fracture zones. With an increase in length of the dipole aerial, easily achieved by adding two additional screw in one-metre lengths, detection of EK signals from even greater depth can be had, e.g., by adding two one meter lengths to a one metre dipole aerial the detection sensitivity is increased by a factor of 2. The sensitivity is governed by equation 46 in Chapter 2, section 2.5 that is seen to be linear.

A coil aerial tested on the Mansfield site did not detect any EK signal that was directly comparable to the dipole aerial. However, there was a small response that appeared to be measuring a surface Raleigh wave which showed the effects of dispersion. The coil aerial was also used for surface studies. This is another interesting response that appears

to be due to an 'S' wave and needs to be investigated further date as it is obviously electro-magnetic in origin. The theory as presented by Pride (1996) will need to re-examined as it is shown in his analysis there is no EK response generated with regard to shear waves. However, papers by (Garamboise S. & Dietrich M. 2001 and 2002) clearly demonstrate electric kinetic responses being generated by 'S' waves

No attempt was made at this stage to tune the coil aerial to the 100 Hz frequency of the seismic source which would have increased its sensitivity. In any future investigations this will be done. As the dipole aerial was more easily deployed and proved to be more successful than the coil aerial in the detection of EK responses and so it was decided to stay with this for the remainder of the EK investigations.

The results of the EK experiments conducted at the Toray Textiles factory Mansfield site were very encouraging indeed, as very clear and well defined EK responses were obtained using the original one metre dipole aerial. A test carried out at the end of the EK investigations at Mansfield with a simple dipole aerial made from two three-metre lengths of standard 15mm copper plumbing tubing proved to be a very successful as a much improved EK signal was obtained amounting to two orders of magnitude.

As a result of this very impressive result, a new improved dipole aerial was designed based on easily available, and low cost, copper plumbing tube. The design incorporated a facility where one metre sections could be screwed into a central boss enabling the dipole aerial length to be adjusted from two metres upwards in steps of two metres. This also made the transportation of it very convenient as it could easily be carried in the average car. The other factor was the very low cost in its construction. The new dipole aerial was used in all of the succeeding investigations, although as a check the original 2 metre dipole aerial was occasionally used in order to compare results.

The EK results for the geotechnical studies conducted at Ospringe were again very successful having achieved good correlations with other geotechnical and geophysical investigations. Of most interest was the EK responses obtained from very shallow depths, < 1 metre. The EK response at water table was also seen, i.e. the EK response at 24 milliseconds figure 4.33 in Chapter 4.

The EK results obtained from the site at Ospringe had a considerable amount of noise

superimposed on the EK recordings. This was thought to be due to a fault in the seismic recorder being used. However, this was removed by the noise removal software developed in this project, as shown on a number of the recording in Chapter 4.

10.2 EK field investigation results.

A summary of all of the EK investigation data are presented below in the order in which they were conducted.

10.2.1 *Mansfield EK investigations*

The results of the EK investigations conducted at the Mansfield site showed that the EK responses obtained were indeed electro-kinetic in origin and not electro-seismic, i.e., where the travelling electric field follows that of the seismic head wave. In addition, this travelling electric field does not radiate independent electromagnetic energy and is only detected on the dipole aerial as the co-seismic wave passes by. However, this travelling electric field does exhibit moveout that matches that of the direct seismic wave.

After careful analysis of the EK data it became clear that fracture zones above the water table, in the right conditions can be detected as well as those below it Chapter 4, section 4.5.5. In addition the water table was successfully identified as well as a small response at 33ms which corresponds to a depth of 24 metres. From the borehole log the geological features are that it is fairly well cemented red sandstone with few pebbles and horizontal fractures due to bedding planes.

10.2.2 *EK field results for Ospringe in Kent*

The EK results obtained from the geotechnical ground investigations at the Ospringe brick earth site in Kent provided a wealth of information on EK responses that were obtained from depths as shallow as 300mm after compaction. These shallow EK data correlated very closely with data obtained from a Dynamic Cone Penetrometer (DCP), together with a number of other techniques. These data were used to confirm the effective depth of the compaction being over the range of 50 to 650 mm.

The compaction data from the DCP was confirmed with the data from a Prema-100 dynamic plate and German dynamic plate tests. A high resolution seismic refraction survey was not only able to resolve details in the 0.1 m range, but correlated very well

with all of the other methods employed, Widess (1973). The depth of the water table was also clearly detected at a depth of 10.7 metres, corresponding to an EK response at 24 milliseconds (see figure 4.36).

The proof that the EK response obtained from the above two sites is truly EK in origin has been clearly demonstrated by the results in Chapter 4, section 4.5 by noting that the first arrival of EK signals from an increasing range of distances from the shot point are all received at the same time, e.g., no EK move out is observed.

For all of these EK investigations shallow seismic refraction surveys were undertaken in order to be able to correlate the EK data with the travel time of the seismic wave down to the water table as an EK response will no be generated until the seismic wave is refracted at the interface of the soil water table interface. It was realised that for future EK investigations the necessity of conducting a seismic survey could be eliminated by noting the fall off of peak amplitude of the EK response with distance, see results table 4.4 and figure 4.5. There is a very clear mathematical dependence of the measured peak dipole electric field versus distance form the source of the dipole electromagnetic variation. Use of this relationship would be employed to determine the depth to the water table.

10.2.3 *The laboratory experimental results.*

The laboratory experiments presented a number of difficulties the first being with the serious ringing of the ultrasonic transducer (see figure 5.8a Chapter 5) this is seen to persist long after the excitation pulse of 3.5 microseconds. Investigating this ringing problem revealed that, in a number of applications, such as flaw testing, this is quite normal as it is the first arrival of the ultrasonic pulse that is important. In most cases this is acceptable. However, for these investigations in order to overcome this ringing problem the length of the specimen was selected to be longer than any flaws along its length, i.e., no flaws close to either end. Another problem encountered was with the recording equipment. The Tecktronix digital phosphor recording oscilloscope was excellent for most of the work however, it was not possible to stack the data. The EK spectrometer was designed to stack at a low repetition rate, i.e. once every five seconds or so. In the time available it was not possible to go back and modify the software to cope with repetition rates of 100 per second. Zhena and Toksöz (2001) stacked their data 128 times. For future laboratory investigations the EK spectrometer will be

modified to do this.

Despite these problems, the data obtained from a sandstone sample, and in particular a fine bedding plane fault within it, (figure 5.6 Chapter 5), were found to give rise to an EK response. The specimen was reversed and similar EK responses were observed once an allowance for the differing travel times was taken into account. The EK arrival times for the normal and reversed specimen correlated very well once an allowance was made for experimental errors. Time was very limited and further investigations with other soil types was not Despite the experimental problems, the results gained were very encouraging and quite clearly point the way forward to conduct further research in this area both theoretical and applied.

As a concluding statement it can be said that the use of EK as a shallow non-invasive ground investigation tool using the new dipole aerial has been successfully demonstrated.

10.3 Recommendations for future research:

10.3.1 *Determination of ground permeability using EK*

The possibility of the determination of ground permeability has been discussed in Chapter 9, section 9.5.1 indicating a clear way forward on how to proceed with this line of research. The determination of permeability using EK is very difficult due to the limited research having taken place in this area. However, having demonstrated the effectiveness of EK in the detection of bedding planes in the laboratory, (see Chapter 5), using the dipole aerial provides a possible way forward to further to investigate the use of EK in achieving this result.

10.3.2 *Investigation of the effects of the double layer in various geological profiles*

The double layer model has been used to describe electro-kinetic phenomena in most geophysical investigations. For some geological profiles this may be appropriate such as in the case of clay or mudstone. However, in the case of sandstone it is wholly inappropriate owing to the grain sizes involved, the typical grain size for fine sand being in the range 0.2 – 0.06 mm. The water grain interface is thus considerably different from that of clay. Even after taking into account the chemical nature of this difference, the effects of cementation between grains where clay could be involved, the differences

between the main clay groups and also the nature of the grain boundary at the interface should be taken into account.

10.3.3 *Creation of an EK ground characterisation database.*

The results in this thesis indicate clear differences in the nature of an EK response in differing geological profiles. The problem of ground characterisation is complex as the differing conditions within a given geological environment have to be taken into account. However, to encourage of the use of EK, a database of EK responses in a range of different geological profiles would be required. This would be an ongoing project requiring the co-operation and collaboration of a number of institutions here in the UK and elsewhere worldwide.

10.3.4 *Measurement of EM moveout with distance from a source*

In the discussion of the results of the EK investigations, Chapter 9, section 9.3.1, it was noted that the EK response should not follow the seismic move out. In reality, there is a small move out associated with the electromagnetic (EM) response, which will be in the nanoseconds range as the EM radiation travels at 3.2 ns per metre. Even at the maximum distance of 24 m used for the EK surveys described in this thesis, this would correspond to a time 78.8 ns or 0.0788 μ-sec, too short to be observed on a normal seismic recording system.

It would be possible to measure this moveout using a modern digital oscilloscope such as the Tektronix TDS3032 digital phosphor oscilloscope or Nicolet Sigma 90-4 digital storage oscilloscope to obtain an estimate on the true velocity of the EK signal and therefore determine the permittivity of the subsurface at EK frequencies.. As part of the investigation careful measurements would be made of the variation of peak EK amplitude with distance. - Two contrasting geological environments such sandstone and a clay environment should be selected for these investigations.

10.4 Concluding remarks

The research into the considerable advantages of the new dipole aerial method for detection of seismically induced electro-kinetic responses has not only demonstrated its advantages over other methods of detection in two differing geological environments but opened up a whole new range of other related geophysical applications such as fault zones and its potential use in contaminated land.

References

Adler, M., Le Mouel, J.L. Zlotnicki, J. 1999. Electrokinetic and magnetic fields generated by flow through a fractured zone: a sensitive study for La Fournaise volcano. Geophysical Research Letters, 26 (6), 795-798.

Alkafeel, S.F. Gochin, R.J. & Smith, A.L. 1999. Surface Potential and Permeability of Rock Cores Under Ashaltenic Oil Flow Conditions. Society of Petroleum Engineers SPE 30539 report, 1-9.

ANSI. 1997 ASCII American Standard Code for Information Interchange Specification for standard set of 128 characters,

Bachrach, R., Dvorkin, J. & Nur, A. M. 2000. Seismic velocities and Poisson's ratio of shallow unconsolidated sands. Geophysics. 65, (2), 559-564.

Bachrach, R & Nur, A. 1998. High-resolution shallow seismic experiments in sand., Part 1: Water table, fluid flow , and saturation. Geophysics, 63, 4, 1225-1233.

Bachrach, R & Nur, 1998. A. High-resolution shallow seismic experiments in sand., Part 11: Velocities in shallow unconsolidated sand. Geophysics, 63, 4, 1234-1240.

Baker G. S, Schmeisser and Steeples D. W. 1999. Seismic reflections fro depths of less than two metres. Geophysical Research Letters 26, (2), 279-282.

Barton, P.G. and Rawlins, A.D. 1998. Acoustic diffraction by a semi-infinite plane with different face impedances. Journal of the Institute of Applied Mathematics. 52 (3), 469-487.

Beamish, D. 2000. Quantative 2D VLF data interpretation. Journal of Applied Physics 45, 33-47.

Beamish, D. & Peart, R.J. 1998. Electrokinetic geophysics. Terra Nova, 10, 48-55.

Beamish, D. 1998. Three-dimensional modelling of VLF data. J. Applied Geophysics, 39, 63-76.

Beamish, D. & Peart, R.J. 1997. Electrokinetic sounding applied to well and borehole siting: an appraisal. British Geological Survey Technical Report WC/97/59

Bendix is the trademark of the Bendix Corporation of America.
Beeson. 1950. The Kobe Porisometer and the use of oil well research. American Institute of Minerals and Met Eng. 189, 313-318.

Biot, M.A. 1962. Generalised theory of acoustic propagation in porous dissipative media. The Journal of the Acoustical Society of America. 34, (9), 1254-1264.

Biot, M.A. 1962, Mechanics of deformation and acoustic propagation in porous media. Journal of Applied Physics. 33, (4), 1482-1498.

Biot, M.A. & Willis, D.G. 1957. The elastic Coefficients of the theory of Consolidation. Journal of Applied Mechanics. 57, 594-601.

Biot, M.A. 1956. Theory of Propagation of elastic waves in a Fluid saturated Porous Solid. II. High-Frequency Range. The Journal of the Acoustical Society of America. 28 (2), 179-191.

Biot, M.A. 1956. Theory of Propagation of elastic waves in a Fluid saturated Porous Solid. I. low-Frequency Range. The Journal of the Acoustical Society of America. 28, (2). 168-178.

Biot, M.A. 1956. General Biot, Solutions of the Equations for Elasticity and Consolidation for a porous Material. Journal of Applied Mechanics. Transactions American Society |Mechanical Engineers. 78, 91-96.

Biot, M.A. 1956. Theory of Deformation of a Porous Viscoelastic Anistropic Solid. Journal of Applied Physics. 27, 459-467.

Biot, M.A. 1955. Theory of Elasticity and Consolidation for a Porous Anisotropic Solid. Journal of Applied Physics. 26, 182-185.

Bockris, J. & Reddy, AKN (1970). Editors. Modern Electrochemistry, Vol. 1. New York: Plenum Press.

Brigham, E. Oren, 1988, The Fast Fourier Transform and Its Applications, Englewood Cliffs, NJ: Prentice-Hall, Inc., 448 pp.

Buckingham E., 1907. Studies on the movement of soil moistures. U.S. Department of Agriculture, Bur. Soils Bullatin 38.

BURR-BROWN corporation is a subsidiary of Texas Instruments.

Butler, K.E., Russell, R.D., Kepic, A.W & Maxwell, M. 1996. Measurement of the seismoelectric response from a shallow boundary. Geophysics, 61, (6), 1769-1778.

Butler, K.E, & Russel, R.D. 1993. Subtraction of power line harmonics from geophysical records, Geophysics. 58, 898-903

Butler, K.E, Flemming, S.W and Russel, R.D. 1999. Field Test for the linearity of Seismoelectric conversion. Canadian Journal of Exploration Geophysicists. 35, 20-33

Callen H. B, & Welton T. A. 1951. Irreversibility and generalised noise, Physics Review. 83, (1), 334-40

Carcione, J.M. & Quiroga-Goode, G. 1995. Some Aspects of the Physics and Numerical Modelling Biot Compressional Waves. Journal of Computational Acoustics. 3, (4), 261-280.

Carnie, S. L., & Tottie, G. M. 1984. The statistical mechanics of the electric double layer, Advances in Chemical Physics. 56, 141-253.

Chandler, R.N. 1981. Transient streaming potentials measurements on fluid saturated structures : an experimental verification of Biot's slow wave in the quasi-static limit. Journal of the Acoustical Society of America. 70, 116-245.

Chapman, L. 1913 " A contribution to the theory of electrocapillarity", Philosophical Magazine. Se.6 25, 148. 475-481

Clark, S. P. 1996. Handbook of Physical Constants. The Geological Society of America, Memoir 97. 197-209

Clarke, R.H., Millar, J. W.A., & Knaggs D. 1999. Electrokinetic soundings at cape hill brewery Birmingham UK. Internal report, 'Groundflow Ltd'. Unpublished. 1-12.

Chandler, R.N. 1981. Flow Permeability Transient Streaming Potential Measurements. Schlumberger-Doll-Research, P.O Box 307 Ridgefield, CT 06877.

Musso, G. 2000. Clay Mineralogy and Double layer in clays. PhD thesis, Polilecnco di Torina. Chapter 3, 19–37.

Chung, H & Lawton, D. C. 1995. Frequency Characteristics Of Seismic Reflections From Thin Beds. Canadian Journal of Exploration Geophysics. 31 1 & 2, 32-37.

Coelho, D, Shapiro, M, Thovert, J. F. &. Adler, P.M. 1996. Electro-osmotic phenomena in porous media, Journal of Colloid and Interface. Science. 181, 169-190.

Computer Boards, inc. 1996. Universal Library Programmers Manual, Revision 3.3V.

Computer Boards, inc. 2001. Distributing 32-bit applications that use Computerboard's Universal Library.

Crampin, S., 1999. Calculable fluid-rock interactions. Journal of the Geological Society, London. 156, 501-514.

Curie, J. and Curie, P. 1880 Developpment par compession de lelectricite polaire dans les cristaux hemiedres a faces inclinees. Bulletin de la Societe Mineralogie de France, 3, 90. Bulletin 4.

Daniels, D. J, 1996. Surface Penetrating Radar. IEE Radar, Sonar Navigation and Avionic series. 19-27

Davis, J.L, & Annan, A.P. 1989. Ground Penetrating Radar for High-Resolution Mapping of soils and Rock Stratigraphy. Geophysical Prospecting. 37, 531-551.

Darcy, H. 1969. "Détermination des lois d'écoulement de l'eau à travers le sable". In The Theory of Ground-Water Motion and Related Papers, by M. K. Hubbert, Hafner Pub. Co., New York. pp. 287-310. (Reprints of three papers with corrections, plus a

facsimile of Darcy's Appendix D in French. This is the ultimate theoretical discussion of Darcy's Law.)

De Jong, M. 1996. Sub-Poissonian shot noise. Physics World, 22-26.

der Ziel, V. 1954 A. *Noise*. Englewood Cliffs, NJ: Prentice-Hall, Inc.

Dekker A., J. 1967. Solid State Physics. MacMillian & Co. 148-154.

Deresiewiez, H. & Rice, J.T. 1964. The effect of boundaries on wave propagation in a liquid filled porous solid versus transmission across a plane interface. Bulletin of the Seismological Society of America. 54(1), 409-416.

Dietrich, M., Garambois, S. & Glangeaud, F. 1996. Seismo-electric effects: A field example over a shallow aquifer, Proc. EEGS. 2nd Annual Meeting, Nantes, France, 82-84.

Dukhin, A.S., and Goetz, P.J. 2001. Acoustic and Electroacoustic Spectroscopy for Characterizing Concentrated Dispersions and Emulsions", Advances in Colloid and Interface Science., 92, 73-132.

Elmofy, S. E., and Shokir, E. M. El-M., 2003. Effect Of Surface Active Agents On Electrokinetic And Wettability Changes of Reservoir Rocks. Emirates Journal for Engineering Research, 8(1), 35-40.

Evans, R.D., Jefferson, I.F., Kumar, R., O'Hara-Dhand, K. and Smalley, I.J. 2004 The nature and early history of airborne dust from North Africa: in particular the Lake Chad basin. Journal of African Earth Sciences. In press

Fitterman D.V. 1978. Electrokinetic and magnetic anomalies associated with dilatant regions in a layered earth. Journal of Geophysical Research. 83, 5923-5928.

Fleming P.R, M.W. Frost and Rogers C.D. 2000. A comparison of devices for measuring stiffness in-situ.. Proceedings of the fifth international Symposium on unbound aggregates. 193-200.

Frenkle, J. 1944. On the theory of seismic and seismoelectric phenomena in a moist soil. Journal of Physics, 8(4), 230-244.

Gao, Y. and Crampin, S. 2004. Temporal variations of shear wave splitting in field and laboratory in China. Proceedings 10th International Workshop on Seismic Anisotropy, Tutzing, 2002. Journal of Applied Geophysics.

Garamboise S. & Dietrich M. 2001. Seismoelectric wave conversions in porous media: Filed measurements and transfer function analysis. Geophysics, (66) 3, 1417-1430.

Garamboise S. & Dietrich M. 2002. Full waveform numerical simulations of Seismoelectromagentic wave conversions in fluid-saturated stratified porous media. Journal of Geophysical Research, (107), B7, 1000-1029.

Gaskill, J. D., 1978, Linear Systems, Fourier Transforms, and Optics, New York: John Wiley & Sons, 554 pp.

Graben, P.B. 2001. Estimating and improving the signal to noise ratio of time series by symbolic dynamics. Physical Review E, 64, 64-78.

Grahame, D.C. 1947. The electrical double layer and the theory of electrocapillarity. Chemical Review. 41, 441-510.

Green R. 1962 The Hidden layer problem. Geophysical Prospecting. 10, 166-177.

Grimshaw, R. & Gottwald, G. 2001. Models for Instability in Geophysical flows. Proceeding of the UUTAM Symposium on Advances in the Mathematical Modelling of the Atmosphere and Ocean Dynamics, Limerick, ed. P.F. Hodnett. Kluwer Dordrecht, 153-160.

Guervich, B., Marschall, R. & Shapiro S.A. 1994. Effect of Fluid Flow On Seismic Reflections from a thin layer in a porous medium. Journal of Seismic Exploration, 3, 125-140.

Guzina, B, B. & Madyarov. 2004. On the spectral analysis of Love waves. University of Minneapolis. Unpublished

Haartsen, M, Matthijis W., Zu Zhenya & Toksoz, M. Naji. 1995 Seismoelectric experimental data and modelling in porous layer models at ultrasonic frequencies. 65th Annual International Meeting Society of Exploration Geophysicists, Exploration Geophysics, 696-699.

Haartsen, M., Dorg, W. & Tolksöz, M.N. 1998. Dynamic streaming currents from seismic point sources in homogeneous poro-elastic media. Geophysical Journal International, 132, (2), 256-274.

Haartsen, M. & Pride, S.R. 1997. Electroseismic waves from point sources in layered media. Journal of Geophysical Research, 102, (B11), 24, 745-769.

Helmholtz, H.L.F., 1879. Studen uber electrische grenzschicten. Ann. Physik. 7, 337-382.

Hillier, A. 1996. EM Electroseismic Survey Modelling and assessment of its potential for petroleum exploration. Imperial College Paper submitted in part fulfilment of the MSc in Petroleum Exploration, 1- 48. Unpublished.

Hipp, J. E., 1974. Soill electromagnetic parameters as functions of frequency, soil density and soil moisture. Proceeding of the IEEE, 62, 98-103.

Hunt, C.W. & Worthington, M. H. 2000. Borehole electrokinetic responses in fracture dominated hydraulically conductive zones. Geophysical Research Letters, (9)27, 1315-1318.

Ishido, T. & Mizutani H. 1981. Experimental and Theoretical Basis of Electrokinetic Phenomena in Rock-Water Systems and its Application to Geophysics. Journal of Geophysical Research, 86, (B3), 1763-1775.

Ivanov, A.G., 1940. The seismoelectric effect of the second kind. Izvestiya Academii Nauk SSSR, seriya geograficheskaya i geofizicheskaya, 4(5), 699-727 (English translation from US Library of Congress).

Ivanov, A.G., 1939. Effects of electrization of earth layers by elastic waves passing through them. Comptes Rendus (Doklady) de l'Academie Sciences de'URSS, 24, (1), 42-45.

Jiang, Y.G, Shan, F.K, Jin H.M & Zhou L.W. 1998. A method for measuring electrokinetic coefficients of porous media and its potential application in hydrocarbon exploration. Journal Geophysical Research. 25, (10), 1581-1584.

Jiracek, G.R. 1990. Near-surface and topographic distortion in electromagnetic induction surveys. Survey Geophysics. 11, 163-203.

Jouniax L. & Pozzi J-P, 1995. Permeabilty dependence on streaming potential in rocks for various fluid flow conductivities. Geophysical Research Letters, 22(4), 485-488.

Joičič, V. & Cooper, M.R. 1997. Stiffness of coarse-grained soils at small strains. Gèotechnique. 47, (3), 545-561.

Keiswetter, D.A. & Steeples, D.W, 1995. A field investigation of source parameters for the sledge hammer. Geophysics, 60, (4), 1051-1057.

Kepic, A, W, Michael Maxwell, M, & Russell, R, D. Field trials of a seismoelectric method for detecting massive sulfides. Geophysics, 60:365-373, 1995.

Keshner, M.S, 1982. "1/f noise". Proceedings of the IEEE. (3)70, 212 – 218.

Lee K.H. & Xie G. 1993. A new approach to imaging with low frequency electromagnetic fields. Geophysics.. 58, (6), 780-796.

Lensky N. and Lyakhvsky V. and Navon O., 2002. Expansion dynamics and volatile-supersaturated liquids and bulk viscosity of bubbly magmas, Journal Fluid Mech. 460, 39-56

Long, L.T. & Rivers, W.R. 1975. Field measurement of electroseismic response. Geophysics, 40, (2), 233-245.

Longhurst, R. S., 1967 Geometrical and Physical Optics. 2nd Edition, Longmans, pp 199-204

Lorne, B., Perrier, F, and Avouc, J-P. 1999. Streaming potential measurements 1. Properties of the electrical double layer from crushed rock samples. Journal of Geophysical Research. 104 (B8), 17,857-17,877.

Lorne, B., Perrier, F, and Avouc, J-P. 1999. Streaming potential measurements 2. Relationship between electrical and hydraulic flow patterns from rock samples during deformation. Journal of Geophysical Research. 104 (B8), 17,879-17,896.

Lorrain, C. and Corson, D. R. 1970. Electromagnetic Fields and Waves. W.H . Freeman and Company. pp 595-635.

Lugwig, J. Rainer, Iutrrino J. G., & Rona A.P. 1998. Seismic velocity-porosity relationship of sulphide, sulphate and basalt samples from the Tag hydrothermal mound. Proceedings of the Ocean Drilling Program, scientific results, vol. 158, pp 313-326.

Liu, Z., Rector, J.W., Nihei, K.T., Tomutsa, Myer, L.R.,L.R. & Nakagawa, S. 2001 Extensional wave attenuation and velocity in partially-saturated sand in the sonic range. Rock Mechanics International Meeting. 1-5

McBride M, B., & Baveye P. 2002 Diffuse Double-Layer Models, Long-Range Forces, and Ordering in Clay Colloids. DIVISION S-2—"Particle interactions in colloidal systems ". Soil Science Society of America Journal 66:1207-1217

McDowell P. W., *et al.* 2002. Geophysics in engineering investigations (C562) ISBN: 0-86017-562-6

McNeil, J.D. 1980. Electrical conductivity of soils of soils and rocks. 1980. 'Geonics Ltd'. Technical note TN-5. Unpublished.

Matthijis, W., Haartzen, Zhenya Zhu, & Toksoz M.N. 1995. Seismoelectric experimental data and modelling in porous layer models at ultrasonic frequencies. 65th Annual International Meeting of the Society of Exploration Geophysicists. 1155-1158

Martner, S.T, & Sparks, N.R.. 1959. The electroseismic effect. Geophysics, 24, 297-308.

Measurement Computing. 2000. User's Manual, Revision 2, for PC-Card, DAS16/16.

Medina L, Moreno E, González G & Leija L. 2003 Circular ultrasonic transducer characterisation: Theoretical and experimental results. Revista Mexicana De Fīsica. 49 511-518.

Mikhailov, O.V, Haartsen M. W & Toksoz, M.N. 1997. Electroseismic Investigation of

the shallow subsurface: Field measurements and numerical modelling. Geophysics. 62, (1), 97-105.

Mikhailov, O.V, and Toksoz, M.N. 1998. Borehole electroseismic measurements in dolomite. Society of Engineering Geologists. Expanded Abstract

Mikhailenko, B.G & Soboleva O.N. 1996. Mathematical modelling of seismomagnetic effects in an elastic medium. Advanced Mathematics: Computations and Applications. 722-730.

Mikhailenko, B.G & Soboleva O.N. 1996. Mathematical modelling of seismomagnetic effects arising in the seismic wave motion in the earth's constant Magnetic field. Applied Mathematical Letters. 10, (3), 47-51.

Miller, J.W.A., & Clark, R.H. 1995. The application of electrokinetic surveying to mining. Report to MIRO members (Ref. IC 110). Unpublished.

Mitchell, J.K. 1993. Fundamentals of Soil Behaviour, 2nd Edition John Wiley & Sons. 116-117.

Mizutani, H.T., Ishido, T., Yokokura, T. & Ohnishi. 1976. Electrokinetic phenomena associated with earthquakes. Geophysical Research Letters. 3, 365-368.

Mooney, H.M. 1974. Some Numerical Solutions for Lamb's Problem. Bulletin of the Seismological Society of America. 64, (2), 473-491.

Moore, J.R, Glaser, S.D & Morrison H.F. 2004. The streaming potential of liquid carbon dioxide in Berea sandstone. Geophysical Research Letters. 31, L17610 1-4.

Morgan F.D, & Pride S. 1989. On the Importance of Electrokinetic forces in the Acoustics of Porous Media. Journal Geophysical Research. 94, 12449-12461

Murty, Y.S. 1985. First results on the direct detection of ground water by seismo-electric effect, a field experiment. Bulletin Australian Society Exploration Geophysicist. 16, 254-255.

Neev, J & Yeats, E.R. 1989. Electrokinetic effects in fluid-saturated poroelastic media. Physical Review B, 40, (13), 9135-9141.

Northmore KJ, Jefferson I, Jackson P. D, Entwisle D. C, Milodowski A. E, Raines M. R, Gunn D. A, Boardman D. I, Zourmpakis A, Nelder L. M, Rogers C. D. F, Dixon N,

Nourbrechect B. 1963. Irreversible thermodynamic effects in inhomgenous media and their applications in certain geological problems. PhD thesis, Massachusetts Institute of Technology (MIT). Cambridge, MA. Unpublished

Smalley I. J, Karri R. S, Rouaiguia A & Derbyshire E. (2004). On-Site Characterisation of Loessic Brickearth Deposits at Ospringe, Kent, UK. Geotechnical Engineering, Proceedings on the Institution of Civil Engineers. (Submitted for review)

Nyquist, H. 1928 Certain topics in telegraph transmission theory, Trans. AIEE, (47), 617-644.

Oberbeek, J. Th.G. 1952. Electrochemistry of the double layer. Colloid Science, Vol. 1, Irreversible Systems, Ed. H.R. Kruyt, Elservier, New York, 115-193.

O'Hara-Dhand K. A., Neep J. P., Sams M. S., & Worthington M. H. 1996. Measurement of seismic attenuation from high-resolution crosshole data. Geophysics 61, (4), 1175-1188.

O'Hara-Dhand, K.A & Evans, R. 2001. Report on Geophysical and Geotechnical Investigations at Ospringe Brickearth Quarry. Nottingham Trent University, School of Property and Construction. Working paper. GH-01-01. 1-36. Unpublished.

Parkhomenko E.I. & Gaskarov I.V. 1971. Borehole and laboratory studies of the seismoelectric effect of the second kind in rocks. Izv. Earth Physics. 9, 88-92.

Patella, D. 1997 Introduction to ground surface self-potential tomography. Geophysical Prospecting 45, (4), 653-681. 65-2478.

Pride, S.R. & Morgan, F.D. 1991. Electrokinetic dissipation induced by seismic waves. Geophysics. 54, (7), 916-923.

Pride, S. 1994. Governing equations for the coupled electromagnetics and acoustics of porous media. Physical Review. B. 50(21), 678-694

Pride, S.R. & Haartsen, M.W. 1996. Electroseismic wave properties. Journal Acoustical Society of America. 100, 1301-1315.

Proakis, J. G., & Manolakis, D. G. Digital Signal Processing: Principles, Algorithms and Applications. Upper Saddle River, NJ: Prentice Hall.

Pullan, S.E., 1990. Recommended Standard for seismic and radar data files in the personal computer environment. Geophysics, 58, (9), 1260-1271.

Reuss, F.F. (1809), "Sur un nouvel effet de l'électricité glavanique." Mémoires de la Societé Impériale des Naturalistes de Moscou, Vol. 2, 327-337.

Revil, A., Darot, M. & Pezard, P.A. 1996. From surface electrical properties to spontaneous potentials in porous media. Surveys in Geophysics. 17, 331-346.

Revil, A., Darot, M. & Pezard, P.A. 1996. Influence of the electrical diffuse layer and microgeology on the effective ionic diffusion coefficients in porous media. Geophysical Research Letters. 23, (15), 1989-1992

Russel, R.D, Butler, K.E, Kepic, A.W. & Maxwell, M., 1997. Seismoelectric exploration. The Leading Edge. Nov. 1611-1615.

Shapiro, S.A., Audigane, P., Royer, J., & Fehler, M. 1999. Large-scale in situ permeability tensor of rocks from induced seismicity. Geophysical Journal International. (137), 207-213

Shapiro, S.A., Audigane, P., Royer, J, and Fehler, M. 1999. An inversion for the permeability tensor by using seismic emission. Society of Engineering Geophysicists-Annual Meeting Abstracts 1783-1786.

Smoluchowski, M. 1914. In: L. Graetz (Ed.) *Handbuch der Elektrizitat und Magnetismus*. 2, J.A. Barth, Leipzig.

Soske J. L. 1959 The Blind Zone Problem in Engineering Geophysics. Geophysics 24, 359-365.

Spunt E.S, Mercer T.B. & Djabbarah N.F. 1994. Streaming potential from multiphase flow. Geophysics 59, (5), 707-711

Statham and Blau (1935), Internal memo, of the Humble Oil Company.

Stern, O. 1924. Zur Theorie der Elecktrolischen Doppelschicht, Z. Electrchem., 30, 508.

Suslov, S. K, 2001. An Introduction to Basic Fourier Series. Department of Mathematics and Statistics, Arizona State University Tempe, AZ 85287-1804 USA, Kluwer Academic Publishers Dordrecht, Boston, London Developments in Mathematicss. Vol. 9. Chapters 1, 2 & 3.

Thompson, A.H. & Gist, G.A. 1993. Geophysical applications of electrokinetic conversion. The Leading Edge. Dec, 1169-1173.

Thompson, R.R., 1936. The seismoelectric effect. Geophysics, 1, 327-335.

TI INA118 data sheet. SC Design Center and SC, S&C, E&PS, Digital Imaging Sales Texas Instruments Limited 800 Pavilion Drive Northampton Business Drive Northampton NN4 7YL United Kingdom. Phone: +44 1 604 66 30 00

Tuekolsky, S.A., Vettering, W.T. & Fannery, B.P. 1992. Sample section from Numerical Recipes in C: The Art of Scientific Computing 2nd Ed. Chapter 13. Cambridge University Press.

Volarovich M.P. & Parkhomenko E.I. 1959 Modelling the connection between seismic phenomena and disturbances in the electric field of rocks due to the piezoelectric effect, Bull. (Izv.) Acad. Sci., USSR, Geophys. Ser. and pp.90-92,

Volarovich M.P., Sobolev G.A. & Parkhomenko E.I. 1962. The piezoelectric effect in pegmatite and quart veins, Bull. (Izv.) Acad. Sci., USSR, Geophys. Ser. and pp.103-107,

Walker, D.W. 2000. Experimental Evidence of Near-field Superluminally Propagating Electromagnetic fields. Royal Institute Of Technology, KTH_Visby. Department of Electrical Engineering. 1-17.

Walker, D.W. 2000. Experimental Evidence of Near-field Superluminally Propagating Electromagnetic fields. Royal Institute Of Technology, KTH_Visby. Department of Electrical Engineering. 1-17.

Wang, Y. & Guo, J. 2004 Modified Kolsky model for seismic attenuation and dispersion. Journal of Geophysics and Engineering. 1, 187-196.

Welch, P.D. 1967. The Use of the Fast Fourier Transform for the Estimation of Power Spectra: A Method Based on the Time averaging Over Short, Modified Periodograms. IEEE Transactions. Audio Electroacoustics. AU-15, 70-73.

Wemp, W, & Mavko, M. 2001. Three distinct porosity domains defined physically, hydraulically, electrically and elastically. The Leading Edge. (Feb), 198-199.

White, P.A. 1994. Electrode arrays for measuring ground water flow direction and velocity. Geophysics. 59, (2), 192-201.

Widess, M. B 1973. How thin is a thin bed. 1973. Geophysics 38, 6, 1176-1180.

Willink, R. 2001. An integral inequality bounding the autocorrelation function of a pulse or sequence at a known Lag. Journal of Inequalities in Pure and Applied Mathematics. 3, (1), 1-21

Wolfe, P.J, Yu, J. & Gerhenzon, N. 1996. Seismoelectric studies in an outwash plain. Dept. of Physics and Geological Sciences. Wright State University, Dayton OH 45435. Symposium on the Applications of Geophysics to Engineering & Environmental problems. 21-30.

Wurnstich, B. & Morgan, F.D. 1994. Modelling of streaming potentials caused by oil well pumping. Geophysics. 59, (1), 46-56.

Yoshida, S., Clint, O.C., & Sammonds, P.R. 1998. Electric potential changes prior to shear fracture in dry and saturated rock. Geophysical Research Letters. **25**(10), 1577-1580.

Zlotnicki, J & Le Moul, J.L. 1990. Possible electrokinetic origin of large magnetic variations at La Fournaise volcano. Nature, 343, 633-635.

Zhena, Z, and Toksö, M. N. 2002. Crosshole Seismoelectric Measurements in Borehole Models with Fractures. Geophysics. 68, (5), 1519-1524.

Appendix A

Outline specification for EK Spectrometer (20th November 2000)

This specification was prepared as a reminder of the main features to be built into the design

1) The spectrometer will be based on a ruggedised laptop computer with a Pentium 500MHz processor, 6.4 G-byte hard disk and 128 m-byte of ram.

   (a) To have a PCMCIA type 2 slot, two serial ports, one USB port and a one parallel port.

   (b) To have the ability to fit a standard modem card.

2) Software to be based on HPVEE 6.0 with embedded 'C' code programmes.

3) The spectrometer is to have 16 differential input channels each with a bandwidth of 0 to 2 kHz. The input noise to be less than 0.1 micro-volt rms.

4) A 16-bit, 16 channel, a-d converter with a conversation rate of 100KHz will be employed; this will give an effective sampling rate of 6.6 kHz per channel. It has a software programmable gain of 1x, 2x, 4x and 8x, allowing an input voltage range of 1.25, 2.5, 5 and 10. At the most sensitive setting it has an input resolution of 19μ-volt. An input buffer amplifier, see (7) below, will enhance the input sensitivity. At the gain setting of X64 on the preamplifier there is a dynamic range of 133 db. With an input amplifier of times 16, 32 or 64 an input signal voltage of (1.2, 0.6 or 0.3) μ-volt can be resolved. The detection level can be further enhanced by the stacking technique as outlined in (13) below.

5) Input signal sample rate to be 0.125ms, 0.25ms, 0.5 or 1ms per channel.

6) Total number of samples 1024, 2048, 4096 and 8192, therefore at the maximum 8192 samples memory needed for all 16 traces is 128K plus space for header information. The timing for this will need to be done within the laptop. However there is a 16 bit counter within the PCMIA card which can be set to count down

for the above intervals. The computer can be doing other things while the conversion process is taking place.

7) Additionally one other feature to be incorporated is the ability to select on channel only and extend the recording time to 16 x 8196 x sampling rate, e.g. at a sample rate of 0.125 ms total recording time would be 16 x 8196 x 0.000125 = 16.392 seconds.

8) To achieve the low input noise a differential buffer amplifier will precede each channel. It will have prefixed gains of x16, X32 and x64. Noise of input amplifier 4.2 nv/√Hz. All gain defining resistors to be 1% low noise metal film. Buffer amplifier module to fit onto base of laptop and to be self- powered, total power drain 6ma. Power supplied by four non-rechargeable AA Ultra Duracell batteries which will give an estimated operating life of 268 hours or 33 days assuming an eight hour day.

9) Each channel's gain to be independently adjustable.

10) Noise monitor to show all channels as this can be useful to detect a faulty channel. Channels may or may not have a transducer attached.

11) Each channel to be independently selectable via the software, i.e., if say only channels 1 to 3 required then channels 4 to 16 can be switched off.

12) External or internal trigger to be software selectable, internal trigger used for noise monitoring purposes only. Manual selection of seismic hammer or geophone trigger.

13) Post trigger delays of 1, 2, 4, 8, 16, 32, 64 and 128 milliseconds.

14) A trace stacking facility must be incorporated, that is the first conversion must be added to the second and so on until the requisite number of data stacks are achieved, maximum 144. It is not necessary to save each individual trace. A noise removal facility must be incorporated based on the 1993 Butler and

Russell paper. The original data must be retained after this process has been applied.

15) Digital low and high pass filtering to be available. Low pass up to 2 kHz and high pass with a similar range. Steps to be decided. A fixed 50 or 60 Hz notch filter to be incorporated for mainly seismic applications. To be applied after the raw data has been recorded. Original traces to be preserved.

16) Results to be displayed on the screen as 16 channels or what ones have been selected with the gain per channel and channel numbers identified.

(a) To have a fill option on positive going peaks.
(b) To be able to display output as voltage or geophone response.

17) All data to be saved in SEGII format. Based on 1990 Pullen paper (1993).

18) Data to be down loaded to a 3.5" high density floppy disc in SEGII format.

19) A parallel port to be available in order to connect a portable battery driven printer.
(a) USB port to be fitted as an option

20) Ruggedised laptop computer to have a battery back up to run from an external 12 volt battery, e.g. sealed lead acid 12 volt 7 ampere hour, also to have a car cigarette lighter power point adapter. Unit must have at least 8 hours operating life in the field. Suitable battery 'Radiospares' Yuasa order code 597-835.

21) To triggered externally either by relay contact closure or on the leading or trailing edge of an electronic or geophone pulse. The trigger pulse to have a maximum amplitude of 5 volts and minimum of 0.5 volts, except in the case of noise monitoring where it will be placed in the continuous sample mode. Trigger input must be protected against high voltage transients, up to five kilovolts, by use of a 5 kv opto-isolator built into the pre-amplifier unit. Input connector to be 'Bendix' 3 pin female PT06A-8-3P(SR). To have cable adapters available to match the connectors on other systems seismic hammers.

22) 10% pre-trigger information to be available.

23) To have a geophone input facility, using two 'Amphenol' NK27 fixed plugs and a software facility for determining slope data from the seismic trace first arrival data. This may include manual selection of the appropriate first arrivals. To have a cursor trackable across the screen trace in order to check on the timing of the first arrival.

24) Desirable features :-

a) To have a GPS input

b) To have a mobile phone link for transmission of data back to base

The above specifications are provisional and may be subject to change

References.

Butler, K.E., Russel, R.D., 1993. Subtraction of power line harmonics from geophysical records, Geophysics (58), 898-903.

Pullan, S.E., 1990. Recommended Standard for seismic and radar data files in the personal computer environment. Geophysics, 58(9), 1260-1271

Revision 1 08-07-01.

Revision 2 24-05-02

Revision 3 19-05-05

KOHD.

Appendix B

Details taken form Measurement Computing Corporation's

data sheet for the PC-Card-DAS 16/16.

Analogue input section

A/D type	AD976A
Resolution	16 bits
Number of channels	16 single ended or 8 differential, software selectable
Input ranges	± 10v, ± 5v, ± 2.5v, ± 1.25 v, fully programmable
A/D pacing	Programmable: Internal counter 82C54
"	External source: A/D external pacer
"	Software polled
External A/D clock	Programmable for rising or falling edge
A/D trigger sources	External gate or edge trigger (A/D external trigger programmable
A/D trigger modes	Rising or falling edge trigger (software programmable) or high or low level gate (software programmable)
Burst mode	Software selectable option burst rate = 100KHz
Data Transfer	From 4 K sample FIFO via REPINSW, interrupt or software polled
A/D conversion time	5µs max
Calibrated throughput	200KHz single channel, 100 KHz multiple channel. Minimum system requirement is Pentium II, 400MHz.
Calibration	Auto calibration, calibration factors for each range being stored on board in non-volatile ram

Accuracy absolute

Range	Absolute accuracy
± 10.00v	± 5.0 LSB Max
± 5.000v	± 5.0 LSB Max
± 2.500v	± 5.0 LSB Max
± 1.250v	± 5.0 LSB Max

Accuracy typical

Range	Typical accuracy
± 10.00v	± 4.5 LSB Max
± 5.000v	± 4.5 LSB Max
± 2.500v	± 4.5 LSB Max
± 1.250v	± 4.5 LSB Max

Power consumption

PC-CARD-DAS 16/16	130 ma typical, 150 ma max.

Accuracy - components

Range	Gain error (LSB)		Offset error (LSB)		DLE (LSB)		ILE (LSB)	
	Max	Typ	Max	Typ	Max	Typ	Max	Typ
± 10.00v	± 3.0	± 2	± 1.5	± 0.5	± 1	± 0.5	± 2	± 1.5
± 5.000v	± 3.0	± 2	± 1.5	± 0.5	± 1	± 0.5	± 2	± 1.5
± 2.500v	± 3.0	± 2	± 1.5	± 0.5	± 1	± 0.5	± 2	± 1.5
± 1.250v	± 3.0	± 2	± 1.5	± 0.5	± 1	± 0.5	± 2	± 1.5

Each card is tested at the factory to assure the boards overall error does not exceed ± 5.0 LSB.

Total board error is a combination of Gain, Offset, Differential Linearity Error (DLE) and Integral Linearity Error (ILE). The theoretical worst case error of the board may be calculated by summing these component errors.

Typical accuracy is derived directly from the various component typical errors. This typical, maximum error calculation for the

Analogue Input Full-scale Gain Drift	± 0.60 LSB/°C max
Analogue Input Zero drift	± 0.15 LSB/°C max
Analogue Input Full-scale Gain Drift	± 0.75 LSB/°C max
Common mode range	± 10v min
CMRR @ 60Hz	- 76db min
Input leakage current	± 20 na max
Input impedance	10 M ohms min
Absolute maximum input voltage	± 55/ -40v. (Fault protected via input MUX)

Noise performance

Noise distribution is determined by gathering 50K samples with inputs tied to ground at the user's connector. Specification refers to both Single-Ended and Differential modes of operation. Input noise is assumed to be Guassian. An RMS noise value from a Guassian distribution is calculated by dividing the peak-to peak bit spread by 6.6.

Noise performance, all ranges	Typical	Maximum
	1.8 LSB RMS	4.7 LSB RMS

Digital Input / output

Digital type	FPGA
PC-CARD-DAS 16/16	Output port of four bits. Programmable as 4 inputs or 4 outputs
Low input voltage	0.8 v max
Input high voltage	2.ov min
Output low voltage (IOL = 4mA)	0.32v max
Output high voltage (IOH +)	3.86v min
Absolute maximum input	- 0.5v, + 5.5v
Power-up / reset state	Input mode (high impedance)
Interrupts	Programmable levels: Levels 2 to 15
Interrupt enable	Programmable
Interrupt source	External (External Interrupt)
"	A/D End of channelscan
"	A/D FIFO not empty
"	A/D FIFO-half full
"	A/D Pacer

Counter section

Counter type	82C54
Configuration	3 down counters, 16 bits each
Counter 1 – User counter	Source: Programmable external (Ctrl Clk) or 100 Hz source
	Gate: Available at connector (Ctrl Gate) pulled to logic high via a 10K resistor
	Output: Available at connector (Ctrl Out)
Counter 2 – ADC Pacer lower divider	Source: Programmable, 1MHz or 10 MHz
	Gate: Available at connector (A/D Pacer) pulled to logic high via a 10K resistor
	Output: Chained to counter 3 clock
Counter 3 - ADC Pacer Upper divider	Source: Counter 2 output
	Gate Internal
	Output: Programmable as ADC Pacer clock. Avai;able at user's connector (ADC Pacer)
Clock input frequency	10 MHz max
High pulse width (Clock input)	30 ns min
Low pulse width (clock input)	50 ns min
Gate width high	50 ns min
Gate width low	50 ns min
Output low voltage	0.8v min
Output high voltage	2.0v min
Output low voltage	0.4v max
Output high voltage	3.0v min
Crystal oscillator frequency	10 MHz
Frequency accuracy	50ppm

Miscellaneous

+ 5 Volts DC	Available at I\O connector (+5.0 v power).
	Protected by resettable fuse : Hold current 350maA max @ 20°C still air
	Trip current700mA min. @ 20°C still air
	Trip and Recovery time : 100 ms max
	On Resistance 1.3 ohms max

Environmental

Operating temperature range	0 to 70°C
Storage temperature range	- 40 to 100°C
Humidity	0 to 95% non-condensing

Appendix B

Details taken form Measurement Computing Corporation's

data sheet for the PC-Card-DAS 16/16.

Analogue input section

A/D type	AD976A
Resolution	16 bits
Number of channels	16 single ended or 8 differential, software selectable
Input ranges	± 10v, ± 5v, ± 2.5v, ± 1.25 v, fully programmable
A/D pacing	Programmable: Internal counter 82C54
"	External source: A/D external pacer
"	Software polled
External A/D clock	Programmable for rising or falling edge
A/D trigger sources	External gate or edge trigger (A/D external trigger programmable
A/D trigger modes	Rising or falling edge trigger (software programmable) or high or low level gate (software programmable)
Burst mode	Software selectable option burst rate = 100KHz
Data Transfer	From 4 K sample FIFO via REPINSW, interrupt or software polled
A/D conversion time	5µs max
Calibrated throughput	200KHz single channel, 100 KHz multiple channel. Minimum system requirement is Pentium II, 400MHz.
Calibration	Auto calibration, calibration factors for each range being stored on board in non-volatile ram

Accuracy absolute

Range	Absolute accuracy
± 10.00v	± 5.0 LSB Max
± 5.000v	± 5.0 LSB Max
± 2.500v	± 5.0 LSB Max
± 1.250v	± 5.0 LSB Max

Accuracy typical

Range	Typical accuracy
± 10.00v	± 4.5 LSB Max
± 5.000v	± 4.5 LSB Max
± 2.500v	± 4.5 LSB Max
± 1.250v	± 4.5 LSB Max

Power consumption

PC-CARD-DAS 16/16	130 ma typical, 150 ma max.

Accuracy - components

Range	Gain error (LSB)		Offset error (LSB)		DLE (LSB)		ILE (LSB)	
	Max	Typ	Max	Typ	Max	Typ	Max	Typ
± 10.00v	± 3.0	± 2	± 1.5	± 0.5	± 1	± 0.5	± 2	± 1.5
± 5.000v	± 3.0	± 2	± 1.5	± 0.5	± 1	± 0.5	± 2	± 1.5
± 2.500v	± 3.0	± 2	± 1.5	± 0.5	± 1	± 0.5	± 2	± 1.5
± 1.250v	± 3.0	± 2	± 1.5	± 0.5	± 1	± 0.5	± 2	± 1.5

Each card is tested at the factory to assure the boards overall error does not exceed ± 5.0 LSB.

Total board error is a combination of Gain, Offset, Differential Linearity Error (DLE) and Integral Linearity Error (ILE). The theoretical worst case error of the board may be calculated by summing these component errors.

Typical accuracy is derived directly from the various component typical errors. This typical, maximum error calculation for the

Analogue Input Full-scale Gain Drift	± 0.60 LSB/°C max
Analogue Input Zero drift	± 0.15 LSB/°C max
Analogue Input Full-scale Gain Drift	± 0.75 LSB/°C max
Common mode range	± 10v min
CMRR @ 60Hz	- 76db min
Input leakage current	± 20 na max
Input impedance	10 M ohms min
Absolute maximum input voltage	± 55/ -40v. (Fault protected via input MUX)

Noise performance

Noise distribution is determined by gathering 50K samples with inputs tied to ground at the user's connector. Specification refers to both Single-Ended and Differential modes of operation. Input noise is assumed to be Guassian. An RMS noise value from a Guassian distribution is calculated by dividing the peak-to peak bit spread by 6.6.

Noise performance, all ranges	Typical	Maximum
	1.8 LSB RMS	4.7 LSB RMS

Digital Input / output

Digital type	FPGA
PC-CARD-DAS 16/16	Output port of four bits. Programmable as 4 inputs or 4 outputs
Low input voltage	0.8 v max
Input high voltage	2.ov min
Output low voltage (IOL = 4mA)	0.32v max
Output high voltage (IOH +)	3.86v min
Absolute maximum input	- 0.5v, + 5.5v
Power-up / reset state	Input mode (high impedance)
Interrupts	Programmable levels: Levels 2 to 15
Interrupt enable	Programmable
Interrupt source	External (External Interrupt)
"	A/D End of channelscan
"	A/D FIFO not empty
"	A/D FIFO-half full
"	A/D Pacer

Counter section

Counter type	82C54
Configuration	3 down counters, 16 bits each
Counter 1 – User counter	Source: Programmable external (Ctrl Clk) or 100 Hz source
	Gate: Available at connector (Ctrl Gate) pulled to logic high via a 10K resistor
	Output: Available at connector (Ctrl Out)
Counter 2 – ADC Pacer lower divider	Source: Programmable, 1MHz or 10 MHz
	Gate: Available at connector (A/D Pacer) pulled to logic high via a 10K resistor
	Output: Chained to counter 3 clock
Counter 3 - ADC Pacer Upper divider	Source: Counter 2 output
	Gate Internal
	Output: Programmable as ADC Pacer clock. Avai;able at user's connector (ADC Pacer)
Clock input frequency	10 MHz max
High pulse width (Clock input)	30 ns min
Low pulse width (clock input)	50 ns min
Gate width high	50 ns min
Gate width low	50 ns min
Output low voltage	0.8v min
Output high voltage	2.0v min
Output low voltage	0.4v max
Output high voltage	3.0v min
Crystal oscillator frequency	10 MHz
Frequency accuracy	50ppm

Miscellaneous

+ 5 Volts DC	Available at I\O connector (+5.0 v power).
	Protected by resettable fuse : Hold current 350maA max @ 20°C still air
	Trip current700mA min. @ 20°C still air
	Trip and Recovery time : 100 ms max
	On Resistance 1.3 ohms max

Environmental

Operating temperature range	0 to 70°C
Storage temperature range	- 40 to 100°C
Humidity	0 to 95% non-condensing

Appendix C

Table E1. Pre-amplifier parts list. Refer to Chapter 6 sections 6.2 and 6.3

Ref	Q'ty	Stock No	Description	Supplier	Price (£)
1	1	121-882	Diecast box (167 x 191 x 76) mm	R/S	21.00
2	1	482-226	Box header 50 way	R/S	2.38
3	6	220-4355	PC screw connector	R/S	6.00
4	1	434-352	Printed circuit development board	R/S	23.12
5	2	543-973	PC card guides	R/S	1.75
6	1	352-187	Miniature switch shaft assembly	R/S	4.54
7	4	352-222	4 pole 3 way switch wafers	R/S	11.92
8	1 box	352-226	Screens	R/S	0.84
9	1 box	352-272	Spacers	R/S	0.74
10	1	318-648	Toggle switch DPDT	R/S	2.24
11	1	321-228	Toggle switch waterproof cover	R/S	1.38
12	2 pks	166-2750	0.25 w metal film resistors 7k15	R/S	5.00
13	2 pks	166-2570	0.25 w metal film resistors 3k33	R/S	5.00
14	2 pks	166-2384	0.25 w metal film resistors 1k54	R/S	5.00
15	4 pks	164-435	0.125 w metal film resistors 20k0	R/S	2.12
16	1 pk	144-245	0.125 w metal film resistors 1k0	R/S	0.53
17	1 pk	144-324	0.125 w metal film resistors 4k7	R/S	0.53
18	1 pk	144-431	0.125 w metal film resistors 39k0	R/S	0.53
19	16	182-8534	IN118 Instrumentation amplifier	R/S	74.40
20	20	447-308	8 Pin DIL gold plated sockets	R/S	12.80
21	2	507-523	AA battery holder	R/S	5.50
22	2	293-533	BC108 Si npn transistor	R/S	0.55
23	1 pkt	271-606	IN4148 Si diode	R/S	0.08
24	1 pkt	180-1573	Tantalum capacitor 10µf 16 volt	R/S	3.10
25	1 bag	560-596	Superdrive Panhead zinc plated screw	R/S	1.08
26	1 bag	530-52	Aerotight stiff nuts M6	R/S	8.21
27	2	NK27C	Cannon 27 way Fixed sockets	GM	150
28	1	PT06A-8-3P	Bendix 3 pin fixed socket	GM	30
				Total	200.34

Appendix D

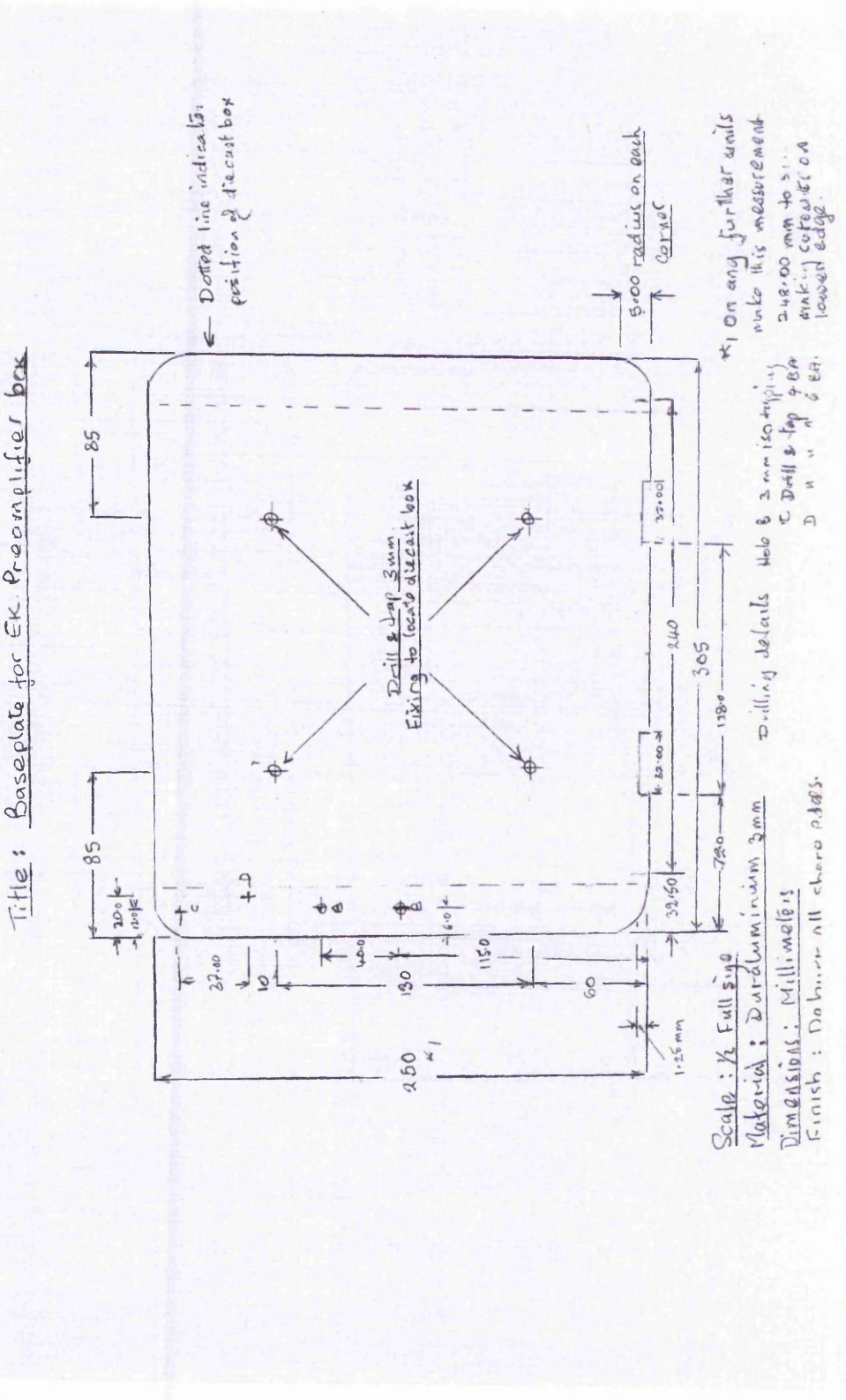

Figure D1 Base plate for EK Preamplifier box.

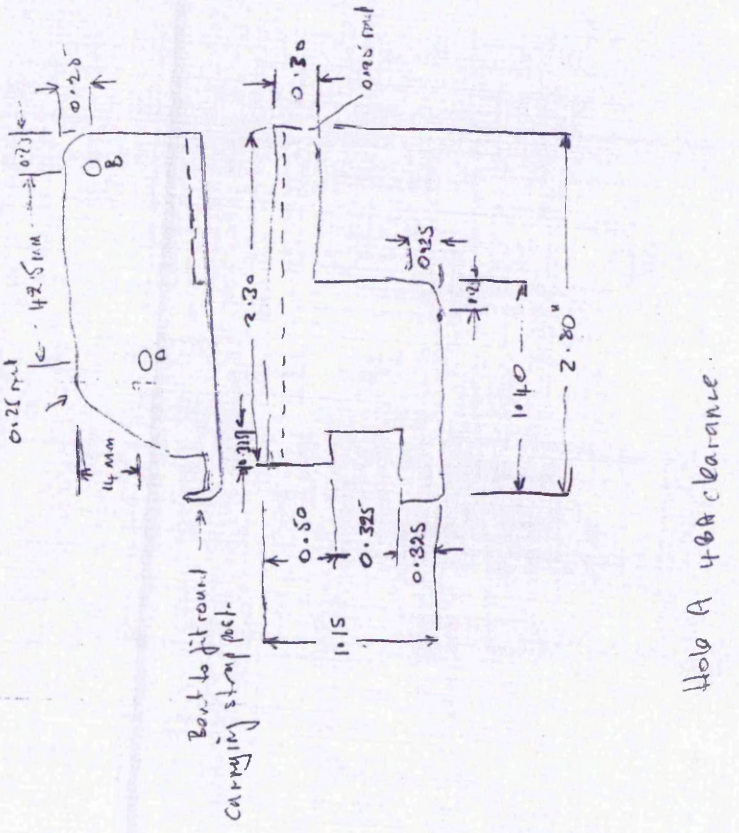

Figure D2. Quick release clip for EK base plate

Appendix E

Wiring for PCMIA DAS 16\16 interconnecting cable							
HD connector		IDC connector		HD connector		IDC connector	
		Row pin No.				Row pin No.	
Pin	Function	A	B	Pin	Function	A	B
1	AGND	1		26	DGND		13
2	CH0 IN		1	27	DIO0	14	
3	CH8 IN	2		28	DIO1		14
4	CH1 IN		2	29	DIO2	15	
5	CH9 IN	3		30	DIO3		15
6	CH2 IN		3	31	DIO4	16	
7	CH10 IN	4		32	DIO5		16
8	CH3 IN		4	33	DIO6	17	
9	CH11 IN	5		34	DIO7		17
10	CH4 IN		5	35	NC	18	
11	CH12 IN	6		36	NC		18
12	CH5 IN		6	37	NC	19	
13	CH13 IN	7		38	NC		19
14	CH6 IN		7	39	CTR1 Clock	20	
15	CH14 IN	8		40	CTR1 Gate		20
16	CH7 IN		8	41	CTR1 Out	21	
17	CH15 IN	9		42	A/D ext pacer		21
18	CH8 IN		9	43	Ext. Interrupt	22	
19	NC	10		44	A/D pacer gate		22
20	NC		10	45	A/D ext. Trigger	23	
21	NC	11		46	NC		23
22	NC		11	47	A/D pacer out	24	
23	NC	12		48	+ V Power		24
24	NC		12	49	NC	25	
25	NC	13		50	DGND		25

Appendix F

Ospringe Geotechnical Data (Oct (2002)
Seismic survey data

File	Channels	Aerial	Notes
1188	1-13	1.0m	Line 1, vertical geophones. 4 Metre 22mm dipole aerial
1189	1-9 & 13	1.0m	Ch. 3 not working and only 8 good geophones, aerial ch. 13 gain70
1190	1-13	1.4m	Channels 1-12 not switched off
1191	"	"	Geophones 11 to 24 metres. 6 metre dipole aerial
1192	"	"	Noise
1193	"	"	Shear phones at 13 m from plate
1194	"	"	Noise
1195	1-9 & 13	3.0m	Shear phones at 13 meters from plate
1196	1-9 & 13	3.0m	Duplication of 1195
1197	1-9 & 13	3.0m	Noise recording
1198	13	4.0m	Aerial only, all other channels switched out
1199	"	5.0m	Aerial only Ch1.
1200	"	5.0m	Duplication of file
1201	"	6.0m	Aerial only Ch1.
1202	"	7.0m	Aerial only Ch1.
1203	"	7.0m	Noise recording
1204	"	8.0m	Aerial only Ch1.
1205	"	9.0m	Aerial only Ch1.
1206	"	9.0m	Noise recording
1207	"	10.0m	Aerial only Ch1.
1208	"	11.0m	Aerial only Ch1.
1209	"	11.0m	Noise recording
1210	"	12.0m	Aerial only Ch1.
1211	"	13.0m	Aerial only Ch1.
1212	"	13.0m	Noise recording
1213	"	14.0m	Aerial only Ch1.
1214	"	15.0m	Aerial only Ch1.
1215	"	15.0m	Noise recording
1216	"	16.0m	Aerial only Ch1.
1217	"	17.0m	Aerial only Ch1.
1218	"	17.0m	Noise recording
1219	"	18.0m	Aerial only Ch1.
1220	"	19.0m	Aerial only Ch1.
1221	"	19.0m	Noise recording
1222	"	20.0m	Aerial only Ch1.
1223	"	21.0m	Aerial only Ch1.
1224	"	21.0m	Noise recording
1225	"	22.0m	Aerial only Ch1.
1226	"	23.0m	Aerial only Ch1.
1227	"	23.0m	Noise recording
1228	"	24.0m	Aerial only Ch1.
1229	"	25.0m	Aerial only Ch1.
1230			No data
1231	1-13	1.0m	Line 2 CH7 no Geophone because of large puddle 1st Geophone at 2m
1232	1-13	2.0m	1st Geophone at 12 m from plate
1233	1-13	3.0m	Shear phones 14-25m from shot point
1234	2-7 & 9-14	4.0m	Line 2 shear phones gap at 7-9m to miss puddle
1235			No data
1236	1-13	1.0m	Aerial to north side of plate ~ 1metre
1237	1-13	2.0m	Shear phone 2-12 m
1238	1-13	3.0m	Vertical geophones at 10-17m

$
Filename..... west-east.pkv
Client code.....
Project number..... ospringe
Name of client..... ntu
Date..... 11 Oct 2001
Prima 100 SN..... S/N-0107201-ORC-0014
Load plate radius (mm). 150
R(1) Radial offset (cm)..... 0

£
Point..... 1
Pavement description... brickearth
Remarks..... pre-compaction
Temperature..... 17

Time (HMS)	Force (kN)	Press (kPa)	Pulse (ms)	D(1) (µm)	E(1) (MPa)
09:24:49	8.69	123	16.8	1399	23.14
09:25:03	8.66	122.5	17	1102	29.26
09:25:07	7.78	110	18.3	965	30.02
09:25:10	6.82	96.5	20.4	934	27.2

£
Point..... 2
Pavement description... brickearth
Remarks..... pre-compaction
Temperature..... 17

Time (HMS)	Force (kN)	Press (kPa)	Pulse (ms)	D(1) (µm)	E(1) (MPa)
09:26:21	8.76	123.9	16.6	6195	5.26
09:26:24	9.13	129.2	16.5	1404	24.21
09:26:28	8.59	121.5	16.5	1208	26.47
09:26:31	8.33	117.9	16.4	1118	27.75

£
Point..... 3
Pavement description... brickearth
Remarks..... pre-compaction
Temperature..... 17

Time (HMS)	Force (kN)	Press (kPa)	Pulse (ms)	D(1) (µm)	E(1) (MPa)
09:26:53	8.52	120.5	16.5	922	34.39
09:26:56	6.78	95.9	15.3	732	34.47
09:26:59	6.94	98.2	15.8	726	35.61

09:27:03	6.6	93.4	15.1	725	33.93

£
Point..... 4
Pavement description... brickearth
Remarks..... pre-compaction
Temperature..... 17

Time (HMS)	Force (kN)	Press (kPa)	Pulse (ms)	D(1) (µm)	E(1) (MPa)
09:27:24	7.93	112.1	16.5	915	32.27
09:27:27	7.48	105.8	16.6	657	42.4
09:27:30	7.44	105.3	16.4	651	42.56
09:27:33	7.67	108.5	16.3	650	43.96

£
Point..... 5
Pavement description... brickearth
Remarks..... pre-compaction
Temperature..... 17

Time (HMS)	Force (kN)	Press (kPa)	Pulse (ms)	D(1) (µm)	E(1) (MPa)
09:27:56	6.85	96.9	16.8	5690	4.48
09:28:00	7.97	112.7	17.7	1810	16.39
09:28:03	6.55	92.7	23.2	3375	7.23
09:28:07	8.91	126.1	16.8	2251	14.74

£
Point..... 6
Pavement description... brickearth
Remarks..... pre-compaction
Temperature..... 17

Time (HMS)	Force (kN)	Press (kPa)	Pulse (ms)	D(1) (µm)	E(1) (MPa)
09:28:32	9.2	130.2	16.6	1116	30.71
09:28:36	8.53	120.7	16.4	854	37.2
09:28:39	7.56	106.9	15.9	852	33.01
09:28:43	7.3	103.3	15.9	847	32.09
09:28:54	0.26	3.6	0	0	Inf

£
Point..... 7
Pavement description... brickearth
Remarks..... pre-compaction
Temperature..... 17

Time	Force	Press	Pulse	D(1)	E(1)

(HMS)	(kN)	(kPa)	(ms)	(µm)	(MPa)
09:29:08	9.23	130.6	16.7	950	36.19
09:29:12	6.86	97.1	16.5	834	30.66
09:29:15	6.87	97.2	16.6	827	30.94
09:29:19	6.9	97.6	16.5	825	31.17
09:29:32	0.56	7.9	0	446	4.65

£
Point..... 8
Pavement description... brickearth
Remarks..... pre-compaction
Temperature..... 17

Time (HMS)	Force (kN)	Press (kPa)	Pulse (ms)	D(1) (µm)	E(1) (MPa)
09:29:44	8.95	126.7	16.7	1282	26.01
09:29:47	9.01	127.5	16.8	967	34.68
09:29:51	8.17	115.5	16.8	887	34.27
09:29:54	7.63	108	17	886	32.07
09:30:06	0.28	4	0	4	252.13

£
Point..... 9
Pavement description... brickearth
Remarks..... pre-compaction
Temperature..... 17

Time (HMS)	Force (kN)	Press (kPa)	Pulse (ms)	D(1) (µm)	E(1) (MPa)
09:30:17	8.44	119.4	17.5	4915	6.39
09:30:22	8.57	121.2	16.8	1718	18.57
09:30:25	8.26	116.8	16.9	1616	19.02
09:30:29	6.66	94.3	17.1	1493	16.62
Point 10					
09:30:52	9.75	138	17.3	968	37.53
09:30:55	9.05	128	16.7	795	42.39
09:30:58	8.35	118.2	16.5	741	41.96
09:31:01	8.64	122.3	16.3	734	43.84

£
Point..... 11
Pavement description... brickearth
Remarks..... pre-compaction
Temperature..... 17

Time (HMS)	Force (kN)	Press (kPa)	Pulse (ms)	D(1) (µm)	E(1) (MPa)
09:31:19	9.18	129.9	16.8	1611	21.22
09:31:22	7.67	108.5	16.7	642	44.49
09:31:25	6.83	96.7	16.9	635	40.09

09:31:28	6.91	97.8	16.9	650	39.59

£
Point..... 12
Pavement description... brickearth
Remarks..... pre-compaction
Temperature..... 17

Time (HMS)	Force (kN)	Press (kPa)	Pulse (ms)	D(1) (µm)	E(1) (MPa)
09:31:45	9.49	134.2	17.1	8069	4.38
09:31:49	9.06	128.1	16.8	774	43.6
09:31:52	9.12	129	16.9	744	45.66
09:31:56	9.21	130.4	16.7	752	45.61

£
Point..... 13
Pavement description... brickearth
Remarks..... pre-compaction
Temperature..... 17

Time (HMS)	Force (kN)	Press (kPa)	Pulse (ms)	D(1) (µm)	E(1) (MPa)
09:32:32	9.26	130.9	16.6	1322	26.08
09:32:36	7.01	99.1	16.8	1265	20.64
09:32:39	6.66	94.2	16.3	1216	20.39
09:32:42	6.8	96.2	16.3	1216	20.84
09:32:52	0.27	3.9	0	262	3.9

£
Point..... 14
Pavement description... brickearth
Remarks..... pre-compaction
Temperature..... 17

Time (HMS)	Force (kN)	Press (kPa)	Pulse (ms)	D(1) (µm)	E(1) (MPa)
09:33:01	8.45	119.5	16.9	1111	28.31
09:33:04	8.87	125.4	16.5	928	35.57
09:33:08	8.59	121.5	16.5	917	34.85
09:33:12	8.7	123	16.3	928	34.91

£
Point..... 15
Pavement description... brickearth
Remarks..... pre-compaction
Temperature..... 17

Time (HMS)	Force (kN)	Press (kPa)	Pulse (ms)	D(1) (µm)	E(1) (MPa)
09:33:30	8.14	115.2	17	974	31.12
09:33:33	7.49	106	16.3	479	58.19
09:33:37	6.76	95.6	16	359	70.08
09:33:40	6.1	86.3	15.2	184	123.66
Point 16					
09:34:07	7.41	104.9	17	1163	23.75
09:34:11	6.54	92.5	15.8	330	73.77
09:34:14	5.81	82.2	16	314	68.92
09:34:18	5.91	83.5	16.3	285	77.12

£
Point..... 17
Pavement description... brickearth
Remarks..... pre-compaction
Temperature..... 17

Time (HMS)	Force (kN)	Press (kPa)	Pulse (ms)	D(1) (µm)	E(1) (MPa)
09:34:32	0.41	5.8	0	0	Inf
09:34:36	7.48	105.9	17.1	1771	15.74
09:34:39	8.11	114.7	17.2	755	39.98
09:34:43	8.46	119.6	17.3	674	46.73
09:34:46	8.5	120.3	17.5	574	55.19

£
Point..... 18
Pavement description... brickearth
Remarks..... pre-compaction
Temperature..... 17

Time (HMS)	Force (kN)	Press (kPa)	Pulse (ms)	D(1) (µm)	E(1) (MPa)
09:35:17	8.11	114.8	17.8	1221	24.74
09:35:20	8.71	123.2	17.9	1213	26.74
09:35:24	8.81	124.6	17.8	1179	27.82
09:35:27	8.9	126	18.5	1142	29.03

£
Point..... 19
Pavement description... brickearth
Remarks..... pre-compaction
Temperature..... 17

Time (HMS)	Force (kN)	Press (kPa)	Pulse (ms)	D(1) (µm)	E(1) (MPa)
09:35:43	8.89	125.7	18	3500	9.45
09:35:46	8.54	120.8	16.8	1871	17
09:35:50	7.91	112	16.9	1701	17.33
09:35:53	7.96	112.6	16.8	1629	18.19

£
Point..... 20
Pavement description... brickearth
Remarks..... pre-compaction
Temperature..... 17

Time (HMS)	Force (kN)	Press (kPa)	Pulse (ms)	D(1) (µm)	E(1) (MPa)
09:39:30	0.39	5.5	0	86	16.94

£
Point..... 20
Pavement description... brickearth
Remarks..... pre-compaction
Temperature..... 17

Time (HMS)	Force (kN)	Press (kPa)	Pulse (ms)	D(1) (µm)	E(1) (MPa)
09:40:45	7.49	106	15.7	1580	17.66
09:40:47	5.69	80.4	14.6	922	22.97
09:40:51	5.81	82.2	15.1	901	24.01
09:40:54	5.71	80.8	14.9	896	23.75

Prima data for NNE line

(c) Keros 2000

$
Filename..... sw-ne.pkv
Client code.....
Project number..... ospringe
Name of client..... ntu
Date..... 11 Oct 2001
Prima 100 SN..... S/N-0107201-ORC-0014
Load plate radius (mm). 150
R(1)
Radial offset (cm)..... 0

£
Point..... 13
Pavement description... brickearth
Remarks.....
Temperature..... 17

Time (HMS)	Force (kN)	Press (kPa)	Pulse (ms)	D(1) (µm)	E(1) (MPa)
11:24:43	9.08	128.4	16.8	375	90.12
11:24:49	7.39	104.5	23.5	474	58.07
11:24:56	7.23	102.2	17.0	305	88.21
11:25:02	7.49	106.0	16.9	288	96.85

£
Point..... 14

Pavement description... brickearth
Remarks.....
Temperature..... 17

Time (HMS)	Force (kN)	Press (kPa)	Pulse (ms)	D(1) (µm)	E(1) (MPa)
11:25:58	7.34	103.9	15.5	311	87.95
11:26:03	5.90	83.5	15.0	19	1133.40
11:26:08	7.40	104.6	15.7	11	2514.94
11:26:12	7.28	102.9	15.8	9	3137.72

£
Point..... 15
Pavement description... brickearth
Remarks.....
Temperature..... 17

Time (HMS)	Force (kN)	Press (kPa)	Pulse (ms)	D(1) (µm)	E(1) (MPa)
11:26:46	8.95	126.6	16.1	333	100.15
11:26:50	8.33	117.9	15.9	230	134.84
11:26:53	8.50	120.2	16.0	208	151.79
11:26:57	8.54	120.9	16.1	221	143.82

£
Point..... 16
Pavement description... brickearth
Remarks.....
Temperature..... 17

Time (HMS)	Force (kN)	Press (kPa)	Pulse (ms)	D(1) (µm)	E(1) (MPa)
11:27:43	7.73	109.4	16.2	510	56.44
11:27:47	8.35	118.1	16.5	279	111.28
11:27:51	6.56	92.8	16.6	279	87.53
11:27:54	6.49	91.8	16.6	262	92.31

£
Point..... 17
Pavement description... brickearth
Remarks.....
Temperature..... 17

Time (HMS)	Force (kN)	Press (kPa)	Pulse (ms)	D(1) (µm)	E(1) (MPa)
11:28:20	9.15	129.5	16.3	645	52.87
11:28:22	9.15	129.5	16.3	455	74.95
11:28:25	9.27	131.2	16.4	435	79.42
11:28:29	9.00	127.3	16.5	367	91.26
11:28:45	0.28	4.0	0.0	1031	1.01

£
Point..... 18
Pavement description... brickearth
Remarks.....
Temperature..... 17

Time (HMS)	Force (kN)	Press (kPa)	Pulse (ms)	D(1) (µm)	E(1) (MPa)
11:28:59	8.66	122.5	16.9	2130	15.14
11:29:03	8.59	121.5	18.5	1235	25.91
11:29:08	7.50	106.1	17.1	996	28.03
11:29:11	6.50	92.0	17.1	941	25.73

£
Point..... 19
Pavement description... brickearth
Remarks.....
Temperature..... 17

Time (HMS)	Force (kN)	Press (kPa)	Pulse (ms)	D(1) (µm)	E(1) (MPa)
11:30:05	8.92	126.2	16.9	1575	21.09
11:30:08	8.87	125.5	17.2	1339	24.69
11:30:11	9.34	132.1	17.3	2739	12.69
11:30:15	8.98	127.1	16.8	1222	27.37
11:30:27	0.40	5.6	25.9	0	Inf

£
Point..... 20
Pavement description... brickearth
Remarks.....
Temperature..... 17

Time (HMS)	Force (kN)	Press (kPa)	Pulse (ms)	D(1) (µm)	E(1) (MPa)
11:30:46	7.82	110.6	16.4	995	29.27
11:30:49	8.50	120.3	16.2	918	34.51
11:30:52	8.39	118.7	16.0	889	35.15
11:30:56	8.01	113.3	16.2	830	35.95

£
Point..... 21
Pavement description... brickearth
Remarks.....
Temperature..... 17

Time (HMS)	Force (kN)	Press (kPa)	Pulse (ms)	D(1) (µm)	E(1) (MPa)
11:31:39	7.17	101.5	16.9	4353	6.14
11:31:42	0.51	7.3	0.0	0	Inf
11:31:46	8.81	124.7	18.5	1280	25.63
11:31:50	8.72	123.4	18.5	1184	27.43
11:31:53	8.69	123.0	18.1	1147	28.22

£
Point..... 22
Pavement description... brickearth
Remarks.....
Temperature..... 17

Time (HMS)	Force (kN)	Press (kPa)	Pulse (ms)	D(1) (µm)	E(1) (MPa)
11:32:33	9.37	132.6	16.6	505	69.11
11:32:37	0.53	7.5	3.9	0	17111.94
11:32:41	8.76	124.0	16.5	361	90.48
11:32:45	6.72	95.1	16.6	296	84.69
11:32:48	6.73	95.3	17.1	276	90.80
11:32:52	6.77	95.7	16.9	281	89.57

£
Point..... 23
Pavement description... brickearth
Remarks.....
Temperature..... 17

Time (HMS)	Force (kN)	Press (kPa)	Pulse (ms)	D(1) (µm)	E(1) (MPa)
11:33:21	9.52	134.7	16.8	1053	33.67
11:33:24	0.83	11.8	0.0	81	38.25
11:33:28	9.08	128.4	17.0	1071	31.56
11:33:31	9.11	128.9	16.8	1024	33.13
11:33:35	8.70	123.0	18.7	1008	32.12
11:33:41	9.34	132.1	16.8	1000	34.75

£
Point..... 24
Pavement description... brickearth
Remarks.....
Temperature..... 17

Time (HMS)	Force (kN)	Press (kPa)	Pulse (ms)	D(1) (µm)	E(1) (MPa)
11:34:26	8.89	125.8	16.9	859	38.55
11:34:31	9.24	130.7	16.7	288	119.59
11:34:34	9.18	129.8	16.8	186	184.04
11:34:38	8.74	123.6	17.0	222	146.43

The system calculates the E-moduli by the following formulas:

E(center) = f x (1- Poisson's ratio^2) x Contact pressure x load plate radius)/ Deflection

E(Not center) = (1- Poisson's ratio^2) x Contact pressure x load plate radius^2 / (Deflection x radial distance)

For the moment the stress distribution factor, f is default 2 and Poisson's ratio 0.35. Is has been discussed that there should bee a field/function where the user can change this. This is most likely to be incorporated into the next software update.

GDP test results

Ospringe, Kent, 11/10/01		
Light Drop Weight Tester (a.k.a. German Dynamic Plate Bearing Test, GDP)		
Survey line: west - east, pre-compaction		
Distance (m) from plate	Evd (MN/m2)	Comments
1	9.59	
2	15.14	
3	16.35	
4	20.77	
5	12.03	Point offset 0.5m to south
6	17.63	
7	19.98	
8	16.5	
9	15.59	
10	19.56	Point at 10.3m
11	13.05	
12	14.39	
13	12.54	
14	15.37	
15	11.46	
16	8.33	
17	8.58	
18	10.48	
19	10.41	
20	16.18	
Average	**14.20**	
Survey line: Southwest - Northeast, non-compacted		
Distance (m) from plate	Evd (MN/m2)	Comments
13	13.31	
14	22.14	Downward sloping ground from this point onwards
15	17.91	
16	15.92	Ground disturbed
17	14.77	
18	13.18	
19	11.99	Un-even ground
20	12.93	
21	19.29	
22	23	Too severe slope to record data
23	18.97	
24	11.52	Wet ground + gravel on surface
25	9.48	Wet ground
Average	**15.72384615**	

Survey line: west - east, post-compaction

Distance (m) from plate	Evd (MN/m2)	Comments
1	5.26	
2	11.21	
3	3.18	
4	3.11	
5	3.38	
6	3.39	
7	3.5	
8	3.23	
9	3.77	
10		Slope - unable to level plate
11	4.26	
12	4.7	
13	3.81	
14	3.53	
15	3.96	
16	5.77	
17	5.19	
18	5.23	
Average	**4.50**	
	Post compaction	**Pre compaction**
1	5.26	9.59
2	11.21	15.14
3	3.18	16.35
4	3.11	20.77
5	3.38	12.03
6	3.39	17.63
7	3.5	19.98
8	3.23	16.5
9	3.77	15.59
10		19.56
11	4.26	13.05
12	4.7	14.39
13	3.81	12.54
14	3.53	15.37
15	3.96	11.46
16	5.77	8.33
17	5.19	8.58
18	5.23	10.48
19		10.41
20		16.18

SPT test results

Standard Penetrometer results

SPT 01 (NNE line)				SPT 02 (W-E line)			
Drop	Reading	Normalised	Penetration	Drop	Reading	Normalised	Penetration
0	65	0	0	0	88	0	0
1	97	32	32	1	158	70	70
2	116	51	19	2	178	90	20
3	135	70	19	3	197	109	19
4	148	83	13	4	218	130	21
5	161	96	13	5	236	148	18
6	181	116	20	6	253	165	17
7	203	138	22	7	270	182	17
8	224	159	21	8	287	199	17
9	241	176	17	9	308	220	21
10	260	195	19	10	330	242	22
11	274	209	14	11	359	271	29
12	285	220	11	12	380	292	21
13	295	230	10	13	406	318	26
14	304	239	9	14	433	345	27
15	315	250	11	15	465	377	32
16	327	262	12	16	495	407	30
17	339	274	12	17	530	442	35
18	354	289	15	18	564	476	34
19	366	301	12	19	600	512	36
20	380	315	14	20	638	550	38
21	396	331	16	21	677	589	39
22	413	348	17	22	713	625	36
23	430	365	17	23	745	657	32
24	446	381	16				
25	464	399	18				
26	484	419	20				
27	505	440	21				
28	528	463	23				
29	551	486	23				
30	575	510	24				
31	600	535	25				
32	624	559	24				
33	649	584	25				
34	672	607	23				
35	695	630	23				

SPT 03				SPT 04			
Drop	Reading	Normalised	Penetration	Drop	Reading	Normalised	Penetration
0	80	0	0	0	0	70	0
1	150	70	70	1	46	116	46
2	224	144	74	2	52	168	52
3	286	206	62	3	62	230	62
4	334	254	48	4	69	299	69
5	362	282	28	5	44	343	44
6	387	307	25	6	31	374	31
7	412	332	25	7	26	400	26
8	438	358	26	8	28	428	28
9	465	385	27	9	27	455	27
10	500	420	35	10	24	479	24
11	534	454	34	11	29	508	29
12	577	497	43	12	27	535	27
13	617	537	40	13	33	568	33
14	658	578	41	14	37	605	37
15	698	618	40	15	39	644	39
16	735	655	37	16	44	688	44
				17	30	718	30
				18	36	754	36

SPT 05				SPT 06			
Drop	Reading	Normalised	Penetration	Drop	Reading	Normalised	Penetration
0	85	0	0	0	75	0	0
1	150	65	65	1	108	33	33
2	190	105	40	2	135	60	27
3	220	135	30	3	159	84	24
4	250	165	30	4	183	108	24
5	277	192	27	5	208	133	25
6	306	221	29	6	230	155	22
7	335	250	29	7	249	174	19
8	368	283	33	8	268	193	19
9	398	313	30	9	287	212	19
10	430	345	32	10	310	235	23
11	459	374	29	11	333	258	23
12	485	400	26	12	354	279	21
13	511	426	26	13	378	303	24
14	535	450	24	14	401	326	23
15	559	474	24	15	425	350	24
16	583	498	24	16	451	376	26
17	605	520	22	17	477	402	26
18	630	545	25	18	506	431	29
19	652	567	22	19	533	458	27
20	680	595	28	20	560	485	27
21	709	624	29	21	588	513	28
22	743	658	34	22	615	540	27
				23	641	566	26
				24	669	594	28
				25	695	620	26
				26	720	645	25

SPT 07				SPT 08			
Drop	Reading	Normalised	Penetration	Drop	Reading	Normalised	Penetration
0	93	0	0	0	93	0	0
1	157	64	64	1	145	52	52
2	190	97	33	2	190	97	45
3	220	127	30	3	231	138	41
4	248	155	28	4	264	171	33
5	271	178	23	5	299	206	35
6	294	201	23	6	330	237	31
7	315	222	21	7	368	275	38
8	339	246	24	8	409	316	41
9	361	268	22	9	449	356	40
10	388	295	27	10	485	392	36
11	414	321	26	11	516	423	31
12	441	348	27	12	544	451	28
13	470	377	29	13	573	480	29
14	503	410	33	14	604	511	31
15	533	440	30	15	637	544	33
16	564	471	31	16	667	574	30
17	594	501	30	17	694	601	27
18	624	531	30	18	720	627	26
19	650	557	26				
20	676	583	26				
21	701	608	25				
22	728	635	27				

SPT 09				SPT 10			
Drop	Reading	Normalised	Penetration	Drop	Reading	Normalised	Penetration
0	85	0	0	0	71	0	0
1	138	53	53	1	125	54	54
2	191	106	53	2	158	87	33
3	244	159	53	3	185	114	27
4	288	203	44	4	209	138	24
5	329	244	41	5	231	160	22
6	364	279	35	6	255	184	24
7	397	312	33	7	278	207	23
8	429	344	32	8	307	236	29
9	458	373	29	9	336	265	29
10	485	400	27	10	365	294	29
11	517	432	32	11	393	322	28
12	546	461	29	12	420	349	27
13	575	490	29	13	448	377	28
14	605	520	30	14	475	404	27
15	631	546	26	15	499	428	24
16	661	576	30	16	522	451	23
17	692	607	31	17	544	473	22
18	718	633	26	18	565	494	21
				19	588	517	23
				20	608	537	20
				21	628	557	20
				22	651	580	23
				23	672	601	21
				24	701	630	29

SPT11				SPT12			
Drop	Reading	Normalised	Penetration	Drop	Reading	Normalised	Penetration
0	78	0	0	0	74	0	0
1	120	42	42	1	113	39	39
2	164	86	44	2	146	72	33
3	190	112	26	3	170	96	24
4	215	137	25	4	190	116	20
5	241	163	26	5	208	134	18
6	267	189	26	6	228	154	20
7	294	216	27	7	243	169	15
8	318	240	24	8	263	189	20
9	346	268	28	9	280	206	17
10	373	295	27	10	303	229	23
11	401	323	28	11	324	250	21
12	429	351	28	12	347	273	23
13	452	374	23	13	370	296	23
14	475	397	23	14	394	320	24
15	494	416	19	15	415	341	21
16	519	441	25	16	435	361	20
17	543	465	24	17	456	382	21
18	560	482	17	18	473	399	17
19	575	497	15	19	488	414	15
20	588	510	13	20	506	432	18
21	602	524	14	21	528	454	22
22	618	540	16	22	555	481	27
23	641	563	23	23	591	517	36
24	670	592	29	24	625	551	34
26	704	626	34	26	658	584	33
27	738	660	34	27	694	620	36
				28	731	657	37

SPT 13				SPT 13			
Drop	Reading	Normalised	Penetration	Drop	Reading	Normalised	Penetration
0	78	0	0	21	472	394	27
1	109	31	31	22	502	424	30
2	129	51	20	23	531	453	29
3	148	70	19	24	558	480	27
4	166	88	18	25	584	506	26
5	180	102	14	26	610	532	26
6	198	120	18	27	641	563	31
7	214	136	16	28	671	593	30
8	233	155	19	29	698	620	27
9	249	171	16	30	725	647	27
10	265	187	16				
11	283	205	18				
12	302	224	19				
13	323	245	21				
14	334	256	11				
15	345	267	11				
16	355	277	10				
17	370	292	15				
18	393	315	23				
19	418	340	25				
20	445	367	27				

SPT combined data for SPT tests 03 and 12

Drop	Reading	Corr. Reading	03	12
0	80	0	0	0
1		39	50	39
2	150	72	72	33
3	224	96	73	24
4	286	116	73	20
5	334	134	74	18
6	362	154	73.5	20
7	387	169	70	15
8	412	189	67	20
9	438	206	62	17
10	465	229	55	23
11	500	250	49	21
12	534	273	31	23
13	577	296	25	23
14	617	320	26	24
15	658	341	27	21
16	698	361	27	20
17	735	382	27.5	20
18		399	30	21
19		414	35	17
20		432	34.5	15
21		454	35	18
22		481	35	22
23		517	41	27
24		551	41	36
26		584	40.25	34
27		620	40.5	33
28		657	40	36
			38	37

SPT combined data for SPT tests 04 and 11

SPT4	SPT4	SPT11	SPT11
Depth mm	Penetration mm	Depth mm	Depth mm
46	46	42	42
98	52	86	44
160	62	112	26
229	69	137	25
273	44	163	26
304	31	189	26
330	26	216	27
358	28	240	24
385	27	268	28
409	24	295	27
438	29	323	28
465	27	351	28
498	33	374	23
535	37	397	23
574	39	416	19
618	44	441	25
648	30	465	24
684	36	482	17
		497	15
		510	13
		524	14
		540	16
		563	23
		592	29
		626	34
		660	34

SPT combined data for SPT tests 07 and 08

dcp 7			dcp 8
Corr. Reading	Penetration mm	Depth mm	Penetration mm
64	64	52	52
97	33	97	45
127	30	138	41
155	28	171	33
178	23	206	35
201	23	237	31
222	21	275	38
246	24	316	41
268	22	356	40
295	27	392	36
321	26	423	31
348	27	451	28
377	29	480	29
410	33	511	31
440	30	544	33
471	31	574	30
501	30	601	27
531	30	627	26
557	26		
583	26		
608	25		
635	27		

Appendix G

Dipole aerial centre mounting boss

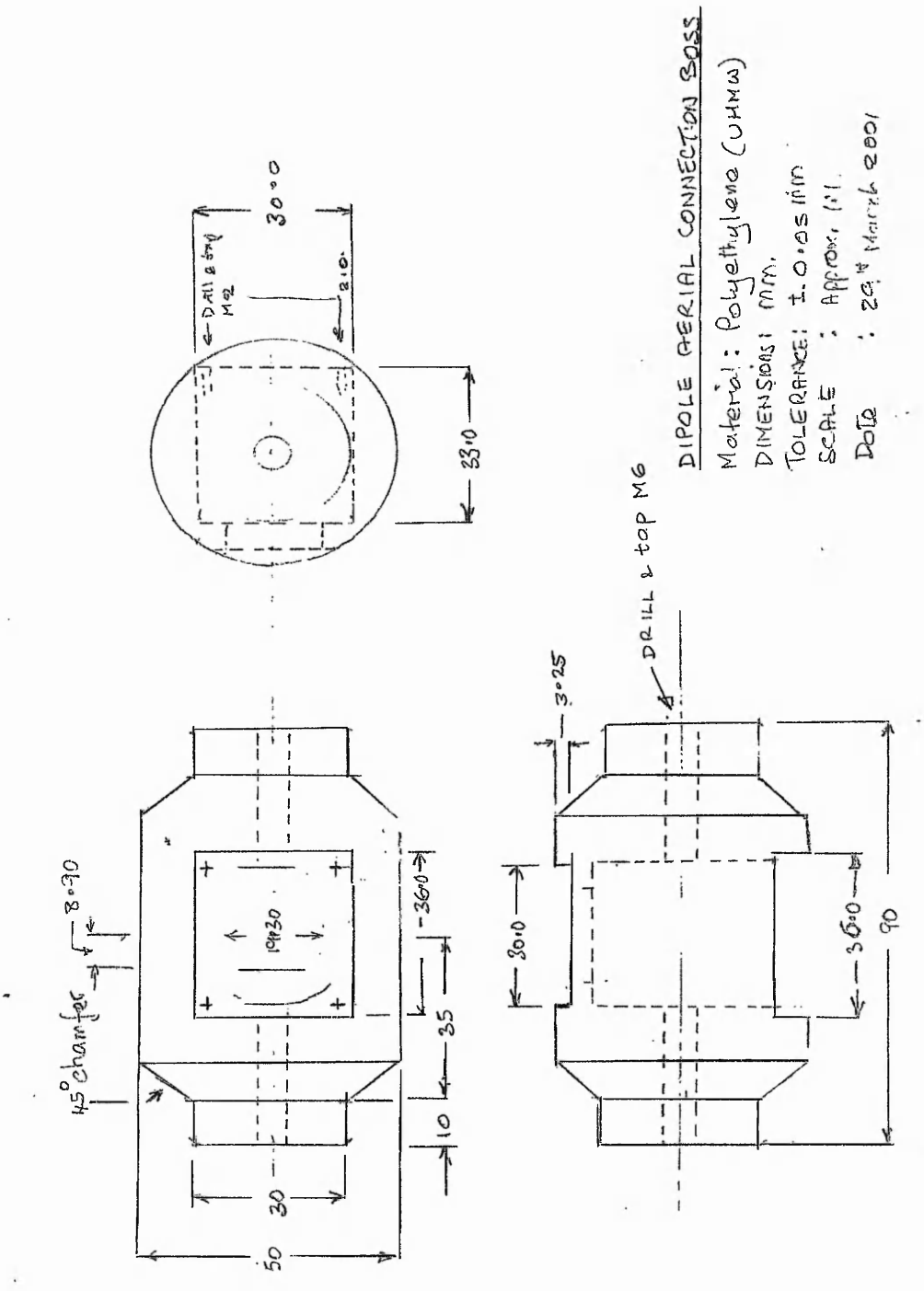

Figure E1. Dipole mounting boss

Appendix H

Ultrasonic transducer high voltage driver circuit

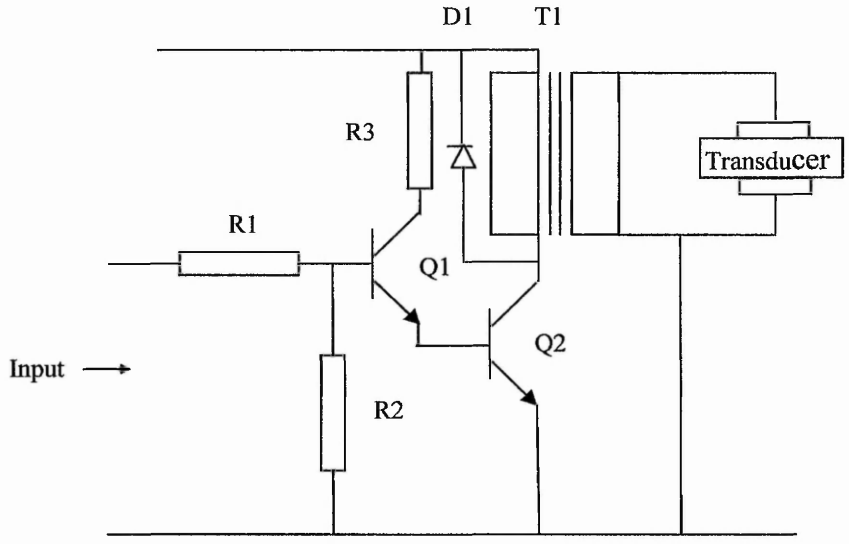

Figure H1 Circuit diagram for ultrasonic high voltage driver circuit

Parts list for figure H1

T1	Ferrite core pulse transformer
Q1	Silicon NPN transistor TIP 47
Q2	Silicon NPN transistor BSX20
R1	12 KΩ 0.25 watt carbon resistor
R2	6K8 Ω 0.25 watt carbon resistor
R3	220 Ω 0.25 watt carbon resistor
D1	Si diode SBYV 28 -200

Winding details for T_1

Primary winding 80 turns 0.25 mm (33 swg) enamelled copper wire

Secondary winding 2500 turns 0.25 mm (33 swg) enamelled copper wire

DC resistance of primary winding 3.1 Ω

DC resistance of secondary winding 35.1 Ω

A photograph of the circuit board is given in plate H1

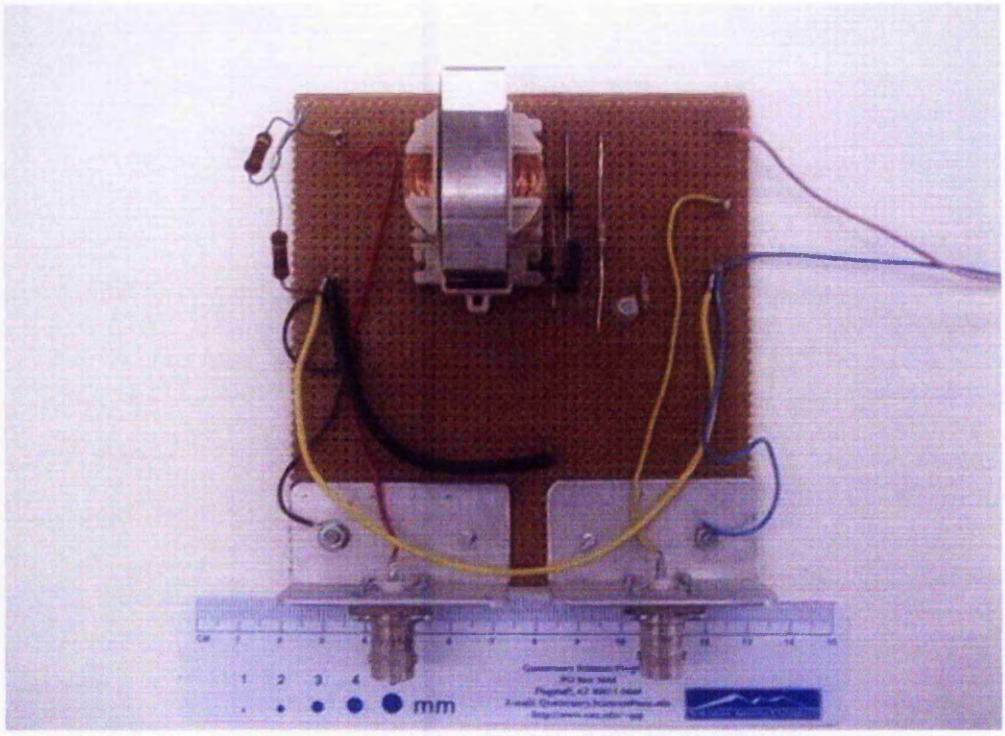

Plate H1 Plan view of high voltage driver circuit for ultrasonic transducer

Appendix I

List of papers

1 O'Hara-Dhand, K. A., Jefferson, I. F., Evans, R. D. 2003. Geophysical ground investigations to assess compaction of problematic soil: in particular loess. Internal report to be submitted for publication in September 2004. 1-11.

2 O'Hara-Dhand, K. A. 2004. A novel method for the detection of electro-kinetic responses and its potential applications. In preparation.

Appendix J

Graphs used to obtain the results of seismic analysis in Chapter 4.

Mansfield results.

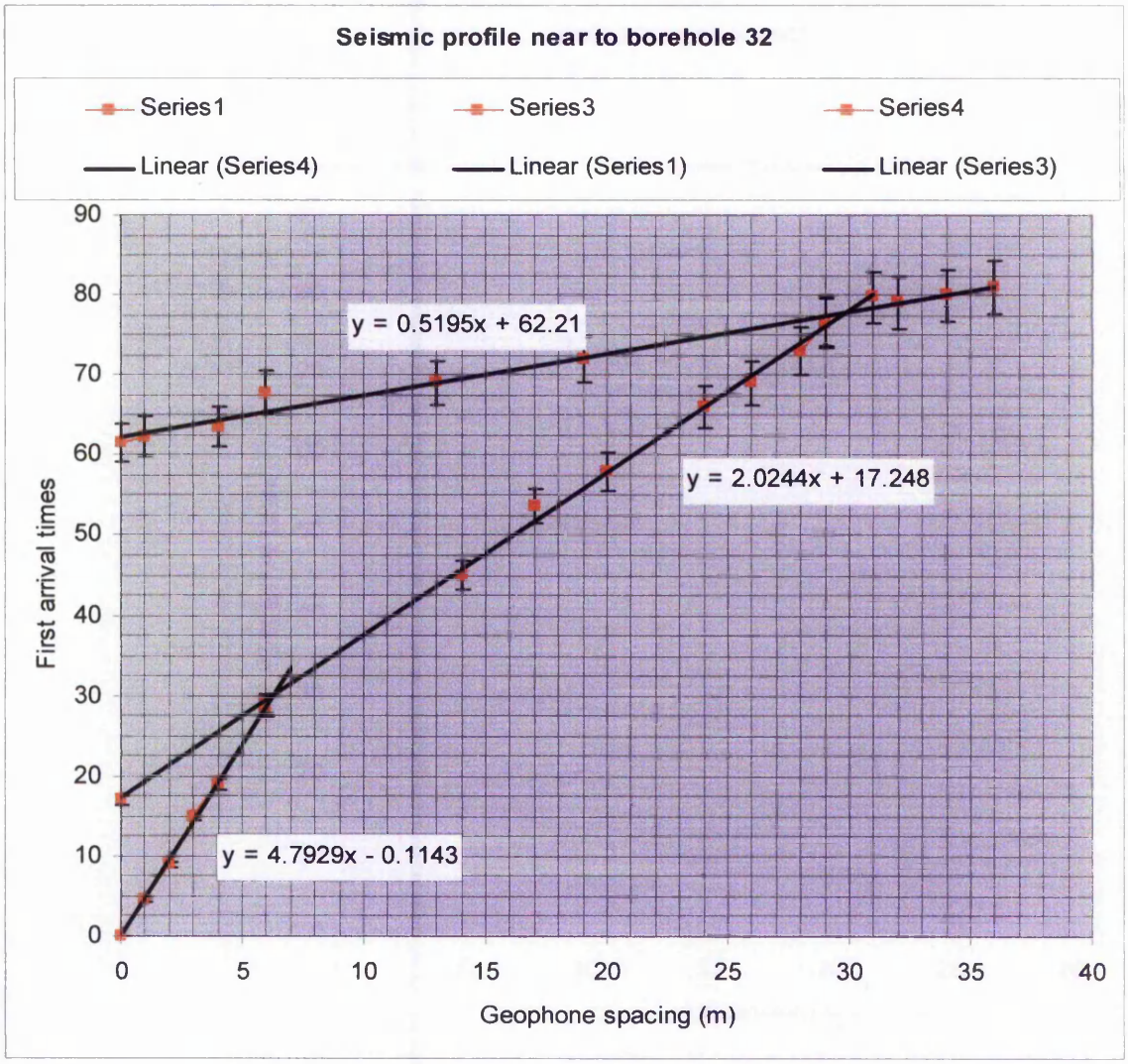

Figure J1 Results of seismic profile taken near to borehole 32. The plotted points have had trend lines fitted in order to determine the seismic velocities of the various layers

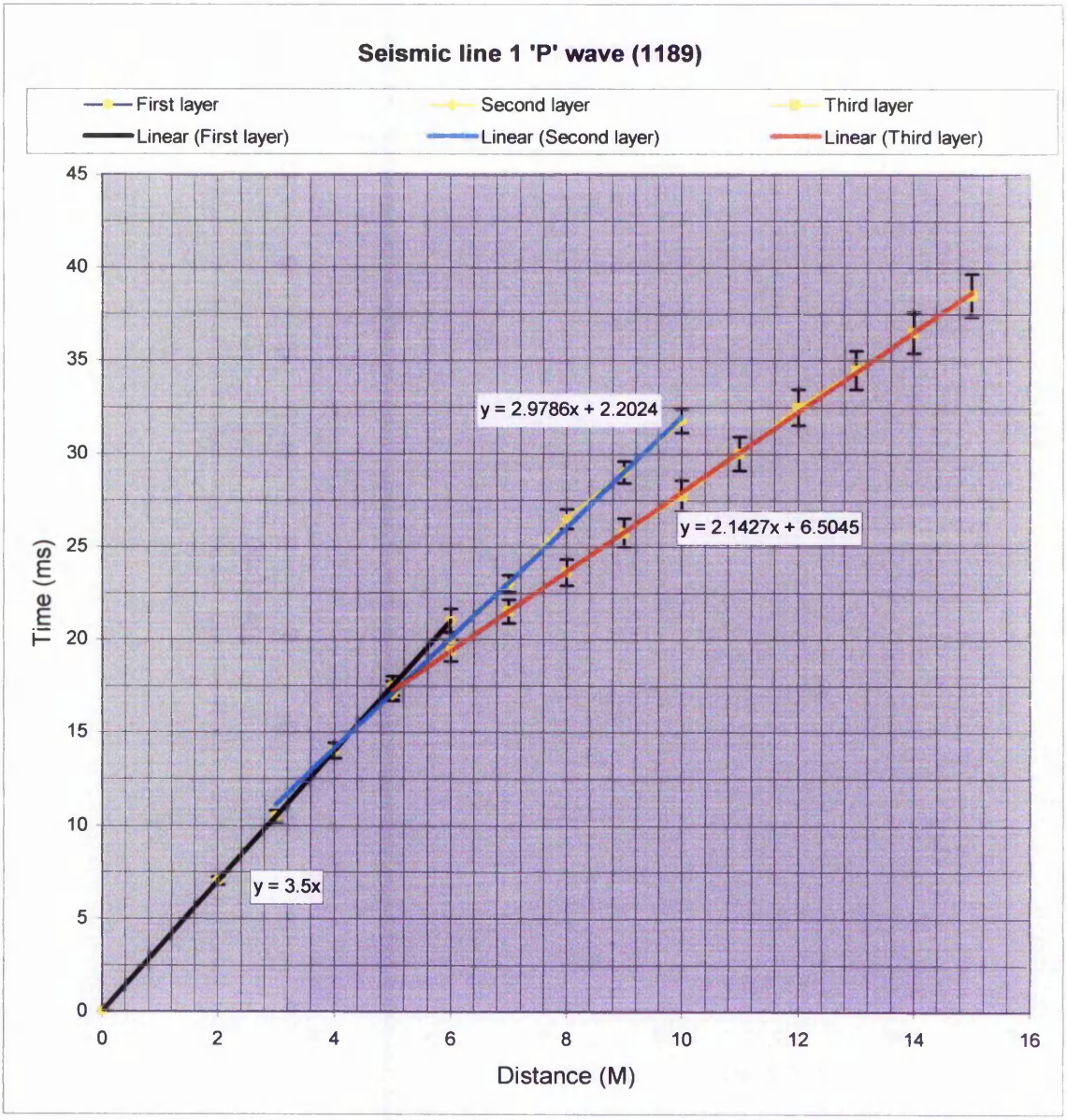

Figure J2. Results from vertical geophone array along line 1 clearly showing the break points for three slopes. These results are pre-compaction. Data point are shown in yellow. All error bars ± 3%.

Results for velocities are given in Chapter 4 table 4.7

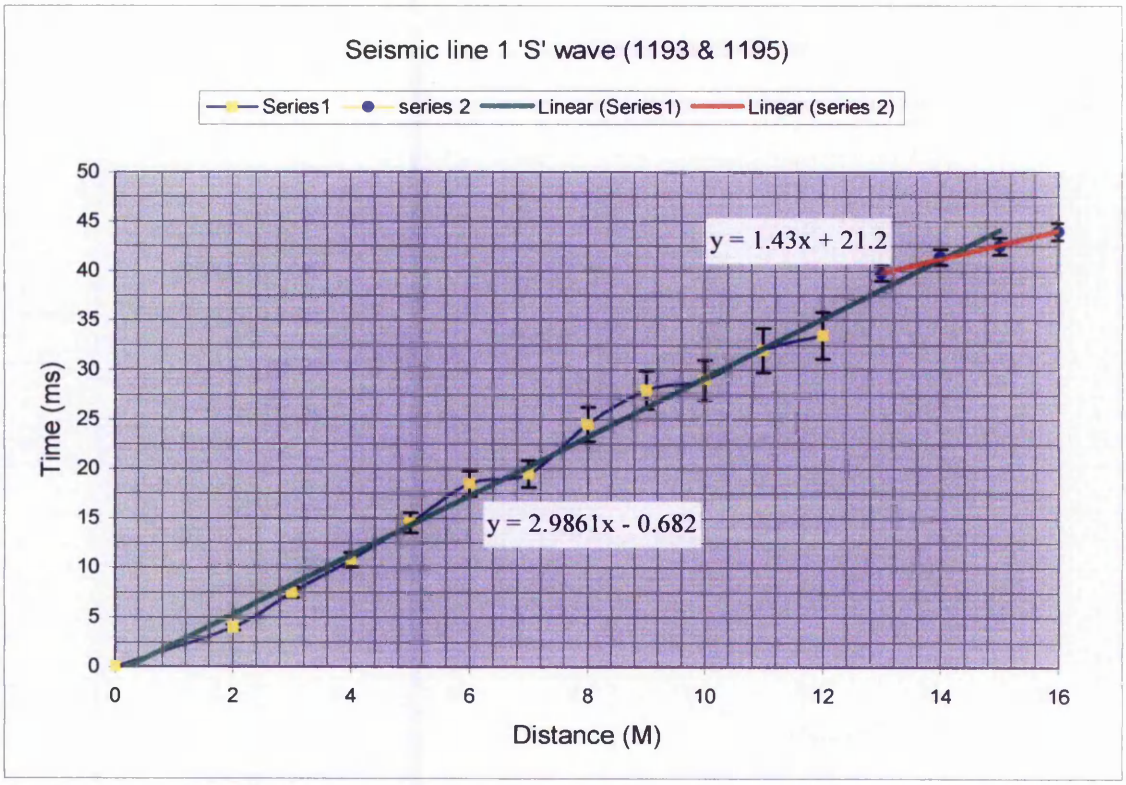

Figure J3. Shear wave geophones start at 2 m out to 24 m. These results are pre-compaction. Data point are shown in yellow. All error bars ± 7%.

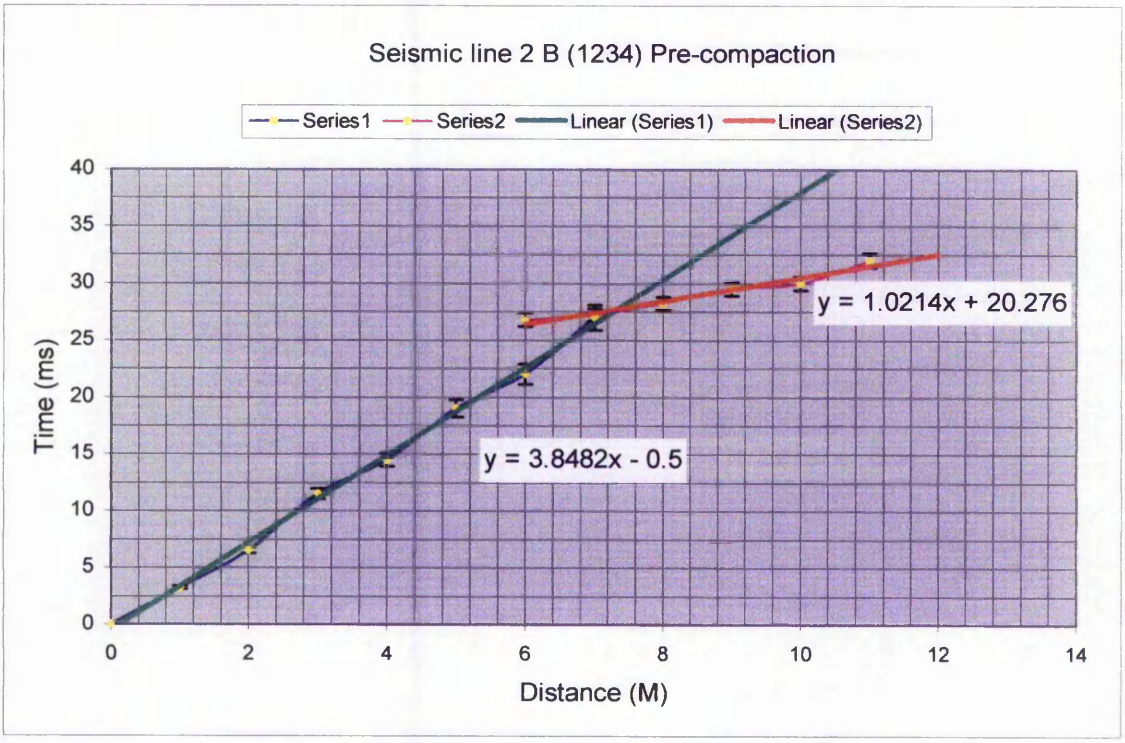

Figure J4 Seismic line 2 pre-compaction. Note the two distinct slopes

Results for seismic velocities are given in Chapter 4 table 4.7

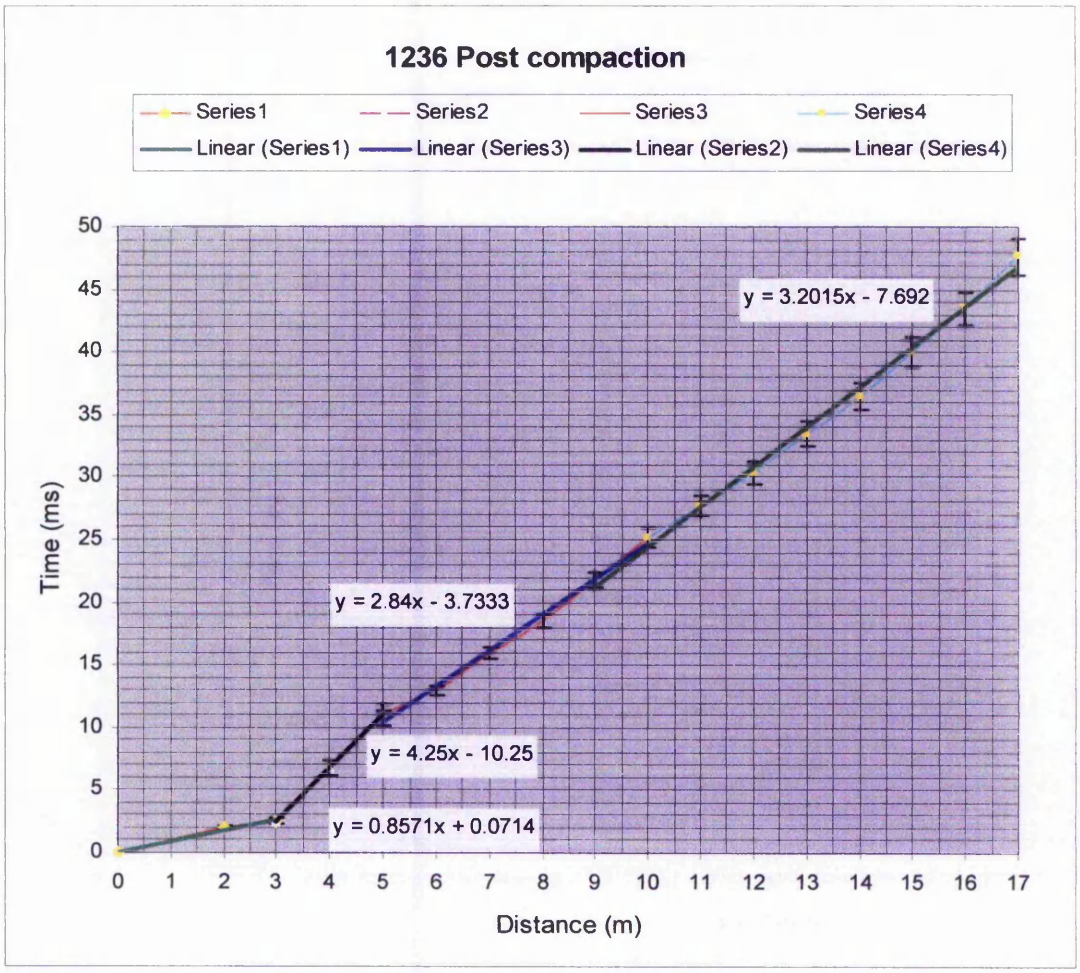

Figure J5 Seismic profile post compaction. Note change in slope for line 2, implies hidden layer

Table J1 DCP test locations and details (See Appendix 'F' for additional details)

Test ref.	Location of test	Compacted	Dist. From shot point
DCP 01	Seismic line at 45^0 NE to east west line 1	N	16 m
" 02	Seismic line approximately east west	Y	1 m
" 03	"	Y	4 m
" 04	"	Y	8 m
" 05	"	Y	12 m
" 06	"	Y	16 m
" 07	"	Y	18 m
" 08	Parallel to above line but 4 m south	N	18 m
" 09	"	N	16 m
" 10	"	N	12 m
" 11	"	N	8 m
" 12	"	N	4 m
" 13	"	N	1 m

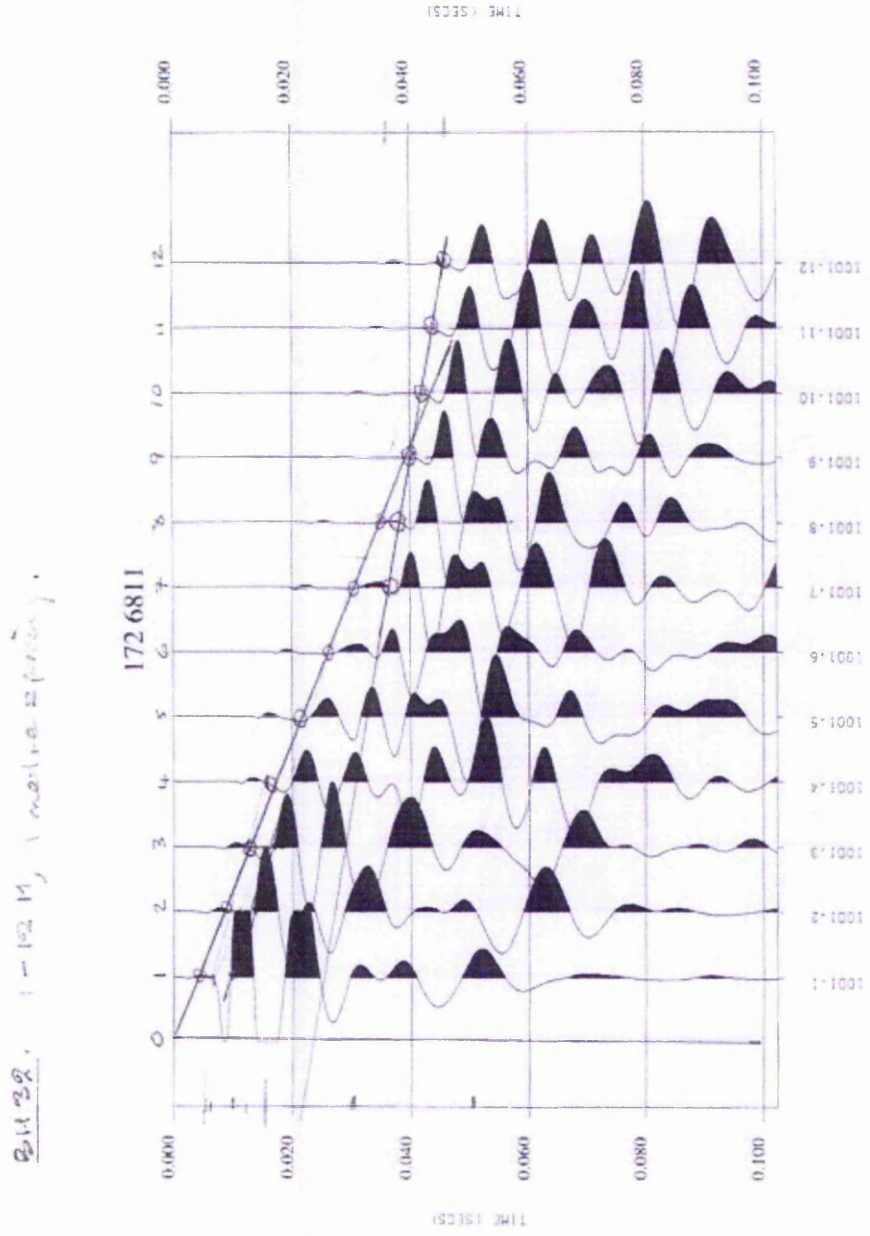

Figure J6. Results of seismic refraction survey at borehole 32